The effect of Mn and Zr additions on Fe impurities and the corrosion performance of Mg

Thesis in the fulfilment of the requirement for the degree of Doctor of Philosophy in Materials Engineering

By

Darren Samuel Gandel

B. Eng (hons.) (Mat. Eng.)

Department of Materials Engineering

Faculty of Engineering

Monash University

October 2013

This page is intentionally left blank

COPYRIGHT NOTICE

.....

Darren Samuel Gandel

This page is intentionally left blank

This thesis is dedicated to my family and friends

Thank you for supporting me on this journey

This page is intentionally left blank

Table of contents

Abstract

Manganese (Mn) and zirconium (Zr) are two common alloying additions in magnesium (Mg) alloys. Both of these elements, while having low solubilities in Mg, each serve a specific purpose when added to Mg. Mn is often added to improve the extrudability and formability of Mg alloys and in aluminium (Al) containing Mg alloys to produce the $Al_8(Mn,Fe)_5$ phase which is able to remove iron (Fe) impurities to dramatically improve the corrosion resistance. Zr is incorporated in Mg mainly due to its unique ability to act as a grain refiner to greatly reduce the grain size and hence improve the mechanical properties of Mg.

The effect of Mn alone on the corrosion of Mg and subsequent Fe impurity levels in the absence of any Al alloying addition is not well documented. Furthermore, the independent role that Zr has on the corrosion of Mg and Mg alloys has also not been reported thoroughly. In this study, Mg alloys containing various levels of Mn, Zr and Fe alloying additions in binary, ternary and quaternary combinations were produced and examined via SEM, EDX and EBSD techniques. The corrosion rates and morphologies of Mg alloy samples were examined via electrochemical polarisation and immersion testing.

It was discovered that Zr additions, while beneficial in being able to remove Fe impurities, has a negative impact on the corrosion rates of Mg. Zr is able to increase both the anodic and cathodic reaction kinetics of Mg, thereby increasing the corrosion rate. Zr dissolved in the Mg solid solution was shown to act as an 'anodic activator', increasing the anodic reaction kinetics and the rate of Mg dissolution. Zr not dissolved in solid solution was present as Zr particles embedded in the Mg matrix. These Zr particles were efficient local cathodes, enhancing the cathodic reaction. The difference in electrochemical potential between these, essentially pure Zr, particles and the surrounding Mg matrix lead to the formation of micro-galvanic couples at open circuit, which increased corrosion rate.

Mn was observed to slightly decrease the cathodic reaction kinetics of Mg when included as an alloying addition. This is rationalised on the basis that Mn will interact with Fe, and not on the basis that Mn can support reduction reactions at lower rates than Mg. This notion also appreciates that there is no Mg metal that has 0% Fe. However, beyond Mn additions of ~2

wt.%, Mn particles which formed in the Mg matrix increased the corrosion rate through the formation of micro-galvanic couples with the Mg matrix. While Mn additions in this study were ineffective at removing Fe from the alloy system, Mn was found to be capable of rendering Fe impurities less detrimental to Mg. Mn additions were found to increase the tolerance limit of Fe in Mg. As such, higher levels of Fe were necessary to increase the cathodic reaction kinetics required for increased corrosion rates. It was observed that the Mn additions form an intermetallic phase with the Fe impurities. At low Fe levels these phases appeared to be Mn particles with Fe dissolved in solid solution within these particles. At higher Fe levels, there were large Fe particles encapsulated by a layer of Mn. It is proposed that this interaction between Mn and Fe decreases the electrochemical potential difference between the Fe impurities and the Mg matrix in a similar manner to the $Al_8(Mn,Fe)_5$ phase observed in Al-containing Mg alloys, thereby, decreasing the driving force to increase the cathodic reaction kinetics through micro-galvanic coupling.

This work has elucidated the interactions and effects of Mn and Zr additions on Mg and has shown that Zr is inherently detrimental to the corrosion resistance of Mg and that Mn can interact with Fe in Mg to reduce the impact that Fe impurities have on Mg alloys in the absence of Al.

This page is intentionally left blank

STATEMENT OF ORIGINALITY

This thesis, except with the Research Graduate School Committee's approval, contains no material which has been accepted for the award of any other degree or diploma in any university or other institution and affirms that to the best of my knowledge the thesis contains no material previously published or written by another person, except where due to reference is made in the text of this thesis.

…….

Darren Samuel Gandel

ACKNOWLEDGMENTS

I would like to express my appreciation and thanks to my supervisors Prof. Nick Birbilis, Dr. Mark Easton and Dr. Mark Gibson. Their incredible help, encouragement and persistence over the past four years have resulted in the culmination of this thesis. My supervisors were continually encouraging me to improve my writing skills and to think ‘outside the box’ and delve deeper into the fundamental aspects of the research to uncover the true novel components behind the science.

I would also like to acknowledge the CAST-CRC which was funded in part by, the Australian Governments Co-operative Research Centres Scheme, which provided the scholarship funding for this research and to Monash Univeristy for all the years of use of their facilities, recourses and help from their personnel.

I would like to thank all the members of Materials Engineering faculty at Monash University who have provided assistance to me over the years. I would like to acknowledge Postdoctoral staff Dr. Kevin Ralston, Dr. Rajeev Gupta, Dr. Xiaobo Chen and Dr. Katherine Nairn for all their support and help with experimental testing and proof-reading of my papers and thesis. I would like to thank to Mr. Sebastian Thomas, Dr. Katharina Strobel, Mr. Serge Gavras, Mr. Andy Yob, Mr. Daniel East, Dr. Ming Sun, Ms. Sherly Simanjuntak, Dr. Trevor Abbott, Dr. Bruce Hinton, Prof. Maria Forsyth and everyone else who helped me over the years, whether in a big way or small, you all helped to bring this work to fruition.

List of Figures

Chapter 2

Chapter 4

Chapter 5.1

Chapter 6

Figure 10: i_{corr} vs. weight loss (determined after 24 h of exposure) for Mg-Zr alloys produced with Microzir and Zirmax master alloys and selected commercial Mg alloys (presented with standard error). Testing was in 0.1M NaCl.

Chapter 7

Figure 1: PANDAT calculated isopleth diagrams depicting phases present in; (A) Mg-Fe-Zr alloy with an increasing Zr content, (B) Mg-Mn-Fe alloy with an increasing Mn content, (C) Mg-Mn-Zr alloy with an increasing Zr content and (D) Mg-Mn-Zr-Fe alloy with increasing Zr content.

Figure 2: (A): BSE-SEM micrograph of Mn-Fe Mg-alloy, (B): Corresponding EDX map of Mg content, (C): Corresponding EDX map of Mn content and (D): Corresponding EDX map of Fe content.

Figure 3: (A): BSE-SEM micrograph of Mn-Zr Mg-alloy, (B): Corresponding EDX map of Mg content, (C): Corresponding EDX map of Mn content and (D): Corresponding EDX map of Zr content.

Figure 4: (A): BSE-SEM micrograph of Mn-Zr-Fe Mg-alloy, (B): Corresponding EDX map of Mn content, (C): Corresponding EDX map of Zr content and (D): Corresponding EDX map of Fe content.

Figure 5: (A): BSE-SEM site 1 micrograph of Zr-Fe Mg-alloy, (B): BSE-SEM site 2 micrograph of Zr-Fe Mg-alloy, (C): Corresponding site 1 EDX map of Fe content, (D): Corresponding site 2 EDX map of Fe content, (E): Corresponding site 1 EDX map of Zr content and (F): Corresponding site 2 EDX map of Zr content.

Figure 6: (A) BSE-SEM image of Mn-Fe particle in Mg alloy Mn-Zr-Fe, (B) Corresponding EDX map of Mg content, (C) Corresponding EDX map of Fe content, (D) Corresponding EDX map of Mn content, (E) EBSD Kikuchi pattern of internal structure of Mn-Fe particle (region denoted as (i)) and (F) EBSD Kikuchi pattern of outside layer of Mn-Fe particle (region denoted as (ii)).

List of Tables

LIST OF PUBLICATIONS FROM PHD

- Journal papers

  - D. S. Gandel, M. A. Easton, M. A. Gibson and N. Birbilis (2013), *"Influence of Mn and Zr on the corrosion of Al-free Mg-alloys, Part I: Electrochemical behaviour of Mn and Zr"*, Corrosion, 69 (7), 666-671, *2013*.
  - D. S. Gandel, M. A. Easton, M. A. Gibson and N. Birbilis (2013), *"Influence of Mn and Zr on the corrosion of Al-free Mg-alloys, Part II: Impact of Mn and Zr on Mg-alloy electrochemistry and corrosion"*, Corrosion, 69 (8), 744-751, *2013*.
  - D. S. Gandel, M. A. Easton, M. A. Gibson, T. Abbott and N. Birbilis (2013), *"The influence of zirconium additions on the corrosion of magnesium"*, Expected publisher: Corrosion Science
  - D. S. Gandel, M. A. Easton, M. A. Gibson and N. Birbilis (2013), *"CALPHAD simulation of the Mg-(Mn,Zr)-Fe system and experimental comparison with as-cast alloy as relevant to impurity driven corrosion of Mg-alloys"*, Expected publisher: Materials Chemistry and Physics

- Conference papers

  - Australasian Corrosion Association conference, Adelaide, Australia, November 2010; *"Influence of Manganese, Zirconium and Iron on the corrosion of Magnesium"*.
  - International Corrosion Congress, Perth, Australia, November 2011; *"The influence of Manganese on the corrosion resistance of Al-free Mg-alloys"*.
  - 9th International Conference on Magnesium Alloys and their Applications, Vancouver, Canada, July 2012; *"Iron and corrosion control in Aluminium-free Magnesium alloys"*.
  - TMS 142nd Annual Meeting and Exhibition, San Antonio, USA, March 2013; *"The influence of Mg-Zr master alloy microstructure on the corrosion of Mg"*.

This page is intentionally left blank

Chapter 1

Introduction

This page is intentionally left blank

Chapter 1: Introduction

1.0 History of magnesium alloys and development

When magnesium (Mg) and Mg alloys were first explored as structural materials early in the 20th century, there were several issues that had to be resolved before Mg alloys could be industrially employed. The most common issue in early castings, such as of Mg-Al-Zn alloys, was severe corrosion in wet or moist conditions [1]. In the late 1920's the impact of this reduced significantly with the discovery that small additions of manganese (Mn) decreased substantially the corrosion rate of Al-containing Mg alloys. The Mn addition was found to combine with heavy-metal impurities, such as Fe, and result in (electrochemically) less detrimental intermetallic particles in the Mg-alloy matrix; it also aided the separation of impurities from the alloy melt during processing [1, 2].

Another issue with early Mg alloy castings was that the grain size was quite variable. This often resulted in poor and inconsistent mechanical properties [1]. Moreover, the values for Mg-alloy proof strength tended to be low, relative to tensile strength. In 1937 it was discovered that zirconium (Zr) had an intense grain-refining effect on Mg when added in sufficient quantities [1]. However, it still took many years before a reliable method was developed to alloy Zr into Mg successfully, on a commercial scale.

Another development was the introduction of high-purity Mg alloys in the mid 1980's. This led to growth in automotive applications of Mg alloy high-pressure die-castings. These alloys were able to provide much lower limits on the heavy-metal impurities, which reduced aqueous corrosion resistance, to obtain a higher quality product. This new approach has allowed Mg alloys to become more competitive with common automotive aluminium die-cast alloys. The corrosion resistance of these high-purity alloys can be as much as 2-3 orders of magnitude higher than that of previous generations of Mg alloys [3]. One of the main goals of industrial engineering in coming decades is to reduce greenhouse gas emissions to lower their growing negative impact on the environment. As such, research is expanding; with the aims of improving the mechanical and corrosion properties to take advantage of the technological, economic and social benefits that Mg alloys present to society [4-6].

2.0 Metallurgy of Mg and Mg-alloys

Mg is an attractive alternative to steel or aluminium alloys in engineering applications where weight reduction and energy savings are a key concern [1, 7]. Commercially-produced magnesium metal is readily available at purities exceeding 99.8%. Mg has the lowest density of all the structural engineering metals [8]. However, it is rarely used for engineering applications without first being alloyed with other metals [1]. The intentional alloying of Mg is to improve both the mechanical properties and corrosion resistance of the final alloy component while retaining the attractive combination of low density, high strength/weight ratio and good castability or workability associated with Mg [9]. Mg alloys can be excellent substitutes for many ferrous and aluminium alloys used in automotive and aeronautical applications [9].

There are six main raw materials commonly used in the production of magnesium: magnesite, dolomite, bischofite, carnallite, serpentine and seawater. As there are a wide variety of sources from which Mg can be produced, there are a large number of production and manufacturing technologies that exist, because of the different approaches required to remove Mg from each source material. Thus, unlike many other metallurgical manufacturing processes, there is no one particular dominant technology used for most of the world's production of Mg [3]. The natural abundance of Mg and the recyclability of Mg alloys ensures a long-term supply of raw resources desired by growing global industrial manufacturing demands [7].

Magnesium has a hexagonal-close-packed atomic structure. This structure is the main reason why Mg alloys are not amenable to cold forming. Below 225°C, only {0001} <1120> basal plane slip is possible, along with pyramidal {1012} <1011> twinning. Because of the limited number of slip systems, pure magnesium and traditionally-cast magnesium alloys demonstrate a propensity for poor room temperature ductility arising from intercrystalline failure and localised transcrystalline fracture at twin zones or {0001} basal planes within large grains. At temperatures above 225°C, pyramidal {1011} planes become active [7] and magnesium alloys become more ductile particularly with certain additional alloying elements (such as certain RE elements) are present to produce the necessary microstructural changes in Mg.

The key metallurgical properties of pure magnesium are contained in Table 1. On the basis of the strength/weight ratio, Mg casting alloys are superior to aluminium casting alloys because

of their lower density [3, 7, 8]. Mg alloys tend to have the lowest densities of all structural metals, ~ 1.7 g/cm³. Their low melting point allows Mg alloys to be cast at lower operating temperatures, facilitating the use of cheaper steel dies in the casting process when proper atmospheric controls are in place. The low specific heat capacity also means that less energy overall is needed to initiate the melting and processing of the alloy. Most Mg alloys also show good machinability and processability. Mg alloys tend to have good damping behaviour, which makes the use of these alloys even more desirable for industrial applications as it increases the life cycle of machine parts and equipment as well as reducing sonic emissions. In general, Mg alloys show higher damping properties than cast-iron components, although these properties are dependant on the heat treatment carried out on the component [7].

Table 1.1 – Chemical and physical properties of Mg [7]

Crystal Structure	HCP
Density	1.738 g/cm³ at RT
Young's Modulus	45 GPa
Ultimate Tensile Strength	80 - 180 MPa
Fracture Elongation	1 - 12%
Melting Point	650°C
Boiling Point	1090°C
Specific Heat Capacity	1.05 kJ/(kg K)
Fusion Heat	195 kJ/kg
Thermal Conductivity	156 W/(mK) (RT)
Shrinkage (Solid-Liquid)	4.20%
Specific Electrical Conductivity	22.4 m/(Ω mm²) (RT)
Normal Potential	-2.37 V (vs.SHE)

Despite all the attractive properties of Mg alloys, there remain some limitations to their broad application. As mentioned previously, HCP-structured Mg alloys have poor cold working ability and relatively low ductility. Certain alloying additions, such as lithium (Li), form crystal structures in Mg alloys that are more compliant during cold working processes [3]. Moreover, these alloys have a complex phase transformation from an HCP structure to a BCC structure which affects the mechanical properties [10, 11]. However, this remains an area of active research. When solidified, Mg has a bulk shrinkage of approximately 4%. This shrinkage leads to microporosity pockets which can cause low toughness values and high

notch sensitivity. Magnesium also has a relatively high thermal expansion coefficient [12], ~10% higher than the corresponding value for Al. This leads to concerns about heat-fatigue and stress-cracking resulting from temperature changes [7].

3.0 Commercial Mg-alloys

Mg needs to be alloyed with other elements to be employed in engineering applications to improve its mechanical properties [3]. Existing commercially available Mg alloys can generally be separated into two main groups: Mg alloys that contain aluminium (Al) as a primary alloying element and alloys free of Al, which may contain small amounts of zirconium (Zr) for grain refinement.

3.1 Aluminium containing Mg-alloys

Al containing Mg alloys generally display good tensile strength (up to 250 MPa) and ductility (up to 20% elongation) [3], however, not both at the same time. These alloys also often contain zinc or a few tenths percent of manganese as alloying additions [1]. These additions can also improve the corrosion resistance of the alloy. High pressure die-casting (HPDC) is a popular method used in the manufacturing of Al containing Mg alloys. These alloys offer specific advantages for both cast and wrought production processes, with HPDC being the most popular for manufacturing near-net-shape products made from Mg. By using HPDC, Mg alloys can easily be made into intricate and thin-walled castings [1]. However, an unfortunate draw-back of introducing Al in Mg is the low creep resistance observed in such alloy systems at high temperatures. This low creep resistance can be attributed to the presence of Al in the Mg alloy creating the $Mg_{17}Al_{12}$ intermetallic phase in the Mg matrix [13].

These alloys tend to be cheaper and easier to produce and make up roughly 90% of the current global market share in Mg alloys. Common Al-containing Mg alloys include AZ91 (Mg-9wt.%Al-1wt.%Zn), AZ31 (Mg-3wt.%Al-1wt.%Zn), AM60 (Mg-6wt.%Al-0.5wt.%Mn) and AE42 (Mg-4wt.%Al-2wt.%Rare earth elements) with such alloys having moderate tensile properties and corrosion resistance [7].

3.2 Al-free Mg-alloys

Al-free Mg-alloys can be resistant to the loss of room temperature tensile properties at higher temperatures due to the absence of the low melting $Mg_{17}Al_{12}$ eutectic phase. Moreover, it is common for these alloys to contain rare earth element additions which allows for further improvements in creep resistance up to temperatures in excess of 300°C, well above the operating temperature of Al containing Mg alloys. The Al-free alloys nominally achieve additional gains in strength by grain refining with the addition of Zr. Such alloys, containing Zr, are generally more expensive due to material and manufacturing costs – justified on the basis of enhanced alloy performance. Zr additions are incompatible with certain alloying elements such as Al, Si, Mn, Sn and Sb [3] as Zr has a tendency to segregate with elements other than Mg. Common Zr-containing Mg alloys include ZE41 (Mg-4wt.%Zn-1wt.%Rare earth elements), ZK60 (Mg-6wt.%Zn-0.5wt.%Zr) and WE54 (Mg-5wt.%Y-4wt.%Rare earth elements) [7].

4.0 Context for research

Magnesium alloys are presently being used in many applications where weight-reduction is a key concern, such as selected automotive and aerospace applications, along with portable consumer electronics. However, as Mg is one of the most reactive metals (and most reactive of the structural metals), coupled with almost all alloying additions to Mg being more noble metals, it is invariably difficult to achieve an Mg alloy composition with good corrosion performance. While there has been a lot of research into Al-containing Mg-alloys; such research has, however, a) been focused on interpreting corrosion of existing alloys as opposed to systematic research that is design focused, and b) been limited to room-temperature applications as Mg-Al alloys are not suited for high-temperature applications. Thus, there is a need to expand the knowledge and understanding of the corrosion properties of Al-free Mg-alloy systems (i.e. the next generation of creep resistant alloys).

Other research studies into Mg alloys have principally focused on altering alloying composition to improve other properties such as mechanical strength, by using alloying elements to achieve better precipitation, solid-solution hardening and other microstructural improvements [13-18]. The research herein is targeted towards a fundamental and platform understanding for key issues that will be relevant to Al-free Mg alloys and with the hope of translating the findings into future commercial Mg-alloy development and innovation.

This page is intentionally left blank

Chapter 2

Literature review

This page is intentionally left blank

Chapter 2: Literature review

1.0 Current commercial alloys and production processes

Unlike other metal systems, there are many elements that are insoluble in Mg. This greatly limits the possible alloy (chemical) formulations to those systems which show some solubility. Pioneering developments in Mg-alloying technology in the 1960's were able to determine which elements could be alloyed successfully with magnesium in significant quantities [8]. This advance in Mg-alloy technology was initially aimed at improving the mechanical properties through either precipitation hardening and/or solid-solution hardening. The best elements to alloy with Mg depend on several factors; including: the concept that while solid-solution hardening is established by differences in the atomic radii of the elements involved, the effectiveness of precipitation hardening in Mg alloys mainly depends on reduced solubility at low temperatures, the Mg content of any resulting intermetallic phase, and its stability at the application temperature.

Thus, an important characteristic of the Mg-alloy system is that the solubility of alloying elements is strongly influenced by the atomic size of the main alloy constituent [19]. In general, solid solubility decreases with decreasing temperature [1]. While Mg forms intermetallic phases with a number of alloying elements, the stability of these intermetallic phases increases with increasing electronegativity of the selected alloying element [7].

The classification system for Mg alloy formulae is standardised worldwide, with each commercial Mg alloy marked with letters indicating the main alloy elements. Table 2 shows the letters for alloying elements used in commercial alloys. These letter designations are followed by the rounded numbers of each significant alloying element in weight percentage terms. The last letter in the classification number is a general indication of the generation of the alloy design (A, B, C …). In some cases, the letters/number classification can also identify the degree of purity of the given magnesium alloy [7].

Table 2.1 – Mg alloying element abbreviations as defined by ASTM International [7]

Abbreviation letter	Alloying element	Abbreviation letter	Alloying element
A	Aluminium	M	Manganese
B	Bismuth	N	Nickel
C	Copper	P	Lead
D	Cadmium	Q	Silver
E	Rare earths	R	Chromium
F	Iron	S	Silicon
H	Thorium	T	Tin
J	Strontium	W	Yttrium
K	Zirconium	Y	Antimony
L	Lithium	Z	Zinc

Current commercial cast- and wrought-Mg alloys can generally be separated into two main groups:

(1) Alloys containing aluminium as a primary alloying element.

(2) Alloys free of aluminium and containing zirconium, usually up to ~1 wt.%, for the purposes of grain refinement [20].

The Al-containing Mg alloys are often alloyed with Mn to assist with corrosion control and Zn to increase strength (i.e. AM60, AZ31, AZ91) [1]. As mentioned previously, these alloys are known to improve the corrosion resistance and mechanical properties of Mg. Mg-Al alloys are usually die-cast and are heat-treatable (although not together), giving them attractive tensile and mechanical properties. Unfortunately, these particular alloys can have a propensity to develop microporosity, and can show poor ductility if not manufactured properly.

While Mg alloys offer specific advantages for both cast and wrought production processes, a large quantity of alloys in the past couple decades have been high pressure die-cast (HPDC) for several reasons [7, 21], including:

1) Most Mg alloys demonstrate high fluidity, allowing castings to be made of intricate and thin-walled parts [1, 22, 23].

2) Mg alloys have a low specific heat per unit volume compared with that of other metals. This allows Mg castings to cool more quickly, thereby facilitating faster production cycle times and reduced die wear and thermal fatigue [22].

3) The low density of Mg alloys reduces the high internal gate pressures generally expected in the die-casting process to relatively moderate pressures (compared to those required for other die-casting metal systems).

4) Iron, used in steel dies in the HPDC process, has very low solubility in Mg alloys. This reduces the risk of components sticking to the die moulds. Moreover, the steel dies used in HPDC for magnesium alloys are far cheaper than the permanent dies used other metal systems [1, 3]. The notion of Fe in Mg however, is addressed elsewhere in this thesis.

Thus, as a result of magnesium alloys having good casting characteristics, the development of the comparatively low melting-point eutectics at the grain boundaries tends to feed and reduce micro-porosity formation [1].

In the second group of Mg alloys, the role Zr has on grain refinement in magnesium alloy systems make it, in some ways, as significant an aspect of the Mg alloy composition as aluminium is in the first group of alloys [24]. The Zr-containing Mg alloys are also regularly alloyed with Zn and rare earth metals (i.e. ZK60, ZE41) [25].

The Zr-containing Mg alloys display good proof stress and ductility and are mostly resistant to loss of tensile properties upon annealing. These alloys contain rare earth elements to allow for great creep resistance up to temperatures in excess of 300°C. The wrought alloys of both Al- and Zr-containing types of Mg alloys generally demonstrate limited cold formability but are readily able to be hot worked [8].

In general, the Zr-containing Mg alloys, both sand-cast and wrought, have been used in the aircraft and military fields. In commercial applications, the Al-containing Mg alloys are more widely used as they are slightly cheaper. Exceptional machinability is another major characteristic of most Mg alloys, and alloys of both main families are readily weldable by inert-gas-shielded arc processes [8].

Rapid solidification (RS) processing of Mg alloys is another manufacturing technique that is currently being further developed. RS processing in known to result in greatly improved mechanical properties by reducing the size of grains and intermetallic particles in Mg alloys, extending the solid solubility levels of alloying elements, the formation of non-equilibrium meta-stable phases and overall improvement in chemical homogeneity of the alloy. All of these properties are known to be factors in improving the corrosion resistance of magnesium [26-28].

1.1 Manganese and Zirconium additions to Magnesium

Manganese (Mn) and zirconium (Zr) have a number of engineering applications. Mn is primarily used as an alloying element in many steels [29] and provides solid solution strengthening in aluminium alloys [1]. Zr-based alloys are mainly used in heavy-water pressure tubes in nuclear reactors because of their strong neutron absorbing capability and high corrosion resistance [30]. In the context of Mg alloys, Mn and Zr, although considered minor alloying elements, can play an important role in alloy performance despite having a limited solid solubility (C_s) in Mg: Mn ≈ 2.1 wt.% [31] (Figure 2.1) and Zr ≈ 2.7 wt.% (Figure 2.2) [32].

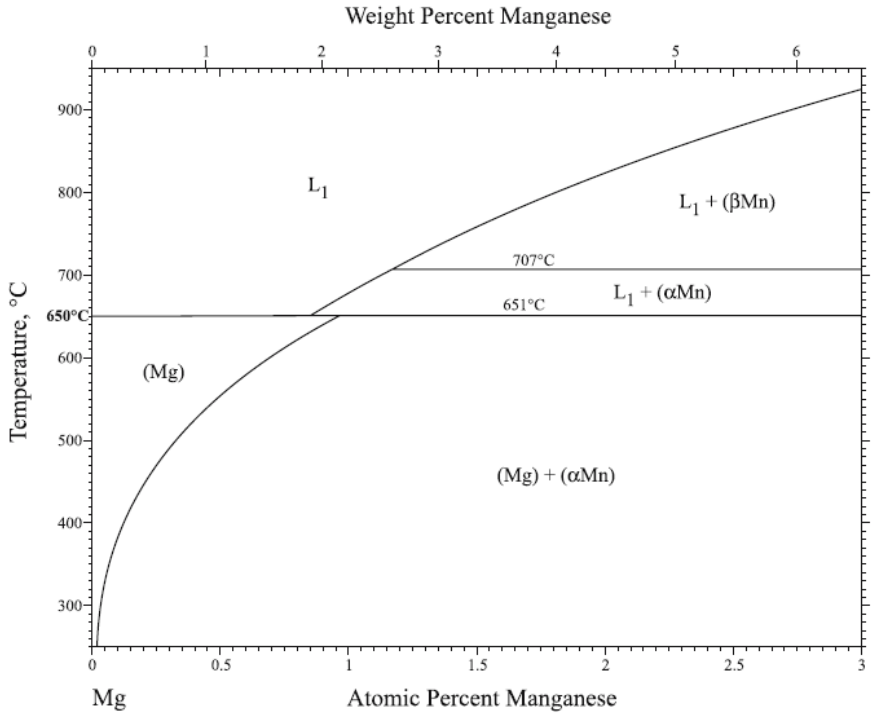

Figure 2.1 - Magnesium-Manganese phase diagram [31]

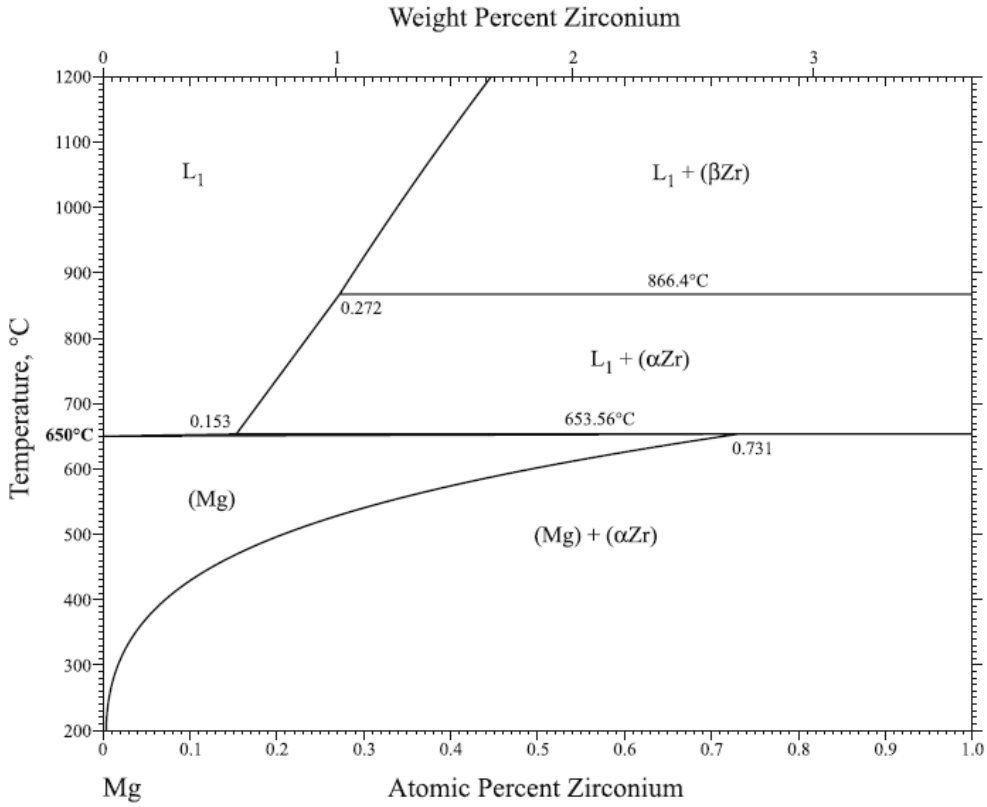

Figure 2.2 - Magnesium-Zirconium phase diagram [32]

1.2 Impurity elements in Magnesium

Iron, nickel, cobalt and copper are impurity elements that are deleterious to the corrosion properties of Mg alloys because they all have very low solid-solubility limits and act as active cathodic sites within the magnesium matrix [8, 33, 34]. Corrosion of Mg alloys could be dramatically improved by controlling the impurity concentrations in the base metal. However, as seen in Figure 2.3, once an impurity is beyond the tolerance limit the corrosion rate begins to increase rapidly.

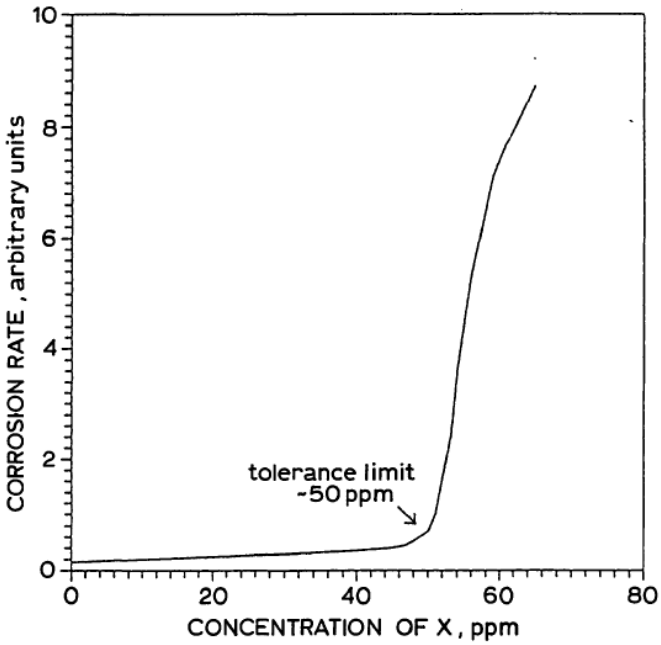

Figure 2.3 – Example of a tolerance limit in magnesium alloy according to Makar [33]. The depicted value does not necessarily correspond to any specific element.

2.0 Corrosion of magnesium

2.1 Electrochemistry of magnesium

Magnesium and its alloys can easily undergo severe corrosion attack in neutral aqueous solutions. The Pourbaix diagram for Mg, as displayed in Figure 2.4, shows the stable species of Mg for changes in pH and electrochemical potential. Mg is unstable in neutral and acidic pH, undergoing dissolution to Mg^{2+}. The Pourbaix diagram also reveals that there is a region at alkaline pH where passivity takes place, in the sense that $Mg(OH)_2$ is stable (insoluble) and capable of forming a protective film on the Mg surface. In the context of an engineering material however, the environmental envelope where Mg is prone to corrosion attack is very large, including most atmospheric conditions.

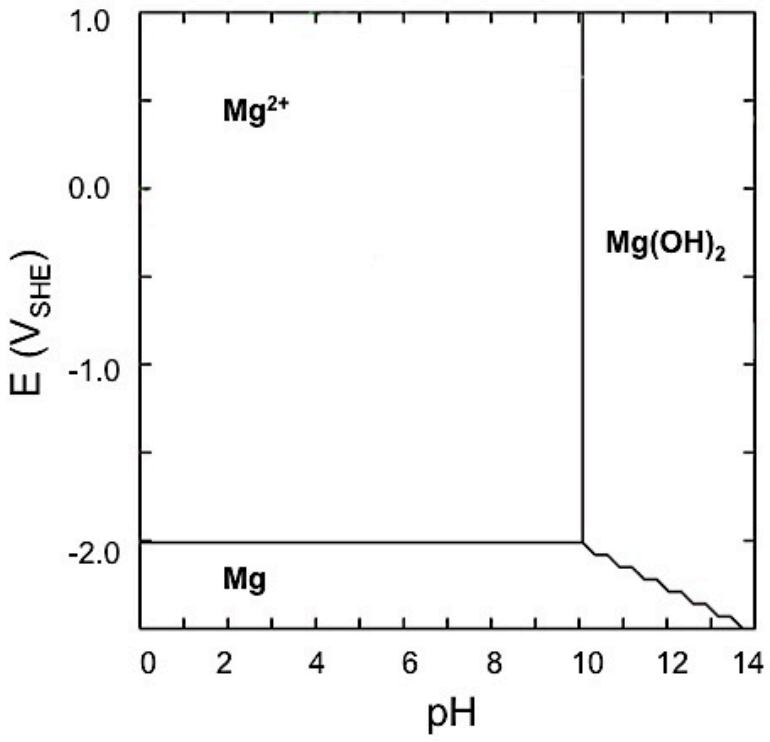

Figure 2.4 – E-pH diagram for the Mg in water H_2O system at 25°C

In atmospheric conditions, Mg corrosion is reduced due to the presence of a mixed oxide/hydroxide film on its surface [36]. However, these films are not a satisfactory protection strategy. In the presence of water, Mg dissolution occurs spontaneously [8, 33, 37]:

$$Mg + 2H_2O \rightarrow Mg(OH)_2 + H_2 \qquad \text{Eqn. 1}$$

This reaction can be further broken down into its anodic and cathodic components:

$$\text{Anodic reaction: } Mg \rightarrow Mg^{2+} + 2e^- \qquad \text{Eqn. 2}$$

$$\text{Cathodic reaction: } 2H^+ + 2e^- \rightarrow H_2 \qquad \text{Eqn. 3}$$

The corrosion rate of an Mg alloy will increase if the rates of one or both of the anodic or cathodic reactions are increased by the addition of alloying elements or second phases (including impurities). Similarly, the corrosion rate will decrease if alloying elements can decrease the relative rates of these reactions.

Other increases in the corrosion rate of Mg are observed to occur from internal micro-galvanic corrosion effects caused by either secondary intermetallic phases or elemental impurities. These impurities nominally act as miniature cathodes (of great efficiency) embedded in the alloy where they can enhance the cathodic reaction given in Eqn. 3 [34]. Such second phases, which are also nominally more noble than Mg, raise the overall electrode potential – which thus promotes further attack of the Mg. In such instances, the principal cathodic reaction remains water reduction (and hence, hydrogen evolution) [38].

It is well known that chloride ions are extremely detrimental to Mg alloys in aqueous solutions [39, 40]. Soluble fluorides on the other hand appear to be chemically inert with Mg alloys [8, 33]. Other ionic salts that are damaging to Mg alloys in an aqueous environment are sulphates and nitrates. A general rule of thumb with Mg alloys is that some sort of corrosion attack can be expected to occur when the alloy is exposed to most electrolytic systems [3, 7, 8].

Electrochemical testing methods are a popular form of 'instant' corrosion testing compared to immersion weight-loss and H_2 collection methods which take long periods of time. In addition, electrochemical methods provide a mechanistic insight regarding anodic and cathodic kinetics.

2.2 Magnesium surface film

The protective film that forms on the Mg-alloy surface is believed to comprise of a three-layered morphology. The inner film layer is made up of thin, porous and hydrated MgO with the outer layer being a thick, less-porous crystalline $Mg(OH)_2$ structure [36, 41, 42]. The intermediate layer is a thin, dense and relatively dehydrated region [42]. Furthermore, films that form on the surface of Mg, protective or semi-protective, can readily dissolve in the presence of ions such as chlorides and sulphates [8].

2.3 Effect of secondary phases on Mg-alloy corrosion behaviour

Despite modern understanding and knowledge of Mg-alloy properties and functionalities, there remain some, greatly overstated, concerns regarding the vulnerability of Mg alloys to corrosion. For more corrosive environments, there are some commercially available surface-coating treatments that offer additional corrosion protection; however, they can not protect the alloy as effectively if there is an alloy defect present, such as an impurity in the microstructure. Early generations of commercial Mg alloys would undergo severe corrosion

attack in moderately damp conditions. There are two main causes for this poor corrosion resistance. The first reason is that the semi-passive hydroxide film that forms on the Mg alloy is not as stable as the oxide films which form on other metal systems, such as aluminium alloys or stainless steels, and consequently does not render the same degree of protection against corrosion. The second reason is due to the internal micro-galvanic corrosion effects from either secondary intermetallic phases or elemental impurities. These intermetallic impurities and the particles that they form in the Mg alloy matrix act as miniature cathodes where they create micro-galvanic cells within the anodic magnesium matrix [8, 33, 40, 43].

When dealing with a two-phase microstructure in a Mg alloy, the overall corrosion rate vary rather dramatically [44], and common secondary phases and impurities in commercial Mg alloys include: $Mg_{17}Al_{12}$, Al_8Mn_5, $Mg_{12}RE$, and Fe, Ni and Cu [38]. Whilst it has been previously posited that if the second phase is finely divided and essentially continuous in contrast to the Mg matrix, then the second phase may be able to act as a corrosion barrier for the Mg matrix [45]. This notion however, as was originally proposed by Song and Atrens [46] is very naïve and wont be considered any further herein, as not only has it not been proven, but: (a) a continuous phase is metallurgically impossible on the basis of common compositions requiring much more solute than present in Mg alloys, and the free energy involved in completely and fully encapsulating grains with a second phase, (b) even if the continuous intermetallic phase occurred, the reaction rates of such intermetallics (namely $Mg_{17}Al_{12}$) in isolation (since the intermetallic wont be presumably be cathodically protected by the matrix) is essentially as high as that of Mg in any case [47].

As such, under open circuit conditions, the corrosion rate for a given Mg alloy is generally controlled by the corrosion reactions observed on the individual constituent phases within that particular alloy. If the Mg alloy contains component phases that are very reactive, then the alloy will usually have low corrosion resistance (nominally observed in the Mg-Ca system [48]). Thus, the reaction mechanisms of pure magnesium are of great importance to researchers, because those reactions provide the foundations for understanding the mechanisms underpinning corrosion for all other Mg alloys [8, 33].

2.4 Modes of corrosion attack observed in Mg alloys

Galvanic corrosion:

Mg alloys are vulnerable to galvanic corrosion. Galvanic corrosion is typically manifest as corrosion of Mg as a result of being connected to a cathode [49]. Cathodes can either be an external cathode, such as another metal in contact with the Mg alloy, or an internal cathode, present as a second phase or impurity particle [50].

During Mg alloy dissolution, stray electrons transfer towards anodic sites to the active cathode in the metal (Figure 2.5). This also leads to hydrogen gas evolution in the case of Mg, as per Eqn. 3. Ionic species present (such as sodium and chloride ions) transport the charge through the electrolyte. The effect of galvanic corrosion between the surrounding magnesium matrix and an inner secondary phase is macroscopically seen as corrosion across the whole alloy surface rather than at a specific location [38]. Galvanic corrosion is an essential issue to overcome since magnesium is so reactive compared to other structural metals (Table 2.2). There are also serious problems when magnesium alloys are joined to all other engineering metals, such as aluminium or steel. Fasteners used in many automotive applications are an example of this very important issue [51].

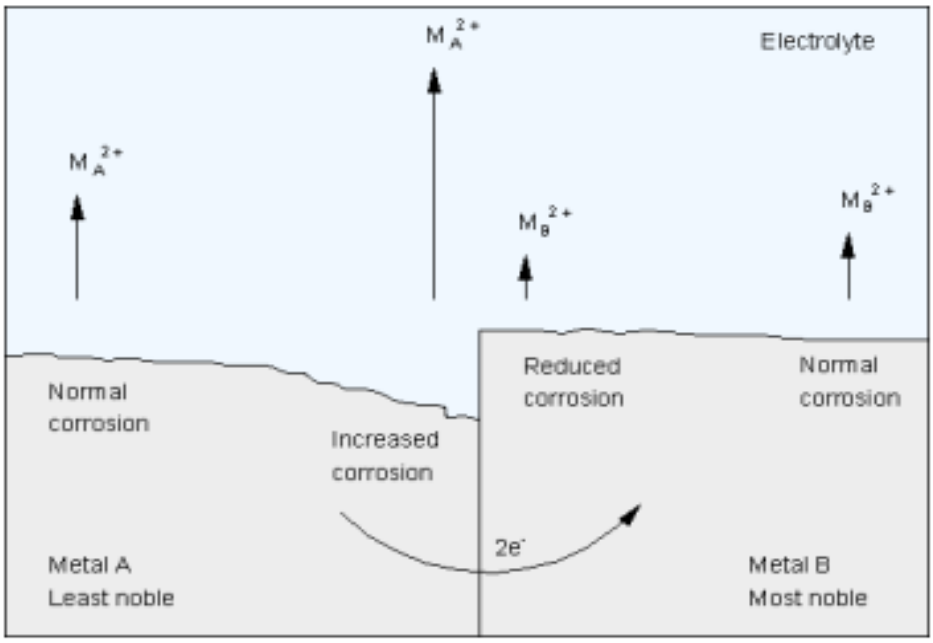

Figure 2.5 – Schematic diagram of electron transfer process during corrosion.

Table 2.2 – Galvanic series of common engineering metals in sea water [52]

Anodic (Most active)
Magnesium
Zinc
Aluminium
Cadmium
Steel
Cast Iron
Lead
Tin
Nickel
Brass
Copper
Titanium
Silver
Gold
Platinum
Cathodic (Least active)

Intergranular corrosion:

Intergranular corrosion generally takes place at the grain boundaries owing to precipitation of secondary phases in the alloy matrix. Corrosion does not have a propensity to propagate along the magnesium grain boundaries, because the grain-boundary phases that form are actively cathodic compared to the interior of the magnesium grain [33, 38]. This can lead to a micro-galvanic coupling effect between the grain boundary and the grain itself [39]. The solute depleted zone in region next to the grain boundary can still be prone to corrosion; the corrosion can then proceed inwards, until it eventually causes the grain itself to become undercut and fall out of the alloy matrix [38].

Localised corrosion:

The localised corrosion of Mg alloys generally starts as pitting on the alloy surface. The pit initiation sites are usually determined by the alloy microstructure for Mg alloys, whilst local attack also occurs upon pure Mg [53, 54]. However, in most cases pits do not extend particularly deep into the alloy surface. This means that the localised corrosion effects seen in Mg alloys tend to be self-limiting, compared to other metal systems where the pit continues

to become more destructive to the alloy and the localised corrosion is accelerated. This self-limiting effect only applies to α-phase Mg alloys. In the case of multi-phase Mg alloys there is a considerable influence from the secondary microstructural phases that changes the overall corrosion behaviour and control mechanisms [51, 53]. The difference between Mg and other engineering alloy systems is that there is considerable alkalisation associated with corrosion, both from the cathodic reaction and the anodic dissolution itself, whereby the Mg^{2+} ion is basic [55]. Another form of localised corrosion is filiform corrosion (also known as 'wormtrack' corrosion). This mode of corrosion occurs when an active corrosion cell moves across the Mg alloy surface. The head of the 'wormtrack' is the anodic end with the tail being cathodic. It has been reported that in Mg alloys the galvanic coupling between the anodic 'wormtrack' head and the cathodic tail leads to hydrogen evolution along the corroded tracks [53]. The mechanism of filiform corrosion on Mg is somewhat different to the commonly accepted mode for coated metals [50, 56] – whereby the filiform corrosion can also be influenced by local pH gradients, so it can be considered a unique form of differential pH corrosion [53].

Crevice corrosion:

Crevice corrosion is reported to not occur within Mg alloys. This is due because magnesium corrosion is fairly insensitive to differences in oxygen concentrations [8]. Although there is a form of corrosion attack that takes place in Mg alloys where narrow gaps or crevices appear, that has a similar appearance to crevice corrosion, it is not a true form of crevice corrosion. This crevice corrosion imitation is caused by retention of moisture in a crevice within the magnesium surface. At this point the moisture is unable to evaporate, leaving water to permit corrosion of the surrounding magnesium in the narrow gap [38].

2.5 Negative difference effect

Mg and its alloys demonstrate an electrochemical phenomenon which is termed the negative difference effect (NDE). The basic laws of electrochemistry classify the net corrosion reaction can be split into a cathodic or anodic reaction. Under normal circumstances, the anodic reaction rate increases if the applied potential is made more anodic. Magnesium, on the other hand, does not follow this rule and appears to contradict the very basics of electrochemical theory with its different hydrogen evolution behaviour. Mg shows experimentally that when the potential is made more anodic, both the magnesium corrosion rate and the hydrogen evolution reaction (HER) rate of the alloy increases, rather than the

latter decreasing as expected [57]. This phenomenon means that the total amount of hydrogen generated increases with an increasing applied anodic current.

The critical characteristic of the NDE is that the cathodic HER rate for Mg increases with a corresponding increase in the electrochemical potential. For many years, researchers have tried to describe the cause of the NDE phenomenon in magnesium alloys by means of electrochemical reaction mechanisms. One proposed mechanism was the creation of unipositive Mg ions [51]; although, to date no one has proven the existence of Mg^{+}. However, more recent work has revealed that there is in fact no unipositive Mg or a need to invoke its presence [54, 58], particularly since the HER has been shown to occur on 'cathodic' sites which increase in intensity with anodic polarisation (as opposed to the reaction of Mg^{+} with water) [55].

3.0 Alloying effects of elements in magnesium

Each element has a unique impact on the properties of Mg and Mg alloys. One of the most significant impacts of these alloying elements is on the corrosion rate of magnesium (Figure 2.6). The corrosion rate of Mg alloys containing different alloying elements varies greatly because of differences in solid solubility and electrochemical potentials of those elements with respect to Mg. As such, certain elements may be added in greater quantities to magnesium without having a deleterious effect on the corrosion properties, while even smaller amounts of other elements can be very detrimental.

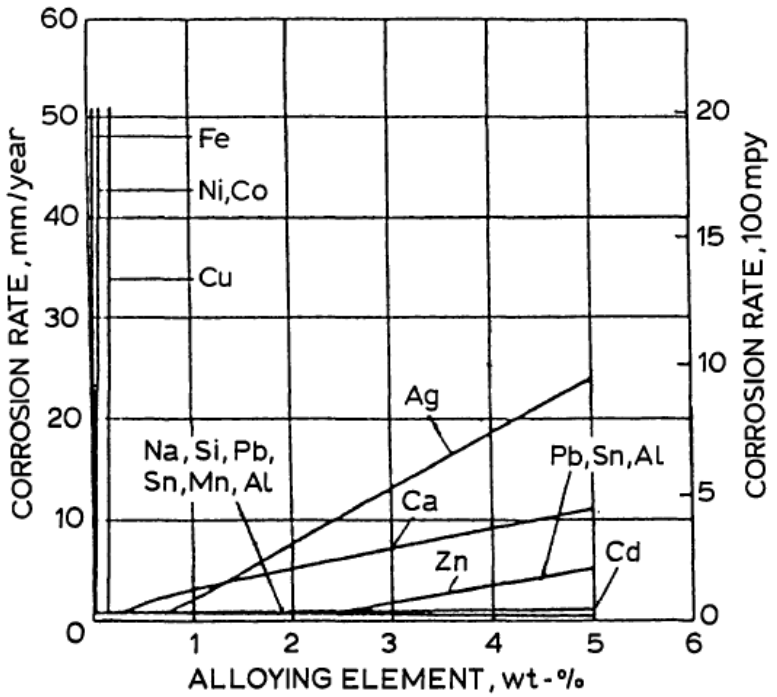

Figure 2.6 – Effects of alloying elements on the corrosion of magnesium in a 3% NaCl solution [33]

As magnesium is one of the most reactive engineering metals, alloying elements that are added to Mg nominally form more noble intermetallic phases in the microstructure [47]. These intermetallic phases have different electrochemical properties, most of them supporting the cathodic reaction at higher rates than Mg. These phases can then influence the corrosion reaction kinetics of the Mg alloys. The characteristic potentials and listing of such intermetallics is presented in Table 4. The potential difference between Mg and the compounds / metals in Table 4 indicates the relative sign of the galvanic interaction (not the rate), and is therefore a useful first order indication of the relative role (anode or cathode) that the compound will take when exposed at open circuit.

Table 2.3 - Electrochemical potentials of common alloying elements, intermetallic phases and impurity elements seen in Mg alloys [47]

Alloy system	Intermetallic phase	Corrosion potential (V_{SCE})
Mg-Ca	Mg_2Ca	-1.75
Mg	N/A	-1.65
Mg-Y	$Mg_{24}Y_5$	-1.60
Mg-La	$Mg_{12}La$	-1.60
Mg-Nd	Mg_3Nd	-1.55
Mg-Si	Mg_2Si	-1.54
Mg-Ce	$Mg_{12}Ce$	-1.50
Mg-Al	$Mg_{17}Al_{12}$	-1.35
Mn	N/A	-1.28
Mg-Zn	$MgZn_2$	-1.03
Al-Mg	Mg_2Al_3	-1.01
Fe	N/A	-0.60
Ni	N/A	-0.22
Cu	N/A	-0.15

3.1 Detrimental elements with low solubilities in magnesium

There are a significant number of elements that are detrimental to Mg corrosion performance and can contaminate Mg-alloy compositions when they are not added intentionally. These elements are termed impurity elements. Studies have indicated that one of the critical factors in the corrosion of Mg alloys is the metal purity [8, 34, 43]. It is known that some transition metals with a low hydrogen overvoltage, such as Ni, Fe, Co and Cu, cause the formation of efficient cathodes when included in Mg alloys and can cause severe galvanic corrosion. The corrosion rate is seen to be lower, up until a tolerance limit where the corrosion rate is accelerated substantially, sometimes by a factor of two orders of magnitude [45]. Other metals that combine an active corrosion potential with a high hydrogen overpotential, such as Al, Zn, Cd and Sn, are much less damaging than Ni, Fe, Co and Cu [33], and can be beneficial when added to Mg alloys in the right proportions.

There are currently two hypotheses as to how impurity elements such as Fe, Ni, Cu and Co can be detrimental when present in Mg in sufficient levels: phase precipitation and surface deposition [45]. Both the phase precipitation and surface deposition theories assume that efficient cathodic sites are produced when the impurities are above the tolerance limit, and both theories presume that these cathodes have a composition rich (if not pure) in the given impurity element. The critical distinction between the two is that the phase precipitation hypothesis relates to the precipitation of a new phase forming inside the Mg alloy, whereas the surface deposition theory relates to the deposition of cathodes on the Mg alloy surface [45].

Current commercial processing techniques work by adding a small amount of some harmless or readily-removable compounds which render the undesirable impurity element insoluble in the magnesium melt so that it can be separated by particle settling on the bottom of holding crucibles. Several possible mechanisms are known to perform this operation:

(a) The added compound (X) can reduce the solubility of the impurity (I) in magnesium, so that the pure (I) precipitates and settles out of the melt.
(b) An insoluble compound (XI) can be formed and settles out of the melt.
(c) (I) may be precipitated out in a fine state of division where it can act as nuclei on which primary crystals of (MgX) may form and thereby permit its removal by settling.
(d) Particles of compound (XY), which is insoluble in the magnesium melt, may be deliberately added to the melt to form nuclei on which (I) will precipitate out [8].

An example of how a high Fe impurity concentration in Mg alloys can be reduced considerably in the magnesium melt prior to casting is by the addition of compounds such as B_2O_3, $MnCl_2$ or TiO_2. These reduce the Fe concentration in the Mg melt and allowing it to settle out at the bottom of the holding vessel as an insoluble sludge with a high Fe content [59, 60].

3.1.1 Iron impurities

Iron is the most common impurity element encountered in Mg alloys. Fe has a very small solubility limit in magnesium, 0.018 wt.% (Figure 2.7) [61]. The corrosion behaviour of many commercial Mg alloys is mainly dominated by their Fe content, when Fe is above the corrosion tolerance limit [2, 34, 62]. When Fe contents are below the tolerance limit for a

given Mg-alloy composition, other factors influence the corrosion behaviour of Mg alloys, such as chemical composition and microstructure [45].

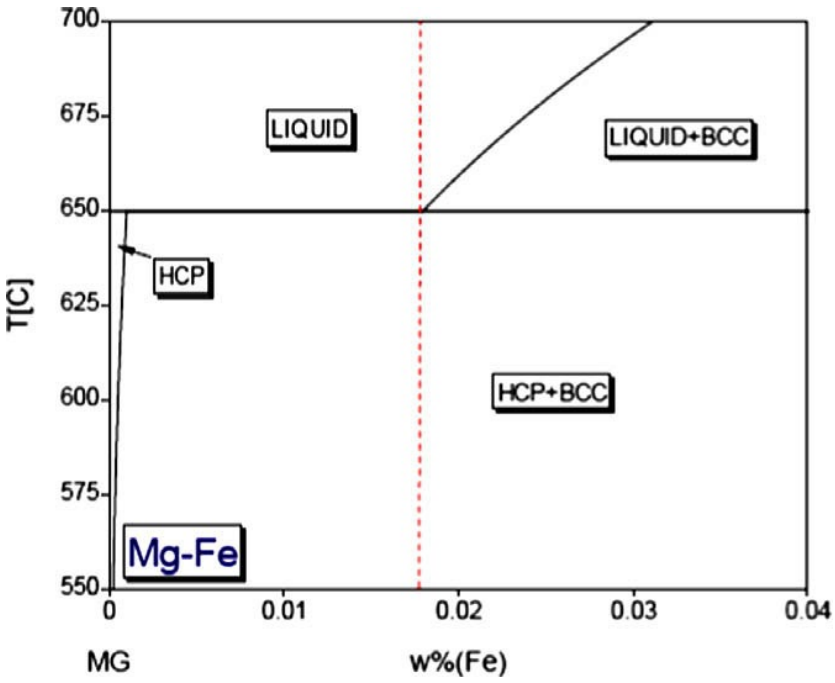

Figure 2.7 – Mg-Fe binary phase diagram calculated with the PANDAT phase diagram calculation (CALPHAD) program [63]. It is noted that the lines / data in this plot have not been experimentally validated by the authors.

Cooling of an Mg alloy containing an Fe content above the tolerance limit is predicted to cause the solidification, from the melt, of a separate body-centred cubic (BCC) iron-rich phase [45, 61]. It is emphasised that this is not an intermetallic phase consisting of Fe and Mg, but essentially pure Fe in pure Mg [64]. This phase is able to act as an efficient cathode, thereby accelerating the corrosion of the alloy by micro-galvanic coupling with the magnesium matrix [43, 45, 62]. Additionally, when pure Fe exists in the matrix, the magnitude of the potential difference of micro-galvanic coupling with the Mg matrix can be as great as 1V in certain circumstances, meaning that the anodic Mg is polarised such that anodic dissolution is enhanced [45].

For an Fe content below the tolerance limit, the calculated phase diagram predicts that upon solidification, the liquid Mg alloy undergoes a eutectic reaction at 650°C to form an α-Mg

matrix containing a small amount of Fe in solid solution as well as the BCC phase (Figure 2.6) [63]. However, in reality, the region for the two phases of liquid Mg and α-Mg is exceptionally small.

This effect is easily demonstrated with current commercial alloys. A clear example is the commercial alloy AZ91C, which generally has a high Fe impurity content (~160ppm [65]) that causes high corrosion rates where the Fe content dominates the corrosion behaviour, overwhelming the influence of the microstructure [66]. The more recent AZ91E Mg alloy, on the other hand, is a high purity alloy with an Fe content well below the tolerance limit (~20ppm [65]). In AZ91E, which has the same overall alloy composition as AZ91C, the corrosion rate is clearly influenced by the alloy microstructure instead of the Fe content [45].

There is a vast number of conflicting values published regarding the tolerance limit of Fe in Mg alloys. It is often found that other alloying elements in Mg alloys can affect the Fe tolerance level. One example is that the Fe tolerance limit decreases with increasing Al content [8].

When even a few weight percent of Al is added to a Mg alloy, the tolerance limit for Fe can decrease from roughly 170 ppm to as little as a few ppm (Figure 2.8). At around 9 wt.% aluminium, the tolerance limit for Fe is reported to be about 20 ppm [40]. This is due to the formation of the Al-Fe phase, Al_3Fe, which has an even more deleterious effect as it is even more active than discrete Fe particles [67]. However, to further complicate matters, the Fe tolerance limit can continue to be influenced by the presence of ternary elements. The Fe tolerance limit for Mg-Al alloys can be radically improved by the addition of Mn [2].

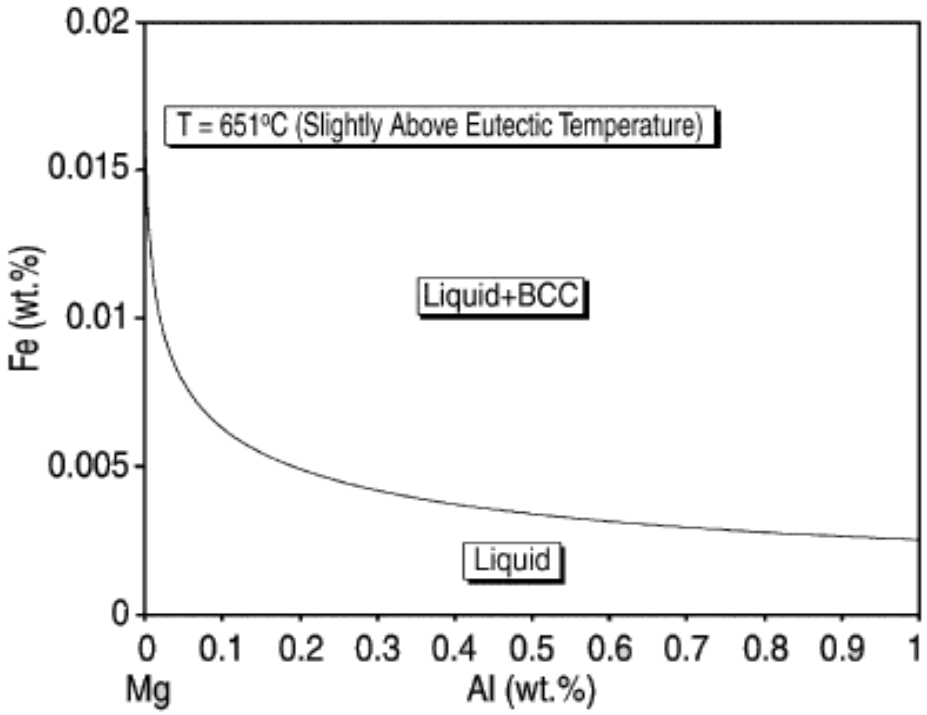

Figure 2.8 – Iron solubility levels in Mg with increasing Al content calculated with the PANDAT phase diagram calculation (CALPHAD) program [45]

Because other (ternary, quaternary, etc.) elements can influence the Fe tolerance limit, there is no concrete agreement in published studies on an exact tolerance limit for Fe across a range of Mg alloys. It was the seminal work by Boyer and McNulty, who initially began researching the tolerance limits of Fe in the late 1920's and early 1940's, which identified how Fe impurities can be targeted and rendered less detrimental in Mg [2, 34]. Their work and later studies that also produced and tested a series of Mg alloys that contained Fe on the exact tolerance limit of Fe in Mg usually range between 160 ppm and 180 ppm [2, 8, 34, 43]. This means there is no discreet tolerance limit, but rather a 'zone' where, depending on the alloy formula and purity, the tolerance limit for Fe may lie. As the need for understanding the microstructural characteristics of Mg alloys is becoming increasingly more important, it is also critical to understand the behaviour of alloying elements on Fe impurities in Mg in order to use Mg alloys most effectively [68].

Steel containers and holding vessels are generally used for melting magnesium and its alloys because Fe of the low solubility of Fe in Mg. However, at the high temperatures at which magnesium melts are prepared, even the small amount of Fe that may be picked up by Mg

from the container walls can remarkably increase the corrosion of the alloys [61]. Under normal commercial operating circumstances the Mn content in the alloy melt is used to suppress the pick-up to ensure that levels of Fe are within the alloy specification limits. However, when problems are encountered with the casting equipment, resulting in long delays, excessive Fe pick-up can be observed. In addition to the issues from the operating equipment, the melt processing temperature is also an important factor in the pick-up of Fe impurities. The higher the processing temperatures employed, the higher the rate of Fe pick-up and solubility of Fe particles [3]. This effect can be seen in Figure 6; as processing temperatures increase the liquidus line shifts to higher Fe contents, allowing more Fe to be dissolved. Thus, Fe contamination is very hard to avoid with current commercial practices. However, it is possible to manage such problems through the overall Mg alloy compositional design and pre-casting alloy processing.

3.1.2 Nickel impurities

Nickel, as an impurity, is more harmful than Fe in both pure magnesium and Mg alloys. This is not only because Ni has a far lower tolerance limit in Mg alloys [33], but the undesirable effect that Ni has on the corrosion reaction kinetics of magnesium is not suppressed by the presence of Mn in the alloy in the same manner that reduces the influence of Fe impurities [8], and that Ni has a high exchanged current density [47].

The tolerance limit for Ni in Mg alloys has been reported to be as low as 5 ppm [1]. The low solid solubility of Ni in magnesium creates a separate nickel-rich phase when alloyed at noticeable levels [8]. However, the tolerance limit for Ni impurities has been found to be dependant on the casting form. Rapid-solidification processing of Mg alloys can also raise the Ni tolerance limit appreciably.

Ni contamination of Mg alloys generally occurs when Ni-bearing steels are used in the machinery intended for Mg-alloy manufacture. The 400 series chrome steels and most carbon steels are often used when dealing with magnesium melts, the 300 series alloy steels, which contain nickel, are usually avoided [3].

3.1.3 Copper impurities

Copper has both negative and positive effects when used as an alloying element in Mg alloys. A relatively small amount of Cu can have a beneficial effect on the creep strength of magnesium castings, however, it strongly accelerates the corrosion rate [3, 8, 69]. With

increasing Cu content in Mg, the Cu particles act as local cathodes that create micro-galvanic couples and the ensuing accelerated corrosion of the Mg matrix [38]. This is because the inherent properties of Cu make it a very efficient cathode, and hence even traces of Cu can rapidly enhance the cathodic reaction kinetics (as seen in Eqn. 3). Recent work has shown that when as little as 0.1 wt.% Cu is present in the commercial alloy AZ91 there is an increase in the measured corrosion current [70].

There is quite some conjecture on the corrosion tolerance limit for Cu in Mg alloys. The reported tolerance limit varies from 1000 ppm to 1300 ppm depending on the specific source [1, 40]. In any case, for corrosion resistant magnesium-alloy design, copper impurities should be minimised. The most common source of Cu contamination found in Mg alloys is unwanted contaminants in the foundries for Al alloys, since aluminium is a common alloying element used in casting Mg alloys. To minimise such potential problems, high-purity grade Al is specifically used to alloy with magnesium melts and machining components that contain Cu (such as brass) are kept to a minimum [3].

3.1.4 Cobalt impurities

Cobalt, like Fe, Ni and Cu, also has strong adverse effects on the corrosion resistance of Mg alloys [8, 33]. However, Co is not an impurity element commonly observed in Mg alloys. It can easily be avoided in the casting and manufacturing process if the machining equipment does not contain any Cobalt.

3.2 Elements with moderate solubilities in magnesium

3.2.1 Al additions

Adding Al to Mg alloys can be both beneficial and detrimental to magnesium corrosion. A prime example of this is the distinction between the corrosion behaviour of the alloys AM50 with approximately 5 wt.% Al and AM100 with approximately 10 wt.% Al [71]. The Al level in the AM50 alloy creates a complimentary microstructure of β-phase particles around the α-Mg grains. However, in the AM100 alloy, the higher Al levels create microstructural features that form adverse distributions of β-$Mg_{17}Al_{12}$ phase particles around the α-Mg grains. This causes the β-phase to start accelerating the corrosion of the Mg alloy via micro-galvanic coupling, generating large amounts of hydrogen as the α-phase in the alloy is dissolved [71].

This effect is observed in other Al-containing Mg alloys, such as as-cast AZ91, where the β-$Mg_{17}Al_{12}$ phase is mainly distributed along the Mg grain boundaries. The β-$Mg_{17}Al_{12}$ phase is formed concurrently in two forms: continuous precipitation (of isolated $Mg_{17}Al_{12}$ particles) and discontinuous precipitation. It is the discontinuous growth of the lamellar β-$Mg_{17}Al_{12}$ that is mainly distributed along the grain boundaries [72, 73]. Thus, depending on the microstructure for a given alloy, the corrosion rate of an Mg alloy of the AZ series can either possess appreciably superior or far worse corrosion resistance than pure magnesium [45, 74].

3.2.2 Zn additions

Zinc is a common alloying addition in Mg alloys, being added to both Al- and Zr-containing Mg alloys and also both cast and wrought Mg alloys [75]. While Zn is an important addition to Mg alloys, it is rarely added in large quantities. Zn has a solid solubility of 6.2 wt.% in Mg at the eutectic temperature [3]. Addition of Zn to Mg-Al alloys leads to strengthening; however, excess Zn can cause hot cracking during the solidification of the Mg alloy [1]. Moreover, Zr additions of up to 11 wt.% have been shown to have little effect on the current density of Mg, indicating that up to these levels, Zn is not detrimental to the corrosion performance of Mg [76].

3.2.3 Ca additions

Calcium is added to the AZ series of Mg alloys to improve their corrosion performance. Addition of low levels of calcium is known to decrease the oxidation rates of AZ Mg alloys by improving the protective nature of the oxide film that forms on the alloy surface through the incorporation of Ca-containing compounds [77]. Moreover, Ca additions can refine the grains and eutectic structure in the alloy microstructure, thereby strengthening the grain boundaries and leading to improvements in the overall tensile strength, creep strength and plasticity [78-80].

3.2.4 Mn additions

Mn is a common alloying addition to Mg alloys. Mn is added to improve not only the mechanical properties of Mg, to increase extrudability (i.e. M1, ME10), but also for corrosion control and mitigation [3, 17, 75, 81, 82]. One of the greatest discoveries contributing towards increasing the corrosion resistance of Mg alloys was the revelation that small amounts of Mn were able to reduce the adverse effect of Fe impurities on the corrosion of Mg-Al alloys [1, 8]. As such, Mn is now predominantly added to reduce the corrosion of Mg

alloys by reducing the impact of Fe impurities. When Mn is added to Al-containing Mg alloys, it combines with Al to form the Al_8Mn_5 phase (Figure 2.9) [83-86], in which Fe can replace Mn in the intermetallic phase and hence be removed from the Mg melt as $Al_8(Mn,Fe)_5$ [8]. Nominally, the $Al_8(Mn,Fe)_5$ particles either settle to the bottom of the crucible during melting and are not included in the final castings, or if they are embedded in the casting during solidification, are rendered less detrimental because of their reduced electrochemical potential [87].

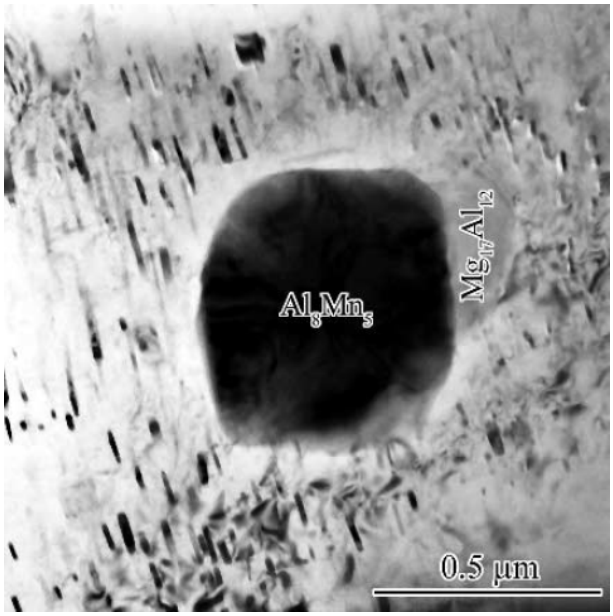

Figure 2.9 – Electron micrograph of Al_8Mn_5 intermetallic phase in Mg alloy AM50 [85]

As mentioned previously, the electrochemical potential difference between pure Mg and Fe is comparatively large at ~0.95V [47]. This leads to severe localised microgalvanic couples around Fe impurity particles, which can easily promote corrosion under immersion/exposure conditions. In contrast, when Mn is added as an alloying addition and the Fe present is incorporated in the $Al_8(Mn,Fe)_5$ intermetallic phase, the effect of the Fe impurity on the corrosion rate is vastly reduced as the electrochemical potential difference between Mg and $Al_8(Mn,Fe)_5$ is much smaller than that between pure Mg and Fe [88]. When considering the mechanism of how Mn reduces the corrosion rate in Mg-Al alloys caused by Fe impurities through incorporating Fe into the $Al_8(Mn,Fe)_5$ phase, older studies proposed that such a mechanism would only work for Al-containing Mg alloys. However, with the need to develop Mg alloys for higher operating temperatures (temperatures which are somewhat limited in Al-containing Mg alloys because of the precipitation of the $Mg_{17}Al_{12}$ phase, as seen in Figure 2.10), recent studies have expanded this area of research to include developing

Al-free Mg alloys that still contain Mn and can have enhanced creep strength at high temperatures [14, 15].

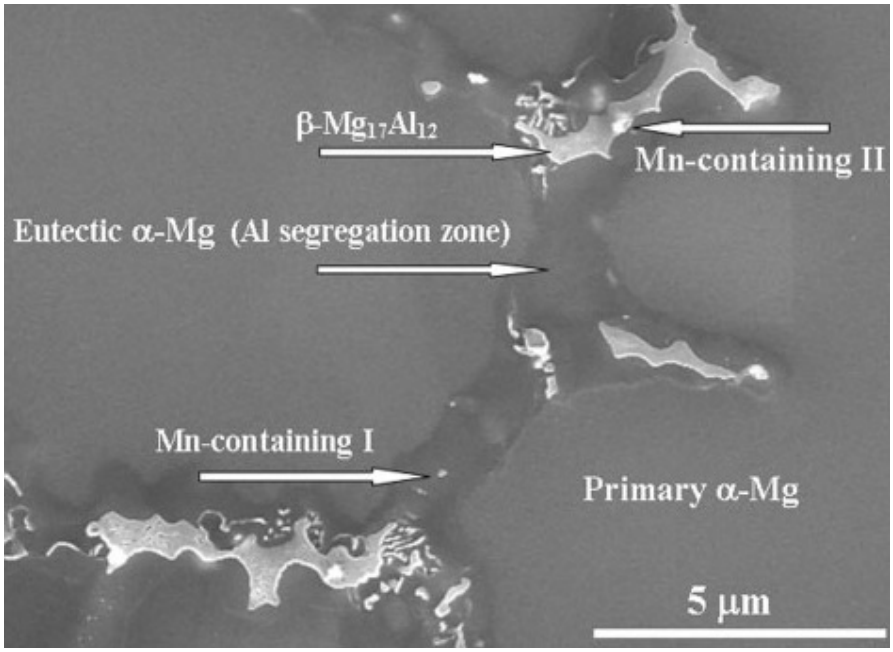

Figure 2.10 - Electron micrograph of the $Mg_{17}Al_{12}$ beta phase in a AM50 Mg alloy [89]

Early research into the effect of Mn on the corrosion of magnesium reported that large Mn alloying additions increased the corrosion rate of Mg alloys [2]. This increase in the corrosion rate was attributed to two factors. The first was an increase in the number of inclusions on the Mg-alloy surface. This caused a weakness in the adherence of the semi-protective surface film to the alloy surface. The second was formation of Mn particles embedded in the Mg matrix at higher Mn-alloying levels. These particles acted as cathodes in micro-galvanic cells and increased the consumption of the Mg matrix [90].

It is important to note that in the Mg-Mn binary system there are no intermetallic phases that form and that the Mn particles that are present in the Mg-alloy matrix are essentially pure Mn particles [31, 81]. Research into the dual component system has developed the binary phase diagram of Mg and Mn (Figure 2.1) which shows that the Mn particles that form in the Mg-Mn binary alloy are insoluble inclusions.

The latest research on the corrosion of Al-free Mg-alloys, which also contain Mn proposes that Mn is still able to suppress the deleterious effect of Fe impurities, despite the absence of Al [91]. When Al is not present, the mechanism by which Mn counteracts the damaging effects of Fe (which previously was only hypothesised and remains un-validated) is that Mn

is capable of encapsulating the Fe particles and separating them from direct contact with the magnesium matrix [92-95]. This would theoretically reduce the overall cathodic reaction kinetics imposed on the Mg-alloy system retarding the galvanic-coupling that takes place when the Fe particles are in direct contact with the Mg matrix and thereby reducing the corrosion rate of the alloy. However, the targeted use of Mn in this manner has two main disadvantages. Firstly, the majority of the Mn added to the alloy is usually found within the grains themselves rather than at the boundaries [24] and, secondly, depending on when Fe comes out of the Mg melt, that the precise ratio of Fe to Mn necessary to counteract the negative effect of Fe on the corrosion resistance is difficult to achieve [60]. Thus, the precise levels of Mn addition that are required to counteract the negative effects of Fe impurities, of a specific concentration, in a Mg alloy and the subsequent changes in the electrochemical reaction kinetics of the Mg matrix are still somewhat unknown.

Another study has shown that when Mn is the only alloying addition in Mg, the open circuit potential (OCP) initially moves to less noble values with the addition of low levels of Mn (reportedly up to 0.18wt.%) [90]. This initial decrease in the corrosion rate with the addition of Mn was attributed to two main factors. The mode of corrosion attack across the Mg alloy surface became more uniform with less overall pitting and the nature and the stability of the $Mg(OH)_2$ film formed on the surface of the Mg alloy changed to provide greater protection. Higher Mn levels then cause the OCP to shift towards the less-negative direction, which is interpreted as a reduction in the cathodic reaction kinetics. Still, the higher Mn levels lead to a greater number of inclusions on the alloy surface which have been proposed to be able to weaken the adherence of the surface film and increase the corrosion rate [90].

3.2.5 Zr additions

Zirconium is well known for its potent grain refining ability in Mg alloys (Figure 2.11) [8, 20, 24, 96-99]. Mg has a Hall-Petch coefficient of around 280-320 MPa/μm and the addition of Zr allows the subsequent reduction in the Mg alloy grain size to greatly increase the tensile strength, improves casting quality and allow better control of the alloy texture [100-102]. Aside from the gain in mechanical properties that comes from having a smaller average grain size, there can be benefits to the corrosion properties as well. As the intermetallics or particles on the grain boundary can act as a physical corrosion barrier, smaller average grain sizes create more grain boundaries in total to prevent corrosion from more easily spreading across the alloy surface. There have been published studies which confirm that after Zr is

added to Mg alloys to refine the grain size, the corrosion resistance is noticeably enhanced [24].

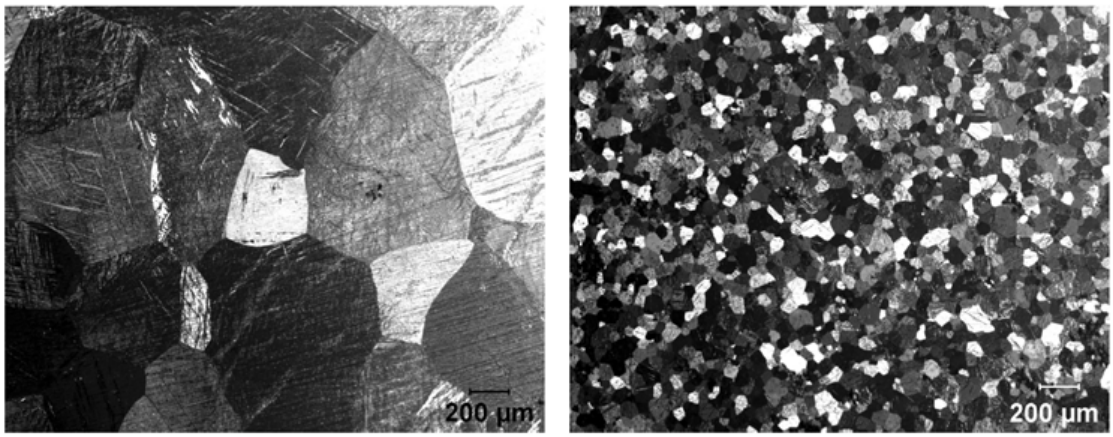

Figure 2.11 – (A) Microstructure and grain size of Mg alloy without Zr and (B) Microstructure and grain size of Mg alloy with 1 wt.% Zr [103]

Zr additions in Mg do not lead to the formation of a Mg-Zr intermetallic phase [104]. The Mg-Zr system (Figure 2.2) satisfies two key requirements of a grain refining system: the presence of potent nucleant sites and a solute with a high growth restriction factor. Moreover, Zr will segregate into the α-Mg because it is a peritectic system. The resultant microstructure consists of a reasonably homogeneous distribution of fine grains [96].

This important feature has allowed Zr to be included in commercially available alloys such as ZE41, WE43 and ZK60. Moreover, the significant interest in Mg-alloy development has seen newer Mg alloys, such as Elektron 21 and AM-SC1, being specifically developed to incorporate Zr as one of the main alloying elements for this ability [105-109]. Zr-containing Mg alloys are also being explored and tested for use in biomedical applications [110].

The addition of Zr to Mg alloys has been reported to contribute to decreasing the corrosion rate of Mg alloys [20, 24, 96, 97]. However, these studies have usually focused on specific commercial Mg alloys. The Zr in these commercial alloys is usually considered a minor addition and the alloys include several other alloying elements or impurities in the Mg matrix. The Zr present is believed to react with oxygen and become incorporated in the semi-protective surface film layers of the Mg alloy. This would increase the stability of the oxide films formed in aqueous solutions and increase the corrosion resistance of the Mg alloys [111].

As common impurities found in Mg alloys, such as Fe, are known to be the cause of deleterious micro-galvanic couples with the Mg matrix, Zr is added to 'scavenge' Fe particles in the Mg melt [20, 24, 61, 96, 97] and combine to form an insoluble phase with nominal composition Fe_2Zr [112]. Because of their large difference in density with that of Mg, Fe_2Zr particles usually settle to the bottom of the melting vessel prior to casting. This effect of forming the Fe_2Zr phase is so strong that when Zr is introduced into a Mg alloy melt, the Zr will first remove a large amount of the Fe impurity from the melt before any grain refining takes place [20]. As such, adding Zr to Mg can be considered to render a Mg alloy to be of higher purity [24, 113], as these alloys generally contain <50 ppm Fe [20]. This low level of Fe impurity in an Mg alloy is below the tolerance limit required to cause a rapid acceleration of the corrosion rate [43, 45].

There are a number of negative effects that Zr particles have on Mg, and the distribution of Zr in the Mg matrix can also influence the corrosion reaction kinetics [38, 114, 115]. Excess amounts of Zr added to Mg lead to the formation of elemental Zr particles embedded in the matrix. This is detrimental for the corrosion properties as these Zr particles can easily act as cathodes in micro-galvanic couples and increase the corrosion rates appreciably [38]. Multiple studies have confirmed that these elemental Zr particles act as micro-galvanic sites with the Mg alloy matrix under open circuit exposure conditions [115, 116]. This micro-galvanic coupling effect is attributed to the difference in electrochemical potential between Zr and Mg. Thus, the Zr particle – Mg matrix interface sites also often experience circumferential pitting attack [115]. Moreover, these elemental Zr particles have also been reported to disrupt the formation of the protective film on the Mg alloy surface [115].

When Zr particles are not homogeneously dispersed throughout the Mg-alloy matrix the corrosion rate increases compared to a situation with a more even distribution of smaller Zr particles [114]. Deep corrosion attack often occurs around these Zr-rich particles in an Mg alloy. The Zr-rich interaction zones become the next most favourable sites for corrosion to occur. In these areas small pits begin to form, followed by severe corrosion [115]. Recently published research has shown that Zr alone as an alloying addition is itself deleterious to the corrosion of Mg, based on its ability to 'activate' the anodic reaction [117]. These conflicting views of the effect of Zr in Mg only increase the value of systematic work focused on elucidating its true effect on the corrosion properties of Mg.

3.2.6 Mn and Zr additions together

It is known that both Zr and Mn do not form any intermetallics with Mg and that, in Mg, Zr combines with Mn to form Mn_2Zr (Figure 2.12). One study has suggested that not only are Fe impurities soluble in the Mn-Zr intermetallic phase, but that Zr, Mn and Fe can all combine to form a new intermetallic phase in the Mg melt [98]. However, there is very little data available on the tolerable levels of Mn and Zr alloying additions present concurrently in Al-free Mg alloys and the distinctive effects these elements have (when added together) on the corrosion rate of Mg.

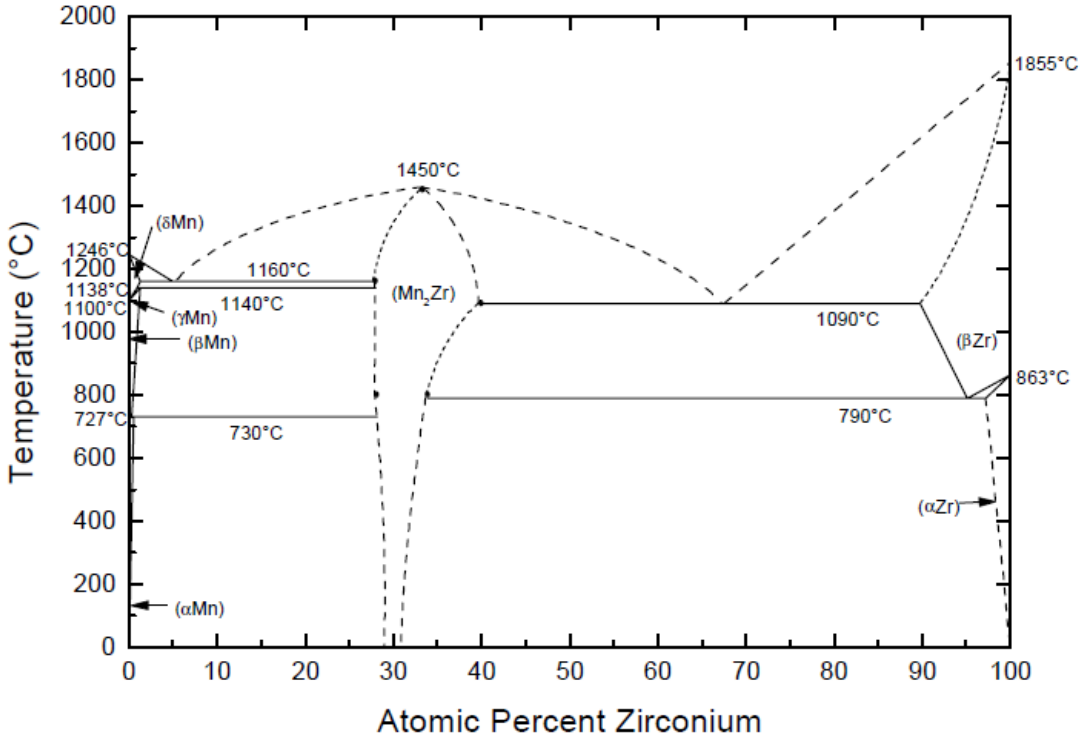

Figure 2.12 – Manganese-Zirconium phase diagram [118]

3.2.7 Rare earth elements

Rare earth metals (RE), such as cerium, lanthanum, neodymium, are being added as alloying elements to both Al-containing and Al-free Mg alloys [119]. RE additions are known to alter the existing microstructure when added to Al-rich Mg-alloys [120]. Improved corrosion resistance can be attributed to the formation of Al-RE intermetallic compounds within the Mg-alloy matrix and inclusion of RE ions in the protective alloy surface film [121, 122]. However, there has been a limited amount of research reported on the corrosion properties of

RE-containing Mg-alloys in the absence of Al; the majority of studies have focused on commercial Mg alloys that do contain Al.

An important effect that RE elements are purported to have, which improves the corrosion resistance of Mg alloys, is the 'scavenger effect' [123]. This is where the RE additions form intermetallic compounds with impurity elements present in the Mg alloy melt. This can remove their harmful effects of these impurities and thereby increase the corrosion resistance of a given Mg alloy. Another effect of RE additions is the inclusion of RE atoms into the surface oxide film, improving the protective nature of the surface film and enhancing the corrosion resistance of the alloy [122, 124, 125].

RE additions in Mg-RE binary alloys have been reported to increase the corrosion resistance of the Mg alloys through changes in the structure of the alloys when different amounts of various alloying additions are added [122]. This assertion however has not only not been reproduced, but is at odds with every other study of Mg-RE alloys. This magnesium-RE dual-phase system will create a network of microgalvanic couples between the Mg-alloy matrix and intermetallics formed by the RE alloying elements; the network accelerates the nominal corrosion rates of the magnesium [120]. As it can be seen in Figure 2.13, increasing RE content in the Mg alloy system will lead to a systematic increase in the corrosion rate.

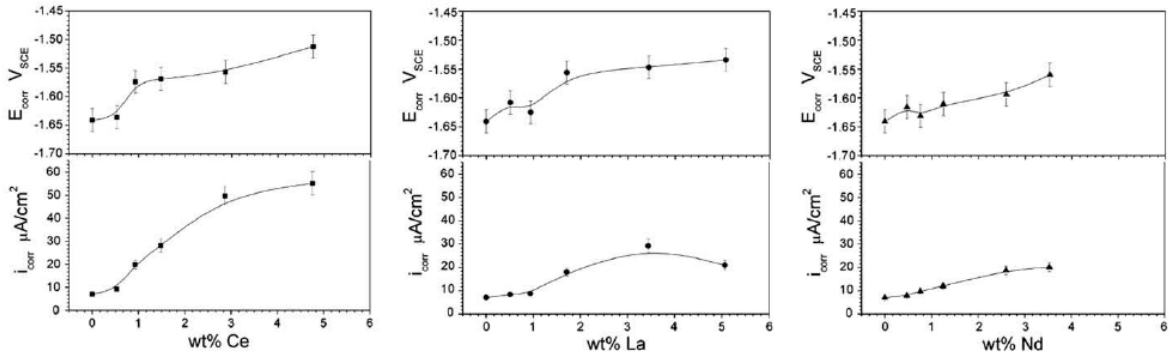

Figure 2.13 – Potentiodynamic E_{corr} and i_{corr} polarisation data for the corrosion rates of binary Mg-RE (Lanthanum, Cerium and Neodymium) alloys with increasing RE content [120]

The polarisation behaviour shows that RE additions are able to retard slightly the anodic reaction kinetics, but that these decreases in reaction rates are not large enough to decrease significantly the overall corrosion rate. This is because of the overwhelming increase in the cathodic reaction kinetics caused by the Mg-RE intermetallic particles that are embedded in the Mg matrix – which enhance the cathodic reaction kinetics. Therefore, while there is an

ennoblement in the value of E_{corr}, there is an overall net increase in i_{corr} values, causing a net increase in corrosion to take place [120]. This behaviour is indicative of a system under cathodic control.

4.0 Unresolved issues from the literature

A review of the literature has shown that while Zr and Mn are both common alloying additions in many Mg-alloys there is a major knowledge gap that needs to be researched. The precise impact of Mn and Zr additions on the corrosion behaviour of Mg needs to be resolved. One obvious issue is that research work to date has largely speculated on the corrosion effects, without any effort to produce alloys with desired compositions (or a range of compositions, which is scientifically more illuminating). This needs to be done. Moreover, while the effect of Zr additions on Fe impurities (which have a great impact on the corrosion performance of Mg) has been widely reported, the effect of Mn addition on Fe impurities in the absence of Al has only been proposed as a Mn-Fe encapsulation mechanism [92, 95] with no research to prove or disprove this theory. These factors need to be addressed to create a foundation of knowledge that can be used in improving currently available commercial Mg-alloys and future alloys that may be developed with these alloying additions. Most recently, several works have also reported calculated phase diagrams as a basis for the interpretation of the corrosion of Mg in the presence of low levels of impurities [45]. Again no experimental validation of such diagrams or alloy production was employed, meaning any assertions in such works are not validated and cannot be considered reliable.

This page is intentionally left blank

Chapter 3

Research aims and methodology

This page is intentionally left blank

Chapter 3: Research aims and methodology

Research hypothesis

A review of the literature reveals that there are few reported studies regarding the specific influence of Mn and Zr individually and in conjunction with high Fe impurity concentrations on the corrosion kinetics of Mg and Mg alloys that do not contain Al.

The hypothesis to be tested is that in absence of Al additions, Mn and Zr alloying additions can improve the corrosion performance of Mg, via:

- Zr additions will remove Fe from Mg melts, which is beneficial to corrosion.
- Mn interacting with Fe to render the Fe particles less detrimental.
- Additionally, a definitive notion of the Fe tolerance limit (in the presence and absence of combinations of Mn and Zr), will also be elucidated such that optimal combinations can be obvious.

Research aims

The key aims of this research are to quantify the corrosion of Al-free Mg alloys in order to:

1. Characterise the electrochemical behaviour of pure Mn and Zr over a range of pH levels.
2. Understand the electrochemical effect and the mechanistic aspects related to corrosion of Mn and Zr additions upon Mg. (i.e. do such alloying additions impact anodic or cathodic kinetics?).
3. Understand the interaction between the Fe impurity and Mn or Zr alloying additions in Al-free Mg systems (i.e. what intermetallics will form, if any).

Alloy production and manufacturing

The 'pure' Mn and Zr samples used in this study were >98% Mn (supplied by Metallium Inc., USA) and 99.95% Zr (supplied by Alfa Aesar, USA). The Mg alloys cast in this study were made by blending Mg-2.12 wt.% Mn, Mg-1.3 wt.% Fe, Mg-25.0 wt.% Zr and Mg-33.3 wt.% Zr master alloys, that were supplied by CSIRO Australia, CAST-CRC and Magnesium Elektron, with commercially pure Mg in a resistance furnace. AM-Cover® was used as a cover gas to reduce oxidation of the Mg alloy melt during the casting process. The commercially pure Mg was initially melted in the furnace to roughly 700°C and then poured into a crucible capable of producing 300g ingots, to which small amounts of the master alloys were added to the Mg melt to attain specific Mn/Zr/Fe contents in the final ingot castings. The melt was poured into a graphite coated cast iron mould and allowed to air cool. The elemental compositions of all the Mg alloys produced herein were independently determined by inductively coupled plasma atomic emission spectroscopy (ICP-AES). The ICP-AES testing was performed by Spectrometer Services, Coburg, Australia.

Electrochemical polarisation testing

The Mg alloy specimens were ground to a 2000 grit finish prior to electrochemical testing. Electrochemical tests were conducted using a 3-electrode flat-cell (PAR) with an exposed sample area of 1 cm^2. It should be noted that the sample surface areas were nominally >> 1 cm^2 and hence did not need to be mounted in epoxy. They were simply metal ingot sections. A saturated calomel (SCE) reference electrode was used, along with a standard test electrolyte of 0.1M NaCl. For the testing of the pure Mn and Zr samples the testing electrolyte solution was buffered to achieve final pH levels of 1, 3, 5, 7, 9, 11 and 13. Buffering of the solutions was achieved via the addition of NaOH (for increasing pH) and HCl (for decreasing pH). In the preparation of the acidic electrolytes, the amount of NaCl added to the solution was reduced at very low pH levels to accommodate the excess Cl^- ions introduced by adding HCl to maintain the molarity of 0.1). The solutions were used in quiescent conditions and were not aerated or deaerated.

A VMP (Biologic) potentiostat was used in this study with potentiodynamic polarisation conducted at 1 mV/s. Prior to polarisation, each specimen was exposed for ten minutes at open circuit to acquire a relatively stable potential. The polarisation curves were used to determine i_{corr} (via a Tafel-type fit) using the EC-Lab software package. As a general rule, the Tafel fits were executed by selecting a section of the curve that commenced >50mV from

E_{corr}, and i_{corr} was subsequently calculated from where the fit intercepted the potential value of the true E_{corr}. Each specimen investigated was re-ground and tested five times and an average result was determined and reported. The polarisation testing was able to visually reveal comparative and quantitative information related to the kinetics of both the anodic and cathodic reactions of the selected alloy specimens, which is shown to be of most critical importance.

Immersion testing

Immersion testing was conducted by measuring the initial weight and dimensions of the selected alloy specimens and then placing them in a 0.1M NaCl solution in quiescent conditions. After a period of 24 hours the samples were removed from the solution weight loss was calculated by subsequent removal of the corrosion products by a light scrubbing following a ~3s immersion in a dilute (15%) HNO_3 solution. Comparisons between the initial and final weight and dimensions of the tested specimens were then used to determine the mass loss per unit area. Each alloy sample was tested three times and an average result was determined.

SEM analysis

The microstructures of the alloys produced in this study were examined via electron microscopy. Specimens were polished to a 1μm diamond paste finish and then imaged using either a FEI Phenom or JEOL 7001F electron microscope in back scattered electron (BSE) mode. The JEOL 7001F microscope was also equipped with energy dispersive X-ray spectroscopy (EDX) (Oxford Instruments X-Max 80 detector) analysis capability. This allowed for the determination of elemental composition through EDX mapping of the particles that were observed in the microstructure.

SEM observations were also carried out on post-corrosion samples (exposed at open circuit) using an FEI-Phenom. Selected Mg alloy specimens were polished to a 1 μm diamond paste finish and immersed in a 0.1M NaCl solution for 30 minutes. The samples were then gently cleaned with a 5% nitric acid solution (normally a dip of a few seconds to remove the hydrated corrosion product) prior to SEM observation. Electron back-scatter diffraction (EBSD) and analysis using HKL was also performed. Samples used in EBSD analysis were prepared using the same techniques for preparing the Mg alloy specimens for SEM observation.

Phase constituent simulation

The CALPHAD-based computer program 'PANDAT', using the PanMg8 database, was used to compute the most likely stable equilibrium phases expected in the Mg-alloys produced in this study. The computer simulation by PANDAT is done using a global minimisation algorithm based on mathematical modelling of the thermodynamic properties of the Gibbs energy functions of the different phases that form in the alloy and then analysing the changes in the energy curves of the alloy systems with changes in the alloy composition. As such, this method uses the phase equilibrium of known alloy systems to predict the phase equilibrium of unknown multi-component systems. A reliable database of thermodynamic parameters for each phase component in a selected alloy system is required to ensure that the calculations simulate the expected interactions between constituent elements accurately.

Phase analysis was calculated by imputing the various alloy components at different contents and allowing PANDAT to determine the phases that form and their respective volume fractions in the alloy. Moreover, isopleths of these various alloy systems were calculated and analysed to present and investigate the more complex interactions that were taking place within the Mg-alloy systems.

This page is intentionally left blank

Chapter 4

Influence of Mn and Zr on the corrosion of Al-free Mg-alloys: Part 1 – Electrochemical behaviour of Mn and Zr

This page is intentionally left blank

Influence of Mn and Zr on the Corrosion of Al-Free Mg Alloys: Part 1—Electrochemical Behavior of Mn and Zr

D.S. Gandel,[‡,*,***] M.A. Easton,[*,**] M.A. Gibson,[**,***] and N. Birbilis[*,**]

ABSTRACT

Electrochemical characteristics of Mn and Zr are reported in a dilute chloride electrolyte (0.1 M sodium chloride [NaCl]) over a wide pH range. This is because the relatively insoluble Mn and Zr are common in newer Al-free Mg alloys; however, little research has been conducted on the isolated effect of these elements upon Mg corrosion. In Part 1 of this study, the properties of Mn and Zr are studied in isolation, and this information is carried on to Part 2, where the influence of Mn and Zr is studied when alloyed with Mg alloys.

KEY WORDS: manganese, magnesium, polarization, zirconium

INTRODUCTION

Mn and Zr have several uses in engineering applications. Mn is used predominantly as an alloying element, serving various functional roles in a range of steels,[1] along with providing solid solution strengthening in Al alloys.[2] Zr-based alloys are used principally in heavy water pressure tubes in nuclear reactors because of a strong neutron-absorbing capability and high corrosion resistance.[3]

In the context of Mg alloys, Mn and Zr play a functional role as minor alloying elements, albeit with a limited solid solubility (C_s) at 650°C in Mg; Mn ≈ 0.95 at%[4] and Zr ≈ 0.73 at%.[5]

Zr has a potent ability to serve as both an Fe scavenger and a grain refiner in Mg alloys.[6-11] Given that Mg has a Hall-Petch coefficient of ~280 MPa/μm to 320 MPa/μm, the reduction of grain size can assist in increasing strength greatly, while also simultaneously allowing texture control.[12-14] Consequently, Zr is added to commercial alloys such as ZE41, WE43, and ZK60. Further to this, given the significant present interest in Mg alloys and that new Mg alloys such as Elektron† 21 and AM-SC1† recently have been developed with Zr as an alloying element,[15-18] the investigation of Zr additions on the corrosion of Mg is warranted.

Of the relatively few investigations on the corrosion behavior of Zr in aqueous solutions, most testing has taken place in highly aggressive solutions, such as nitric (HNO_3), hydrochloric (HCl), and sulfuric (H_2SO_4) acids, or at elevated temperatures and pressures.[3,19-20] The interaction between oxygen anions and the Zr metal surface allows for the establishment of the protective oxide layer zirconium dioxide (ZrO_2).[21]

Recent work has shown that Zr-rich particles that are embedded in the matrix of Mg alloys can disrupt the formation of the protective surface film that forms above pH 11 and allows severe corrosion to take place.[22] This form of accelerated corrosion of Mg is intensified when there is a higher concentration of large Zr particles compared to a more homogeneous distribution of smaller Zr particles[23] and when there are disproportionate amounts of different-sized Zr particles in the matrix.[24] The Zr particle/Mg matrix interface sites

Submitted for publication: September 4, 2012. Revised and accepted: December 16, 2012. Preprint available online: February 3, 2012, http://dx.doi.org/10.5006/0827.

‡ [redacted]
* CAST Cooperative Research Centre.
** Department of Materials Engineering, Monash University, Clayton VIC. 3800, Australia.
*** CSIRO Process Science and Engineering, Clayton, VIC, 3168, Australia.

† Trade name.

ISSN 0010-9312 (print), 1938-159X (online)
13/000121/$5.00+$0.50/0

also often experience circumferential pitting attack as a result of the formation of galvanic couples.[22] This galvanic coupling effect is attributed to the difference in electrochemical potential between Zr and Mg.

Mn is a routine addition to Mg alloys for improving the physical properties, such as extrudability (i.e., M1, ME10), and for corrosion control.[25-27] Arguably, to date, the single biggest contribution toward the corrosion control of Mg alloys has stemmed from the early revelation that small amounts of Mn could serve to moderate the deleterious corrosion effect of Fe impurities in Mg-Al alloys.[2,11] When Mn is added to Mg alloys, which contain Al, Mn forms the compound Al_8Mn_5,[28-29] in which Fe can substitute for Mn and hence be removed from the melt[11] forming $Al_8(Mn,Fe)_5$. If not incorporated into an intermetallic, the very low solubility of pure Fe in Mg (0.00043 at%[30]) ordinarily would cause elemental Fe (i.e., small particles of Fe) to form. The electrochemical potential difference between Mg and Fe is relatively large at ~0.95 V,[31] leading to severe localized corrosion under immersion/exposure conditions. In contrast, the electrochemical potential difference between Mg and $Al_8(Mn,Fe)_5$ is comparatively smaller at ~0.35 V.[32] While this difference in potential is still a concern for corrosion in free corrosion conditions, the damage accumulated is less severe in the case of $Al_8(Mn,Fe)_5$ since the phase is weakly polarized in Mg alloys and not as efficient a cathode as pure Fe.

Considering the mechanism for how Mn controls excessive corrosion arising from Fe impurities, it has been proposed that such a mechanism will work only for Mg alloys that contain some amount of Al. With regard to recent progress in the Mg alloy development, there is a need to attain higher operating temperatures (which are limited in Mg-Al alloys by the precipitation of the $Mg_{17}Al_{12}$ phase) through enhanced creep strength, which has led to the evolution of a family of Al-free Mg alloys.[33-34]

To date, work on the corrosion of Al-free Mg alloys in the presence of Mn suggests that Mn is still able to suppress the detrimental effect of Fe impurities.[35] When Al is absent, it is hypothesized (but invalidated) that Mn counteracts the negative effects of the Fe impurities by encapsulating Fe particles and separating them from the Mg matrix.[36] Unfortunately, the use of Mn in this fashion has two main disadvantages. First, the majority of the Mn added to the alloy is found within the grains rather than in the boundary. Second, the necessary ratio of Fe to Mn for the beneficial effect on corrosion resistance is difficult to achieve.[37] It is established that in the binary system there are no intermetallic phases formed between Mg and Mn and that the particles embedded in the Mg matrix are essentially pure Mn particles.[25]

As early as 1927,[38] it was reported that with the addition of up to 1 wt% Mn, there is an increase in the corrosion rate of Mg. This is attributed to:

—an increase in the number of inclusions on the surface of the alloy, which weakens the adherence of any surface film to the substrate, and
—the higher manganese level leads to the formation of Mn particles, which, in turn, stimulate micro-galvanic cells and enhance the consumption of the magnesium matrix.[39]

In regard to the electrochemical characteristics of pure Mn and Zr, there exists relatively little data reporting their individual electrochemical responses in aqueous solutions such as dilute sodium chloride (NaCl). This may be due to the fact that, in part, they are not typical structural metals (in a commodity sense). As a result of this, we aim to present such elementary information herein, which can be used more generally in the corrosion science field where Mn and Zr are used as alloying elements—particularly in cases where their solubility limit may be exceeded (which is also relevant to Al alloys). Furthermore, dilute NaCl electrolytes represent a typical environmental envelope for structural metals in atmospheric exposure applications.

In Part 1 of this study, an electrochemical investigation for both pure Mn and Zr in a 0.1 M NaCl solution, buffered to yield a range of pH levels, is presented. Such data has not been reported previously in a consolidated manner. The basic data herein also forms the basis for Part 2,[40] which focuses on the effect of Mn and Zr in a large number of Mg alloys custom-produced with varying concentrations both individually and in combination (i.e., binary and ternary alloys)—the combination of the two studies presenting information pertinent to the development of Al-free Mg alloys.

EXPERIMENTAL PROCEDURES

The samples used in this study were >98% Mn (supplied by Metallium Inc., Norwood, Massachusetts) and 99.95% Zr (supplied by Alfa Aesar, Ward Hill, Massachusetts). Specimens were ground to a 2000 grit finish prior to testing. A three-electrode electrochemical flat cell (Princeton Applied Research†) was used. The test electrolyte was 0.1 M NaCl, which was buffered to achieve a final pH of 1, 3, 5, 7, 9, 11, and 13. Buffering was achieved via the addition of sodium hydroxide (NaOH; for increasing pH) and HCl (for decreasing pH). In the preparation of the acidic electrolytes, the amount of NaCl added to the solution was reduced at very low pH levels to accommodate the excess Cl^- ions introduced by adding HCl. The solutions were used in quiescent conditions and were not aerated or deaerated.

A VMP† (Biologic Scientific Instruments, France) potentiostat was used, with potentiodynamic polarization conducted at 1 mV/s. Prior to polarization, samples were exposed for 10 min at open circuit to obtain a relatively stable potential. The polarization curves

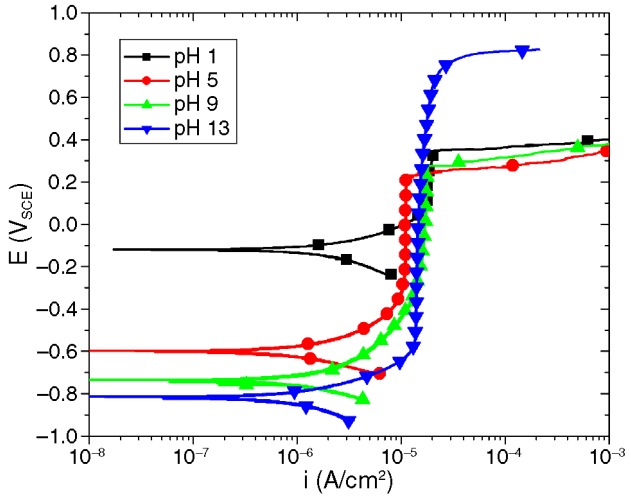

FIGURE 1. *Representative potentiodynamic polarization curves for pure Zr at pH values 1, 5, 9, and 13 in 0.1 M NaCl.*

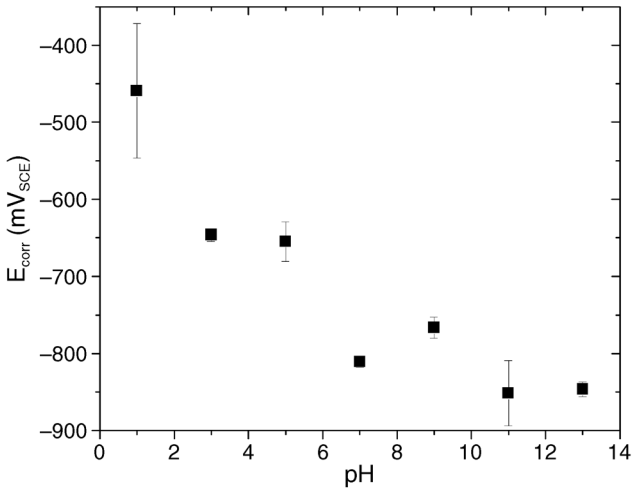

FIGURE 2. *E_{corr} as a function of pH for pure Zr in buffered 0.1 M NaCl.*

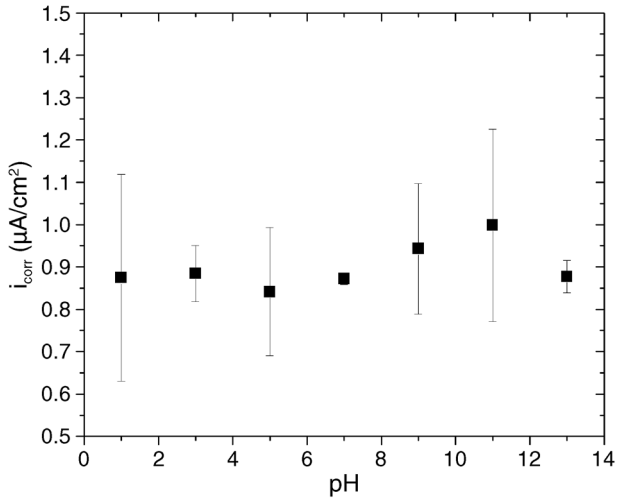

FIGURE 3. *i_{corr} as a function of pH for pure Zr in buffered 0.1 M NaCl.*

were used to determine corrosion current density (i_{corr}) (via a Tafel-type fit) using EC-Lab† software. As a general rule, fits were executed by selecting a portion of the curve that commenced >50 mV from corrosion potential (E_{corr}), and i_{corr} was subsequently estimated from the value where the fit intercepted the potential value of the true E_{corr}. Polarization testing also was able to reveal visually comparative information related to the kinetics of both the anodic and cathodic reactions for the Mn and Zr samples, which is shown to be of most critical importance. Each test condition was repeated at least five times (at each pH) and an average result determined.

RESULTS AND DISCUSSION

Electrochemical Response of Zr in Buffered 0.1 M NaCl

The typical potentiodynamic polarization curves for pure Zr in buffered 0.1 M NaCl are seen in Figure 1. What is obvious from the polarization response is that Zr displays a window of passivity over the entire range of pH tested. The range of passivity varies with pH; however, this is largely a result of the wide differences in the E_{corr} with pH.

The resultant E_{corr} is reported as a function of pH in Figure 2. What is observed is that with increasing pH, E_{corr} decreases somewhat monotonically. Inspection of the polarization curves (which reveal a somewhat similar, passive, anodic character) suggests that this alteration in E_{corr} with pH is a result of significant differences in the rate of the cathodic reaction over the pH range. In the acidic to neutral pH range, the rate of cathodic activity is enhanced. This is related to the cathodic reaction in the acidic regime being water reduction as opposed to oxygen reduction.[41] In acidic solutions, water is reduced to form zirconium oxides and hydrogen evolves in conjunction with the excess H^+ in solution. In more alkaline solutions there is an excess of OH^-, and oxygen in solution is reduced in the production of hydroxyl zirconium compounds, also discussed further below. The ability of Zr to sustain cathodic reactions at relatively high rates compared to other metals is qualitatively expected from its high exchange current density of ~3 × 10^{-5} A/cm^2 at 20°C.[42]

The average i_{corr} values for Zr (Figure 3) vary only slightly over the entire pH range. Over the range of pH, the measured i_{corr} values are within the scatter band of one another. While it may appear that there is a large standard error in the data presented, the scale indicates that the range is small and a standard error of less than 0.5 μA/cm^2 was measured. The characteristic is that the value of i_{corr} remains essentially unchanged while the value of E_{corr} concomitantly decreases (becomes less noble). Since the anodic reaction does not appear to be greatly influenced by pH, the intersection point of the anodic polarization curve

with the cathodic curve as the pH changes (Figure 2) causes a shift in the measured E_{corr}, with minimal change in the i_{corr}.

As also evidenced from the potentiodynamic polarization curve, Zr displays a clear breakdown over the range of pH, allowing for the determination of a pitting potential, E_{pit}. The changes in E_{pit} across the pH range are seen in Figure 4. It appears that there is only a moderate deviation in E_{pit} until pH 13, when E_{pit} increases significantly. In fact, there is also a local trend that the E_{pit} values at highly acidic pH were also more noble than those at pH 5 to 11. This is discussed further below.

Electrochemical Response of Mn in Buffered 0.1 M NaCl

There has been little research conducted on the corrosion of pure Mn in aqueous solutions.[43] However, while it is known that Mn can dissolve readily in dilute acids, the passivation of Mn can be attributed to the development of a visible layer of manganese dioxide (MnO_2) that forms on the metal surface.[44]

The typical potentiodynamic polarization curves for pure Mn in buffered 0.1 M NaCl are seen in Figure 5. What can be seen from the polarization curves is that Mn displays obvious changes to the anodic and cathodic reaction kinetics from the low to high pH ranges tested. This variation in the reaction kinetics with pH results in wide differences in the measured i_{corr} and E_{corr} values at the extreme pH levels of pH 1 and 13, respectively. According to the potentiodynamic polarization curves, Mn does not display a clear E_{pit}.

The resultant E_{corr} for Mn is reported as a function of pH in Figure 6. It is observed that as the pH increases pH 1 to pH 5 and then pH 9, the E_{corr} decreases, then at pH 13 there is a large increase in E_{corr}. The polarization curves for Mn across the various pH levels (Figure 5) show that at pH 13 this increase in E_{corr} (with a pH increase) is a result of considerable differences in the rate of the anodic and cathodic reaction kinetics compared to lower pH levels. As the test electrolyte shifts from an acidic to a more neutral pH range, the rate of cathodic activity is altered, leading to a decrease in the measured E_{corr} value. However, at pH 13, there is also a decrease in the anodic kinetics, leading to an increase in E_{corr}, as illustrated in Figure 5.

The measured i_{corr} values for Mn (Figure 7) decrease with increasing pH. This decrease is most notable at pH 1, which has a measured i_{corr} value over two orders of magnitude larger than the i_{corr} values attained at higher pH levels. From pH 3 to pH 13, the drop in i_{corr} is smaller, with an intermediate plateau where the i_{corr} remains somewhat constant in the (near) neutral regions between pH 5 and pH 9. Again, the distinguishing feature is that the i_{corr} remains effectively unchanged while E_{corr} for the same pH lev-

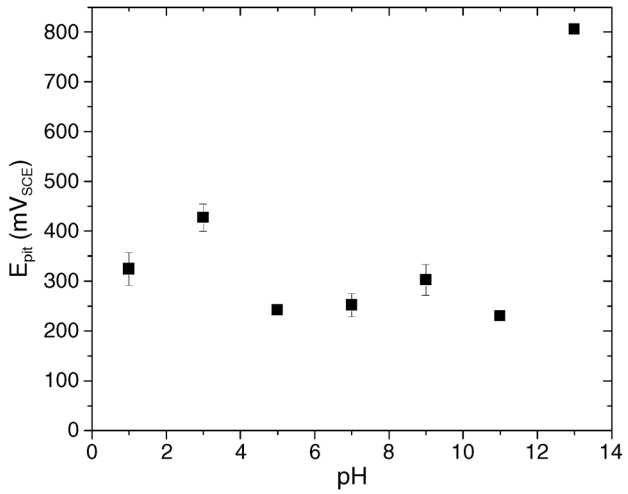

FIGURE 4. *E_{pit} as a function of pH for pure Zr in buffered 0.1 M NaCl.*

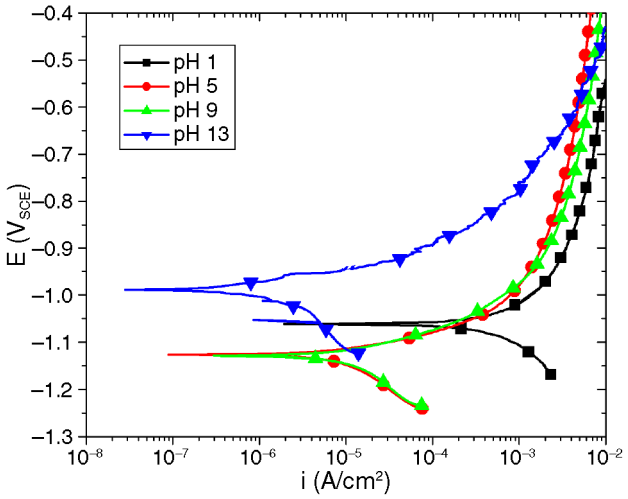

FIGURE 5. *Representative potentiodynamic polarization curves for pure Mn at pH values 1, 5, 9, and 13 in 0.1 M NaCl.*

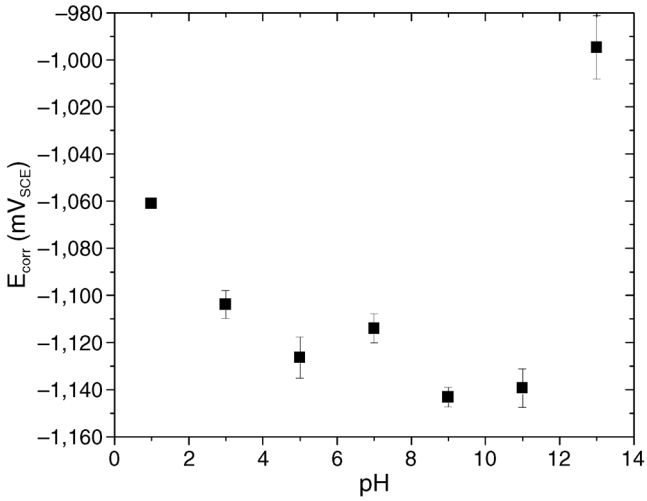

FIGURE 6. *E_{corr} as a function of pH for pure Mn in buffered 0.1 M NaCl.*

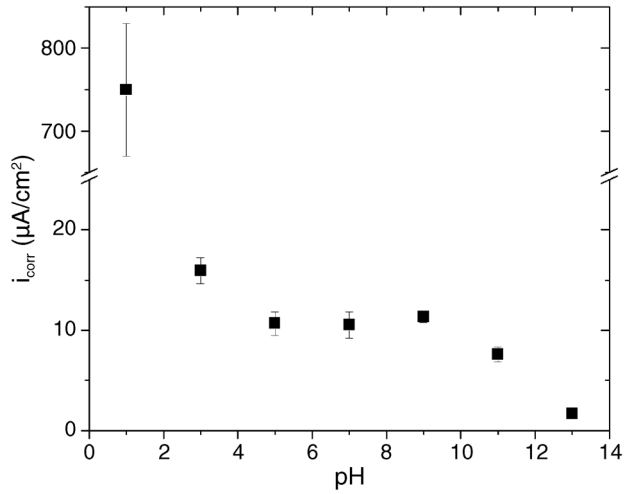

FIGURE 7. *i_{corr} as a function of pH for pure Mn in buffered 0.1 M NaCl.*

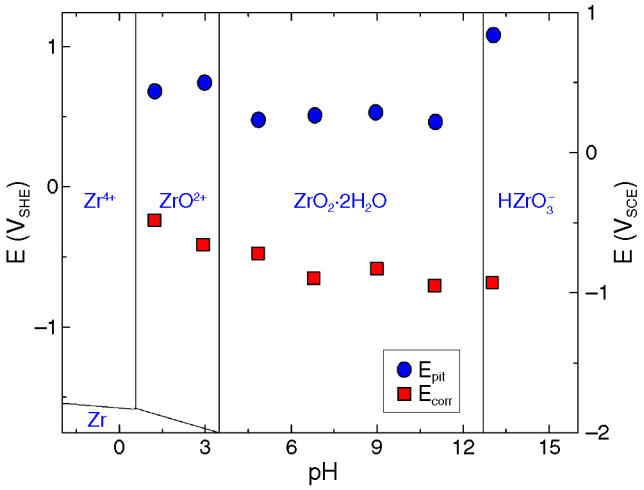

FIGURE 8. *E-pH diagram for pure Zr. Overlaid data represents the values determined herein in buffered 0.1 M NaCl.*

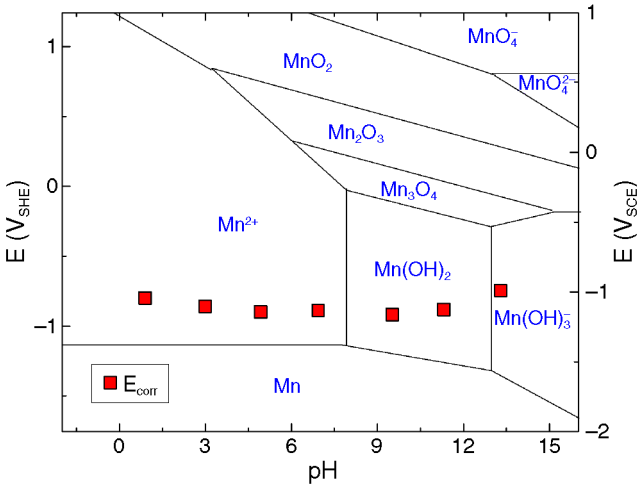

FIGURE 9. *E-pH diagram for pure Mn. Overlaid data represents the values determined herein in buffered 0.1 M NaCl.*

els concurrently decreases; however, at the extremes of pH (1 and 13), the corrosion rate is under cathodic control.

General Discussion

The E-pH diagram for Zr (Figure 8) shows how the Zr metal oxidizes to zirconic ions (Zr^{4+}) in very acid solutions, and then into zirconyl ions (ZrO^{2+}) as pH increases. In more neutral and alkaline solutions, zirconate ions ($HZrO_3^-$) begin to form. Equilibrium calculations (depicted by the fields in the Pourbaix diagram) indicate that there should be domains of corrosion for Zr in very acidic and very alkaline solutions.[45] However, the empirical results presented in the current study indicate that this is not necessarily the case.

Zr demonstrates excellent corrosion resistance in highly acidic environments. It has been reported that the anodic polarization kinetics for Zr are less active in highly reducing acidic environments.[46] ZrO^{2+} ions are expected to form between pH 1 and pH 3. This region correlates to an observed local trend of increased measured E_{pit} values (Figure 8). Thermodynamic calculations indicate that these ZrO^{2+} ions might be able to form numerous zirconyl salt complexes in environments containing HCl.[45] Differently colored corrosion products were observed optically, not only at low pH levels, but also up to pH 13, where the $HZrO_3^-$ ion is predicted by the Pourbaix diagram. We note that pH 13 corresponds to the highest value of E_{pit}, such that if there are insoluble salt complexes that form, they could account for the low rates of dissolution and extension of the passive region, as such compounds on the Zr metal surface are sparingly soluble and block ionic conduction. Therefore, they would act as a further barrier to corrosion and increase the potential required for pitting to commence.

The E-pH diagram for Mn (Figure 9) shows that at sufficiently low pH levels, such as pH 1, the $Mn \rightarrow Mn^{2+} + 2e^-$ anodic reaction readily can take place. Moreover, Figure 5 shows that the cathodic reaction kinetics also increase greatly at pH 1. The large driving force behind the anodic and cathodic reaction kinetics, coupled with the expected lack of a stable oxide product forming of the surface of the Mn at pH 1, leads to a large increase in the current density observed in the polarization testing of Mn (Figure 7) and generates a large driver for the Mn to corrode. In addition, Mn shows that at alkalinities above pH 12 the transition of Mn metal into manganese hydroxide ($Mn[OH]_2$) changes to become $Mn(OH)_3^-$, which only has a very slight solubility in highly alkaline solutions (above pH 11.5). In the presence of oxygen, these new manganous hydroxide ions can form higher volume oxides such as Mn_3O_4 or Mn_2O_3. These oxides, observed by a change in the color of the surface film, can provide a barrier to corrosion.

CONCLUSIONS

The work herein has revealed the general electrochemical response for Zr and Mn over a range of pH in 0.1 M NaCl. Such general data was previously lacking in the open literature and is of direct relevance to light alloy systems that use Zr and Mn as alloying elements. From the survey of the electrochemical characteristics of these metals, the following can be concluded:

❖ Zr metal presents low dissolution rates across the pH spectrum, and i_{corr} remains unchanged, while E_{corr} decreases with increasing pH. The electrochemical response of Zr over the pH range is concomitant with changes in the cathodic reaction rate.

❖ Zr displays a E_{pit} that is dependant on the different Zr ionic species evolving over the various pH ranges where different Zr oxides can be produced.

❖ In the pH regions varying from moderately acidic to moderately alkaline, Mn presents the characteristics that are indicative of a system that is under cathodic control with little change in anodic activity.

❖ At pH 1, both the cathodic and anodic kinetics for Mn are greatly increased, leading to very high current densities.

❖ The large reduction in the anodic reaction kinetics at alkaline pH for Mn results in lower current densities and higher potentials at pH 13.

ACKNOWLEDGMENTS

The CAST Co-Operative Research Centre was established under, and is funded in part by, the Australian Governments Co-Operative Research Centres Scheme. Special thanks to C. Bettles for supplying the pure zirconium.

REFERENCES

1. R.W.K. Honeycombe, H.K.D.H. Bhadeshia, *Steels: Microstructure and Properties*, 3rd ed., ed. E.S. Publishers (Oxford, U.K.: Butterworth-Heinemann, 2006).
2. I.J. Polmear, *Light Alloys*, 3rd ed. (London, U.K.: Arnold, 1995).
3. F. Rosalbino, D. Maccio, A. Saccone, E. Angelini, S. Delfino, *Solid State Electrochem.* 14 (2009): p. 1451-1455.
4. H. Okamoto, *J. Phase Equilib. Diffus.* 29, 2 (2008): p. 208-209.
5. H. Okamoto, *J. Phase Equilib. Diffus.* 28, 3 (2007): p. 305-306.
6. G. Song, D. StJohn, *J. Light Met.* 2 (2002): p. 1-16.
7. P. Cao, M. Qian, D.H. StJohn, M.T. Frost, *Mater. Sci. Technol.* 20 (2003): p. 585-592.
8. M. Qian, D.H. StJohn, *Int. J. Cast Met. Res.* 22, 1-4 (2009): p. 256-259.
9. M. Qian, D.H. StJohn, M.T. Frost, "Zirconium Alloying and Grain Refinement of Magnesium Alloys," in Magnesium Technology 2003, ed. H.I. Kaplan (Warrendale, PA: The Minerals, Metals and Materials Society [TMS], 2003), p. 209-214.
10. M.A. Easton, C.H.J. Davies, M.R. Barnett, F. Pravdic, *Mater. Sci. Forum* 539-543 (2007): p. 1729-1734.
11. E.F. Emley, *Principles of Magnesium Technology*, 1st ed. (Manchester, U.K.: Pergamon Press, 1966).
12. W. Yuan, S.K. Panigrahi, J.Q. Su, R.S. Mishra, *Scr. Mater.* 65 (2011): p. 994-997.
13. C.D. Lee, *Mater. Sci. Eng. A* 459 (2007): p. 355-360.
14. H. Han, S. Liu, L. Kang, L. Liu, *J. Wuhan Univ. Technol.—Mater. Sci. Ed.* 23, 2 (2007): p. 194-197.
15. P. Lyon, "New Magnesium Alloy for Aerospace and Specialty Applications," in Magnesium Technology 2004, ed. A.A. Luo (Warrendale, PA: The Minerals, Metals and Materials Society [TMS], 2004), p. 311-315.
16. T. Rzychon, J. Michalska, A. Kielbus, *J. Achievments in Mater. Manufact. Eng.* 21, 1 (2007): p. 51-54.
17. C.J. Bettles, M.A. Gibson, S.M. Zhu, *Mater. Sci. Eng. A* 505 (2009): p. 6-12.
18. A.C. Hanzi, F.H.D. Torre, A.S. Sologubenko, P. Gunde, R. Schmid-Fetzer, M. Kuehlein, J.F. Loffler, P.J. Uggowitzer, *Philos. Mag. Lett.* 89, 6 (2009): p. 377-390.
19. C. Proff, S. Abolhassani, M.M. Dadras, C. Lemaignan, *J. Nucl. Mater.* 404 (2010): p. 97-108.
20. L.L. Shreir, G.T. Burstein, R.A. Jarman, *Corrosion,* 4th ed., ed. E.S. Publishers (Oxford, U.K.: Butterworth Heinemann, 2010).
21. *Encyclopedia of Electrochemistry of the Elements*, ed. A.J. Bard, vol. 9B (New York, NY: Marcel Dekker, Inc., 1986).
22. W.C. Neil, M. Forsyth, P.C. Howlett, C.R. Hutchinson, B.R.W. Hinton, *Corros. Sci.* 51 (2009): p. 387-394.
23. G. Ben-Hamu, D. Eliezer, K.S. Shin, S. Cohen, *J. Alloys Compd.* 341 (2007): p. 269-276.
24. Z. Rong-Chang, Z. Jin, H. Wei-Jiu, W. Dietzel, K.U. Kainer, C. Blawert, K.E. Wei, *Trans. Nonferrous Met. Soc. China* (2006): p. 763-771.
25. A.F. Smith, *Acta Metall.* 15 (1967): p. 1867-1873.
26. H.E. Friedrich, B.L. Mordike, Magnesium Technology 2006 (Berlin, Germany: Springer-Verlag, 2006), p. 708.
27. L.L. Rokhlin, *Magnesium Alloys Containing Rare Earth Metals* (London, U.K.: Taylor & Francis Group, 2003).
28. C. Liu, F. Pan, W. Wang, *Mater. Sci. Forum* 546-549 (2007): p. 395-398.
29. V.Y. Gertsman, J. Li, S. Xu, J.P. Thomson, M. Sahoo, *Metall. Mater. Trans. A* 36A (2005): p. 1989-1997.
30. A.A. Nayeb-Hashemi, J.B. Clark, L.J. Swartzendruber, *Bull. Alloy Phase Diagr.* 6, 3 (1985): p. 235-238.
31. A.D. Sudholz, N.T. Kirkland, R.G. Buchheit, N. Birbilis, *Electrochem. Solid-State Lett.* 14, 2 (2011): p. C5-C7.
32. Y. Hu, "Electrochemical Polarization Behaviour of Mg-Al Alloys in Near-Neutral Solutions" (Ph.D., Hamilton, Canada, McMaster University, 2012).
33. T.L. Chia, M.A. Easton, S.M. Zhu, M.A. Gibson, N. Birbilis, J.F. Nie, *Intermetallics* 17 (2009): p. 481-490.
34. S.M. Zhu, M.A. Gibson, M.A. Easton, J.F. Nie, *Scr. Mater.* 63 (2010): p. 698-703.
35. D.S. Gandel, N. Birbilis, M.A. Easton, M.A. Gibson, "The Influence of Mn on the Corrosion of Al-Free Mg-Alloys," in 18th Int. Corros. Cong. (Perth, Australia: International Corrosion Congress, 2011), p. 1-9.
36. J.D. Robson, D.T. Henry, B. Davis, *Acta Metall.* 57 (2009): p. 2739-2747.
37. H. Gao, G. Wu, W. Ding, L. Liu, X. Zeng, Y. Zhu, *Mater. Sci. Eng.* (2004): p. 311-317.
38. J.A. Boyer, *The Corrosion of Magnesium and of the Magnesium Aluminum Alloys Containing Manganese* (American Magnesium Corporation, 1927), 417-454.
39. G.T. Parthiban, N. Palaniswamy, V. Sivan, *Anti-Corros. Methods Mater.* 56, 2 (2009): p. 79-83.
40. D.S. Gandel, M.A. Easton, M.A. Gibson, N. Birbilis, *Corrosion* 69, (2013): http://dx.doi.org/10.5006/0828.
41. D.A. Jones, *Principles and Prevention of Corrosion*, ed. D. Johnstone (New York, NY: Macmillan Publishing Company, 1992).
42. M.L. Brown, G.N. Walton, *J. Nucl. Mater.* 58 (1975): p. 321-335.
43. G.J. Browning, S.W. Donne, *J. Appl. Electrochem.* 35 (2004): p. 437-443.
44. S.M.A.E. Haleem, S.A.E. Wanees, E.E.A.E. Aal, *Corros. Eng., Sci. Technol.* 46, 4 (2011): p. 432-438.
45. M. Pourbaix, *Atlas of Electrochemical Equilibria in Aqueous Solutions*, ed. J.A. Franklin (Brussels: Pergamon Press, 1966).
46. P.A. Schweitzer, ed., *Corrosion Engineering Handbook* (New York, NY: Marcel Dekker, Inc., 1996).

This page is intentionally left blank

Chapter 5

Influence of Mn and Zr on the corrosion of Al-free Mg-alloys: Part 2 – Impact of Mn and Zr on Mg alloy electrochemistry and corrosion

This page is intentionally left blank

Influence of Mn and Zr on the Corrosion of Al-Free Mg Alloys: Part 2—Impact of Mn and Zr on Mg Alloy Electrochemistry and Corrosion

D.S. Gandel,[‡,*,**] M.A. Easton,[*,**] M.A. Gibson,[**,***] and N. Birbilis[*,**]

ABSTRACT

A total of 47 alloys were produced to explore the changes in electrochemical and corrosion behavior of binary and ternary Mn- and Zr-containing Mg alloys—in the absence of Al. Up to ~2 wt% Mn was found to slightly reduce cathodic kinetics, while Zr in solid solution increased anodic reaction kinetics. We demonstrate that Zr is an efficient "activator" of Mg, which has not been explicitly shown previously. When Mn and Zr are both added to Mg, there can be an optimized combination/interaction where Mn with Zr works in conjunction to moderate the corrosion rate compared to an Mg-alloy with either Zr or Mn as singular additions. This has ramifications in emerging Al-free Mg alloys.

KEY WORDS: magnesium, manganese, microstructure, polarization, scanning electron microscopy, zirconium

INTRODUCTION

Part 1 of this study focused on electrochemical investigation of both pure Mn and pure Zr in 0.1 M sodium chloride (NaCl), buffered to yield a range of pH levels.[1] Such baseline data was collected with the view of providing a platform for understanding the role of Mn and Zr on the corrosion of Mg alloys that contain either one, or both, of Mn and Zr, in the absence of Al. As such, the work herein focuses on the effect of Mn and Zr addition in a large number of Mg alloys custom-produced with varying binary and ternary concentrations, providing previously unreported information that is pertinent to the evolving generation of Al-free Mg alloys.

Current commercial Mg alloys in general can be separated into two main groups: alloys containing Al as a primary alloying element and alloys free of Al, which may contain up to ~1% Zr for grain refinement.[2] The Mg alloys that contain Al often are alloyed with Mn to assist with corrosion control and sometimes Zn to increase strength (i.e., AM60, AZ31, AZ91).[3] The Zr-containing alloys regularly have Zn and rare earth metals as additions (i.e., ZK60, ZE41).[4]

From as early as the 1920s Mn has been used as an alloying addition for corrosion control in Mg alloys,[5-7] even though Mn itself also has a relatively low solid solubility in Mg ($C_S \approx 0.95$ at%). Theoretical calculations and previous work has indicated that there are no intermetallic phases that form between Mg and Mn.[8-9] Additions of Mn often are targeted at reducing the effect of the Fe impurity content in the alloy to manage the overall corrosion of Mg-Al alloys.[10-11] In the presence of Al and Fe, additions of Mn produce the $Al_8(Mn,Fe)_5$ phase, which reduces the free Fe content and, consequently, the corrosion rate. This is significant because almost all Fe in Mg is ostensibly insoluble and forms a pure-Fe (body-centered cubic [bcc]) phase in the Mg matrix.[12] These pure Fe particles not only have a large potential difference with the surrounding Mg matrix (and hence have

Submitted for publication: September 4, 2012. Revised and accepted: December 19, 2012. Preprint available online: February 5, 2013, http://dx.doi.org/10.5006/0828. Part 1 of this manuscript appeared in Corrosion 69, 7 (2013): p. 666-671, http://dx.doi.org/10.5006/0827.

[redacted]

* CAST Cooperative Research Centre.

** Department of Materials Engineering, Monash University, Clayton, VIC, 3800, Australia.

*** CSIRO Process Science and Engineering, Clayton, VIC, 3168, Australia.

ISSN 0010-9312 (print), 1938-159X (online)
13/000133/$5.00+$0.50/0

significantly different local currents in open-circuit conditions), but they efficiently support cathodic reactions.[13] Nominally $Al_8(Mn,Fe)_5$ particles settle to the bottom of the crucible during melting or are embedded in the casting during solidification.[14]

The development of future Mg alloys with preferably lower corrosion rates, therefore, suggests that an essential precursor is a comprehensive and elementary understanding of the role of key alloying elements and how they interact with impurities. The precise levels of Mn addition necessary to counteract the detrimental effect of any Fe impurities and the overall electrochemical kinetic changes it has on the Mg matrix are still somewhat unknown. However, it has been proposed that the interaction between Mg and Mn causes a reduction in the corrosion rate of Mg alloys.[15]

It also has been reported that the addition of small amounts of Mn to Mg initially shifts the potential of the alloy in a less-noble direction,[15] which we interpret as being attributed to reduction in cathodic kinetics. Furthermore, it was postulated that in the context of anode alloys, Mn addition improves the nature and the stability of the magnesium hydroxide ($Mg[OH]_2$) film formed on the surface of the Mg alloy to provide greater protection; however, this ought to have been associated with lower rates of anodic kinetics (and ennobled potentials), which is not necessarily the case,[15] indicating that the work to be presented herein will contribute toward this topic.

Zr has a low solid solubility in the Mg matrix (C_S ~ 0.73 at%) and no intermetallic phases form between Mg and Zr,[16] yet Zr is predominantly added to refine the grain size of Mg alloys and for improved strength. There are some few cases where the addition of Zr to Mg alloys has been attributed to decreasing the corrosion rate.[2,17-19] One cause of this reduction in corrosion rate is the potential removal of Fe impurities.[2] This may arise if Fe present in the melt combines with Zr to form insoluble particles, typically Fe_2Zr, which can settle at the bottom of the melt crucible owing to density. Addition of Zr can render Mg alloys as "higher purity" alloys,[17] with commercial Mg alloys containing Zr generally containing less than 50 ppm of Fe.

However, there are studies that indicate when Zr is not uniformly distributed within the Mg matrix, the corrosion rate can increase compared to a more homogeneous distribution of smaller Zr particles.[20] Moreover, excess amounts of Zr added to Mg can lead to the formation of elemental Zr particles in the matrix, which is deleterious for corrosion.[21] This elemental Zr has been reported to cause microgalvanic couples within Mg alloys and disrupt the formation of the protective film on the alloy surface.[22] These conflicting views indeed suggest the value of systematic work to elucidate the role of Zr in Mg.

Part 1 of this study indicates that Zr has a significantly more noble electrochemical potential[1] than Mg at pH 1 to 13. As such, it can be inferred that Zr particles embedded in an Mg matrix may act in a similar manner to Fe particles—of a similar electrochemical potential and contribute toward microgalvanic coupling and enhanced corrosion. To study this, a unique and previously unreported range of Mg-Zr alloys were custom-produced.

From the limited number of studies on ternary Mg-Mn-Zr systems, it is suggested that Zr also might combine with Mn to form Mn_2Zr. One such reported study suggests that not only are Fe impurities soluble in the Mn-Zr intermetallic phase, but that Zr, Mn, and Fe combine to form additional intermetallic phases in the Mg melt.[23] Overall, however, there is little to no data available on the tolerable level of Mn and Zr additions present concurrently (or individually) in Al-free Mg alloys and the distinct effect of these elements on the corrosion rate of Mg. In the context of Al-free Mg alloy corrosion, when contrasted with studies on common alloying elements and impurities seen in Mg alloy systems, studies on the effect of either Mn or Zr upon Mg remain scarce. This is the knowledge gap that this study seeks to fill by the combination of this two-part study.

EXPERIMENTAL PROCEDURES

Alloy Production

Mg alloys were made by blending the master alloys Mg-2.12 wt% Mn, Mg-25.0 wt% Zr, and Mg-33.3 wt% Zr, acquired from CSIRO (Normandy Road, Clayton South, VIC, Australia), AMT (George Street, Sydney, NSW, Australia), and Magnesium Elektron (Rake Lane, Manchester, England), with commercially pure Mg (<40 ppm Fe) in a resistance furnace. AM-Cover[†] was used as a cover gas to reduce oxidation during the casting process. Commercially pure Mg initially was melted in a crucible capable of producing 300 g ingots, to which small amounts of the master alloys were added (and regularly stirred) to achieve specific Mn/Zr levels in the final castings. The melt was poured into a graphite-coated cast iron mold and allowed to air cool. Three alloy series were produced, two with only Mn or Zr as binary additions and one with both Mn and Zr as ternary additions. The ternary alloys have a roughly constant Mn content of ~2 wt%, with variable Zr concentration ranging from 0.017 wt% to 0.77 wt%. The compositions of all the alloys produced are displayed in Appendix 1 and were determined independently using inductively coupled plasma atomic emission spectroscopy, ICP-AES (Spectrometer Services, Coburg, Australia).

Corrosion Assessment

Alloy specimens were ground to 2000 grit and electrochemically tested using a three-electrode flat-

[†] Trade name.

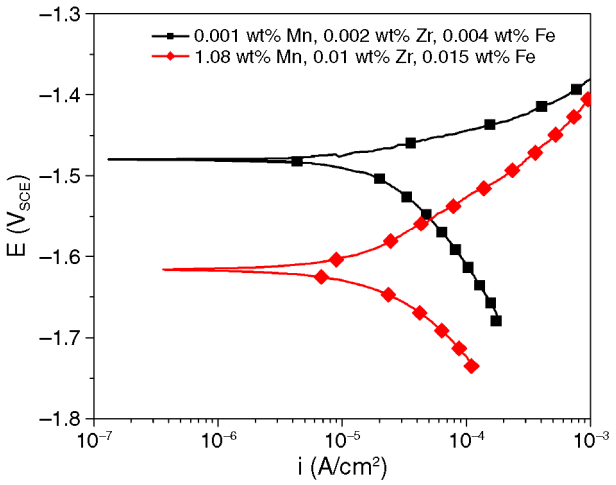

FIGURE 1. *Potentiodynamic polarization curves in 0.1 M NaCl for pure Mg and Mg specimen with high levels of Mn (1.08 wt% Mn).*

cell (Princeton Applied Research†) with an exposed sample area of 1 cm^2. A saturated calomel (SCE) reference electrode was used. The test electrolyte was 0.1 M NaCl in all cases. Potentiodynamic polarization was carried out at 1 mV/s using a BioLogic VMP 3Z† potentiostat. Prior to polarization, samples were allowed to stabilize for 10 min at open circuit to establish a relatively stable potential. The polarization curves were used to determine corrosion current density (i_{corr}) (via a Tafel-type fit) using EC-Lab† software.

As a general rule, fits were executed by selecting a portion of the curve that commenced >50 mV from corrosion potential (E_{corr}), and i_{corr} was subsequently estimated from where the fit intercepted the potential value of the true E_{corr}. Also of critical importance, polarization testing could reveal visually comparative information related to the kinetics of both the anodic and cathodic reactions for samples tested. Each sample was re-ground and tested five times, and an average result was determined and reported.

In parallel, immersion testing was carried out by measuring the initial weight and dimensions of the alloy samples and then placing them in a 0.1 M NaCl solution. After a period of 24 h, the samples were removed from the solution and mass loss per unit area was determined. Each alloy sample was tested three times and an average result was determined.

To observe visually the post-corrosion surface of the specimens, SEM observations were carried out on exposed samples (at open circuit) using an FEI-Phenom†. Such specimens were polished to a 1 μm diamond paste finish and immersed in a 0.1 M NaCl solution for ~30 min and then gently cleaned with a 5% nitric acid (HNO_3) solution (normally a dip of a few seconds to remove the hydrated corrosion product) prior to SEM observation. This rather short exposure was performed on well-polished specimens since the immersion testing generated rather significant weight loss and surface corrosion in many cases (i.e., microscopy of specimens subject to 24 h immersion did not reveal any additional information other than excessive corrosion product).

RESULTS AND DISCUSSION

Electrochemical Effect of Mn in Mg

Rather than show all the raw data, a key example is given, and in the following section the data is described overall. The polarization response of an Mg-Mn specimen with 1.08 wt% Mn, 0.01 wt% Zr, and 150 ppm Fe (Figure 1) is compared to that of commercially pure Mg with approximately 40 ppm Fe. There is a noticeable decrease in the cathodic reaction kinetics when Mn is added to Mg. This is despite the Mn-containing specimen having an Fe content of ~150 ppm, which is considered to be just below the critical threshold of Fe (after which corrosion rates dramatically increase[12,24]). This indicates that the cathodic kinetics decrease with the Mn content depicted, even without reducing the overall Fe content.

However, as also seen in Figure 1, the addition of Mn at the level of 1.08 wt% also increases the anodic kinetics slightly, such that the i_{corr} value between the two specimens depicted is rather similar. As previously suggested, Mn is known to be efficient at inhibiting the harmful effect of Fe impurities in Mg alloys in the presence of Al;[15,25] however, in this instance, the addition of Mn is found to be beneficial in reducing cathodic kinetics in the absence of Al, which has not been detailed explicitly previously. Mn has a solid solubility in Mg of ~2 wt%,[9] and additions below this limit can allow for Mn to moderate corrosion rate when added to Mg, described in more detail below.

Electrochemical Response of Zr in Mg

In the case of Zr additions, again, a typical example is presented to typify the raw data followed by a general discussion below. In the case of Mg with a Zr addition of 0.19 wt% (below the solid solubility limit), the polarization curve (Figure 2) shows that (for an Fe content of 60 ppm) there is an increase in the anodic reaction kinetics while the cathodic kinetics are essentially unaltered. At this concentration, while Zr is in solid solution, it appears as though Zr acts as an anodic activator of Mg, thereby increasing the overall corrosion rate. The ability of relatively low levels of Zr (including below the solubility limit) to activate Mg has not been discussed previously, and is dealt with further below.

Other studies that have posited the addition of Zr is beneficial for the corrosion resistance of Mg,[2,17] examined alloys with Mg alloys that contain other elements, such as rare earths, and therefore do not reflect the direct interaction between only Zr and Mg. Any decreases in corrosion rate in such studies are likely from secondary interactions with ternary or

quaternary elements—which, in turn, also impact the corrosion of the particular alloys studied.

Electrochemical Response of Mg Alloys Containing Mn and Zr

With a high Mn and low Zr content, there is still a reduction in the cathodic reaction kinetics compared to pure Mg (Figure 3). Overall, the level of reduction in the cathodic kinetics is comparable to that seen in the polarization curve of the Mg sample with a Mn addition of 1.08 wt% (Figure 1). However, there is a slight increase in the anodic reaction kinetics compared to the sample containing 1.08 wt% Mn, which also has almost no Zr. This increase is attributed to the additional Zr in the Mn-containing specimen, because the increase in anodic kinetics is similar to that seen in Mg specimen that contains Zr at concentrations of 0.19 wt% and almost no Mn (Figure 2), which has a similar overall Zr content.

When Mg has a high Zr and low Mn content (Figure 4), increased Zr content continues to contribute toward an increase in the corrosion rate. The relatively small addition of Mn (0.146 wt%) does not appear to minimize the impact of the Fe impurity in the Zr-containing sample with a content of 170 ppm Fe.[15] Similarly, as one might expect on the basis of Part 1 of this study, an increase is observed in the cathodic reaction kinetics from the formation of Zr particles in the matrix that can form at such Zr levels. As such, there is an increase in the cathodic reaction kinetics when Zr is present at such high levels.

Overall, for the Mg-Mn-Zr alloys produced herein, there is a noticeable interaction between the Mn and Zr, which will be described and differs from the relationships observed for binary Mn or Zr additions.

General Discussion of the Impact of Mn and Zr Additions

The measured i_{corr} values as a function of composition for all the samples were analyzed and placed into the three alloy groups (Figure 5[a]). In the Mg-Mn alloy group, increased Mn content slightly decreases the i_{corr} value. This is a result of the reduction in the cathodic reaction kinetics as Mn is introduced into Mg.

The Mg-Zr group displays an increase in the i_{corr} value as the Zr content is increased (Figure 5[b]). This increase can be attributed to the increase in the anodic reaction kinetics caused by the addition of Zr, while the Zr is in solid solution, and then an increase in the cathodic reaction kinetics when the Zr content is beyond the solid solubility limit. The samples with only Zr as an addition display higher corrosion current densities than the Mg-Mn and Mg-Mn-Zr alloy groups. In Figure 5(c) we see that the Mg-Mn-Zr ternary alloys reveal relatively lower corrosion rates with respect to the Mg-Mn and Mg-Zr alloys, as depicted according to the Mn:Zr ratio in the ternary alloys. The

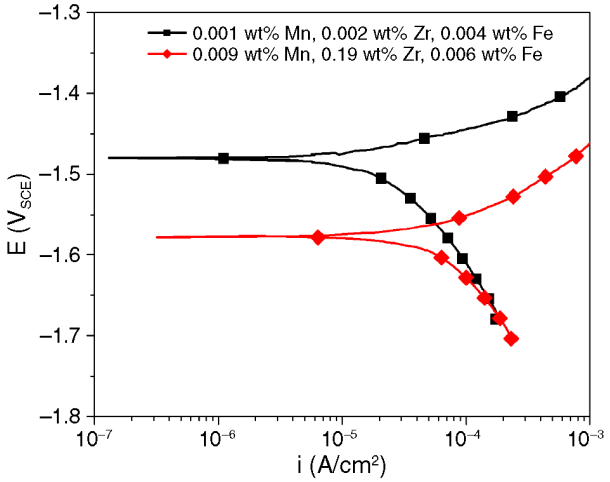

FIGURE 2. *Potentiodynamic polarization curves in 0.1 M NaCl for pure Mg and Mg specimen with high levels of Zr (0.19 wt% Zr).*

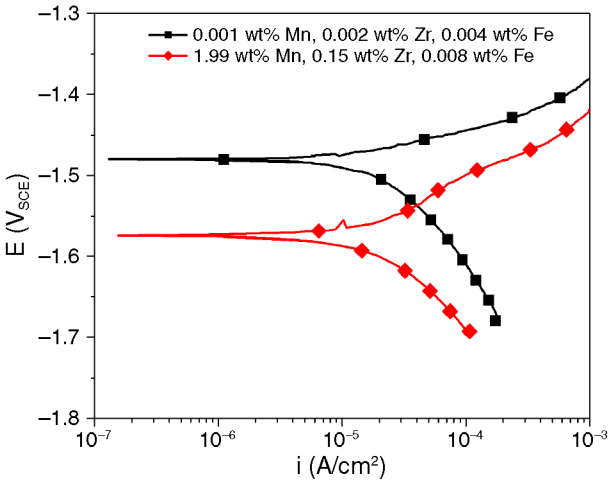

FIGURE 3. *Potentiodynamic polarization curves in 0.1 M NaCl for pure Mg and Mg specimen with high levels of Mn and low levels of Zr (1.99 wt% Mn, 0.15 wt%).*

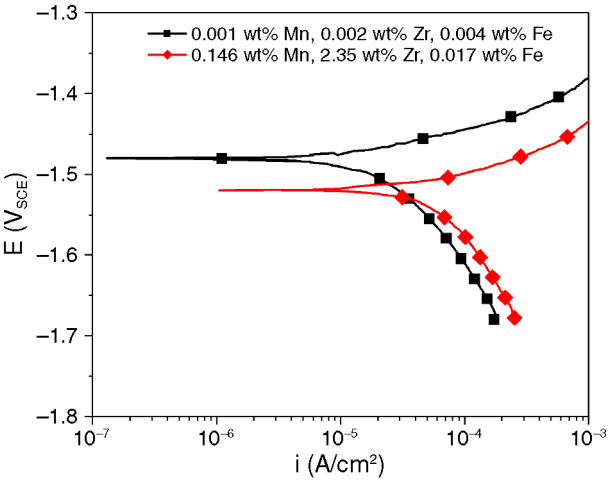

FIGURE 4. *Potentiodynamic polarization curves in 0.1 M NaCl for pure Mg and Mg specimen with high levels of Zr and low levels of Mn (2.35 wt% Zr, 0.146 wt% Mn).*

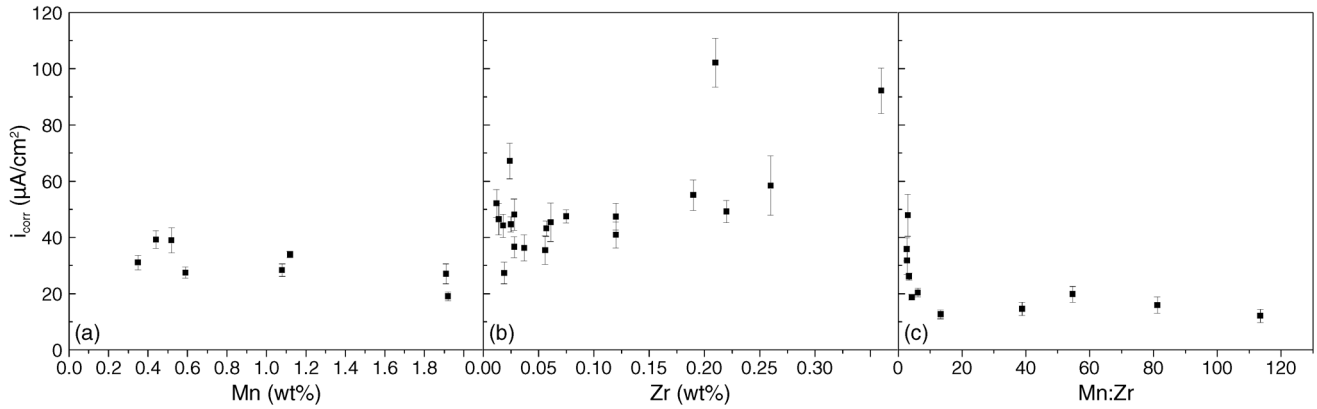

FIGURE 5. *i_{corr} values determined in 0.1 M NaCl plotted against increasing alloying content for: (a) binary Mg-Mn specimens, (b) binary Mg-Zr specimens, and (c) ternary Mg-Mn-Zr specimens.*

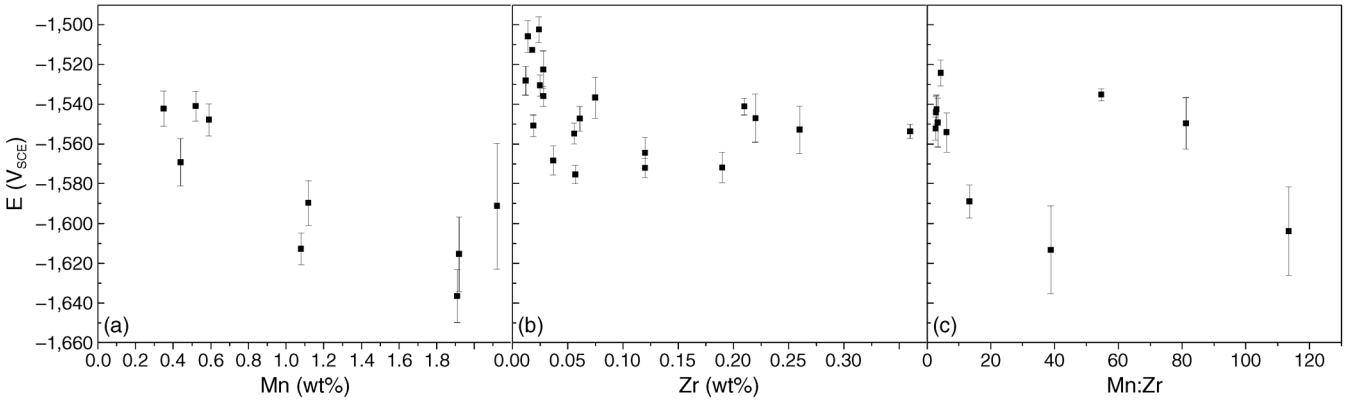

FIGURE 6. *E_{corr} values determined in 0.1 M NaCl plotted against increasing alloying content for: (a) binary Mg-Mn specimens, (b) binary Mg-Zr specimens, and (c) ternary Mg-Mn-Zr specimens.*

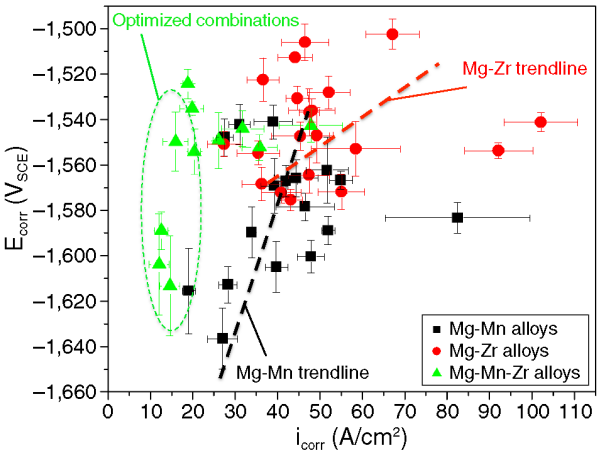

FIGURE 7. *i_{corr} vs. E_{corr} for the three Mg-alloy series produced in this work. These are binary Mg-Mn, binary Mg-Zr, and ternary Mg-Mn-Zr. All tests were conducted in 0.1 M NaCl.*

lower i_{corr} values correspond to higher Mn:Zr ratios, which is a significant observation.

Figure 6 reveals the corresponding E_{corr} values as a function of alloy composition. The data reveals that Mg-Mn alloys have an increasingly less noble E_{corr}. Mg-Zr alloys have a relatively stable E_{corr}, in spite of large variations in i_{corr} that are dictated by the combination of changes in anodic (<C_s), then cathodic, kinetics (>C_s). The Mg-Mn-Zr alloys have a complex variation.

To understand better the elementary mechanisms at play, the E_{corr} vs. i_{corr} relationship for all alloys produced and tested is seen in Figure 7.

It is shown that for the Mg-Mn alloy group, the trend observed is as i_{corr} increases, the E_{corr} value increases, which is interpreted as an indicator that the Mg-Mn system varies under the influence of the cathodic reaction kinetics. The range of E_{corr} for all the Mg-Mn alloys is ~100 mV.

In the case of the Mg-Zr alloy group, the trend is not as obvious as the Mg-Mn alloys, with a large scatter in the data and a linear fit revealing a much more subtle slope (than from Mg-Mn). The relative nobility of Zr is manifest as generally higher E_{corr} values than the Mg-Mn alloys; a variation in E_{corr} of ~80 mV between all alloys tested corresponds to significant variations in i_{corr}. The relationship between E_{corr} and i_{corr} for the Mg-Zr alloy group is under the mixed control of anodic control and later cathodic control.

The lowest measured i_{corr} values were observed for the Mg-Mn-Zr group. There is a so-called optimized region where there is little change in i_{corr} with and approximate range of 120 mV of E_{corr}. This indicates that in this Mg alloy composition region, where the Mn and Zr additions are interacting to modify anodic and cathodic kinetics (based on the Mn:Zr ratio).

Immersion Test Results

While the polarization data is indispensable in providing information about the rate-controlling mechanisms that dictate corrosion, immersion testing also was carried out to benchmark the trends observed (and to compare instantaneously collected data with a longer term metric). For the alloys tested herein, there is an obvious trend between the polarization test data and mass loss from immersion results (Figure 8). The data has been left in its native units, to avoid any complications or errors from having to assume a uniform corrosion for the polarization data. It is to be observed from this relationship in Figure 8 that for i_{corr} values below ~25 μA/cm^2, the mass-loss rates are quite low and have little variance. When the i_{corr} values are above ~60 μA/cm^2, there are high mass-loss rates with a large degree of variability. As such, the Mg-Mn-Zr alloy mixtures, which presented an i_{corr} value below ~25 μA/cm^2, are seen to have low mass loss. Between 25 μA and 60 μA, there is a wide range where the mass-loss rates appear to be more dependent on the alloy composition (and is most likely caused by variations in corrosion morphology that are outlined in the subsequent section).

Corrosion Morphologies

While the level of the Zr and Mn additions in some of the Mg alloys studied herein is below the theoretical solubility limit, there is still evidence of metallic Zr and Mn particles observed in the Mg matrix, which can influence the corrosion morphology. The presence of such particles is attributed to the combination of a necessity for infinite hold times to reach equilibrium (which is not met) and because of the master alloys used containing Zr and Mn well above the solubility limits. Elemental Zr and Mn particles were present in the master alloys and perfect mixing is also difficult to achieve during the manufacture of Mg alloys.

Mn-containing Mg alloys (Figure 9[a]) are observed generally to have uniform corrosion over the entire alloy surface. The hydroxide film that usually forms on the surface of Mg is absent from the regions that have Mn particles present (for alloys with high Mn levels). These Mn particles are essentially elemental Mn since there are no compounds that form between Mn and Mg. Pits are observed to form around the circumference of the Mn particles. This region of intensified corrosion around the Mn particles is most likely from the increased local galvanic activity in the region between the Mn particles and the Mg matrix,[15] albeit

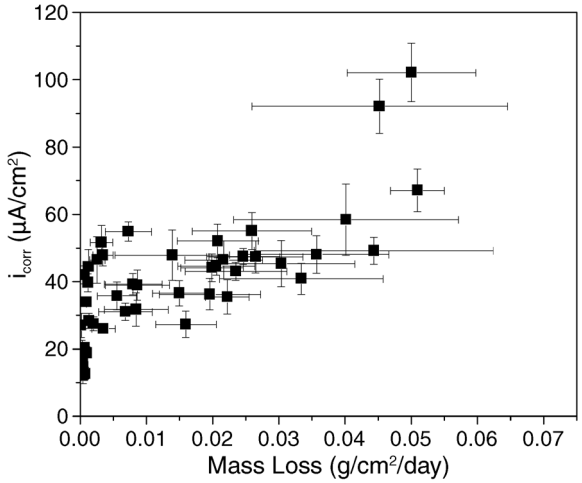

FIGURE 8. *Electrochemically determined i_{corr} vs. mass loss from immersion tests for all Mg alloy specimens reported herein. Testing was in 0.1 M NaCl solution.*

to a lesser degree than an impurity such as Fe because of the closer electrochemical potential of Mg and Mn.[13] Mechanistically, the origin of this local attack requires further work to elucidate, since any local alkalization would be expected to passivate the Mg, meaning that the mechanism of localized trenching in Mg alloys is yet to be resolved fundamentally.

Mg alloys containing low levels of Zr (Figure 9[b]) still tend to have a number of Zr particles embedded in the Mg matrix (albeit that one must attempt to seek their location by scanning the specimen) because of the low solid solubility of Zr in Mg.[16] These Zr particles are also essentially elemental Zr with no compounds forming between Zr and Mg. The particles are posited to cause microgalvanic coupling effects and inhibit the formation of protective oxide films.[22] However, in the work herein there was essentially no corrosion (at the composition in Figure 9[b]) associated with the Zr particles alone. However, significant corrosion had occurred, as evidenced by cracks extending across the alloy surface, again not appearing to be localized near Zr particles. The extensive surface corrosion and cracks are attributed to the Zr acting as an "anodic activator," which rather dramatically increases corrosion of the Mg matrix.

A Mg alloy containing high Mn and low Zr contents (Figure 9[c]) displays less intense corrosion attack across the surface compared to the high Mn-containing alloy. However, there also appears to be a reduction in the generalized corrosion over the surface and an increase in the intensity of the pitting around the Mn particles. This may be caused by either the increased Mn content further increasing the microgalvanic activity or the dissolved Zr decreasing the corrosion rate of the surrounding Mg matrix. With a high Zr content (above the Zr solid solubility limit) and a low Mn addition, Mg displays extensive corrosion across much of the metal surface (Figure

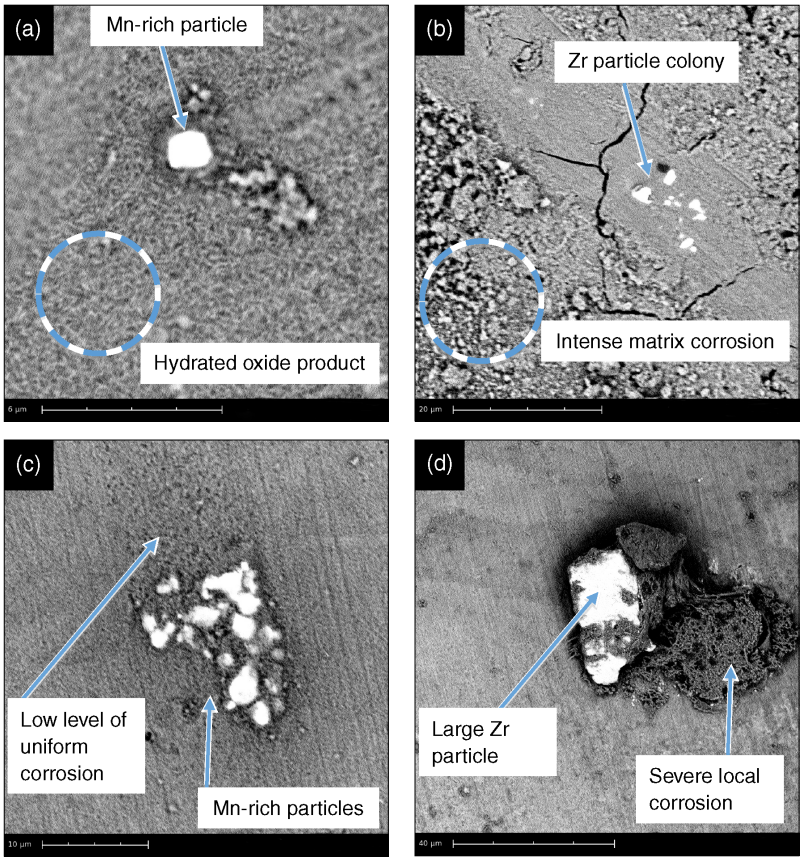

FIGURE 9. *SEM image of an (a) Mg-1.92 wt% Mn specimen after immersion in 0.1 M NaCl for 30 min, (b) Mg-0.19 wt% Zr specimen after immersion in 0.1 M NaCl for 30 min, (c) Mg-1.99 wt% Mn-0.15 wt% Zr specimen after immersion in 0.1 M NaCl for 30 min, and (d) Mg-2.35 wt% Zr-0.146 wt% Mn specimen after immersion in 0.1 M NaCl for 30 min.*

9[d]). There are much larger regions of corrosion damage spread across most of the surface compared to the sample with only Zr as an addition. Deep pits and cracks form along and near Zr particles embedded in the matrix. To give typical examples of the above phenomena, the scales of the images in Figure 9 vary for each situation.

The work herein has provided a rather comprehensive set of data and a framework for interpreting the role of Mg-Mn-Zr alloys more generally. It is obvious that further work to provide a more detailed characterization of the interaction between Mn and Zr with the Mg matrix could be conducted using SVET (the scanning vibrating electrode technique),[26] such that SVET might help to elucidate interactions within the microstructure to a greater degree than SEM alone, providing the mechanistic basis for the moderated corrosion arising from the interaction of Zr and Mn.

CONCLUSIONS

❖ The relatively low levels of Mn and Zr additions (albeit in some cases in excess of their limited solubility in Mg) reveal a marked influence on the electrochemical response and corrosion of Mg.

❖ There is a mild decrease in the corrosion of Mg as a result of a decrease in the cathodic reaction kinetics when Mn is added up to additions of ~2 wt%. This phenomenon was also concomitant with a qualitatively observed reduction in the extent of pitting on the alloy surface.

❖ There is an increase in the corrosion rate of Mg when Zr is added to Mg. Zr in solid solution in Mg acts as an anodic activator, causing what can be severe generalized attack of the matrix. Further increases in the Zr content in the binary context lead to further increases of the corrosion rate by continually enhancing the anodic activation, while simultaneously increasing the cathodic reaction kinetics, because pure Zr particles are more efficient cathodes than Mg. As such, in spite of being highly noble as a pure element, the major impact of Zr was not that of electrochemical mismatch but anodic activation.

❖ A ternary Mg-Mn-Zr alloy with Mn at ~2 wt% combined with Zr at ~0.1 wt% demonstrated the lowest corrosion rate. A corrosion rate was observed as low as 0.00026 g/cm^2/day. This complex interaction between Mn and Zr, posited to be a result of Mn-Zr interactions, was studied by investigating the effect of the Mn:Zr ratio, the E_{corr} vs. i_{corr} relationships for the

alloy classes tested. Mn was able to moderate the tolerance limit for Zr additions, which was reconciled via SEM analysis, and this is very important for commercial Mg alloys.

❖ It is obvious that further mechanistic interpretations will require detailed microscopy to elucidate the microchemical basis for such effect.

ACKNOWLEDGMENTS

The CAST Co-Operative Research Centre was established under, and is funded in part by, the Australian Governments Cooperative Research Centres Scheme. M. Sun, S. Simanjuntak, N. Kirkland (all of Monash University), A. Yob, and D. East (of CSIRO) are gratefully acknowledged for their assistance in preparing the alloys used in this research. All alloys produced in this study were made at CSIRO Process Science and Engineering, Clayton, Australia.

REFERENCES

1. D.S. Gandel, M.A. Easton, M.A. Gibson, N. Birbilis, *Corrosion* 69, 7 (2013): p. 666-671.
2. P. Cao, M. Qian, D.H. StJohn, M.T. Frost, *Mater. Sci. Technol.* 20 (2003): p. 585-592.
3. I.J. Polmear, *Light Alloys*, 3rd ed. (London, U.K.: Arnold, 1995).
4. Q. Peng, Y. Huang, K.U. Kainer, N. Hort, *Adv. Eng. Mater.* 14, 3 (2012): p. 178-184.
5. H.E. Friedrich, B.L. Mordike, *Magnesium Technology* (Berlin, Germany: Springer, 2006), 708.
6. L.L. Rokhlin, *Magnesium Alloys Containing Rare Earth Metals* (London, U.K.: Taylor & Francis Group, 2003).
7. J.A. Boyer, T*he Corrosion of Magnesium and of the Magnesium Aluminum Alloys Containing Manganese* (American Magnesium Corporation, 1927), 417-454.
8. A.F. Smith, *Acta Metall.* 15 (1967): p. 1867-1873.
9. H. Okamoto, *J. Phase Equilib. Diffus.* 29, 2 (2008): p. 208-209.
10. X. Zhang, D. Kevorkov, I.-H. Jung, M. Pekguleryuz, *J. Alloys Compd.* 482 (2009): p. 420-428.
11. P. Cao, M. Qian, D. StJohn, *Scr. Mater.* 54 (2006): p. 1853-1858.
12. M. Liu, P.J. Uggowitzer, P. Schmutz, A. Atrens, *J. Mater.* 60, 12 (2008).
13. A.D. Sudholz, N.T. Kirkland, R.G. Buchheit, N. Birbilis, *Electrochem. Solid-State Lett.s* 14, 2 (2011): p. C5-C7.
14. S.L. Sin, D. Dube, R. Tremblay, *Mater. Charact.* 58 (2007): p. 989-996.
15. G.T. Parthiban, N. Palaniswamy, V. Sivan, *Anti-Corros. Methods Mater.* 56, 2 (2009): p. 79-83.
16. H. Okamoto, *J. Phase Equilib. Diffus.* 28, 3 (2007): p. 305-306.
17. G. Song, D. StJohn, *J. Light Met.* 2 (2002): p. 1-16.
18. M. Qian, D.H. StJohn, M.T. Frost, "Zirconium Alloying and Grain Refinement of Magnesium Alloys," in *Magnesium Technology 2003*, ed. H.I. Kaplan (Warrendale, PA: The Minerals, Metals, and Materials Society [TMS] 2003).
19. M. Qian, D.H. StJohn, *Int. J. Cast Met. Res.*22, 1-4 (2009): p. 256-259.
20. G. Ben-Hamu, D. Eliezer, K.S. Shin, S. Cohen, *J. Alloys Compd.* 341 (2007): p. 269-276.
21. Z. Rong-chang, Z. Jin, H. Wei-Jiu, W. Dietzel, K.U. Kainer, C. Blawert, K.E. Wei, *Trans. Nonferrous Met. Soc. China* (2006): p. 763-771.
22. W.C. Neil, M. Forsyth, P.C. Howlett, C.R. Hutchinson, B.R.W. Hinton, *Corros. Sci.* 51 (2009): p. 387-394.
23. M.A. Easton, C.H.J. Davies, M.R. Barnett, F. Pravdic, *Mater. Sci. Forum* 539-543 (2007): p. 1729-1734.
24. J.E. Hillis, "The Effects of Heavy Metal Contamination on Magnesium Corrosion Performance," in *Light Metal Age* (Warrendale, PA: SAE International, 1983), p. 25-29.
25. J.G. Kim, A.J. Koo, *Corros. Sci.* 56, 4 (2000): p. 380-388.
26. G. Williams, K. Gusieva, N. Birbilis, *Corrosion* 68, 6 (2012): p. 489-498.

APPENDIX 1

Composition of alloys produced in this study as tested via ICP-AES.

Sample ID	Mg wt%	Mn wt%	Zr wt%	Fe wt%
Mg-Mn no.1	~Bal.	1.92	<0.01	0.015
Mg-Mn no.2	~Bal.	1.91	<0.01	0.012
Mg-Mn no.3	~Bal.	1.08	<0.01	0.015
Mg-Mn no.4	~Bal.	1.12	<0.01	0.02
Mg-Mn no.5	~Bal.	1.11	<0.01	0.043
Mg-Mn no.6	~Bal.	0.72	<0.01	0.027
Mg-Mn no.7	~Bal.	0.7	<0.01	0.023
Mg-Mn no.8	~Bal.	0.65	<0.01	0.023
Mg-Mn no.9	~Bal.	0.59	<0.01	0.007
Mg-Mn no.10	~Bal.	0.52	<0.01	0.008
Mg-Mn no.11	~Bal.	0.44	<0.01	0.016
Mg-Mn no.12	~Bal.	0.35	<0.01	0.011
Mg-Mn no.13	~Bal.	0.6	<0.01	0.054
Mg-Mn no.14	~Bal.	0.77	<0.01	0.071
Mg-Mn no.15	~Bal.	0.81	<0.01	0.048
Mg-Mn-Zr no.1	~Bal.	1.93	0.017	0.006
Mg-Mn-Zr no.2	~Bal.	1.95	0.024	0.006
Mg-Mn-Zr no.3	~Bal.	1.97	0.036	0.007
Mg-Mn-Zr no.4	~Bal.	1.98	0.051	0.005
Mg-Mn-Zr no.5	~Bal.	1.99	0.15	0.008
Mg-Mn-Zr no.6	~Bal.	2.03	0.33	0.013
Mg-Mn-Zr no.7	~Bal.	2.04	0.48	0.019
Mg-Mn-Zr no.8	~Bal.	2.07	0.61	0.018
Mg-Mn-Zr no.9	~Bal.	2	0.72	0.018
Mg-Mn-Zr no.10	~Bal.	2.04	0.77	0.021
Mg-Mn-Zr no.11	~Bal.	2.03	0.68	0.025
Mg-Zr-Mn no.1	~Bal.	0.146	2.35	0.017
Mg-Zr no.1	~Bal.	0.018	0.028	0.01
Mg-Zr no.2	~Bal.	0.015	0.012	0.008
Mg-Zr no.3	~Bal.	0.015	0.061	0.01
Mg-Zr no.4	~Bal.	0.015	0.014	0.008
Mg-Zr no.5	~Bal.	0.014	0.12	0.011
Mg-Zr no.6	~Bal.	0.014	0.019	0.005
Mg-Zr no.7	~Bal.	0.014	0.22	0.014
Mg-Zr no.8	~Bal.	0.014	0.037	0.006
Mg-Zr no.9	~Bal.	0.014	0.36	0.016
Mg-Zr no.10	~Bal.	0.014	0.26	0.013
Mg-Zr no.11	~Bal.	0.008	0.028	0.006
Mg-Zr no.12	~Bal.	0.008	0.018	0.006
Mg-Zr no.13	~Bal.	0.009	0.057	0.006
Mg-Zr no.14	~Bal.	0.009	0.025	0.005
Mg-Zr no.15	~Bal.	0.009	0.12	0.001
Mg-Zr no.16	~Bal.	0.009	0.056	0.005
Mg-Zr no.17	~Bal.	0.009	0.19	0.006
Mg-Zr no.18	~Bal.	0.009	0.075	0.013
Mg-Zr no.19	~Bal.	0.01	0.21	0.13
Mg-Zr no.20	~Bal.	0.009	0.024	0.017

This page is intentionally left blank

Chapter 5.2

Effect of Mn and Zr on the corrosion behaviour of Mg – Continued

This page is intentionally left blank

Chapter 5.2: Effect of Mn and Zr on the corrosion behaviour of Mg – Continued

5.2.1 Introduction

The purpose of this section (§5.2) is to provide further information and context that is not covered in the associated paper (§5.1), however which is relevant to the dissertation overall.

As has been outlined in this dissertation, Manganese (Mn) and zirconium (Zr) are two possible candidates for alloying additions to potentially counter the detrimental effects of Fe impurities in Mg; however more generally, even in the absence of beneficial effects, their influence warrants critical research.

The sections §3.3.2 and §5.1 provide original research to address the paucity of published reports on Mg alloys which contain both Mn and Zr. However, a review of the available literature suggests that not only are Fe impurities in Mg alloys soluble in the Mn-Zr intermetallic phases which form, but that Zr, Mn and Fe may combine to become a unique intermetallic particles in the Mg melt prior to casting. These particles are then able to settle out of the Mg melt to the bottom of the processing vessel as 'sludge' [98], which is descriptive word to indicate the combination of elements more dense than Mg that can settle due to gravity.

This section herein gives principal focuses on the impact of Fe when Mn and/or Zr are added to Mg during the casting process, expressly on the relative effectiveness of Mn and/or Zr on Fe removal and control. This is a key component of the thesis (since it firmly addresses the Mn and Zr versus Fe aspect. Hence, this section is included as a unique thesis portion.

5.2.2 Experimental Methods

5.2.2.1 Samples

Mg alloys were produced by combining Mg-Mn, Mg-Zr and Mg-Fe master alloys with commercially pure Mg (>99.9%) in a resistance furnace with Sulfur Hexafluoride (SF_6) as a cover gas. The pure Mg was initially melted in the furnace and small amounts of the master alloys were weighed and added according to their calculated Mn/Zr/Fe contents to achieve specific Mn/Zr/Fe levels in the cast alloys. After melting, the alloys were poured into a cast iron mould and allowed to air cool. Three series of alloys were produced, two with only Mn or Zr as singular additions and one with both Mn and Zr as additions. All three series had Fe added into the melt. Table 5.2.1 below shows the levels of each alloying addition in the specimens tested as well as a commercially pure Mg test specimen. The composition of each alloy determined by inductively coupled plasma atomic emission spectroscopy (ICP-AES) by Spectrometer Services (Coburg, Vic, Australia). All alloy compositions reported are those taken after solidification.

Table 5.2.1 – Elemental compositions of Mg-alloys produced for this study. The notation "S" refers to Mg-Zr alloys that were stirred prior to casting and "US" refers to un-stirred. All compositions are in wt. %.

Sample ID	Mg%	Mn%	Zr%	Fe%
Mg-Mn-Fe no.1	~Bal	1.92	<0.01	0.015
Mg-Mn-Fe no.2	~Bal	1.91	<0.01	0.012
Mg-Mn-Fe no.3	~Bal	1.08	<0.01	0.015
Mg-Mn-Fe no.4	~Bal	1.12	<0.01	0.02
Mg-Mn-Fe no.5	~Bal	1.11	<0.01	0.043
Mg-Mn-Fe no.6	~Bal	0.72	<0.01	0.027
Mg-Mn-Fe no.7	~Bal	0.7	<0.01	0.023
Mg-Mn-Fe no.8	~Bal	0.65	<0.01	0.023
Mg-Mn-Fe no.9	~Bal	0.59	<0.01	0.007
Mg-Mn-Fe no.10	~Bal	0.52	<0.01	0.008
Mg-Mn-Fe no.11	~Bal	0.44	<0.01	0.016
Mg-Mn-Fe no.12	~Bal	0.35	<0.01	0.011
Mg-Mn-Fe no.13	~Bal	0.6	<0.01	0.054
Mg-Mn-Fe no.14	~Bal	0.77	<0.01	0.071
Mg-Mn-Fe no.15	~Bal	0.81	<0.01	0.048
Mg-Mn-Fe no.16	~Bal	0.61	<0.01	0.012
Mg-Mn-Fe no.17	~Bal	1.13	<0.01	0.035
Mg-Mn-Fe no.18	~Bal	2.31	<0.01	0.056
Mg-Mn-Fe no.19	~Bal	4.07	<0.01	0.061
Mg-Mn-Fe no.20	~Bal	3.94	<0.01	0.002
Mg-Mn-Zr no.1	~Bal	1.93	0.017	0.006
Mg-Mn-Zr no.2	~Bal	1.95	0.024	0.006
Mg-Mn-Zr no.3	~Bal	1.97	0.036	0.007
Mg-Mn-Zr no.4	~Bal	1.98	0.051	0.005

Sample ID	Mg%	Mn%	Zr%	Fe%
Mg-Mn-Zr no.5	~Bal	1.99	0.15	0.008
Mg-Mn-Zr no.6	~Bal	2.03	0.33	0.013
Mg-Mn-Zr no.7	~Bal	2.04	0.48	0.019
Mg-Mn-Zr no.8	~Bal	2.07	0.61	0.018
Mg-Mn-Zr no.9	~Bal	2	0.72	0.018
Mg-Mn-Zr no.10	~Bal	2.04	0.77	0.021
Mg-Mn-Zr no.11	~Bal	2.03	0.68	0.025
Mg-Zr AM no.1 S	~Bal	0.018	0.028	0.01
Mg-Zr AM no.1 US	~Bal	0.015	0.012	0.008
Mg-Zr AM no.2 S	~Bal	0.015	0.061	0.01
Mg-Zr AM no.2 US	~Bal	0.015	0.014	0.008
Mg-Zr AM no.3 S	~Bal	0.014	0.12	0.011
Mg-Zr AM no.3 US	~Bal	0.014	0.019	0.005
Mg-Zr AM no.4 S	~Bal	0.014	0.22	0.014
Mg-Zr AM no.4 US	~Bal	0.014	0.037	0.006
Mg-Zr ZIR no.1 S	~Bal	0.008	0.028	0.006
Mg-Zr ZIR no.1 US	~Bal	0.008	0.018	0.006
Mg-Zr ZIR no.2 S	~Bal	0.009	0.057	0.006
Mg-Zr ZIR no.2 US	~Bal	0.009	0.025	0.005
Mg-Zr ZIR no.3 S	~Bal	0.009	0.12	0.001
Mg-Zr ZIR no.3 US	~Bal	0.009	0.056	0.005
Mg-Zr ZIR no.4 S	~Bal	0.009	0.19	0.006
Mg-Zr ZIR no.4 US	~Bal	0.009	0.075	0.013
Pure Mg	~Bal	0.001	0.002	0.001

2.2 Electrochemical and Weight loss testing

Prior to testing, the metal surfaces were ground to a 2000 grit surface finish. A 3-electrode electrochemical flat-cell with an exposed sample area of 1 cm^2 was used in conjunction with a 0.1M NaCl electrolyte. A VMP 3Z potentiostat was used, with potentiodynamic polarisation conducted at 1 mV/s. Prior to polarisation, samples were conditioned for ten minutes at open circuit to ascertain a relatively stable potential. The polarisation curves were used to determine i_{corr} (via a Tafel-type fit) using EC-Lab software. Such fitting is inherently difficult; however the ability of EC-lab to allow manual control is critical. As a general rule, fits were executed by selecting a portion of the curve that commenced >50mV from E_{corr}, and i_{corr} was subsequently estimated from the value where the fit intercepted the potential value of the true E_{corr}. Polarisation testing was also able to visually reveal comparative information related to the kinetics of both the anodic and cathodic reactions of the various Mg specimens. Each sample was tested five times and an average result was determined.

Weight loss testing was also done to provide a longer-term comparison of alloy corrosion and was determined by immersion of samples in 0.1M NaCl for a period of 24 hours. The corrosion products were subsequently removed by light scrubbing following a 3s immersion in dilute (15%) HNO_3. The mass loss was determined on three unique samples and an average result was determined and reported.

2.3 SEM and EDXS

The microstructures of the alloys were examined via scanning electron microscopy. Alloy samples were polished to a 1μm diamond paste finish and etched with a picric acid solution. They were then imaged using either an FEI Phenom or JEOL 840A; the latter microscope also capable of EDXS analysis for determination of elemental composition of the particles observed in the alloy microstructure.

5.2.3 Results

Iron (Fe) was deliberately added to the Mn and Zr containing alloys to have an approximate concentration of several hundred ppm, ensuring that the Fe content was above any reported Fe tolerance limit in Mg from the literature [1, 45]. As the Mn content in Mg is increased, the Fe concentration appears to have no correlation to the Mn content (i.e. this implies that Mn is

not having a systematic effect at removing Fe from the melt via gravity or sludge formation). This is quite evident as a number of the samples with up to 1 wt.% Mn still have a Fe level of over 400ppm (Figure 5.2.1). The low(er) Fe levels in the high Mn containing samples appears to be fortuitous – but (as described below) indicative of the scatter and not of any systematic purification. As such, the purpose of Figure 5.2.1 is to visually indicate no trend where additional Mn reduces the Fe content.

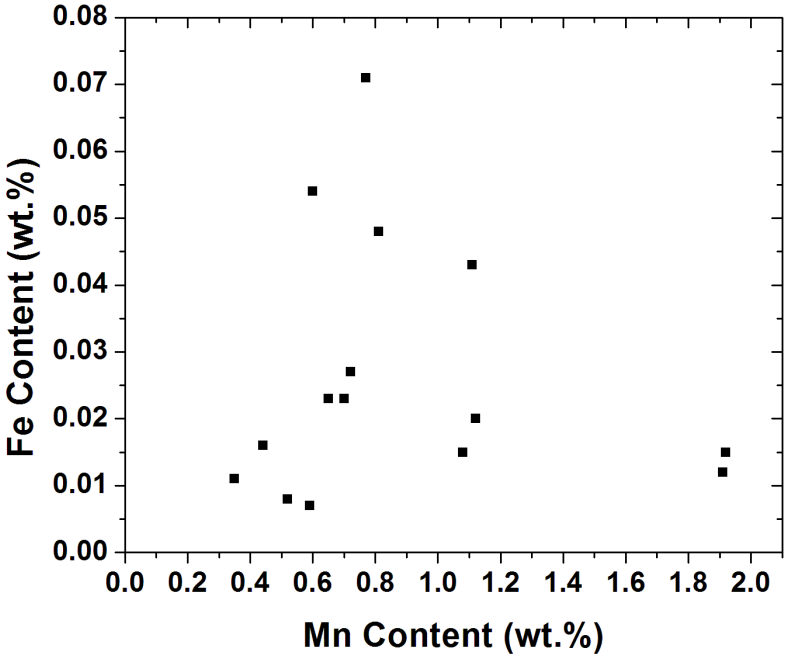

Figure 5.2.1 - Mn content (wt.%) vs. Fe content (wt.%) as determined by ICP-AES for the Mg-Mn(-Fe) alloys investigated.

When Zr was added to Mg (Figure 5.2.2), it is observed that there is systematically a lower Fe content. The data in Figure 5.2.2 also indicates that the Fe content in the Zr containing alloys will be lower irrespective of the overall Zr content. Such results confirm assertions in published studies in that the addition of Zr is effective at lowering the Fe impurity content in the Mg alloy [8, 20, 24]. None the less, as elementary and straightforward as Figure 5.2.2 appears, such information over a range of custom alloys and indicating the extent of the effect has not been previously shown.

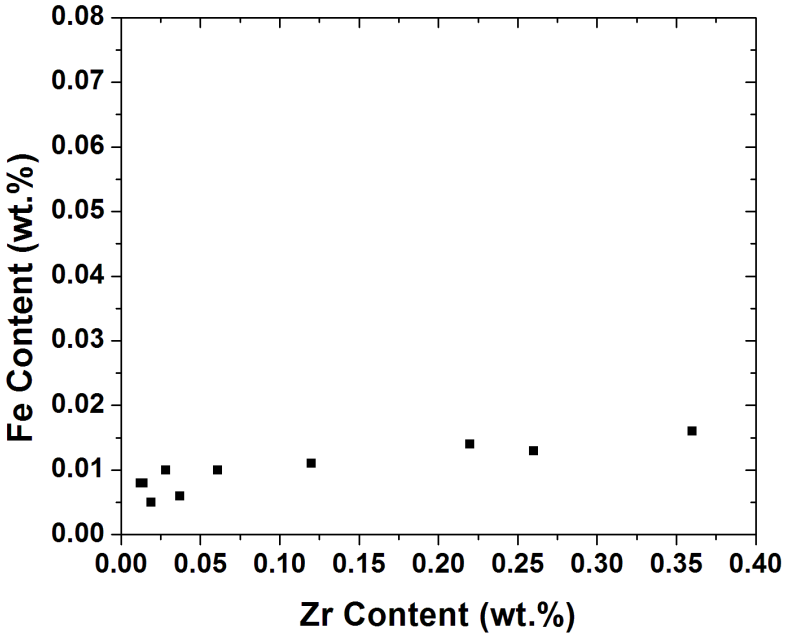

Figure 5.2.2 - Zr content (wt.%) vs. Fe content (wt.%) as determined by ICP-AES for the Mg-Zr(-Fe) alloys investigated.

The relative effects of Mn, Zr and Fe on Mg are best presented via contour plots where their compositional contents are presented in contrast with the measured corrosion rates - providing a visual assessment of the overall test results obtained. The contour plots were constructed using Origin®, and the darker shaded (viz. tending to dark blue) areas display regions with lower measured corrosion rates, whereas increasing brightness (viz. tending to red) on the contour plots depicts an increase in the overall corrosion rate. The grey dots on the contour plots correspond to the actual compositions of the Mg alloy samples tested.

Figure 5.2.3 reveals the contour plot of the Mg-Mn(-Fe) alloys presenting the Mn and Fe contents versus their corrosion rate as determined from 24 hr weight loss. The contour plot indicates that as the Fe content is increased there is an increase in the corrosion rate of Mg, as anticipated. However, as the Mn content is increased, the corrosion rate of Mg initially decreases before starting to increase again at higher Mn levels. This reduction in the corrosion rate of Mg caused by the addition of Mn is observed to behave in a roughly linear fashion, even in the presence of higher Fe levels in the alloy.

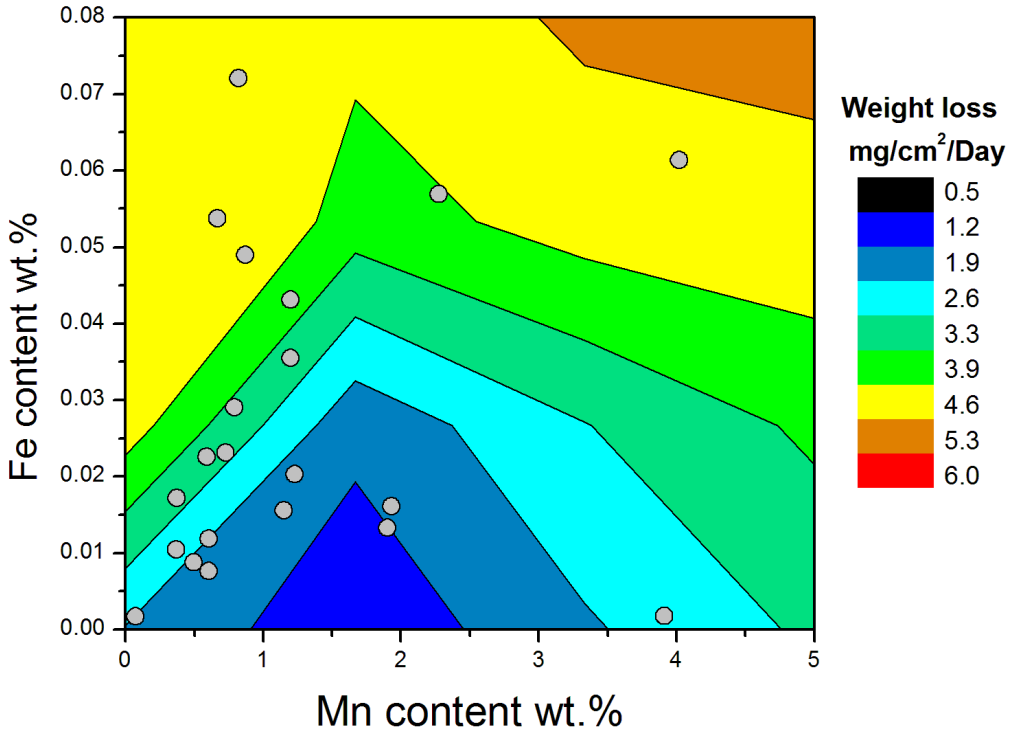

Figure 5.2.3 - Contour plot of the corrosion rate (expressed here as mg/cm^2/day from 24 h weight loss testing) as a function of Mn wt.% vs. Fe wt.%.

EDXS analyses of the Mn particles that are present in the Mg matrix confirm that they are not Mg-Mn intermetallic phases (Figure 5.2.4) and that the Fe present in the Mg matrix is combined with an Mn component where they form an Mn-Fe intermetallic particle in the matrix (a notion expanded elsewhere in the thesis by more advanced characterisation).

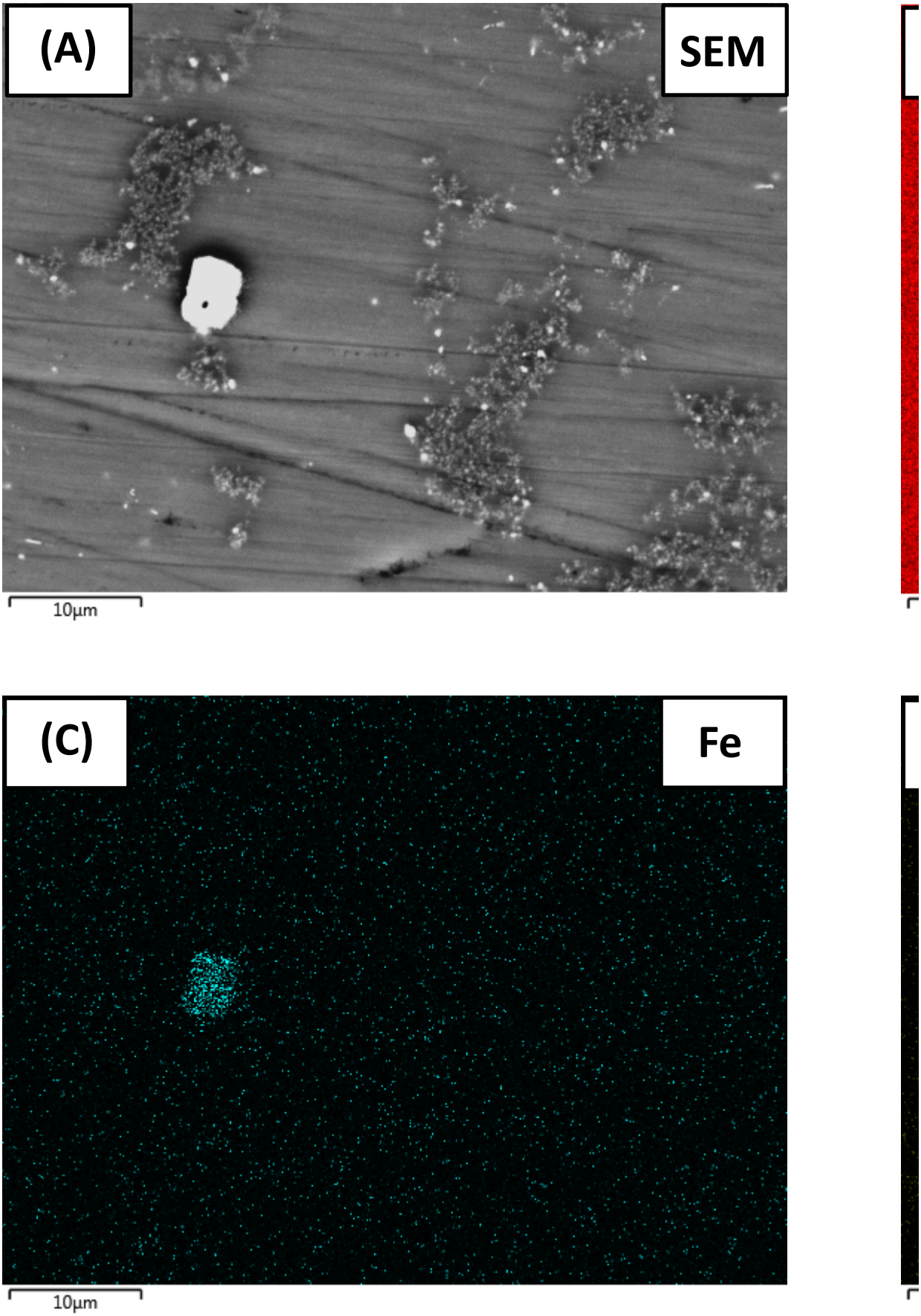

Figure 5.2.4 – EDXS map of a Mn-Fe particle in the Mg-Mn-Fe no.5 alloy of the Mg-Mn-Fe

series produced in this study.

The contour plot of the calculated i_{corr} values for the Mg specimens containing Zr and Fe shows that with increasing Fe content the corrosion rate increases (Figure 5.2.5). However, Zr has a negative impact on the corrosion rate of Mg. As the Zr content of the Mg alloy was increased the corrosion rate continued to increase. EDXS analysis of the Zr particles that are present in the Mg matrix confirm that they are essentially pure Zr particles and are not Mg-Zr intermetallic phases (Figure 5.2.6).

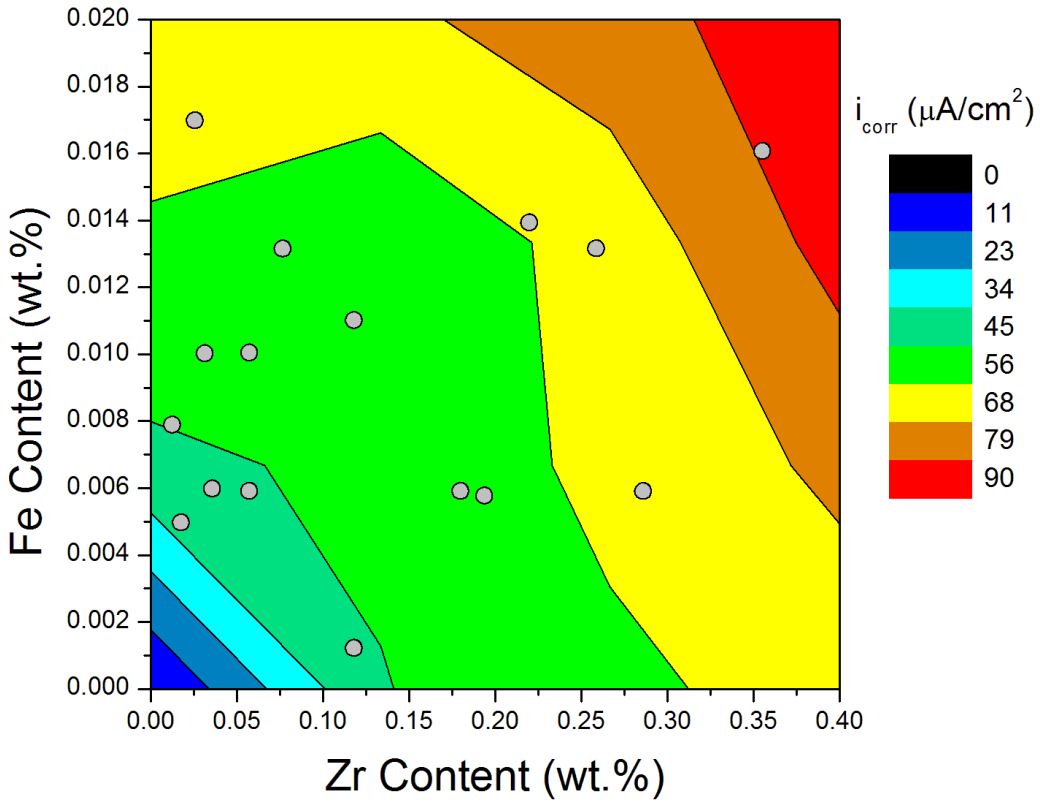

Figure 5.2.5 - Contour plot of the corrosion rate as a function of Zr wt.% vs. Fe wt.%.

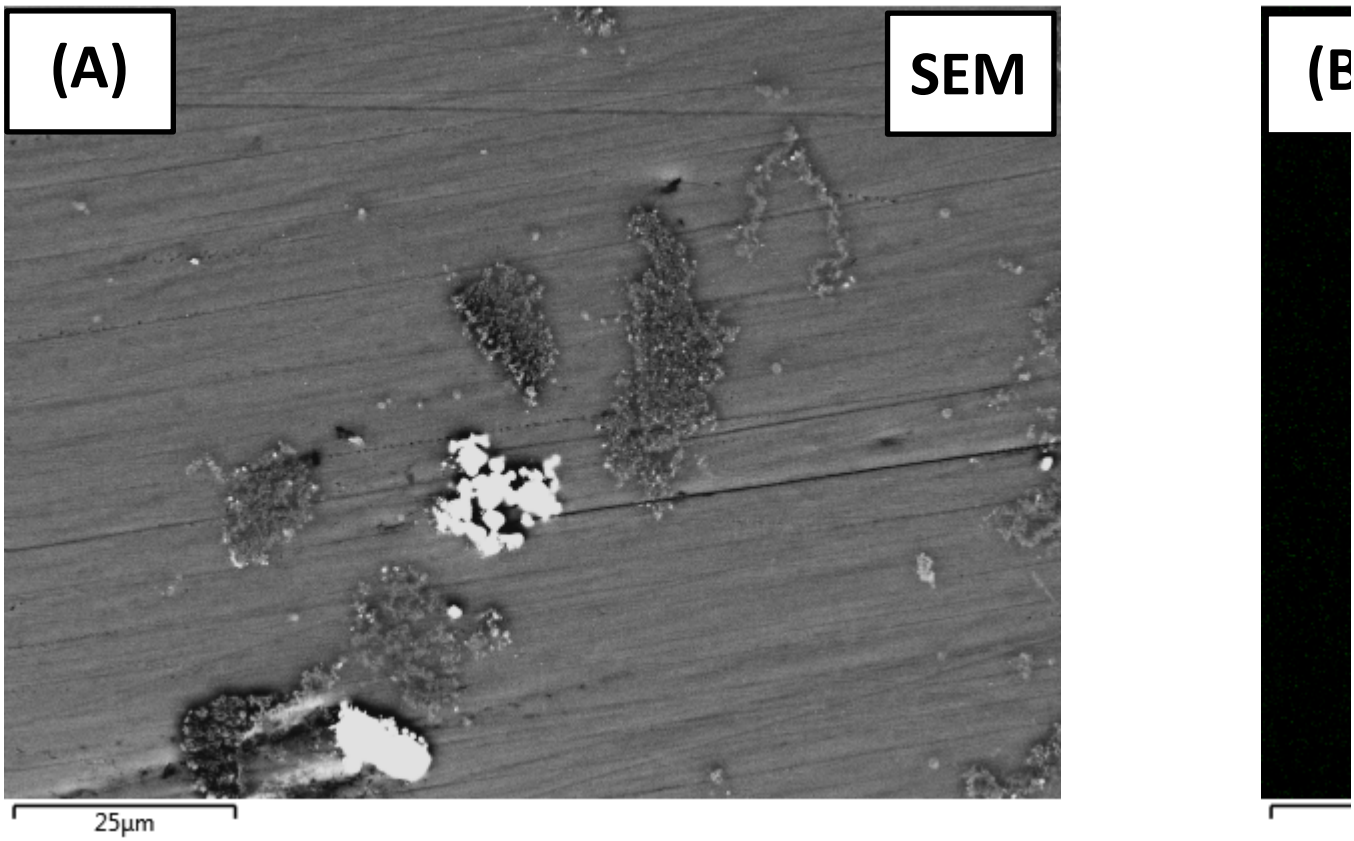

Figure 5.2.6 – EDXS map of a Zr particle in the Mg-Zr no.3 AM S alloy of the Mg-Zr series produced in this study.

The electrochemical polarisation behaviour of a Mg-Mn specimen with 1.08wt.% Mn and 150ppm Fe was compared to that of Pure Mg with approximately 40ppm Fe (Figure 5.2.7). The polarisation curves reveal a significant decrease in the cathodic reaction kinetics when Mn is added to Mg compared to the pure Mg specimen. This is despite the fact that the Mn containing specimen has an Fe impurity content of 150ppm, which is close to the critical Fe tolerance limit that leads to increased corrosion rates [1, 43]. This behaviour demonstrates that Mn can decrease the corrosion rate despite the presence of a large Fe content. The physical reason for why Mn may retard the high cathodic kinetics associated with Fe impurities is the basis for the chapter 7 further below.

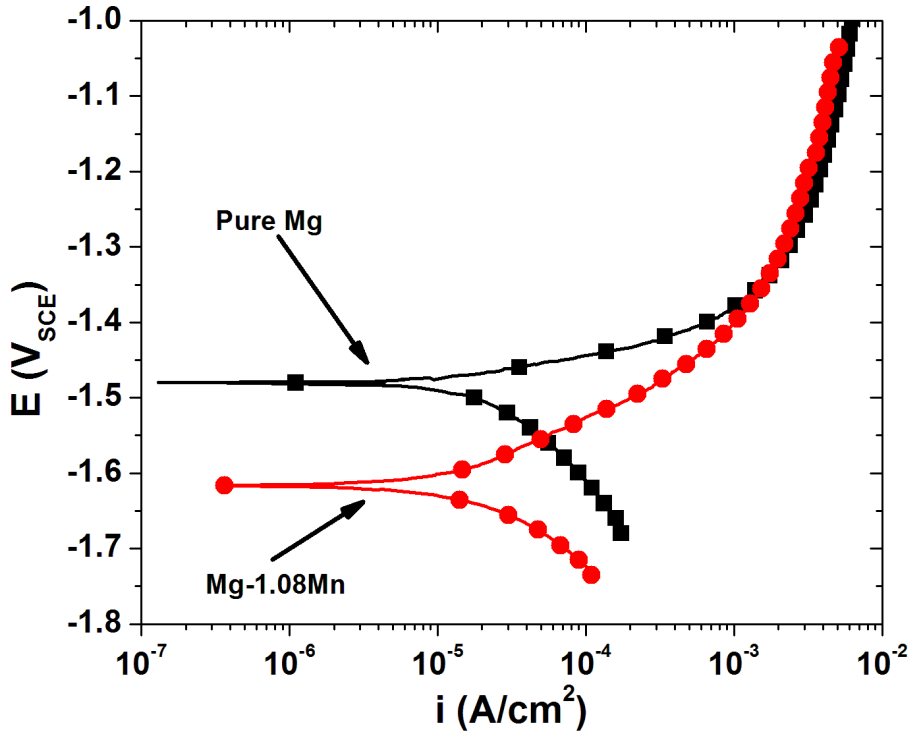

Figure 5.2.7 - Polarisation curves for the Pure Mg (40 ppm Fe) and Mg-Mn-Fe no.3 (1.08 wt.% Mn and 150 ppm Fe) alloy samples measured in a 0.1M NaCl solution.

The calculated i_{corr} values and standard error for the individual Mg-Mn-Zr, Mg-Mn-Fe and Mg-Zr alloys with the lowest i_{corr} values from each alloy group are seen in Figure 5.2.8. The data indicates that the Mg alloy with the lowest current density is the Mg-Mn-Zr no.5 alloy. The Mg-Mn-Zr no.5 alloy has a Mn content of ~2 wt.% Mn and 0.15 wt.% Zr. The next alloy group to show the next best corrosion performance was the Mg-Mn-Fe series with the Mg-Zr alloys showing the highest corrosion rates.

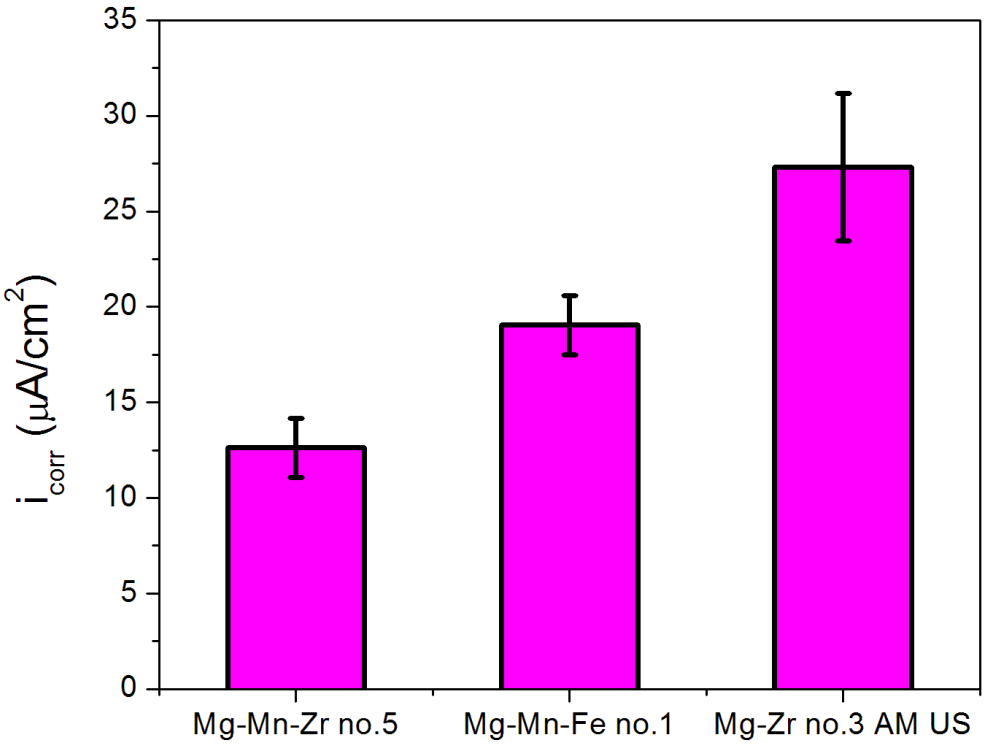

Figure 5.2.8 - Lowest i_{corr} values measured during electrochemical polarisation testing in a 0.1M NaCl solution for the alloys: Mg-Mn-Zr no.5 (with and Mn content of 1.99 wt.% and a Zr content of 0.15 wt.%), Mg-Mn-Fe no.1 (with and Mn content of 1.92 wt.% and a Fe content of 0.015 wt.%) and Mg-Zr no.3 AM US (with and Zr content of 0.019 wt.% and a Fe content of 0.005 wt.%).

5.2.4 Discussion

According to Figure 5.2.1, there does not appear to be the commonly misreported 'scavenging' effect [93] of Mn on Fe in the Mg-Mn alloy group as the Fe content seems to be unaffected by the Mn content. However, Mn is still very effective at inhibition of the deleterious effect of the Fe impurities present in the Mg matrix. As shown in Figure 5.2.3, when the Fe content increases, the corrosion rate increases, yet, when the Mn content increases, the corrosion rate decreases despite an elevated Fe content. This behavior is also observed in the polarisation kinetics in Figure 5.2.7, where the cathodic corrosion kinetics of Mg are reduced when Mn is added, despite the high Fe content which should lead to an increase in the cathodic kinetics. It has been reported [47] that pure Mn has lower cathodic

kinetics than pure Fe, and how this point may be manifest into the behavior observed herein is elaborated in Chapter 7, further below.

On the basis of the corrosion data alone, one can assert an interaction between Mn and Fe that is capable of increasing the Fe tolerance limit in Mg, allowing higher Fe impurity levels to be present before the impurities begin to cause detrimental and rapid corrosion. Thus, while Mn does not appear to remove Fe from the Mg alloy, it is still very effective in reducing the negative impact of Fe impurities on Mg – most importantly, in the absence of Al in the alloy composition.

Despite the fact that the Mg-Zr alloys produced herein all have varying levels of Fe (Figure 5.2.2), Zr is itself detrimental for the corrosion of Mg alloys. It is revealed in this dissertation (chapter 6) that both Zr present in solid solution acts as an anodic activator of Mg and Zr particles that form in the Mg matrix act as micro-galvanic sites for accelerated corrosion [117]. The increase in the corrosion rate can be observed when either the Fe or Zr levels are increased (Figure 5.2.5). Thus, while Zr is very effective at removing the detrimental Fe impurities from Mg, Zr additions invariably lead to further issues that increase the corrosion rate of Mg.

While it is known that the Zr-Fe interaction removes Fe impurities from Mg, recent work has put forth that Mn_2Zr particles can also remove Fe impurities from Mg [98]. However, the Mn_2Zr particles that form when both Mn and Zr are added to Mg are also insoluble, and can settle out of the Mg melt during processing. The combined Mg-Mn-Zr no.5 alloy with approximately ~2 wt.% Mn and 0.15 wt.% Zr has the lowest i_{corr} levels of 12.5 $\mu A/cm^2$ (and a corresponding weight loss of 0.42 $mg/cm^2/day$). When compared to the Mg-Mn and Mg-Zr alloy groups, the specimens with the lowest measured i_{corr} values of 19 $\mu A/cm^2$ and 27 $\mu A/cm^2$ respectively, the i_{corr} value of 12.5 $\mu A/cm^2$ for the Mg-Mn-Zr alloy is statistically below these values (Figure 5.2.8). This decrease in the corrosion rate may be attributed to two factors; firstly that the Zr addition initially removes the Fe impurities and secondly that the Zr addition is then itself removed by the addition of Mn to the Mg melt. This produces an Mg alloy with both low Fe and Zr levels.

5.2.5 Summary

- The addition of Mn was observed to be beneficial in reducing the deleterious impact of Fe impurities on Mg, even in the absence of Al. This was asserted based on the outcomes of polarisation and weight loss testing. Whilst it is not mechanistically elaborated here from a physical sense (done elsewhere in the thesis), it appears that the presence of Mn is able to moderate cathodic kinetics in situations when Fe is present. This is the electrochemical rationalisation of the effect. We note that that Mn is inefficient at removing Fe from the Mg alloy. At higher levels of Mn (i.e. > ~1.6 wt.%) , Mn is also capable of increasing the corrosion rate of Mg.
- The critical tolerance limit for Fe in Mg (which is often reported as a fixed value of roughly ~170ppm [1, 45]) is not observed to be a fixed/single value when Mn is added to Mg. With an increasing Mn content, the Fe tolerance limit is also increased, with the precise tolerance limit dependant on the combination of both Mn and Fe (as likely any functional alloying additions to the alloy) present in the Mg alloy. These findings are original on the basis that prior works have not systematically produced alloys for the purposes of work such as that herein.
- Zirconium is effective at removing the Fe from the Mg melt, however the Zr itself is deleterious for corrosion of Mg. This is rationalised (electrochemically) on the basis that the anodic reaction kinetics are increased by Zr dissolved in solid-solution, and the cathodic reaction kinetics are increased as Zr particles are present in the Mg matrix above the Zr solubility limit, respectively [117].
- Of the Mg alloys produced and examined herein, an alloy with higher levels of Mn combined with low levels of Zr demonstrated the lowest corrosion rate. The cause of this is posited to be that the Zr additions first removed the Fe, and then the Mn removed the excess Zr and rendered the remaining Fe and Zr less detrimental in the Mg matrix.

This page is intentionally left blank

Chapter 6

The influence of zirconium additions on the corrosion of magnesium

This page is intentionally left blank

Corrosion Science 81 (2014) 27–35

Contents lists available at ScienceDirect

Corrosion Science

journal homepage: www.elsevier.com/locate/corsci

The influence of zirconium additions on the corrosion of magnesium

D.S. Gandel [a,b,*], M.A. Easton [a,b], M.A. Gibson [a,c], T. Abbott [a,d], N. Birbilis [a,b]

[a] CAST Cooperative Research Centre, Australia
[b] Department of Materials Engineering, Monash University, Clayton, VIC 3800, Australia
[c] CSIRO Process Science and Engineering, Clayton, VIC 3168, Australia
[d] Magontec Limited, Sydney, NSW 2000, Australia

ARTICLE INFO

Article history:
Received 23 April 2013
Accepted 29 November 2013
Available online 5 December 2013

Keywords:
A. Magnesium
A. Zirconium
B. Polarisation
B. Weight loss
B. SEM

ABSTRACT

Sixteen custom binary Mg–Zr alloys and four commercial Zr-containing Mg-alloys were used to investigate the role of Zr on the corrosion of Mg. Mg–Zr alloys were manufactured with a range of different Zr concentrations. It was observed that the Mg–Zr alloys with a smaller mean Zr particle size had more Zr dissolved in solid solution. Both the Zr in solid solution and in metallic particle form were observed to have a deleterious effect on the corrosion rate of Mg. However, this deleterious effect is less pronounced to effect in alloys with multiple alloying additions.

1. Introduction

Zirconium (Zr) is a common alloying element in magnesium (Mg) alloys. It has a low solid solubility of 0.73 at.% in Mg and does not form any intermetallic phases with Mg [1]. Zr is added to Mg alloys because of its unique and potent ability to refine the grain size of Mg alloys [2–4]. The subsequent reduction in grain size significantly improves both the casting quality and mechanical properties of Mg alloys [5–7], traits that are desired and modified for specific industrial applications. For this reason, Zr is incorporated into several commercially available alloys such as WE54, ZE41, ZK60 and AM-SC1 [8–11]. More recent developments have seen Mg alloys that contain Zr being tested for use in biomedical applications [12]. Thus, there is a substantial and growing interest in Mg alloys, necessitating a fundamental understanding of the influence of Zr additions on the corrosion of Mg.

Some previous studies have reported that the addition of Zr to Mg is beneficial for improving the corrosion resistance [13,14]. However, such studies have usually focused on singular commercial Mg-alloys, where Zr is a minor addition and which include other elements or impurities in the Mg matrix; as opposed to the Mg–Zr binary system. Furthermore, in these studies the Zr content was not altered. Other common alloying additions, such as aluminium (Al) and manganese (Mn), are known to form intermetallic phases with Zr in Mg alloys. Impurities, such as iron (Fe), are known to cause detrimental micro-galvanic couples with the Mg matrix. Zr additions can however scavenge Fe in the melt [4,13–16], combining to form insoluble particles with the nominal composition of Fe_2Zr [17]. Owing to a large difference in density with Mg, Fe_2Zr particles settle to the bottom of the melt prior to casting. This generally renders Mg alloys containing Zr to be of higher purity [18], as they usually contain <50 ppm Fe [14], which is below any tolerance limit for Fe in Mg to cause a rapid acceleration of corrosion rate [19,20]. However, the influence of Zr when added in isolation, for a series of binary alloys has not been previously reported. In addition, studies to date have not reported results of the fundamental influence of Zr upon Mg alone.

A review of the reports regarding the effect of Zr on corrosion of Mg have also indicated there are negative effects of Zr particles in Mg, and that the distribution of Zr in the Mg matrix may also affect the corrosion kinetics [21–23]. Ben-Hamu observed that when Zr particles are not homogeneously dispersed throughout the Mg matrix, the corrosion rate increases compared to a more even distribution of smaller Zr particles [21]. In another study, Neil observed deep corrosion attack around Zr-rich regions in the Mg alloys ZE41 [22]. Moreover, Neil reported that accelerated corrosion rates appeared to be associated with the variance in size of the Zr-rich particles, with a greater number of both larger and smaller particles found within the grain interiors in ZE41. Both Neil and Song proposed that these elemental Zr particles are detrimental when embedded in the matrix [22,24], acting as micro-galvanic sites with the Mg-alloy matrix under open circuit exposure conditions. However, further mechanistic aspects were not described.

* Corresponding author at: Department of Materials Engineering, Monash University, Clayton, VIC 3800, Australia. [redacted]

0010-938X/$ - see front matter © 2014 Published by Elsevier Ltd.
http://dx.doi.org/10.1016/j.corsci.2013.11.051

Whilst such studies have commented on the effect of Zr particles on the corrosion of Mg-alloys, they have not detailed the electrochemical impact or kinetic changes that occur, nor have they studied variations of Zr content in Mg. In regard to this latter point, another variable of interest is the relative proportion of Zr dissolved in solid solution. As such, there exists a paucity of information contrasting the effect of Zr dissolved in solid solution to elemental Zr particles embedded in the Mg matrix, and relating such interactions to changes in the electrochemical kinetics of Mg.

In this study, the effect of systematic Zr additions (for the unique purposes of investigating the effect of Zr variations) on the corrosion rate of Mg is examined. Electrochemical testing is augmented by mass-loss testing to capture the effect of Zr on corrosion for Mg–Zr alloys made from the two commercially available Mg–Zr master alloys, Microzir (formally known as AM-Cast) and Zirmax. These master alloys contain different Zr particle sizes which result in Mg–Zr alloys with varying contents of Zr dissolved in solid solution. Production of such master alloys is specialised, since Zr has a low solubility in Mg, and Zr-containing Mg-alloys have the Zr introduced via such master alloys as opposed to the addition of pure (high melting point) Zr.

2. Experimental methods

2.1. Alloy production and characterisation

The Mg–Zr master alloys used in this study were Microzir (nominally Mg–27 wt.% Zr), supplied by Magontec, and Zirmax (nominally Mg–33 wt.% Zr) supplied by Magnesium Elektron. Melting was carried out in a resistance furnace using AM-Cover® as a cover gas. Pure Mg was initially melted in a steel crucible at 700 °C, to which small amounts of either Mg–Zr master alloy was added to attain specific Zr levels, up to roughly 0.2 wt.%, in the final ingot castings. The Mg melt was poured into a graphite coated cast iron mould and the ingots were allowed to air cool.

During each of the production runs for the Microzir and Zirmax containing Mg–Zr alloys the Zr addition levels were calculated and added to the Mg melt to achieve similar nominal compositions. Stirred and unstirred alloy samples were taken from the same nominal melt charge. Stirred alloys were vigorously stirred immediately prior to casting; whereas the unstirred alloys were held for 20 min prior to casting. The Mg–Zr alloys investigated in this study had Zr additions below the levels required for significant grain refinement to occur [25]. Four commercially available Zr containing Mg alloys with were also selected for examination in this study. The chosen commercial alloys were ZE41, ZK60, WE54 and AM-SC1 with heat treatment for peak strength conditions. These commercial alloys contain Zr for the purpose of grain refinement and combinations of additional alloying elements such as zinc, yttrium and other rare earth elements for additional improvements to the mechanical properties of the alloys.

The compositions of the alloys (custom and commercial) were analysed independently via inductively coupled plasma – atomic emission spectroscopy, ICP-AES (Spectrometer Services, Coburg, Australia). The specific compositions of the binary Mg–Zr alloys produced in this study are given in Table 1 and the commercial alloys tested are in Table 2. The values for overall Zr content and percentage of Zr dissolved in solid solution were measured via an acid pre-treatment procedure prior to ICP-AES analysis as per Crawley [26]. The soluble Zr content was determined by dissolving the sample in a 10% HCl solution. The total Zr content was determined by dissolving the specimen in a 50% HCl–6% HF solution.

Several alloys were examined via scanning electron microscopy (SEM). Mg–Zr alloy specimens and both Mg–Zr master alloys were polished to a 1 μm diamond paste finish and then imaged using a JEOL 7001F SEM in back scattered electron (BSE) mode. The microscope was equipped with energy dispersive X-ray spectroscopy (EDX) (Oxford Instruments X-Max 80 detector). Post-corrosion SEM and EDX analysis was also performed on selected Microzir and Zirmax specimens. The samples were polished to a 1 μm diamond paste finish and immersed in a 0.1 M NaCl solution for 15 min. They were then cleaned by immersion in ethanol before being examined in the JEOL 7001F SEM.

2.2. Electrochemical and corrosion testing

Specimen surfaces were ground to a 2000 grit surface finish. A 3-electrode flat-cell with an exposed sample area of 1 cm^2 was used in conjunction with a VMP 3Z potentiostat. All testing was carried out in 0.1 M NaCl, and potentiodynamic polarisation was conducted at 1 mV/s with a saturated calomel electrode (SCE). Prior to polarisation the samples were conditioned for ten minutes at open circuit to ascertain a close to stable potential. The polarisation curves were used to determine i_{corr} (via a Tafel-type fit) using EC-Lab software. Tafel-type fits were executed by selecting a portion of the curve that commenced >50 mV from E_{corr}, and i_{corr} was estimated from the value where the fit intercepted the potential value of the true E_{corr}. It is noted that the Tafel slopes presented herein include some curvature, to which a linear fit was executed for the purposes of analysis. Importantly however,

Table 1
Composition (tested via ICP-AES) and corrosion properties of alloys produced in this study.

Sample ID	Mg wt.%	Zr wt.% (total)	Overall % of Zr (total) in solid solution	Fe wt.%	i_{corr} (A/cm^2)	E_{corr} (mV_{SCE})	β_a (mV/decade)	β_c (mV/decade)
Microzir-1 Stirred	~Bal	0.028	42.9	0.010	$4.8\ (\pm0.5) \times 10^{-5}$	−1535 (±5)	59 (±4.2)	−228 (±5.7)
Microzir-1 Unstirred	~Bal	0.012	33.3	0.008	$5.2\ (\pm0.5) \times 10^{-5}$	−1529 (±7)	42 (±2.6)	−218 (±6.3)
Microzir-2 Stirred	~Bal	0.061	36.1	0.010	$4.5\ (\pm0.7) \times 10^{-5}$	−1547 (±7)	51 (±2.3)	−214 (±9.5)
Microzir-2 Unstirred	~Bal	0.014	42.9	0.008	$4.6\ (\pm0.6) \times 10^{-5}$	−1504 (±5)	46 (±2.3)	−226 (±5.6)
Microzir-3 Stirred	~Bal	0.120	45.0	0.011	$4.1\ (\pm0.5) \times 10^{-5}$	−1572 (±5)	82 (±1.9)	−188 (±5.1)
Microzir-3 Unstirred	~Bal	0.019	47.4	0.005	$2.7\ (\pm0.4) \times 10^{-5}$	−1549 (±6)	57 (±2.8)	−196 (±8.3)
Microzir-4 Stirred	~Bal	0.220	47.3	0.014	$4.9\ (\pm0.4) \times 10^{-5}$	−1546 (±12)	68 (±5.0)	−225 (±7.5)
Microzir-4 Unstirred	~Bal	0.037	51.4	0.006	$3.6\ (\pm0.5) \times 10^{-5}$	−1569 (±8)	53 (±5.5)	−218 (±7.6)
Zirmax-1 Stirred	~Bal	0.028	25.0	0.006	$3.7\ (\pm0.4) \times 10^{-5}$	−1522 (±10)	45 (±4.4)	−222 (±7.9)
Zirmax-1 Unstirred	~Bal	0.018	22.2	0.006	$4.4\ (\pm0.4) \times 10^{-5}$	−1513 (±2)	56 (±5.1)	−220 (±6.5)
Zirmax-2 stirred	~Bal	0.057	15.8	0.006	$4.3\ (\pm0.3) \times 10^{-5}$	−1576 (±5)	65 (±3.8)	−208 (±3.5)
Zirmax-2 unstirred	~Bal	0.025	16.0	0.005	$4.5\ (\pm0.3) \times 10^{-5}$	−1531 (±5)	63 (±3.9)	−222 (±3.9)
Zirmax-3 stirred	~Bal	0.120	10.0	0.001	$4.7\ (\pm0.5) \times 10^{-5}$	−1564 (±8)	89 (±2.5)	−206 (±12.0)
Zirmax-3 unstirred	~Bal	0.056	8.93	0.005	$3.5\ (\pm0.5) \times 10^{-5}$	−1555 (±5)	51 (±6.3)	−200 (±4.1)
Zirmax-4 stirred	~Bal	0.190	10.5	0.006	$5.5\ (\pm0.5) \times 10^{-5}$	−1572 (±8)	85 (±6.3)	−243 (±6.0)
Zirmax-4 unstirred	~Bal	0.075	8.00	0.013	$4.7\ (\pm0.2) \times 10^{-5}$	−1536 (±10)	67 (±4.7)	−225 (±4.3)
Commercial purity Mg	~Bal	0.002	N/A	0.001	$3.2\ (\pm0.4) \times 10^{-5}$	−1502 (±11)	75 (±8.7)	−239 (±5.2)

Table 2
Composition (tested via ICP-AES) and corrosion properties of commercial Zr-containing Mg-alloys (RE represents the sum of La, Ce, Nd, Y, Gd and Pr).

Sample ID	Zr wt.% (solid solution)	Zr wt.% (total)	Overall % of Zr (total) in solid solution	Fe wt.%	Remain. wt.%	i_{corr} (A/cm^2)	E_{corr} (mV$_{SCE}$)
ZE41	0.49	0.77	63.6	0.001	4.00Zn, 1.25RE	1.0 (±0.2) × 10^{-5}	−1520 (±11)
WE54	0.45	0.53	84.9	0.001	4.86Y, 2.60RE	1.4 (±0.2) × 10^{-5}	−1678 (±7)
ZK60	0.54	0.61	88.5	0.006	5.41Zn	1.3 (±0.1) × 10^{-5}	−1584 (±7)
AM-SC1	0.54	0.66	81.8	0.002	0.54Zn, 2.29RE	1.7 (±0.1) × 10^{-5}	−1627 (±12)

polarisation testing was also able to visually reveal comparative information related to the kinetics of both the anodic and cathodic reactions of the various Mg specimens – which was deemed an important aspect of the work. Each sample was tested five times and an average result was determined.

To supplement the electrochemical testing, weight loss testing was also executed to provide a longer-term comparison of alloy corrosion, and was determined by immersion of samples in 0.1 M NaCl for a period of 24 h. The corrosion products were subsequently removed by light scrubbing following a 3s immersion in dilute (15%) HNO_3. The mass loss was determined on three unique samples and an average result was determined and reported.

3. Results and discussion

3.1. Mg–Zr alloy characterisation

ICP-AES analysis of the Mg–Zr alloys (Table 1) indicates that stirring the Mg melt prior to casting of the Mg–Zr ingots was found to increase the overall Zr content in the alloys. The lower total Zr content in the unstirred alloys is due to Zr particles that have not dissolved into the Mg melt, settling to the bottom of the crucible (due to their density) during the extended holding time prior to casting. Stirring did not affect the average percentage of the amount of Zr in solid solution from either of the two master alloys used.

The Microzir containing alloys have, on average, a higher percentage of Zr dissolved in solid solution than the Zirmax containing Mg–Zr alloys. This can be attributed to the different size of Zr particles introduced into the Mg melt prior to casting [27]. A qualitatively more uniform distribution of smaller Zr particles in the Microzir master alloy, ranging primarily between 1 and 5 μm in size [25,28,29] (Fig. 1A), is in contrast to that of the Zirmax master alloy which has a larger and more variable Zr particle size (Fig. 1B). The finer size of Zr particles in the Microzir master alloy means that a greater amount of Zr is dissolved in solid solution. The smaller Zr particles are apparently dissolved into the Mg matrix more readily; concomitant with fewer large Zr particles remaining suspended in the Mg melt prior to casting and consistent with a higher level of Zr in solid solution [4,30–32].

The overall percentage of Zr dissolved in solid solution increases as the overall Zr content increases in the Microzir Mg–Zr alloys (Fig. 2A). The majority of the Zr particles (between 1 and 5 μm in size) were presumably dissolved or broken up from particle clusters through stirring of the melt, while larger particles are likely to settle to the bottom of the crucible. In contrast, the Mg–Zr alloys produced using Zirmax show that as the overall Zr content increases the percentage of Zr dissolved in solid solution decreases. In the Zirmax alloys, the larger Zr particles are less rapidly dissolved in Mg and as the Zr content is increased, and the proportion of Zr particles remaining embedded in the Mg matrix increases. Despite the lower levels of Zr in Mg, these trends are also seen in the unstirred Mg–Zr alloys (Fig. 2B). The four selected commercial Mg alloys all have a greater percentage of Zr dissolved in solid solution compared to the binary Mg–Zr alloys. This is most likely due to the post-processing operations and particular solution treatments on the selected alloys increasing solubility for Zr.

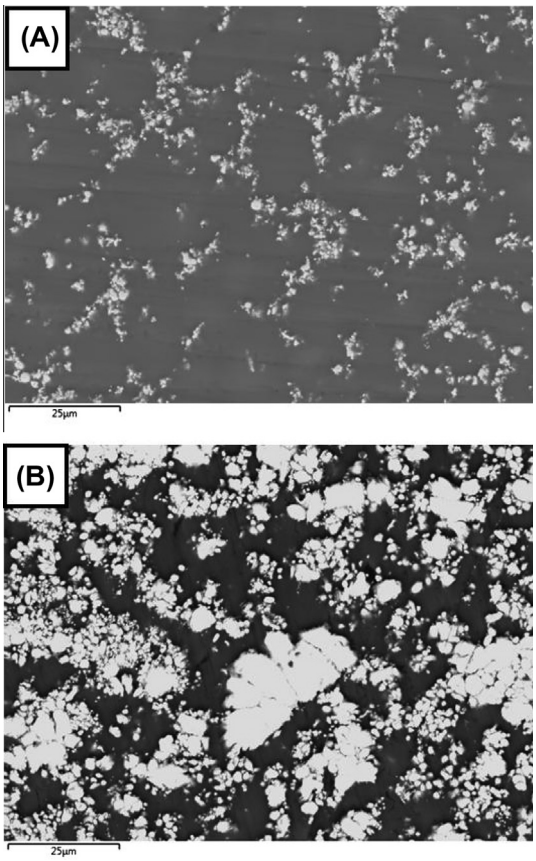

Fig. 1. BSE-SEM micrograph of (A) Microzir master alloy and (B) Zirmax master alloy.

Whilst the electrochemical testing results are described further below, the abridged values of the corrosion current density, i_{corr}, are presented along with the alloy characteristics in Fig. 2 in order to allow some initial assertions to be made. The corrosion current density, i_{corr}, for the custom alloys studied herein is in all cases higher than pure Mg (i.e. >30 μA/cm^2), whereas for example, pure Mg has been previously observed to have a corrosion current density of <10 μA/cm^2 [33]. In the instance of vigorous stirring prior to casting, for the Zirmax alloys, i_{corr} increases as the Zr content increases. The i_{corr} in the stirred Microzir alloys initially decreases, prior to an increase at the highest Zr content (Fig. 2C). The relative proportion of Zr in or ex- solid solution is deemed to play a role in the ultimate corrosion rate. For example, the stirred Microzir-4 alloy has a lower i_{corr} for a similar total Zr content compared to the stirred Zirmax-4 alloy (Table 1). This difference in the percentage of Zr dissolved in solid solution for the same Zr content is the cause for the change in i_{corr} between the two alloys.

The comparison of the influence of total Zr vs. soluble Zr is important for interpreting the evolution of corrosion current as

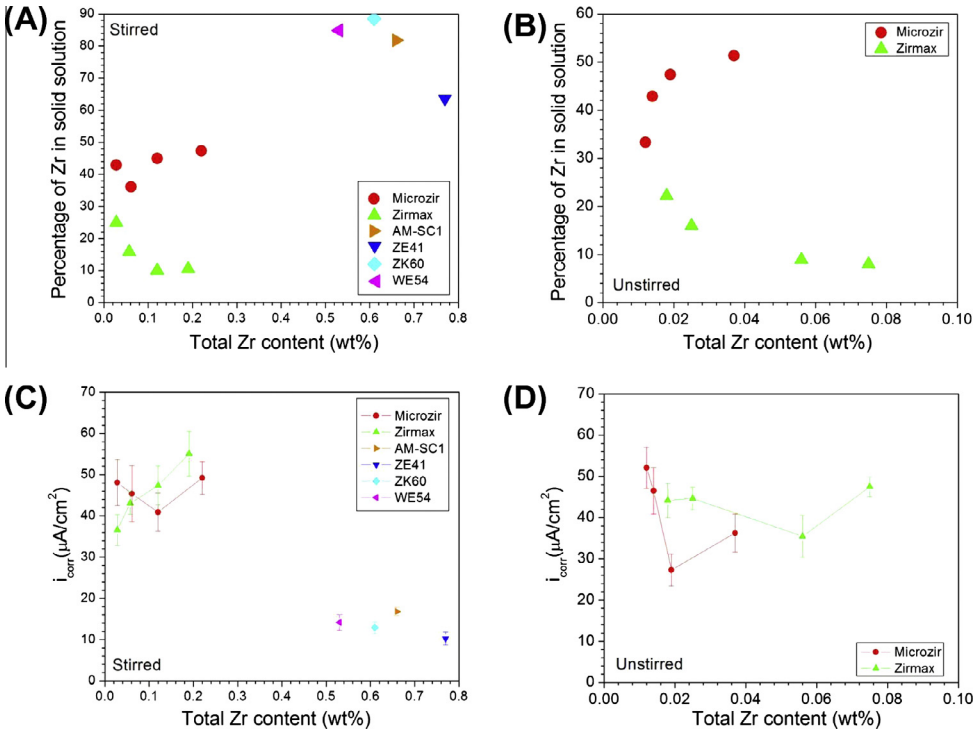

Fig. 2. (A) Zr in solid solution vs. total Zr content for stirred Mg–Zr alloys and selected commercial alloys, (B) Zr in solid solution vs. total Zr content for unstirred Mg–Zr alloys, (C) total Zr content (wt.%) vs. i_{corr} for stirred Mg–Zr alloys and selected commercial alloys (presented with standard error) and (D) total Zr content (wt.%) vs. i_{corr} for unstirred Mg–Zr alloys (presented with standard error). Testing was in 0.1 M NaCl.

the Zr content of the unstirred Mg–Zr alloys are comprehensively lower than the stirred Mg–Zr alloys (Table 1). There is an overall decrease in i_{corr} for the unstirred Microzir alloys and an increase in i_{corr} for the unstirred Zirmax alloys (Fig. 2D). The variance in the measured i_{corr} values for the unstirred alloys is not only greater than that for the stirred alloys, but the majority of specimens tested lie within the standard error scatter range for the stirred alloys of a similar overall Zr content.

The four Zr-containing commercial alloys tested all have i_{corr} values below those of the Mg–Zr binary alloys. Apart from thermo-mechanical treatment, the additional alloying elements in the commercial alloys may further alter the reaction kinetics in a manner that changes the overall i_{corr} values that are observed compared to when only Zr is added [33,34]. This phenomenon will not be studied fully in the current work, but it is nonetheless important and therefore warrants further dedicated study. It is obvious that the role of Zr on the corrosion of magnesium alloys is in need of further dedicated investigation, with this initial study of binary Mg–Zr should be followed by an investigation varying the concentration of Zr in more complex ternary systems.

3.2. Mg–Zr alloy corrosion morphology

Alloys produced using either Zirmax or Microzir master alloys contained Zr particles embedded in the Mg matrix (Fig. 3). This indicates that while the Zr additions are below the theoretical solid solubility limit, equilibrium has not been achieved. The majority of the elemental Zr particles present and the Zr dissolved in solid solution in the two Mg–Zr alloy groups have different morphologies in the Mg matrix, which may have an influence on the mode/morphology of corrosion attack. Due to the very low Fe content in both of the Mg–Zr alloys, no discernable Fe-particles or significant Fe related peaks were seen while performing EDX testing on the selected specimens.

It was observed in the Zirmax containing Mg–Zr alloys that corrosion was mostly concentrated around the Zr particles present in the matrix (Fig. 3C). With less Zr in solid solution, the proportion of Zr particles to contribute to localised corrosion increases (since Zr not in solid solution is present as Zr particles). The Microzir containing alloys show a more generalised corrosion attack across the surface (Fig. 3F). There were many large pits beginning to form across the alloy surface where corrosion was concentrated [35].

The visual identification of either a local anode or cathode via observation of the micrographs is rather complex and not straightforward in real-time or post-corrosion analysis. This is caused by changes in the localised 'active' anodic sites that convert to 'cathodes' after a critical, yet unknown, period of time for Mg and its alloys. It has been shown using SVET [36] that sites of earlier anodic activity can later change to act as local cathodes. As a result, the post exposure micrographs cannot intrinsically isolate these overlapping effects, and the micrographs are a part of a greater collection of data which complements the electrochemical, mass loss and compositional analyses.

3.3. Effect of Zr additions on the electrochemical reaction kinetics of Mg

As Zr is added to Mg, the anodic reaction kinetics increase and the electrochemical potential, E_{corr}, of the Mg–Zr alloy concomitantly decreases (Fig. 4). This phenomenon, which is akin to 'anodic activation' [37–39], is not generally reported for elemental additions to Mg, as it is itself active. Exceptions include highly active additions such as calcium [34,40], however Zr is itself a noble metal addition, and hence the phenomenon is one of anodic activation. It has been reproducibly shown in essentially all of the

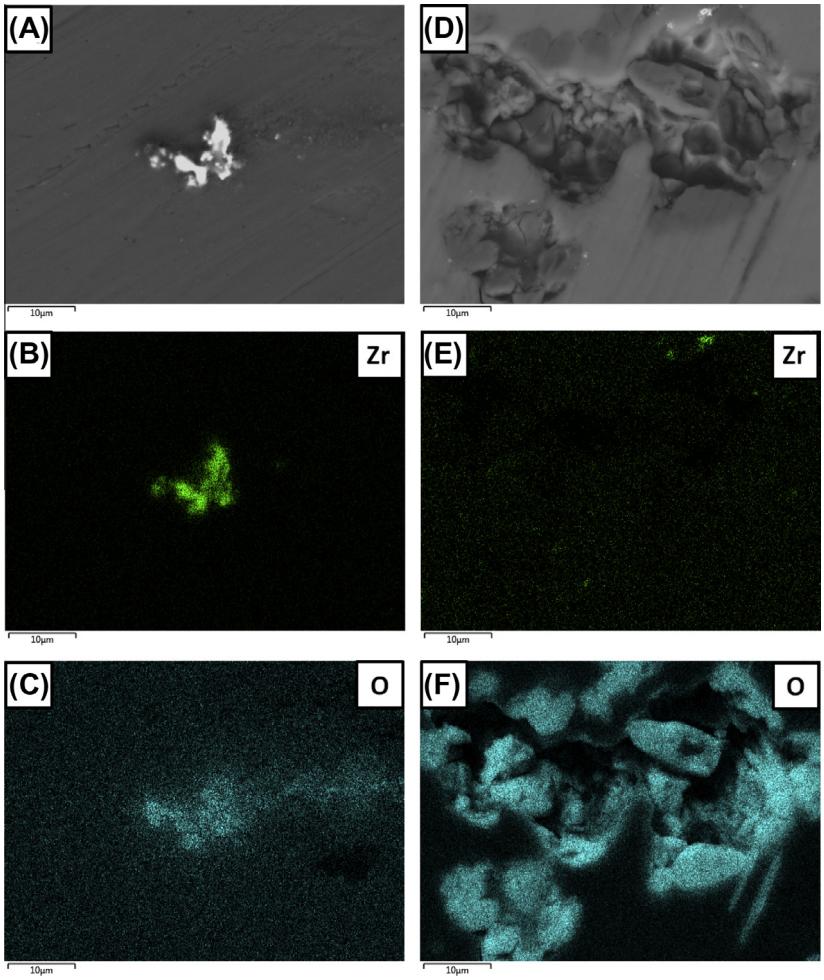

Fig. 3. (A) BSE-SEM micrograph of Mg–0.19Zr following 0.5 h immersion in 0.1 M NaCl (i.e. post-corrosion) produced with Zirmax master alloy, (B) EDX map of Zr content in (A), (C) EDX map of O content in (A), (D) BSE-SEM micrograph of Mg–0.22Zr following 0.5 h immersion in 0.1 M NaCl (i.e. post-corrosion) produced with Microzir master alloy, (E) EDX map of Zr content in (D) and (F) EDX map of O content in (D).

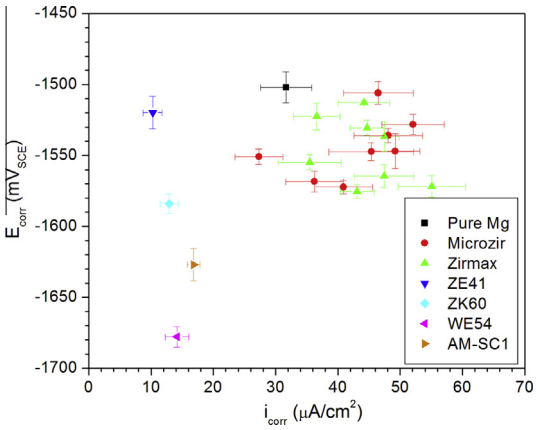

Fig. 4. Measured E_{corr} vs. i_{corr} values in 0.1 M NaCl for Microzir and Zirmax containing binary Mg–Zr alloys and selected commercial Mg alloys containing Zr compared with commercially pure (nominally Zr free) Mg (presented with standard error).

binary Mg–Zr alloys produced in this study that Zr additions are capable of increasing the anodic reaction kinetics, which has not been previously reported.

Whilst this marked increase in the anodic reaction kinetics occurs in both Mg–Zr alloy groups (Fig. 5A), the Zirmax alloys also display a notable increase in the cathodic reaction kinetics (Fig. 5B). The increase in cathodic kinetics would be expected in the case where a higher fraction of elemental Zr particles, which are more efficient at supporting cathodic reactions, exists. The anodic activation effect is apparent even at low levels of Zr. Both alloy systems, made from either Microzir or Zirmax Mg–Zr master alloys, display similar levels of anodic activation at similar total Zr contents. It is possible that Zr additions may be disrupting the partially protective film that forms on the surface of Mg, however, this mechanism is still not fully understood and further analysis is warranted.

In order to assess all the alloys using a standard criterion for the alteration of anodic and catholic rates with Zr content (and bearing in mind all the alloys had a differing E_{corr}) – it was decided to determine the relative anodic and cathodic current density measured at 50 mV_{SCE} either side of E_{corr}). When there is a greater amount of Zr not dissolved in solid solution and present as elemental Zr particles, the cathodic reaction kinetics increase. This is represented in Fig. 6 that shows alloy compositions with a greater amount Zr dissolved in solid solution are represented by transitioning into the colour red. These regions correlate with increased cathodic reaction kinetics compared to areas transitioning into the green coloured regions with a lesser percentage of Zr dissolved in solid solution and having lower cathodic kinetics. As such, the notion that Zr may decrease corrosion rates by purifying the alloy [18]

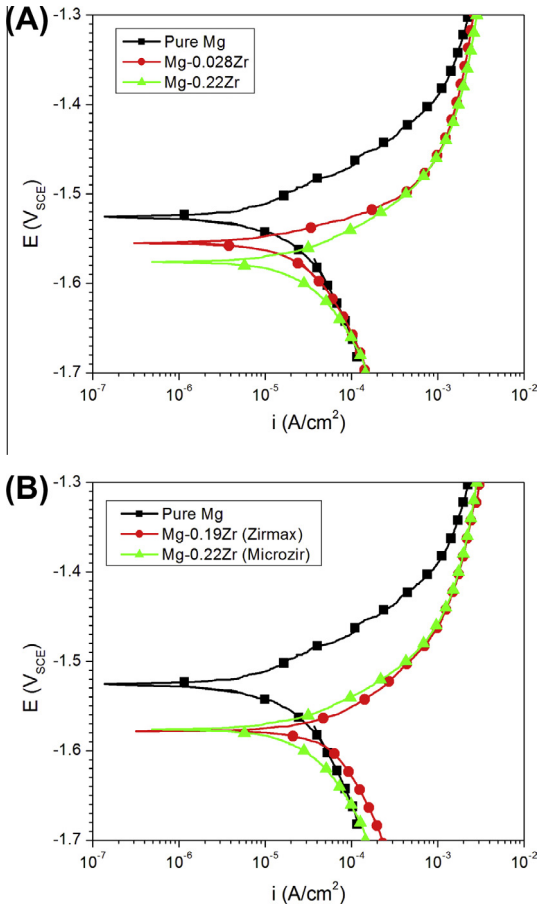

Fig. 5. Polarisation curves for (A) Microzir1 stirred and Microzir4 stirred Mg–Zr alloys, compared with commercially pure Mg, and (B) For stirred Microzir4 and Zirmax4 Mg–Zr alloys compared with commercially pure Mg. Testing was in 0.1 M NaCl.

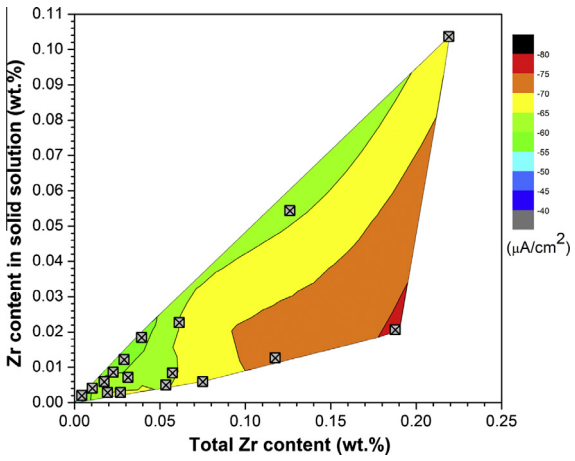

Fig. 6. Contour plots of the current density measured at E_{corr} – 50 mV_{SCE} vs. overall Zr content and Zr content in solid solution. Testing was in 0.1 M NaCl.

and removing metallic Fe (via the formation of Fe_2Zr intermetallic particles), does not take into account the anodic activation effect of Zr – which is in itself a strong effect.

There is a more complex relationship governing the anodic current density of the alloy systems at a given electrochemical potential. It is observed that as the anodic current density (measured at +50 mV_{SCE} from E_{corr}) increases the electrochemical potential of the alloy increases as well (Fig. 7). This relationship between the anodic current density and the electrochemical potential of the alloy leads to an initial increase in anodic current density with an increasing percentage of Zr dissolved in solid solution, followed by a decrease in the anodic current density (Fig. 8A). As there is not a strong relationship between the cathodic current density and the potential, the cathodic current density initially does not change significantly and only starts to decrease at higher percentages of Zr dissolved in solid solution (Fig. 8B). Thus, the effect of Zr dissolved in the Mg matrix on the cathodic reaction kinetics is minimal when compared to the effect of elemental Zr particles.

The interaction between relative changes in cathodic kinetics altering corrosion rates is linked to the aforementioned 'anodic activation' effect of Zr on Mg alloys. When several of the Mg-Zr binary alloys, with varying percentages of Zr dissolved in solid solution, studied herein, are compared with pure Mg it can be seen that at they all roughly intersect at the same current density at a potential of −1.45 V_{SCE} (Fig. 9A). Thus, the rate of increase of the anodic current density will increase as the E_{corr} of the alloy becomes more electropositive. A similar trend can be observed in the four commercial alloys studied (Fig. 9B).

These effects of Zr on both the anodic and cathodic reaction kinetics have not been reported previously as prior studies did not separately analyse the anodic and cathodic kinetics with a variation in the Zr content as particles and in solution and the effects reported herein are not obvious when studying the role of Zr in more complex (ternary and higher order) alloys.

3.4. Comparison between long and short term corrosion testing

Electrochemical testing via potentiodynamic polarisation provides valuable information about the mechanisms influencing the corrosion rate and the relative influence of anodic and cathodic reaction variations from alloy to alloy. Such tests are however 'instant' and immersion (weight loss) testing allows a benchmark to compare the observed short-term (electrochemical) trends with longer-term corrosion effects. For the Mg–Zr alloys tested herein, there was a notable correlation from the polarisation test data (i.e. i_{corr}) and mass loss from immersion results (Fig. 10). The relationship shows that as the current density, i_{corr}, increases the mass loss also generally increases. The data is presented in its native units to avoid errors from assuming uniform corrosion for the electrochemical data, particularly since it was observed that corrosion was localised.

The increase in i_{corr} appears to be similar for both the Microzir and Zirmax alloys; however, there is a divergence in the weight

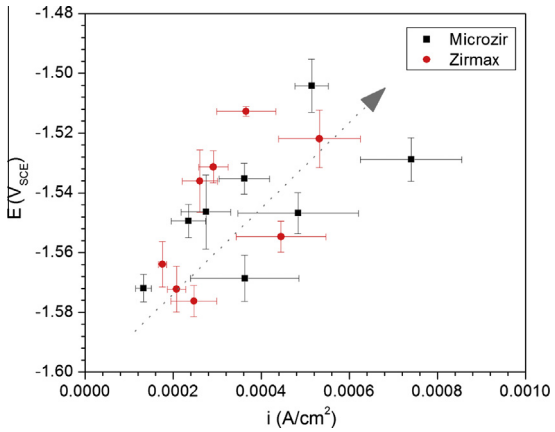

Fig. 7. The corresponding potential (E in V_{SCE}) vs. the anodic current density measured at E_{corr} + 50 mV_{SCE} in 0.1 M NaCl (presented with standard error).

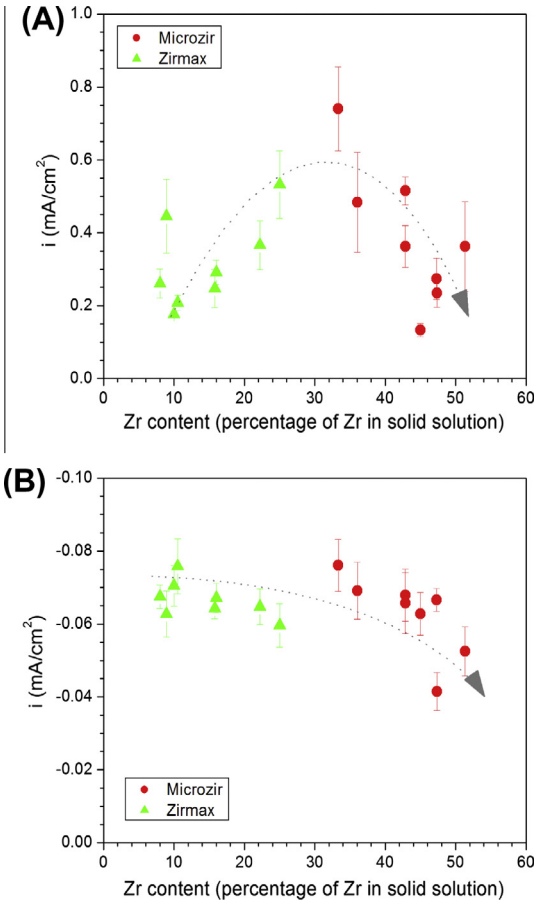

Fig. 8. Absolute percentage of Zr dissolved in solid solution measured against: (A) the anodic current density measured at E_{corr} + 50 mV_{SCE} (presented with standard error), and (B) the cathodic current density measured at E_{corr} − 50 mV_{SCE}. Overlaid arrows are not a fit, but an aid-to-the-eye (presented with standard error). Testing was in 0.1 M NaCl.

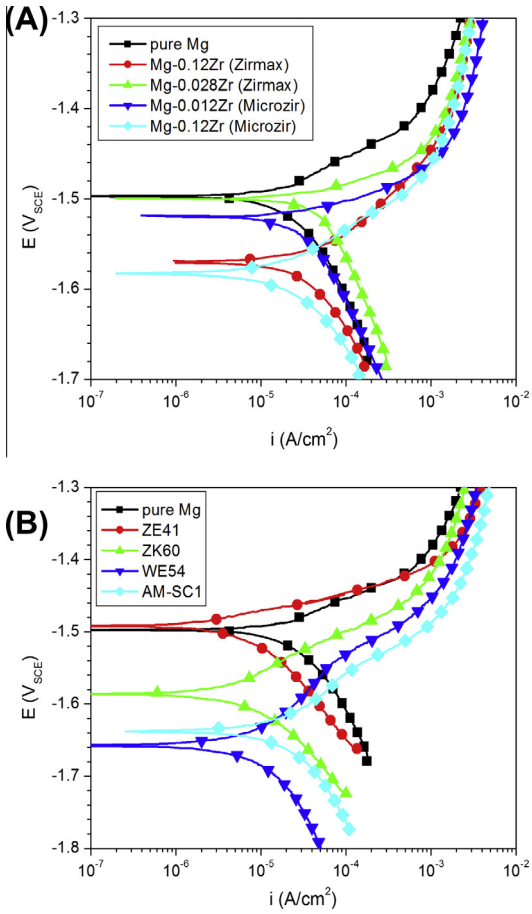

Fig. 9. Polarisation curves collected in 0.1 M NaCl for (A) binary Mg–Zr alloys with varying percentages of Zr dissolved in solid solution, compared with commercially pure Mg, and (B) commercial Mg alloys containing Zr compared with commercially pure Mg.

loss values for the two groups. The Microzir alloys have a higher average weight loss and a larger calculated standard error as i_{corr} increases. As the Zirmax and Microzir alloys have similar overall Zr contents (Table 1), the cause for the increased weight loss per unit time observed in the Microzir alloys can be explained by the difference in Zr content dissolved in solid solution affecting the corrosion morphology of the Mg alloys. The higher amount of Zr in solid solution in the Microzir alloy leads to a greater amount of generalised corrosion attack across the alloy surface compared to the Zirmax alloy which has localised corrosion around large Zr particles in the Mg matrix. The higher Zr content in solid solution has been observed to lead to a greater amount of deep pitting (Fig. 3F) and a larger area of the alloy surface that has undergone oxidation. The overall weight loss per unit time will be greater given the more wide spread mode of corrosion attack. Thus, the variance in the corrosion rates in such cases can be qualitatively attributed to the corrosion morphology [41].

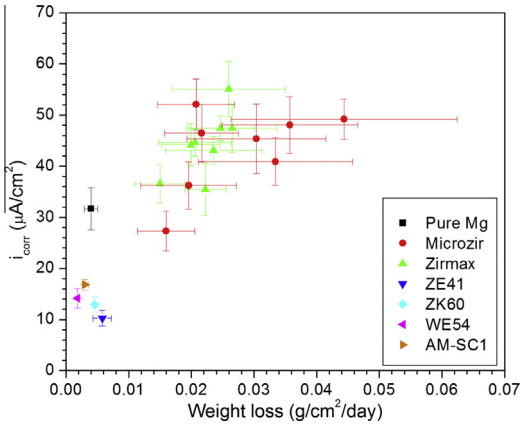

Fig. 10. i_{corr} vs. weight loss (determined after 24 h of exposure) for Mg–Zr alloys produced with Microzir and Zirmax master alloys and selected commercial Mg alloys (presented with standard error). Testing was in 0.1 M NaCl.

3.5. General discussion

The presence of Zr has been shown to increase both the anodic and cathodic reaction kinetics of Mg. The increase in the anodic kinetics appears to be unaffected by which master alloy is used as with both the Microzir and Zirmax alloys there is a component of Zr that is dissolved in solid solution. Overall, the higher Zr content dissolved in solid solution and the electrochemical potential has been shown to affect the rate of increase of the anodic current density. However, the increase in cathodic reaction kinetics has been shown to be dependent on the Zr particle size in the Mg–Zr master alloy.

While it is reported that Zr can refine the grain size of Mg alloys [4,27], there was no significant grain refinement observed in these alloys, and hence grain characterisation is not reported. The overall Zr content in the alloys herein is lower than commercial Zr

additions that are specifically designed to refine the grain size. The smallest grains observed are roughly 300–400 μm across and the largest were over 1000 μm across. Given the large variations in corrosion rate observed as a function of chemical changes, it is posited that the effect of grain size has negligible on the electrochemical response, i.e. the chemical effect of the Zr additions supplants the structural changes that affect the corrosion characteristics of Mg.

The higher percentages of Zr in solid solution for a given total Zr content appear to increase the long-term corrosion rates of Mg, due to a greater influence on the anodic reaction kinetics causing generalised corrosion attack across the alloy surface. The four commercial Zr containing Mg alloys analysed in this study were found to have high levels of Zr in solid solution (Table 2). This would indicate that the Zr present in the alloys would likely have a greater influence on the anodic reaction kinetics rather than the cathodic kinetics based on the rationale deduced from binary alloys. However, this effect of Zr on the anodic kinetics is difficult to ascertain in the commercial alloys unless the Zr content in the commercial alloys is varied in a similar manner to the binary alloys. It can be seen from the abridged electrochemical data (Fig. 4), that the commercial alloys have less noble values of E_{corr} however this could have arisen from the relatively large amounts of ternary elements (including rare earths) present. These additional elements can additionally alter the relative anodic and cathodic kinetics. Rather than speculate on the behaviour of commercial Zr alloys herein, for an initial study it can be nonetheless asserted that without the comparisons made between the Mg–Zr binary alloy and the commercial Mg alloy data presented herein the claims that Zr additions improve the corrosion resistance of Mg could not previously be challenged. Most previous studies have included additional alloying elements which do not reveal the negative influence of Zr on Mg in a corrosion context.

4. Conclusions

1. The morphology and size range variation of the Zr particles present in the Mg–Zr master alloy used for production of the Mg–Zr alloys affects the extent and mode of corrosion. This was attributed to the difference in Zr content in solid solution and the fraction and morphology of remnant Zr particles. It was seen that Microzir presented lower corrosion rates than Zirmax for the same nominal overall Zr content.
2. Higher levels of Zr dissolved in solid solution in Mg effect the anodic reaction kinetics, akin to anodic activation. This activation accelerates the general corrosion of the alloy matrix and increases the long-term corrosion rates from mass loss testing.
3. A greater extent of Zr particles embedded in the Mg matrix (i.e. concentrated Zr particles in excess of Zr in solid solution) increase cathodic reaction kinetics, increasing localised corrosion attack at the Zr particle–Mg matrix interface and increasing short-term corrosion rates. Zr particles serve as efficient local cathodes. Zr can, depending on its morphology in the Mg matrix, lead to significant increases in corrosion rate via modification of the anodic reaction, or the cathodic reaction.
4. The complex interactions which occur in ternary (and higher order) alloys with Zr appear to operate under a different regime that will need future work to elucidate. However, the data herein demonstrates that although Zr has a detrimental effect on the corrosion of Mg, Mg alloys with multiple element additions and post-manufacturing processing can still have acceptable corrosion properties for commercial applications.

Acknowledgments

The CAST Co-operative Research Centre was established under, and is funded in part by, the Australian Governments Co-operative Research Centres Scheme. Andy Yob, Ming Sun and Sherly Simanjuntak are gratefully acknowledged for their technical assistance.

References

[1] H. Okamoto, Mg–Zr (magnesium–zirconium), JPED 28 (2007) 305–306.
[2] I.J. Polmear, Light Alloys, third ed., Arnold, London, England, 1995.
[3] E.F. Emley, Principles of Magnesium Technology, first ed., Pergamon Press, Manchester, 1966.
[4] M. Qian, D.H. StJohn, Grain nucleation and formation in Mg–Zr alloys, Int. J. Cast Met. Res. 22 (2009) 256–259.
[5] K.V. Kutniy, I.I. Papirov, M.A. Tikhonovsky, A.I. Pikalov, S.V. Sivtzov, L.A. Pirozhenko, V.S. Shokurov, V.A. Shkuropatenko, Influence of grain size on mechanical and corrosion properties of magnesium alloy for medical implants, Mater. Wiss. Werkst. 40 (2009) 242–246.
[6] C.D. Lee, Effect of grain size on the tensile properties of magnesium alloy, Mater. Sci. Eng. A-Struct. 459 (2007) 355–360.
[7] H.E. Friedrich, B.L. Mordike, Magnesium Technology, Springer, Berlin, 2006.
[8] P. Lyon, New magnesium alloy for aerospace and specialty applications, in: A.A. Luo (Ed.), Magnesium Technology, TMS, 2004, pp. 311–315.
[9] C.J. Bettles, M.A. Gibson, S.M. Zhu, Microstructure and mechanical behaviour of an elevated temperature Mg-rare earth based alloy, Mater. Sci. Eng. A-Struct. 505 (2009) 6–12.
[10] A.C. Hanzi, F.H.D. Torre, A.S. Sologubenko, P. Gunde, R. Schmid-Fetzer, M. Kuehlein, J.F. Loffler, P.J. Uggowitzer, Design strategy for microalloyed ultra-ductile magnesium alloys, Philos. Mag. Lett. 89 (2009) 377–390.
[11] S.C. Wang, C.P. Chou, Effect of adding Sc and Zr on grain refinement and ductility of AZ31 magnesium alloy, J. Mater. Process. Technol. 97 (2007) 116–121.
[12] X. Gu, Y. Zheng, Y. Cheng, S. Zhong, T. Xi, In vitro corrosion and biocompatability of binary magnesium alloys, Biomaterials 30 (2008) 484–498.
[13] G. Song, D. StJohn, The effect of zirconium grain refinement on the corrosion behavior of magnesium-rare earth alloy MEZ, J. Light Met. 2 (2002) 1–16.
[14] P. Cao, M. Qian, D.H. StJohn, M.T. Frost, Uptake of iron and its effect on grain refinement of pure magnesium by zirconium, Mater. Sci. Technol. 20 (2003) 585–592.
[15] M. Qian, D.H. StJohn, M.T. Frost, Zirconium alloying and grain refinement of magnesium alloys, in: H.I. Kaplan (Ed.), Magnesium Technology 2003, The Minerals, Metals and Materials Society, 2003, pp. 209–214.
[16] T. Haitani, Y. Tamura, T. Motegi, N. Kono, H. Tamehiro, Solubility of iron in pure magnesium and cast structure of Mg–Fe alloy, Mater. Sci. Forum 419–422 (2003) 697–702.
[17] D. Pierre, F. Bosselet, M. Peronnet, J.C. Viala, J. Bouix, Chemical reactivity of iron base substrates with liquid Mg–Zr alloys, Acta Mater. 49 (2000) 653–662.
[18] A. Prasad, P.J. Uggowitzer, Z. Shi, A. Atrens, Production of high purity magnesium alloys by melt purification with Zr, Adv. Eng. Mater. 14 (2012) 477–490.
[19] J.E. Hillis, The effects of heavy metal contamination on magnesium corrosion performance, in: Light Met. Age, SAE, Detroit, 1983, pp. 25–29.
[20] M. Liu, P.J. Uggowitzer, P. Schmutz, A. Atrens, Calculated phase diagrams, iron tolerance limits, and corrosion of Mg–Al alloys, JOM 60 (2008) 39–44.
[21] G. Ben-Hamu, D. Eliezer, K.S. Shin, S. Cohen, The relation between microstructure and corrosion behaviour of Mg–Y–RE–Zr alloys, J. Alloy Compd. 341 (2007) 269–276.
[22] W.C. Neil, M. Forsyth, P.C. Howlett, C.R. Hutchinson, B.R.W. Hinton, Corrosion of magnesium alloy ZE41 – the role of microstructural features, Corros. Sci. 51 (2009) 387–394.
[23] Z. Rong-chang, Z. Jin, H. Wei-Jiu, W. Dietzel, K.U. Kainer, C. Blawert, K.E. Wei, Review of studies on corrosion of magnesium alloys, Trans. Nonferr. Metal. Soc. 16 (2006) 763–771.
[24] G.L. Song, Recent progress in corrosion and protection of magnesium alloys, Adv. Eng. Mater. 7 (2005) 563–586.
[25] M. Sun, M.A. Easton, D.H. StJohn, G. Wu, T.B. Abbott, W. Ding, Grain refinement of magnesium alloys by Mg–Zr master alloys: the role of alloy chemistry and Zr particle number density, Adv. Eng. Mater. (2012) 1–6.
[26] R.H.A. Crawley, Determination of soluble and insoluble zirconium in magnesium alloys, Anal. Chim. Acta (1961) 281–284.
[27] M. Sun, G. Wu, M.A. Easton, D.H. StJohn, T. Abbott, W. Ding, A comparison of the microstructure of three Mg–Zr master alloys and their grain refinement efficiency, in: W.J. Poole, K.U. Kainer (Eds.), 9th International Conference on Magnesium Alloys and their Applications, Vancouver, BC, Canada, 2012, pp. 873–880.
[28] M. Qian, L. Zheng, D. Graham, M.T. Frost, D.H. StJohn, Settling of undissolved zirconium particles in pure magnesium melts, J. Light Met. 1 (2001) 157–165.
[29] M. Qian, D.H. StJohn, M.T. Frost, A new zirconium-rich master alloy for the grain refinement of magnesium alloys, in: K.U. Kainer (Ed.), 6th International Conference Magnesium Alloys and their Applications, Wiley-VCH Verlag Gmbh & Co., Wolfsburg, Germany, 2003, pp. 706–712.
[30] M. Qian, D.H. StJohn, M.T. Frost, M.R. Barnett, Grain refinement of pure magnesium using rolled Zirmax master alloy (Mg–33.3Zr), in: H.I. Kaplan (Ed.), Magnesium Technology 2003, TMS (The Minerals, Metals & Materials Society), 2003, pp. 215–220.
[31] M. Qian, D.H. StJohn, M.T. Frost, Characteristic zirconium-rich coring substructures in Mg–Zr alloys, Scripta Mater. 46 (2002) 649–654.

[32] M. Qian, D.H. StJohn, M.T. Frost, Heterogeneous nuclei size in magnesium–zirconium alloys, Scripta Mater. 50 (2004) 1115–1119.
[33] A.D. Sudholz, N. Birbilis, C.J. Bettles, M.A. Gibson, Corrosion behavior of Mg-alloy AZ91E with atypical alloying additions, J. Alloy. Compd. 461 (2009) 109–115.
[34] A.D. Sudholz, N.T. Kirkland, R.G. Buchheit, N. Birbilis, Electrochemical properties of intermetallic phases and common impurity elements in magnesium alloys, Electrochem. Solid St. 14 (2011) C5–C7.
[35] G. Song, A. Atrens, Understanding magnesium corrosion, Adv. Eng. Mater. 5 (2003) 837–858.
[36] G. Williams, K. Gusieva, N. Birbilis, Localized corrosion of binary Mg–Nd alloys in chloride-containing electrolyte using a scanning vibrating electrode technique, Corrosion 68 (2012) 489–498.
[37] B. Graver, A.T.J.v. Helvroot, K. Nisancioglu, Effect of heat treatment on anodic activation of aluminium by trace element indium, Corros. Sci. 52 (2010) 3774–3781.
[38] A.R. Despic, D.M. Drazic, M.M. Purenovic, N. Cikovic, Electrochemical properties of aluminium alloys containing indium, gallium and thallium, J. Appl. Electrochem. 6 (1976) 527–542.
[39] J.T.B. Gundersen, A. Aytac, J.H. Nordlien, K. Nisancioglu, Effect of heat treatment on electrochemical behaviour of binary aluminium model alloys, Corros. Sci. 46 (2004) 697–714.
[40] N.T. Kirkland, N. Birbilis, J. Walker, T. Woodfield, G.J. Dias, M.P. Staiger, In-vitro dissolution of magnesium–calcium binary alloys: clarifying the unique role of calcium additions in bioresorbable magnesium implant alloys, J. Biomed. Mater. Res. Part B Appl. Biomater. 95B (2010) 91–100.
[41] E. Ghali, W. Dietzel, K.-U. Kainer, General and localised corrosion of magnesium alloys: a critical review, J. Mater. Eng. Perform. 13 (2003) 7–23.

This page is intentionally left blank

Chapter 7

CALPHAD simulation of the Mg-(Mn,Zr)-Fe system and experimental comparison with as-cast alloy microstructures as relevant to impurity driven corrosion of Mg-alloys

This page is intentionally left blank

Materials Chemistry and Physics 143 (2014) 1082–1091

Contents lists available at ScienceDirect

Materials Chemistry and Physics

journal homepage: www.elsevier.com/locate/matchemphys

CALPHAD simulation of the Mg–(Mn, Zr)–Fe system and experimental comparison with as-cast alloy microstructures as relevant to impurity driven corrosion of Mg-alloys

D.S. Gandel [a,b,*], M.A. Easton [a,b], M.A. Gibson [a,c], N. Birbilis [a,b]

[a] CAST Cooperative Research Centre, Australia
[b] Department of Materials Engineering, Monash University, Clayton, VIC 3800, Australia
[c] CSIRO Process Science and Engineering, Clayton, VIC 3168, Australia

HIGHLIGHTS

- Alloy microstructure of the Mg-(Mn,Zr, Fe) system was analysed and reported.
- CALPHAD analysis was used in conjunction with traditional SEM analysis techniques in this study.
- A proposed Mn–Fe interaction within Mg has been observed for the first time.
- Experimental validation of calculated phases is required to understand the effect of Mn and Zr on Mg .

ARTICLE INFO

Article history:
Received 11 July 2013
Received in revised form
20 September 2013
Accepted 3 November 2013

Keywords:
Alloys
Computer modelling and simulation
Electron microscopy
Corrosion

ABSTRACT

Four Mg alloys with variations in the ratio of Mn, Zr and Fe additions were cast and their microstructures analysed via electron microscopy. Thermodynamic calculations of the expected phases using PANDAT were evaluated with actual as-cast microstructures. Some of the as-cast alloys did appear to form phases similar to those anticipated from the PANDAT calculations. Furthermore, there was a new Mn–Fe particle interaction observed that was not predicted, but which is posited to be responsible for the increase in corrosion resistance among Mn containing Mg alloys with Fe impurities. The experimental work herein has been shown to be invaluable in the understanding of this practically important system with sparingly soluble Fe and its potential influence on the corrosion of Mg alloys.

1. Introduction

Magnesium has the lowest density of all the engineering metals [1], making it a desirable substitute for steel or aluminium where weight reduction and energy savings are a key concern [2,3]. However, it is well known that the service life of Mg alloys due to corrosion is a critical factor in the wider use of these materials [4]. As such, there is significant drive to develop Mg alloys with improved corrosion resistance [5], most notably in relation to the removal, or control, of deleterious Fe impurities [6,7] using specific alloying additions. Consequently, two key factors are noteworthy in the context of Mg corrosion.

(1) There exist a large number of common elements that are either insoluble or sparingly soluble in Mg; these include Cu, Fe and Ni. As these elements are insoluble, they form as isolated nano/micro-particles in the Mg matrix, leading to intense microgalvanic corrosion under open circuit exposure [8,9]. However, Fe pickup from most production and processing routes is the most prominent concern.
(2) In the Mg–Al alloy system, which has traditionally been the most utilised system for commodity Mg alloys, the deleterious effect of Fe was counteracted by additions of Mn, to form an $Al_8(Mn,Fe)_5$ particle, which is less problematic for microgalvanic corrosion following the seminal work of Boyer [8]. However, future Al-free Mg alloys will not be able to rely on this scavenging effect, and a renewed investigation of the Mg–Fe interaction is warranted.

Prior studies have proposed that Mn and Zr are two leading contenders as alloying-based approaches to counter the adverse

* Corresponding author. CAST Cooperative Research Centre, Australia. [redacted]

0254-0584/$ – see front matter © 2013 Published by Elsevier B.V.
http://dx.doi.org/10.1016/j.matchemphys.2013.11.008

effects of Fe impurities in Al-free Mg alloys, to improve overall alloy functionality and service life [6,10,11]. Mn and Zr play important roles as alloying elements and have low solid solubility limits, C_s, at 650 °C in Mg:Mn ≈0.95 at.% [12] and Zr ≈0.73 at.% [13]. The families of Mg alloys presently used commercially can be split into two main groups: Mg alloys that contain aluminium (Al) and Mg alloys that are Al-free and contain Zr for the purpose of grain refinement [14]. The Zr containing Mg alloys also frequently incorporate Zn and rare earth metals as additions (i.e. ZK60, ZE41) [15]; however, Zr is not added to Al containing Mg alloys because of the interaction with Al forming Al_3Zr intermetallics which negate the grain refining effect [16].

Mn is commonly added to Mg alloys for improving physical properties, such as solution strengthening and extrudability (i.e. M1, ME10) [17–19]. Whilst the role of Mn in Mg–Al alloys is clear with respect to corrosion, in Al-free Mg alloys it is hypothesised (but previously unproven) that Mn contributes to corrosion control of Mg by forming an encapsulating layer around Fe particles and separates them from direct contact with the magnesium matrix [20]. This is an important knowledge gap in the field that the present work seeks to address.

Zr is mainly added to Mg alloys as a grain refiner [1,5,14,21–23]. The reduction in grain size observed in Zr containing Mg alloys can increase the tensile strength greatly, improve casting quality and allows better control of the alloy texture [24–26], traits which can be required for specific engineering applications. As such, Zr is currently integrated into several commercially available Mg alloys such as WE54, ZE41, ZK60 and AM-SC1 [11,27–30]. Zr also has an Fe scavenging effect by forming Fe_2Zr, which can settle at the bottom of the Mg-alloy melt, decreasing the Fe content of Mg products. However, it has been shown recently that Zr is in itself deleterious to the corrosion of Mg, based on its ability to 'activate' the anodic reaction [31].

Previous work has proposed that Fe impurities are soluble in the Mn–Zr intermetallic phases when both Mn and Zr are incorporated in Mg [23]. While it is known that Mn, Zr and Fe do not form intermetallic phases with Mg [12,13,32], few studies have, however, delved further into the interactions between these elements and the alloy microstructure that forms within these Mg alloy systems. Calculation of the likely phases present for such a quaternary alloy system with a CALPHAD-based program such as PANDAT® can give an insight into the constituents of the likely microstructure which form, without having to engage in an extensive experimental program of Mg-(Mn, Zr, Fe) alloys. PANDAT calculates thermodynamics of multi-component systems to identify different equilibrium phases that form using the Gibbs energy function and the stable phase equilibrium of selected alloy compositions [33,34]. Moreover, information detailing the formation of those systems, such as the alloy cooling rates and resultant microstructures development can also be simulated [35].

Due to the cost-effectiveness, speed and widespread availability of CALPHAD software applicable to commercial alloy systems there has been an increase in published studies using these tools [36]. Unfortunately, for systems with very low solubility or major influences in properties as a result of trace elemental additions, incomplete validation of the predictions from thermodynamic databases raise doubts over the analyses that have been reported. Despite these limitations, CALPHAD simulation is still a popular tool as outputs from CALPHAD-based programs can further be used in other modelling programs to calculate additional properties such as particle size, particle distribution and even the mechanical properties of some alloy systems [37].

Despite the prevalence of published studies using CALPHAD programs there are only a limited number which attempt to verify the thermodynamics of the simulated alloy systems by comparing the models with real-world alloy analogues of the same alloy systems modelled [38,39]. This comparison between experimentally observed and modelled alloy systems leads to a better understanding of how the computer simulations can be used as a tool to predict interactions that can take place between alloying constituents in real alloy microstructures and improve predictions. An example of this is how alloying elements may interact with Fe impurities present in Mg alloys, as there has been the long standing corrosion issue for Fe in Mg and its alloys since the work of Boyer [8] and Hanawalt [9].

The work herein uses the theoretical calculations and models derived from the PANDAT software to predict the interactions taking place between the alloying constituents in the as-cast alloys. This study aims to relate the commonly used PANDAT predictions [33] to the interactions of specific elements in analogous Mg alloys. Furthermore, this study elucidates the role of how Mn and Zr alloying additions interact with Fe impurities to enhance the corrosion resistance of Mg alloys (of greatest relevance to the emerging class of Al-free creep resistant Mg alloys).

2. Experimental methods

2.1. Computer modelling

PANDAT (Computherm, Madison, WI. USA) was used to calculate the equilibrium phases expected in the Mg alloys produced herein. Phase analysis was carried out by inputting the various alloying elements Mn, Zr and Fe at different levels and allowing PANDAT to calculate the phases that form and their respective mass fractions in the alloy at selected temperatures. The PANDAT database PanMg8 was used in the calculations.

2.2. Alloy production

Mg alloys were made by blending the master alloys Mg – 2.12 wt.% Mn, Mg – 1.3 wt.% Fe and Mg – 25.0 wt.% Zr, supplied by CSIRO Australia, CAST-CRC and Magnesium Elektron, respectively, with commercially pure Mg (<40 ppm Fe) in a resistance furnace at 700 °C. AM-Cover® was employed as a cover gas to reduce oxidation during the casting process. The commercially pure Mg was initially melted in a crucible capable of producing 300 g ingots, to which small amounts of the master alloys were added to achieve specific Mn, Zr and Fe levels in the final castings. The melt was held at temperature for 20 min, during which it was mixed, and then poured into a graphite coated cast iron mould and allowed to air cool. The compositions of all the alloys produced were independently determined by inductively coupled plasma atomic emission spectroscopy, ICP-AES (Spectrometer Services, Coburg, Australia).

2.3. Electron microscopy

The microstructures of the alloys produced were examined via scanning electron microscopy (SEM). Specimens were polished to a 1 μm diamond paste finish and then imaged using a JEOL 7001F electron microscope in back scattered electron (BSE) mode. The microscope was equipped with energy dispersive X-ray spectroscopy (EDX) (Oxford Instruments X-Max 80 detector) capability, which allowed for the determination of elemental composition through EDX mapping of the particles that were observed in the microstructure. Electron back-scatter diffraction (EBSD) and analysis using HKL were also performed.

2.4. Corrosion determination

Specimen surfaces were ground to a 2000 grit surface finish. A 3-electrode flat-cell with an exposed sample area of 1 cm^2 was used in conjunction with a VMP 3Z potentiostat. All testing was carried out in 0.1 M NaCl, and potentiodynamic polarisation was conducted at 1 mV s^{-1}. Prior to polarisation the samples were conditioned for 10 min at open circuit to ascertain a close to stable potential. The polarisation curves were used to determine i_{corr} (via a Tafel-type fit) using EC-Lab software.

Tafel-type fits were executed by selecting a portion of the curve that commenced >50 mV from E_{corr}, and i_{corr} was estimated from the value where the fit intercepted the potential value of the true E_{corr}. Polarisation testing was also able to visually reveal comparative information related to the kinetics of both the anodic and cathodic reactions of the various Mg specimens – which was deemed an important aspect of the work. Each sample was tested five times and an average result was calculated.

Weight loss testing was also executed to provide a longer-term comparison of alloy corrosion, and was determined by immersion of samples in 0.1 M NaCl for a period of 24 h. The corrosion products were subsequently removed by light scrubbing following a 3s immersion in dilute (15%) HNO_3. The mass loss was determined on three unique samples and an average result was determined and reported.

3. Results and discussion

3.1. Alloy selection and characterisation

Four Mg alloys were prepared for analysis based on unique alloying contents to examine the interactions between the different alloying elements Mn, Zr and Fe. The four alloys were part of a series of alloys made in previous studies to examine the corrosion characteristics of Mg alloys with Mn, Zr and Fe as alloying additions [31,40]. These specific alloys were chosen from the alloy series based on their variation of Mn, Zr and Fe levels. ICP-AES analysis confirmed the relative amounts of each element in the alloys in this study (Table 1). The levels of Fe additions were above the solid solubility limit in all cases and Mn and Zr were below their solid solubility limits in Mg except for the Mg alloy containing both Mn and Zr [12,13,32].

Despite the Fe content of the Mn–Fe alloy being half of the Zr–Fe alloy, the Fe content is still well over the solubility limit in Mg, and the reported tolerance threshold of ~0.017 wt.% [41]. If perfect mixing were observed individually for these alloying levels in a binary system, Mn and Zr particles would only be expected to form in the Mn–Zr alloy as it is the only alloy examined with Mn and Zr contents above their solid solubility limits. All of the remaining alloys would then be expected to contain Mn and Zr in solid solution. Fe particles should be observed in all of the systems to which it was added.

However, as the alloy systems are not binary, but rather ternary and quaternary, the alloying additions interact with one another in a more complex manner that has not been observed previously. While it has been shown that Mn and Fe interact with one another in Mg, theories as to the nature of this interaction have not previously been proven experimentally. Moreover, Zr forms compounds with both Mn and Fe. As such, while each element can be expected to interact with Mg on its own, the interactions with the other additions alter the practical phase fractions (and types) that are present. As the Mg alloy system becomes more complex, the alloy matrix composition becomes more difficult to predict, necessitating the use of CALPHAD calculation in conjunction with microstructural analysis.

3.2. Corrosion analysis

Short-term electrochemical polarisation and long-term immersion weight-loss corrosion tests were performed to determine the corrosion characteristics of the four Mg alloys. The Zr–Fe alloy has the highest short and long-term corrosion rates, followed by the Mn–Zr–Fe alloy (Table 2). The addition of Mn into Mg alloy systems with a lower number of alloying additions that are known to be detrimental to Mg (Zr and Fe) is beneficial for improved corrosion control. However, the Mn–Zr and Mn–Fe alloys each have the lowest short-term and long-term corrosion rates, respectively.

The differences in the long and short-term corrosion rates for the Mn–Zr or Mn–Fe Mg alloys are likely caused by a number of factors. Microstructural properties, such as the effect of the alloying addition on the Mg matrix and the interactions of the additions on impurities are the likely controlling factors of the long-term immersion weight loss corrosion rates. Other properties that are intrinsic to the specific Mg alloy may be how the alloying additions affect the semi-protective surface film which affects the short-term polarisation corrosion rates.

In either case, it can be shown that while Fe is overall detrimental for the corrosion control of Mg, the effect of Mn and Zr on the corrosion of Mg warrants further attention. PANDAT modelling and SEM analysis of these systems can elucidate the interactions between these elements and how they effect the corrosion of Mg.

3.3. PANDAT analysis

For all four Mg alloys, PANDAT compositional phase analysis using both the Lever rule (equilibrium) and the Scheil condition (non-equilibrium) was performed. The results of both methods were very similar, predicting that the vast majority of the phase mass fraction (over 99%) will be essentially pure Mg with small amounts of intermetallics forming from the alloying additions interacting with one another at the point of solidification (Table 3). This difference in the phase mass fraction is expected as the alloying levels are low (Table 1) and that none of the studied alloying elements form intermetallic phases with Mg [12,13,32] – which is why they are so important in influencing the corrosion of Mg. The phase assembly results presented herein are of the Scheil condition (non-equilibrium) results.

Compositional phase analysis for both the Zr–Fe and Mn–Fe containing alloys are expected to have a single phase present other than the Mg matrix for the precise alloy contents of the Mg alloys. The mass fractions of these phases are very low due to the low

Table 1
ICP-AES elemental analysis of alloys produced.

Alloy ID	Mg wt.%	Mn wt.%	Zr wt.%	Fe wt.%
Zr–Fe	~Bal	<0.01	0.21	0.13
Mn–Fe	~Bal	0.77	<0.01	0.07
Mn–Zr	~Bal	2	0.72	<0.005
Mn–Zr–Fe	~Bal	0.88	0.35	0.13

Table 2
Corrosion related parameters for the alloys studied.

Alloy ID	Mass loss (mg cm^{-2} day^{-1})	i_{corr} (μA cm^{-2})
Zr–Fe	50(±9.7)	102.1(±8.7)
Mn–Fe	3.4(±1.5)	47.9(±3.2)
Mn–Zr	8.5(±4.8)	31.8(±5.0)
Mn–Zr–Fe	33(±19)	82.5(±17.0)

Table 3
PANDAT phase analysis of predicted alloy phases formed using the Scheil condition and total phase fractions at the end of solidification.

Alloy ID	Phase 1		Phase 2		Phase 3	
	ID	wt.%	ID	wt.%	ID	wt.%
Zr–Fe	Mg	99.915	Fe_2Zr	0.085	None	0
Mn–Fe	Mg	99.95	Mn–Fe (FCC)	0.05	None	0
Mn–Zr	Mg	99.41	Mn_2Zr	0.59	None	0
Mn–Zr–Fe	Mg	99.715	Mn_2Zr	0.205	$Fe_{23}Zr_6$	0.08

levels of alloying elements. PANDAT predicts that the expected additional phase in the Zr–Fe alloy is Fe_2Zr. Modelled isopleths predict that when the Zr content is varied in the Zr–Fe alloy it is predicted to change the Zr–Fe intermetallic phase that forms in the liquid domain of the Mg melt as the alloy is cast into a mould and allowed to cool (Fig. 1A).

The extra Mn–Fe phase in the Mn–Fe alloy, which was predicted by PANDAT to be an FCC phase, consisted of 61.3% Fe and 38.7% Mn. The Fe-Mn phase diagram indicates that the FCC austenitic phase of Fe would allow for a high level of Mn to be dissolved in solid solution [42]. The isopleth for the Mg–Mn–Fe system shows that when the Mn content is varied in the Mn–Fe alloy there are three main regions where there is a single extra phase. Other than Mg and two narrow bands separating these three regions where there is a transitional zone with two phases present (Fig. 1B). Another aspect of note in the high temperature solid state transformations of this alloy is the change from FCC and HCP at 600 °C to CBCC and HCP at 500 °C (Mn–Fe alloy in Table 1). In theory, if this transformation is non-equilibrium and does not go to completion, it may create a Mn–Fe phase where a (Fe-rich) FCC core is encapsulated by a (Mn-rich) CBCC phase.

The Mn and Zr additions in the Mn–Zr alloy are also predicted to combine and form a single Mn_2Zr phase. This particular phase has the largest mass fraction of just under 0.6% due to the higher levels of Mn and Zr present in the alloy compared to the alloying content levels of the three other compositions. PANDAT predicts that there will be an Mn phase in the Mg matrix at an Mn content of 2 wt.%. As the Zr content of the Mn–Zr alloy is increased a second phase, the Mn_2Zr phase, will begin to form in the Mg alloy matrix (Fig. 1C).

For the Mn–Zr–Fe alloy, the PANDAT compositional phase analysis has two phases forming other than the Mg matrix. This is due to the addition of all three alloying elements creating a more complex system where multiple interactions are taking place simultaneously. Calculations predict that the Mn_2Zr and $Fe_{23}Zr_6$ phases will form. In the case of three alloying additions (quaternary alloy) a PANDAT calculated isopleth of the Mn–Zr–Fe alloy reveals the associated complexity of this system (Fig. 1D). With an increasing Zr content and Fe and Mn contents at the same levels as

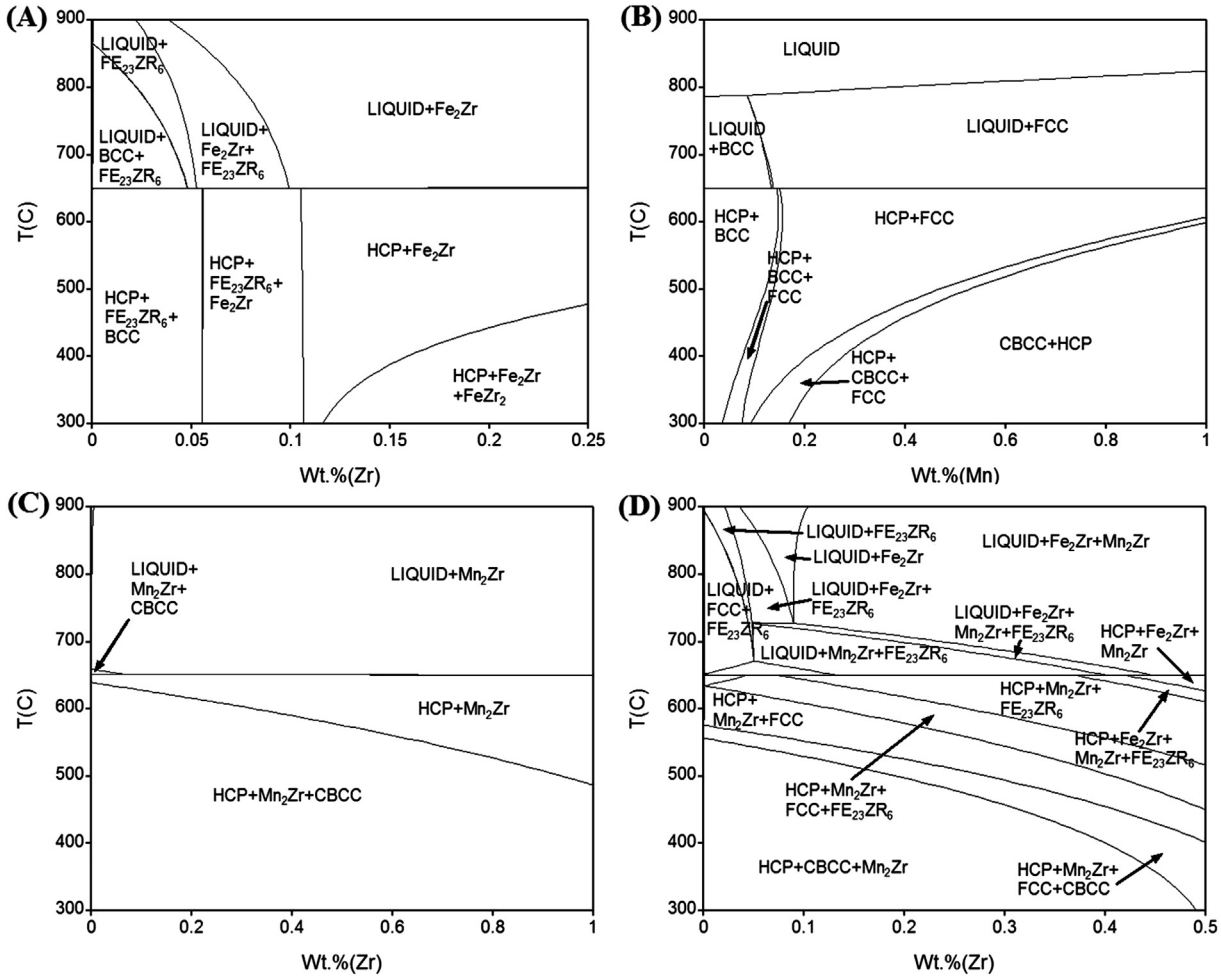

Fig. 1. PANDAT calculated isopleth diagrams depicting phases present in (A) Mg–Fe–Zr alloy with an increasing Zr content, (B) Mg–Mn–Fe alloy with an increasing Mn content, (C) Mg–Mn–Zr alloy with an increasing Zr content, and (D) Mg–Mn–Zr–Fe alloy with increasing Zr content.

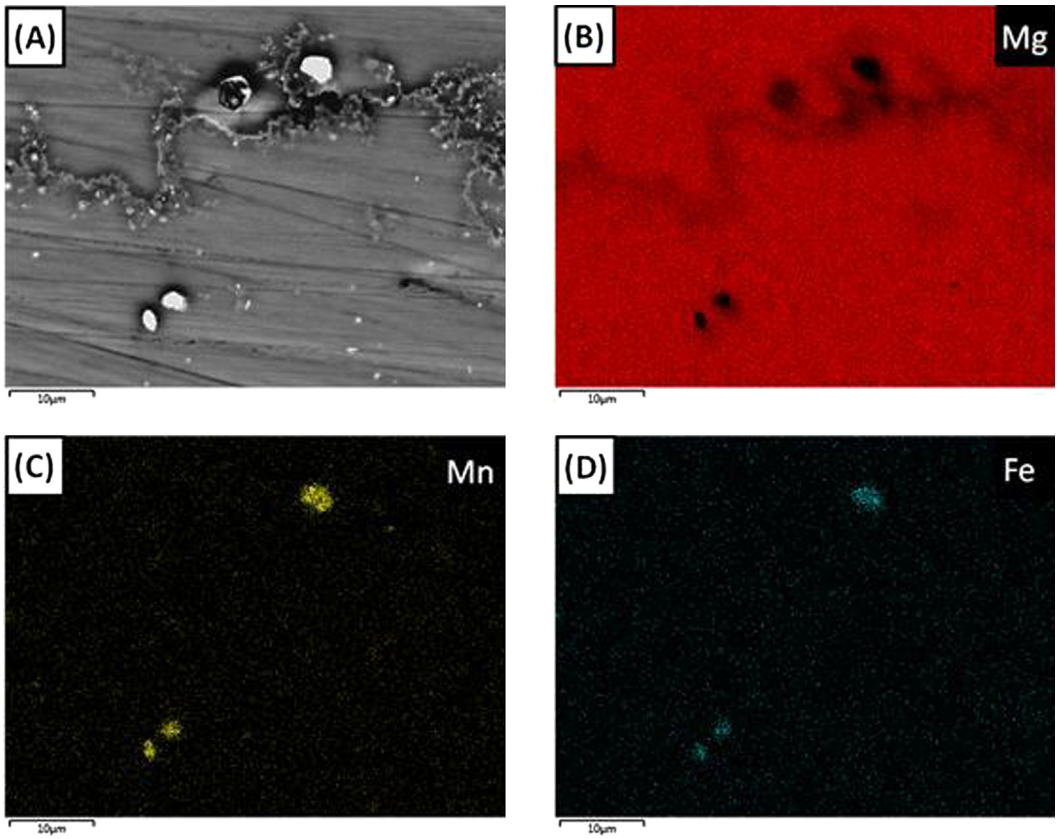

Fig. 2. (A) BSE-SEM micrograph of Mn–Fe–Mg-alloy, (B) corresponding EDX map of Mg content, (C) corresponding EDX map of Mn content, and (D) corresponding EDX map of Fe content.

the Mn–Zr–Fe alloy there are many phases predicted to form, made up from Mn–Zr and Zr–Fe intermetallic phases and elemental Mn and Fe phases.

3.4. SEM and EDX analyses and microstructural assessment

SEM analysis and EDX mapping were employed to identify particles and phases present in the Mg alloy matrix. The microstructures of the as-cast alloys were examined to ascertain how the relative amounts of each alloying element as measured from the ICP-AES data were distributed within the alloys following casting and solidification.

The Mn–Fe alloy contains particles ranging mainly from 1 to 20 μm in size embedded in the Mg-matrix (Fig. 2A). EDX analysis distinguishes that these particles are not Mg containing intermetallic phases (Fig. 2B) but are actually particles that contain mostly elemental Mn and sometimes with Fe integrated into the Mn particles (Fig. 2C and D). While there is some trace amount of Mn and Fe detected in the matrix, there are large clustered Mn particles and Fe EDX peaks where these particles are located. Further analysis of the particles revealed that while the small Mn particles do not contain Fe there were a very small number of large (over 50 μm) Fe particles that were surrounded by Mn. The only place Fe was detected other than in the Mg matrix (i.e. Fe dissolved in solid solution) was in association with Mn. There were also some small (<5 μm) elemental Mn particles observed.

Despite the difference in morphology between the smaller and larger Mn–Fe particles in the matrix, the PANDAT simulations showed that a distinct Mn–Fe phase would form via an interaction between the two elements. As Fe is well known to be detrimental to the corrosion control of Mg, simulating the Mg–Mn–Fe alloy system with PANDAT can show that Mn will interact with Fe without forming an intermetallic with Mg. The addition of alloying elements specifically designed to target Fe impurities without affecting the corrosion characteristics of Mg is a high priority for both materials researchers and manufacturers.

There are many large particles throughout the matrix of the Mn–Zr alloy that EDX confirms do not contain any Mg (Fig. 3A and B). There is also a detectable amount of Mn dissolved in solution in the Mg alloy matrix (Fig. 3C) and only a small amount of Zr present in solid solution (Fig. 3D) due to the larger amount of Mn added to the alloy (Table 1) and the higher solid solubility limit of Mn in Mg compared to Zr. The particles present are distinct in that they are in fact separate elemental Mn and elemental Zr particles. Overall there are a greater number of Zr particles in the matrix than Mn particles. Again this may be due to either the lower solid solubility of Zr in Mg preventing all the Zr from being dissolved in solid solution or a portion of the Zr introduced into the melt as part of the Mg-Zr master alloy not dissolving completely, there-by leaving behind non-equilibrium Zr particles. There does not appear to be any signs of mixed Mn–Zr particles present.

Although only separate elemental Mn and Zr particles were observed during the SEM testing, the PANDAT simulations predicted that the Mn and Zr additions would combine and form a Mn_2Zr intermetallic phase in Mg. This does not exclude the possibility that no Mn_2Zr was created during the casting process. As with the Fe_2Zr particles in the Zr–Fe alloy, the Mn_2Zr particles can settle out of the melt during processing. Although there has also been very little research into Mn–Zr interactions in Mg, the Mn_2Zr phase has been observed experimentally [23]. The PANDAT calculations,

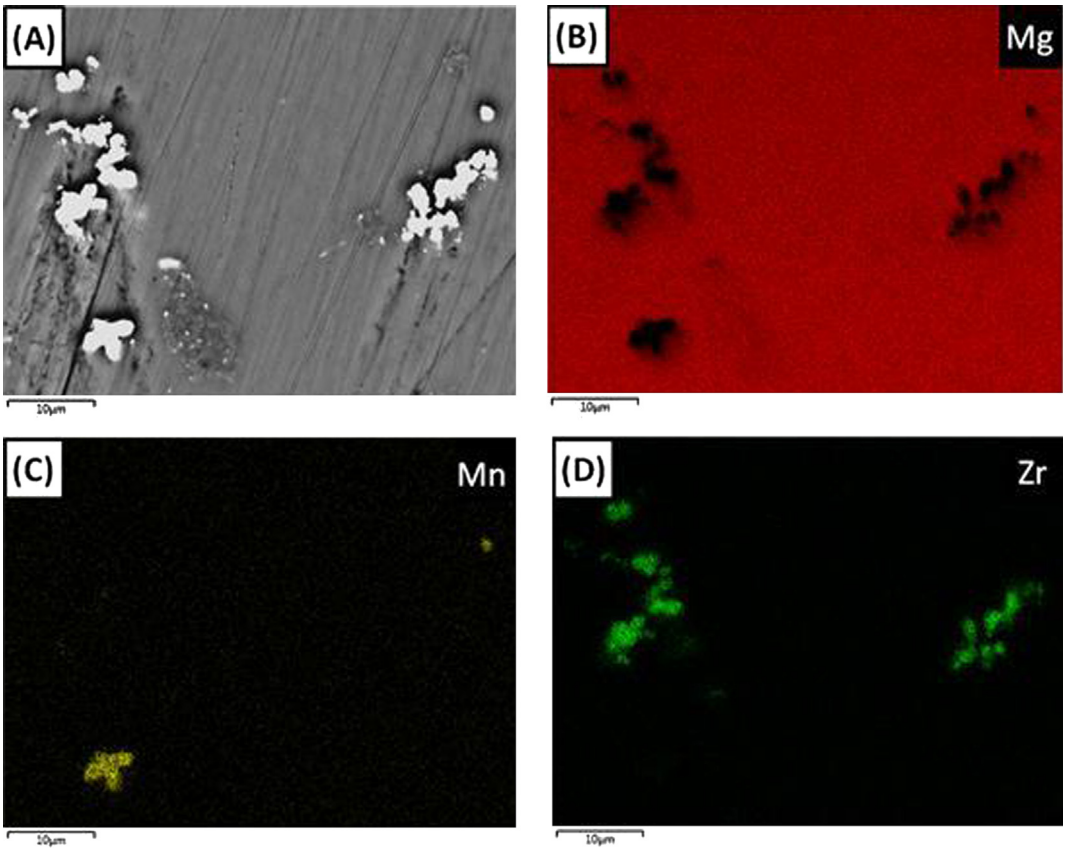

Fig. 3. (A) BSE-SEM micrograph of Mn–Zr–Mg-alloy, (B) corresponding EDX map of Mg content, (C) corresponding EDX map of Mn content, and (D) corresponding EDX map of Zr content.

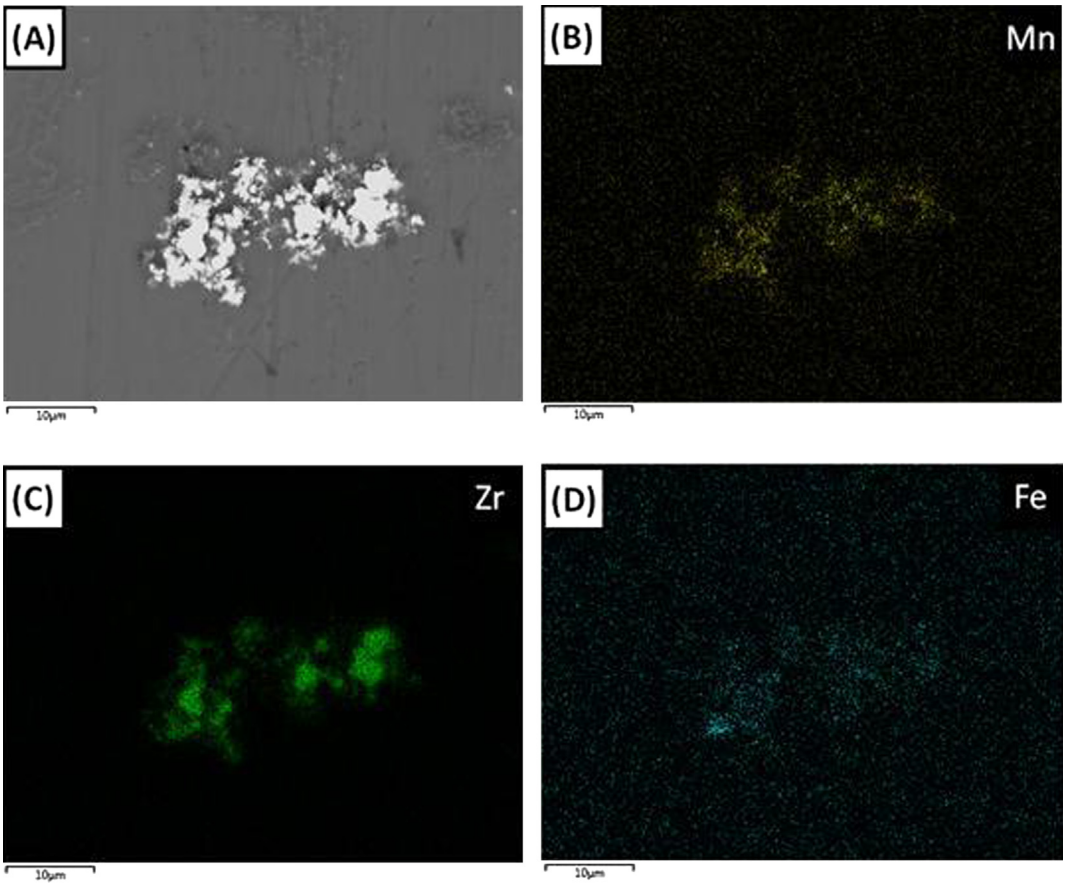

Fig. 4. (A) BSE-SEM micrograph of Mn–Zr–Fe–Mg-alloy, (B) corresponding EDX map of Mn content, (C) corresponding EDX map of Zr content, and (D) corresponding EDX map of Fe content.

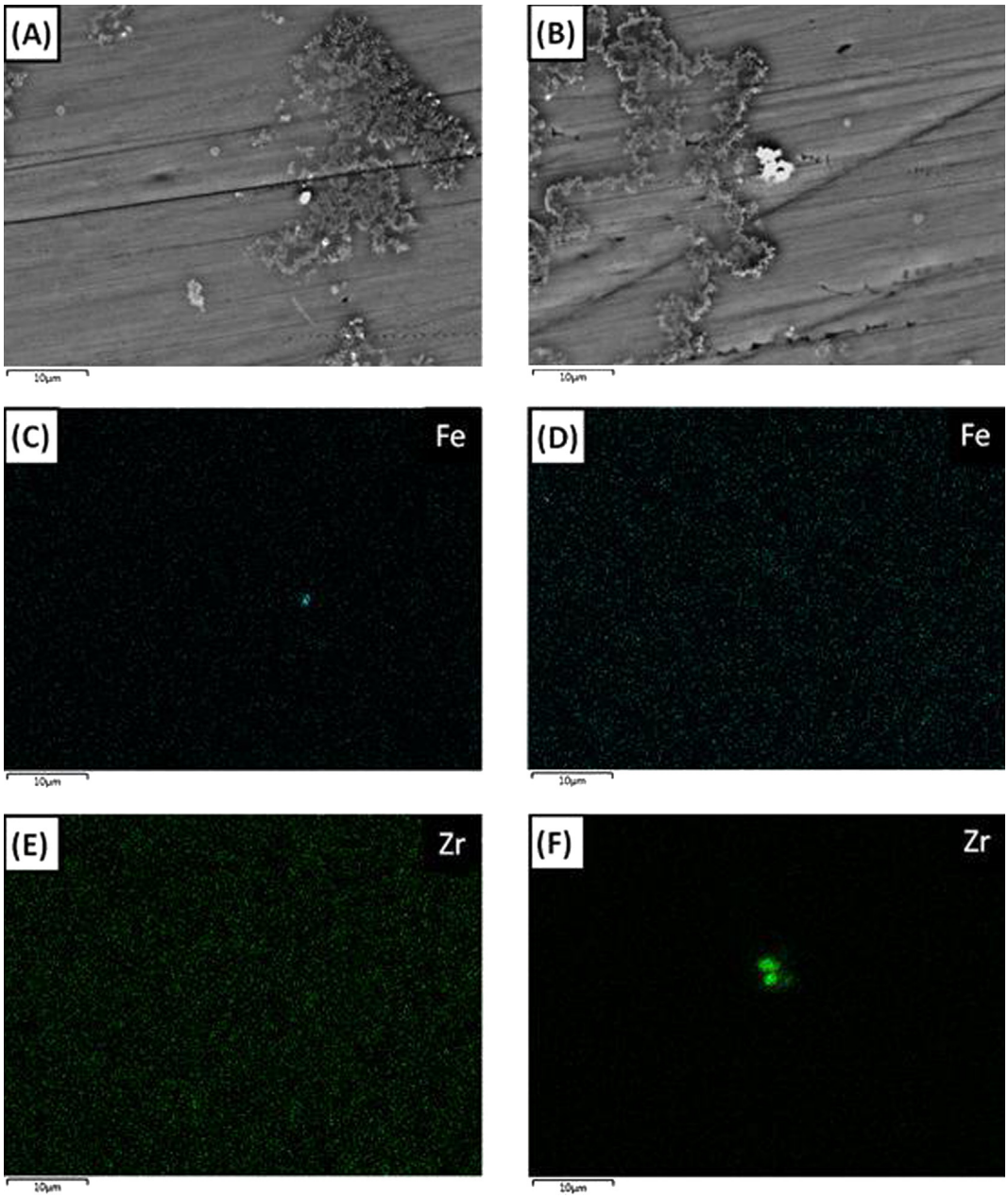

Fig. 5. (A) BSE-SEM site 1 micrograph of Zr–Fe–Mg-alloy, (B) BSE-SEM site 2 micrograph of Zr–Fe Mg-alloy, (C) corresponding site 1 EDX map of Fe content, (D) corresponding site 2 EDX map of Fe content, (E) corresponding site 1 EDX map of Zr content, and (F) corresponding site 2 EDX map of Zr content.

which are based on the thermodynamics driving the interaction between the alloying elements and is not designed to take into account the processing of the melt or the difference in densities between the Mg melt and the new Mn_2Zr particles that form before the ingot is cast.

There are a number of particle clusters embedded in the Mg matrix of the Mn–Zr–Fe alloy (Fig. 4A). These particle clusters contain Mn and Zr. The cores of the particles are Zr-rich regions with some Mn and occasionally there were Fe intermetallic phases around these Zr cores. Upon further inspection of the Mg matrix, Mn and Fe are present dissolved in the Mg matrix (Fig. 4B and D), however, there is relatively little Zr dissolved in solid solution (Fig. 4C). There were also large Fe particles present (up to 100 μm) that were encapsulated by Mn in areas that were largely devoid of Zr.

The PANDAT simulations predicted that these phases are Mn_2Zr and $Fe_{23}Zr_6$ (Table 3). However, as PANDAT has shown in the Mg–Mn–Fe system, Mn and Fe can also interact with one another in Mg. The simulations for the Mn–Zr–Fe Mg alloy are based on 'perfect mixing' scenarios where the reaction kinetics drive the expected interactions between each alloying element until the reaction is complete and one of the two elements in the reaction has been used up. As these are real-world casting situations there are incomplete reactions which can leave individual alloying elements present in the Mg alloy which they themselves can continue to interact with other elements present in the system. This is evident by the Mn–Fe particles observed in the Mn–Zr–Fe alloy microstructure. As such, while in this case there were particles present based on interactions between elements that were not explicitly calculated by PANDAT based on the levels of alloying elements

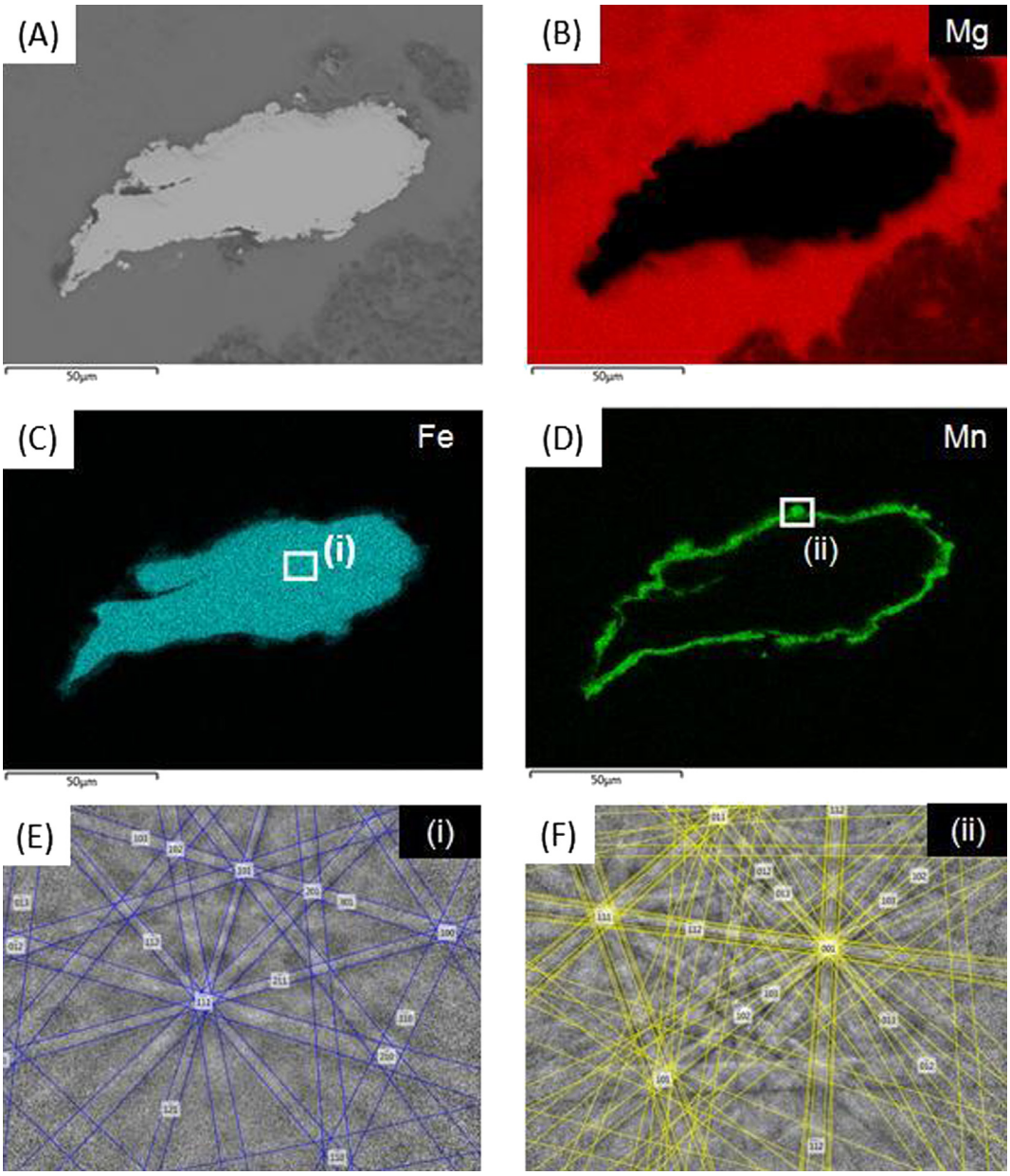

Fig. 6. (A) BSE-SEM image of Mn–Fe particle in Mg alloy Mn–Zr–Fe, (B) corresponding EDX map of Mg content, (C) corresponding EDX map of Fe content, (D) corresponding EDX map of Mn content, (E) EBSD Kikuchi pattern of internal structure of Mn–Fe particle (region denoted as (i)) and (F) EBSD Kikuchi pattern of outside layer of Mn–Fe particle (region denoted as (ii)).

present, PANDAT can determine, on a singular element-to-element basis, all of the possible interactions that can be expected to take place between alloying elements in an Mg alloy system.

Various particles are present in the matrix of the Zr–Fe Mg alloy (Fig. 5A and B). EDX scans of the microstructure reveal that there did not appear to be any Fe_2Zr intermetallic particles present or any significant interaction between Zr and Fe observed in the alloy. There are separate metallic Zr and Fe particles present throughout the alloy microstructure, however, there was little interaction or association between the location and proximity of the elemental particles within the Mg matrix. The regions with elemental particles were observed to have a reduced amount of that particular element dissolved in solid solution (Fig. 5C–F).

As mentioned previously, it is well known that Zr can remove Fe from Mg by forming the Fe_2Zr intermetallic and 'settling out' of the Mg melt during manufacturing and casting processes, leaving the final Mg alloy casting with a lower level of Fe. PANDAT shows the interactions between these elements within the alloy system. The calculations show that this phase will form, driven by the reaction kinetics between Fe and Zr. These calculations, coupled with the published experimental work detailing the Fe_2Zr phase in Mg and how it is empirically known to 'settle out' of the Mg melt during manufacturing can be used in conjunction to predict the expected microstructure of a cast ingot of the Mg–Zr–Fe alloy system [10,14].

3.5. Mn–Fe particle analysis

A more in-depth SEM analysis was performed to identify the interaction taking place between Mn and Fe. During EDX analysis most particles observed in the alloys produced in this study were

smaller than 20 μm and were either particles entirely of a single element, or particles constituted from a mixture of Mn and Fe. However, in the alloys with high Mn and Fe contents there were also a number of non-Mg containing particles present that were up to 100 μm in length (Fig. 6A and B). The Mn–Zr–Fe alloy had several of these large particles located in regions with almost no Zr present. While the inside of the particle is predominantly Fe, there is an encapsulating layer of Mn clearly visible that surrounds the Fe core (Fig. 6C and D). Upon closer inspection of the Mn layer, there is a weaker Fe EDX peak that coincides with the Mn layer. This indicates that there is a small amount of Fe dissolved in the Mn layer. This Mn–Fe particle structure where Mn forms an encapsulating layer around Fe had been previously proposed to occur [20,43], but this is the first documented observation.

If the FCC to CBCC transformation in the PANDAT calculations was incomplete then it may be possible for a Mn–Fe phase with FCC Fe encapsulated by CBCC Mn to form. EBSD was used to differentiate the phase structure of the inside of the large Fe particle and the outer encapsulating Mn layer. Analysis of the inside of the large Fe particle (Fig. 6E) confirms that the Fe particle has a BCC structure compared to the FCC structure predicted by PANDAT. The PANDAT simulations predicted that the Mn–Fe particles would consist of just under 40 wt.% Mn. With this high level on Mn present in solid solution in Fe the γ-Fe (FCC) phase for the Mn–Fe particles should be able to form at the casting and holding temperature of 700 °C [42]. However, there may be other thermodynamic or kinetic interactions taking place that changes the morphology of these Mn–Fe particles, such as the influence of other impurities present in the Mg melt or the methods used in casting the Mg alloy ingot.

Analysis of the outer encapsulating Mn layer around the particle (Fig. 6F) shows that the Mn layer has an α-Mn structure. There is some limited solubility of Fe in α-Mn [42] and the previous EDX micrographs (Fig. 6C and D) show that there is a small amount of Fe present in the encapsulating Mn layer. The Kikuchi band analysis from the EBSD computer software was within the statistical measurement precision allowed by the software for accurate confirmation for both phases presented herein.

This Mn layer around the Fe particle has been the proposed mechanism behind the improvements in the corrosion properties of Mn containing Mg alloy. This has a profound effect on the corrosion kinetics of Mg alloys with Fe impurities as the very low solubility of pure Fe in Mg (0.00043 at.% [32]) would normally cause small elemental Fe particles to form in the matrix. The electrochemical potential difference between Mg and Fe is relatively large (~0.95 V) and leads to severe localised corrosion under immersion/exposure conditions [44]. In contrast, the Mn layer acts as a barrier between the electrochemical potential difference between Mg and Fe, reducing the deleterious effect of Fe impurities on the alloy. While this difference in potential is still a concern for corrosion, the damage accumulated appears to be less severe when Fe is encapsulated in Mn as the phase is more weakly polarised in Mg alloys. In order to relate the work herein with corrosion studies reported in the literature [7–9,45], corrosion measurements for the alloys studied are also presented (Table 2) – although these are not the focus of the present paper.

3.6. Evaluation of the use of PANDAT to predict interactions between Mn, Zr and Fe alloying constituents in Mg

The work herein suggests that while PANDAT can elucidate the interactions that are likely to take place in this alloy system, there are certain limits to the use of PANDAT as a tool to predict the microstructure of an Mg-(Mn, Zr, Fe) alloy. While the precise prediction of the expected microstructure of an alloy simulated in this study can lack a degree of accuracy, the driving forces and expected interactions between the constituent Mn, Zr and Fe alloying elements can provide insight into how the alloy system is expected to find an equilibrium state with a greater degree of certainty.

4. Conclusions

- It was observed experimentally, for the first time, that Mn can, and does, form an apparent encapsulating layer around Fe particles present in Mg. This evidence further proves the benefits of reducing the deleterious effect of Fe impurities via alloying additions of Mn, even in Al-free Mg systems.
- Whilst CALPHAD analysis can offer some insight into the expected interactions between alloying elements in the Mg–Fe system with Mn or Zr present, these calculations are thermodynamic expectations of the equilibrium and optimal mixing scenarios. For the Mg-(Mn, Zr, Fe) system, these calculations show that this very sparingly soluble system can be frustrated by such small alloying additions and the real life scenario of elemental distributions is less likely to match an ideal scenario. The work herein verifies that microstructural analysis is necessary to form a complete understanding of how small, but influential alloying additions such as Mn and Zr can influence the Mg alloy system as a whole.
- EDX mapping and EBSD analysis of the particles present in the as-cast samples show that there are interactions between the alloying elements taking place in a similar manner to those calculated predictions. The experimental validation of phases observed was shown to be invaluable, particularly when relating the properties (such as corrosion rate) to the associated structure/phases.

Acknowledgements

The CAST Co-operative Research Centre was established under, and was funded in part by, the Australian Governments Co-operative Research Centres Scheme. Andy Yob, Ming Sun and Sherly Simanjuntak are gratefully acknowledged for their technical assistance. All alloys produced in this study were made at CSIRO Process Science and Engineering, Clayton, Australia.

References

[1] E.F. Emley, Principles of Magnesium Technology, first ed., Pergamon Press, Manchester, 1966.
[2] K.U. Kainer, Magnesium – Alloys and Technology, Wiley-VCH, 2003.
[3] I.J. Polmear, Light Alloys, third ed., Arnold, London, England, 1995.
[4] N. Birbilis, M.A. Easton, A.D. Sudholz, S.M. Zhu, M.A. Gibson, On the corrosion of binary magnesium-rare earth alloys, Corros. Sci. 51 (2009) 683–689.
[5] G. Song, D. StJohn, The effect of zirconium grain refinement on the corrosion behavior of magnesium-rare earth alloy MEZ, J. Light Met. 2 (2002) 1–16.
[6] G.T. Parthiban, N. Palaniswamy, V. Sivan, Effect of manganese addition on anode characteristics of electrolytic magnesium, Anti-Corros. Methods Mater. 56 (2009) 79–83.
[7] G.L. Makar, J. Kruger, Corrosion of magnesium, Int. Mater. Rev. 38 (1993) 138–153.
[8] J.A. Boyer, The Corrosion of Magnesium and of the Magnesium Aluminum Alloys Containing Manganese, American Magnesium Corporation, 1927, pp. 417–454.
[9] J.D. Hanawalt, C.E. Nelson, J.A. Peloubet, Corrosion studies of magnesium and its alloys, Trans. Am. Inst. Min. Metall. Eng. 147 (1942) 273–298.
[10] A. Prasad, P.J. Uggowitzer, Z. Shi, A. Atrens, Production of high purity magnesium alloys by melt purification with Zr, Adv. Eng. Mater. 14 (2012) 477–490.
[11] T. Rzychon, J. Michalska, A. Kielbus, Corrosion resistance of Mg–RE–Zr alloys, J. Achieve. Mater. Manuf. Eng. 21 (2007) 51–54.
[12] H. Okamoto, Mg–Mn (magnesium–manganese), J. Phase Equilib. Diffus. 29 (2008) 208–209.
[13] H. Okamoto, Mg–Zr (magnesium–zirconium), J. Phase Equilib. Diffus. 28 (2007) 305–306.

[14] P. Cao, M. Qian, D.H. StJohn, M.T. Frost, Uptake of iron and its effect on grain refinement of pure magnesium by zirconium, Mater. Sci. Technol. 20 (2003) 585–592.
[15] Q. Peng, Y. Huang, K.U. Kainer, N. Hort, Development of high performance single-phase solid solution magnesium alloy at low temperature, Adv. Eng. Mater. 14 (2012) 178–184.
[16] F. Kabirian, R. Mahmudi, Effects of Zr additions on the microstructure and impression creep behaviour of AZ91 magnesium alloy, Metall. Mater. Trans. 41A (2010) 3488–3498.
[17] A.F. Smith, The isothermal growth of manganese precipitates in a binary magnesium alloy, Acta Metall. 15 (1967) 1867–1873.
[18] H.E. Friedrich, B.L. Mordike, Magnesium Technology, Springer, Berlin, 2006.
[19] L.L. Rokhlin, Magnesium Alloys Containing Rare Earth Metals, Taylor & Francis Group, 2003.
[20] J.D. Robson, D.T. Henry, B. Davis, Particle effects on recrystallization in magnesium-manganese alloys: particle-stimulated nucleation, Acta Metall. 57 (2009) 2739–2747.
[21] M. Qian, D.H. StJohn, Grain nucleation and formation in Mg–Zr alloys, Int. J. Cast Met. Res. 22 (2009) 256–259.
[22] M. Qian, D.H. StJohn, M.T. Frost, Zirconium alloying and grain refinement of magnesium alloys, in: H.I. Kaplan (Ed.), Magnesium Technology, The Minerals, Metals and Materials Society, 2003, pp. 209–214.
[23] M.A. Easton, C.H.J. Davies, M.R. Barnett, F. Pravdic, Effect of solidification grain refinement on the development of wrought Mg alloys, Mater. Sci. Forum 539–543 (2007) 1729–1734.
[24] W. Yuan, S.K. Panigrahi, J.Q. Su, R.S. Mishra, Influence of grain size and texture on Hall–Petch relationship for a magnesium alloy, Scr. Mater. 65 (2011) 994–997.
[25] C.D. Lee, Effect of grain size on the tensile properties of magnesium alloy, Mater. Sci. Eng. A 459 (2007) 355–360.
[26] H. Han, S. Liu, L. Kang, L. Liu, Refinement role of electromagnetic stirring and calcium in AZ91 magnesium alloy, J. Wuhan Univ. Technol. Mater. Sci. Ed. 23 (2007) 194–197.
[27] P. Lyon, New magnesium alloy for aerospace and specialty applications, in: A.A. Luo (Ed.), Magnesium Technology, TMS, 2004, pp. 311–315.
[28] C.J. Bettles, M.A. Gibson, S.M. Zhu, Microstructure and mechanical behaviour of an elevated temperature Mg-rare earth based alloy, Mater. Sci. Eng. A 505 (2009) 6–12.
[29] A.C. Hanzi, F.H.D. Torre, A.S. Sologubenko, P. Gunde, R. Schmid-Fetzer, M. Kuehlein, J.F. Loffler, P.J. Uggowitzer, Design strategy for microalloyed ultra-ductile magnesium alloys, Phil. Mag. Lett. 89 (2009) 377–390.
[30] S.C. Wang, C.P. Chou, Effect of adding Sc and Zr on grain refinement and ductility of AZ31 magnesium alloy, J. Mater. Process. Technol. 97 (2007) 116–121.
[31] D.S. Gandel, M.A. Easton, M.A. Gibson, T. Abbott, N. Birbilis, The influence of Mg–Zr master alloy microstructure on the corrosion of Mg, in: N. Hort, S.N. Mathaudhu, N.R. Neelameggham, M. Alderman (Eds.), Magnesium Technology, The Minerals, Metals and Materials Society, San Antonio, Texas, USA, 2013, pp. 157–162.
[32] A.A. Nayeb-Hashemi, J.B. Clark, L.J. Swartzendruber, The Fe–Mg (iron–magnesium) system, Bull. Alloy Phase Diag. 6 (1985) 235–238.
[33] S.L. Chen, S. Daniel, F. Zhang, Y.A. Chang, X.Y. Yan, F.Y. Xie, R. Schmid-Fetzer, W.A. Oates, The PANDAT software package and its applications, Calphad 26 (2002) 175–188.
[34] S.L. Chen, F. Zhang, S. Daniel, F.Y. Xie, X.Y. Yan, Y.A. Chang, R. Schmid-Fetzer, W.A. Oates, Calculating phase diagrams using PANDAT and PanEngine, JOM 55 (2003) 48–51.
[35] S. Chen, Y. Yang, W. Cao, B.P. Bewlay, K.-C. Chou, Y.A. Chang, Calculation of two-dimensional sections of liquidus projections in multicomponent systems, J. Phase Equilib. Diffus. 29 (2008) 390–397.
[36] U.R. Kattner, The thermodynamic modeling of multicomponent phase equilibria, J. Mater. 49 (1997) 14–19.
[37] W. Cao, F. Zhang, S.L. Chen, C. Zhang, Y.A. Chang, An integrated computational tool for precipitation simulation, J. Mater. 63 (2011) 29–34.
[38] M. Liu, P.J. Uggowitzer, A.V. Nagasekhar, P. Schmutz, M. Easton, G.-L. Song, A. Atrens, Calculated phase diagrams and the corrosion of die-cast Mg–Al alloys, Corros. Sci. 51 (2008) 602–619.
[39] Y. Guo, J. Li, J. Li, Z. Yang, J. Zhao, F. Xia, M. Liang, Mg–Gd–Y system phase diagram calculation and experimental clarification, J. Alloys Compd. 450 (2008) 446–451.
[40] D.S. Gandel, N. Birbilis, M.A. Easton, M.A. Gibson, Influence of manganese, zirconium and iron on the corrosion of magnesium, in: Corrosion and Prevention 2010, Australasian Corrosion Association, Adelaide, Australia, 2010, pp. 1–11.
[41] J.E. Hillis, The effects of heavy metal contamination on magnesium corrosion performance, in: Light Metal Age, SAE, Detroit, 1983, pp. 25–29.
[42] V.T. Witusiewicz, F. Sommer, E.J. Mittemeijer, Reevaluation of the Fe–Mn phase diagram, J. Equilib. Diffus. 25 (2004) 346–354.
[43] J.G. Kim, A.J. Koo, Effect of alloying elements on electrochemical properties of magnesium-based sacrificial anodes, Corros. Sci. 56 (2000) 380–388.
[44] A.D. Sudholz, N.T. Kirkland, R.G. Buchheit, N. Birbilis, Electrochemical properties of intermetallic phases and common impurity elements in magnesium alloys, Electrochem. Solid-State Lett. 14 (2011) C5–C7.
[45] R.E. McNulty, J.D. Hanawalt, Some corrosion characteristics of high purity magnesium alloys, in: R.B. Mears (Ed.), Eighty-first General Meeting, Nashville, Tennessee, USA, Transactions of the Electrochemical Society, 1942, pp. 423–433.

This page is intentionally left blank

Chapter 8

Summary

This page is intentionally left blank

Chapter 8: Summary

8.1 Conclusions

In this section, an attempt is made to conclude with not only the findings from individual presented manuscripts, but also to summarise the overall outcomes in terms of the implications of the individual pieces of work, when combined with the literature review regarding Mn and Zr, and how they affect the corrosion behaviour of Mg. Moreover, prior to this study, there was little to no data available on the corrosion behaviour of pure Mn and Zr. The initial corrosion testing conducted on these metals was not only done to relate how these elements affect the corrosion of Mg when they are included in the alloy composition, but to also expand the fundamental understanding of these elements that has been unavailable until now.

Mn is commonly added to Mg-alloys to improve the extrudability and machinability of the alloy [3, 75, 82]. However, Mn is also added to improve the corrosion performance of Mg alloys that contain Al as an alloying addition. The formation of the $Al_8(Mn,Fe)_5$ phase, which renders the Fe impurities less detrimental in the Mg-alloy has been well reported on in the literature [1, 2, 8]. However, there have been a number of papers published which propose that Mn can 'encapsulate' Fe particles in the Mg matrix, yet there has been no evidence presented to support this mechanism [92, 93]. The results in this study are the first definitive proof, with visual presentations of SEM micrographs and EDX and EBSD analysis of this Mn-Fe particle interaction, that this encapsulation of Fe by Mn does take place and that it is by this interaction that Mn reduces the detrimental effect of Fe impurities on Mg. Moreover, the results also indicate that apart from affecting the Fe impurities in Mg, low levels of Mn additions can reduce the cathodic reaction kinetics and the overall corrosion rate of Mg as well.

The main use of Zr in Mg has been to refine the grain size and increase the mechanical properties of current commercial Mg-alloys. Almost all studies on the effect of Zr on the corrosion behaviour of Mg alloys has been to observe the corrosion performance of those specific commercially available alloys or how their corrosion is affected when Zr is added to a commercially available alloys which did not previously include Zr as an alloying addition. Reports on the effect of Zr alone on Mg in the Mg-Zr binary system has been lacking in the literature until now. Whilst commercial alloys have been reported to have a decrease in

corrosion rates when Zr is added, this is most often reported to be due to a reduction in the Fe content or changes in the alloy microstructure due to the grain refining ability of Zr impacting on the intermetallic phases present from the other alloying additions and not due to Zr affecting the Mg matrix itself. The true negative nature of Zr upon Mg corrosion has been shown herein without other alloying elements present to mask the detrimental effects of Zr upon Mg.

Further, studying the effect of Mn and Zr as related to Fe impurities in Mg was also a key task. As Fe is the main impurity element found in Mg-alloys, the corrosion behaviour of Mg with these two alloying additions may not have been a true representation of the corrosion response if the Fe content and the effect of either Mn or Zr upon Fe impurities in Mg were not taken into consideration and reported herein. The results in this study have built upon the reported detrimental effects of Fe impurities on the cathodic reaction kinetics of Mg. The data has shown that both Mn and Zr additions can reduce the negative impact of these impurities. Mn can interact with Fe by forming an intermetallic phase with the Fe present in the alloy and reduce the micro-galvanic coupling effect on the Mg matrix, whilst Zr can remove Fe from the melt during the casting processes.

The work in this thesis has built upon the state-of-the-art as per the literature, principally achieved by an important parcel of empirical work involving alloy production and experimental research (microscopy and corrosion testing). The conclusions drawn from the work that constitutes this thesis are as follows:

- The electrochemical behaviour of pure Mn and Zr were analysed over a range of pH levels. Pure Zr has low dissolution rates across the entire pH range with a low and consistent current density and a decreasing potential with increasing pH. Moreover, Zr displayed a pitting potential that was dependant on the pH level and the ionic species that evolve on the surface of the metal at those pH's. The electrochemical behaviour of pure Mn presents a system that is under cathodic control across the majority of the pH range. At a very low pH level (e.g. pH 1) both the anodic and cathodic reaction kinetics are greatly increased and the current density is very high. At a very high pH level (e.g. pH 13) the current density and anodic reaction kinetics of the system are greatly reduced and the electrochemical potential is increased significantly. There was no observed pitting potential for pure Mn across the entire pH range.

- In the practical sense, it is noted that the requisite alloys which contained appropriate relative proportions of Mn/Zr/Fe were produced successfully. This is a summary point, as the production of such alloys is not trivial, with challenges in alloying with sparingly soluble elements (in particular, Fe and Zr). Also, the production and testing of such alloys fills a significant knowledge gap in the literature, particularly since there are several recent works [45, 148] that base assertions regarding the effect of sparingly soluble elements without any empirical (be it corrosion or microscopy) validations.
- Manganese additions were found to decrease the corrosion rate of Mg alloys despite the absence of Al from the Mg alloy composition. This is an important revelation of the thesis in its own right, and practically important in the present era of Al-free Mg-alloy developments (for sheet and creep resistant applications). At Mn additions below roughly ~2 wt.% the cathodic reaction kinetics were found to decrease (relative to alloys with the same level of impurity Fe), resulting in a decrease in the rate of hydrogen evolution and the overall corrosion rate. However, at Mn contents above ~2 wt.%, the cathodic reaction kinetics increased, resulting in a concomitant increase in the corrosion rate of Mg. In open circuit exposure, this was attributed to the formation of more micro-galvanic couples between the Mg alloy matrix and the increased number of Mn particles (on the micron scale) found in the the Mg matrix – which was herein validated by SEM observations.
- Despite several published studies reporting the contrary [86, 90, 93], the results in this study have indicated that Mn is not a good scavenger of Fe. Mn and Fe were added to Mg in varying quantities to determine if there was a correlation between the overall Fe impurity content with increasing Mn content. No such pattern was observed experimentally. Fe contents were found to be independent of Mn content. As such, Mn does not improve the corrosion resistance of Mg alloys through the mechanism of scavenging Fe impurities. This point relates to the analysis of ICP data which has quantified the relative Mn:Fe proportions.
- Following on from the point above, it was, however, shown systematically that Mn alloying additions in Al-free Mg alloys are still able to moderate the deleterious effect of Fe impurities in Mg alloys in regards to corrosion, despite the absence of Al in the alloy. While in Al containing Mg alloys the Al and Mn additions form together with the Fe impurities to make an Al-Mn-Fe phase, when Al is absent Mn and Fe still

combine to form an Mn-Fe phase. Because of this interaction, increasing levels of Mn additions raise the tolerance limit of Fe. This was shown in Figure 5.2.3, where at ~0.5wt.% Mn, an Fe tolerance limit may be ~150ppm, whilst at ~1.5wt.% Mn, an Fe tolerance limit may be ~350ppm, and so forth.

- The Fe impurities in the Mn containing Mg alloys were (always, for those observed herein) found to be located in proximity to Mn, forming a Mn-Fe particle in the Mg matrix. Furthermore, the up-close electron microscopy examination of these Mn-Fe intermetallic particles, which includes EDX and EBSD analysis, provides the first physical evidence that Mn can encapsulate Fe in an Mg alloy that does not contain Al. It is this formation from an initial mixed Mn-Fe intermetallic phase that was previously theorised to neutralise the negative effects of Fe on the corrosion behaviour of Mg. The mechanism of the 'encapsulation' is posited (by aid of CALPHAD) to occur when either Fe particles do not fully dissolve within the Mn phase or the particle reaches a maximum level of Fe solubility within the Mn constituent, leaving a pure Fe core within the particle There is likely a critical Mn:Fe ratio that is necessary for this phenomenon to occur. A possible Mn:Fe ratio has been proposed by Makar and Kruger of 0.032 [33].
- The results herein have provided significant empirical evidence to (re)confirm that Zr is able to scavenge Fe from the Mg melt during alloy processing. In this manner, Zr can be considered beneficial for improving the corrosion resistance of Mg alloys as it can reduce the overall levels of impurities that influence corrosion on one hand. However, beyond this fact, Zr itself was found to have an inherently negative impact on the corrosion of Mg.
- Zirconium was found to act as an anodic activator while in solid solution in Mg alloys. This effect was observed even with low levels of Zr additions (below traditional commercial alloy levels required for grain refinement). The addition of Zr increases the anodic reaction kinetic rates and the rate of dissolution of metallic Mg. This increases the overall corrosion rate of Mg alloys, rather dramatically. The notion that a noble metal such as Zr is an anodic activator is an original finding. Nominally, alloying elements (with the exception of very reactive metals such as Ca) do not enhance the anodic kinetics of Mg, and for this phenomenon to occur via noble metal (i.e. Zr) additions is an important finding. The mechanism of the activation warrants further study via surface analytical methods including XPS (for characterisation) and

also likely scanning probe (SVET, SECM) to interpret the phenomenon electrochemically.

- In parallel to the anodic activation effect, zirconium particles were found to act as micro-galvanic couples when embedded in the Mg matrix during open circuit exposure. This effect was generally observed at slightly elevated levels of Zr additions and when a large portion of the Zr addition was not dissolved in solid solution (however, still below the levels reported for Zr content in several commercial alloy). The Zr particles in this regard, act in a similar manner to Fe impurities serving as sites where corrosion attack is localised. The presence of such particles (which is clearly evident from SEM investigations) results in a corresponding increase in the cathodic reaction kinetic rates and the rate of hydrogen evolution. This also increases the overall corrosion rate of Mg alloys. In some cases shown herein, the combination of the anodic activation effect, and the enhanced cathodic kinetics from Zr particles, leads to very rapid corrosion rates (i.e. > 55μA/cm²).
- The negative effect of Zr additions on Mg on corrosion can easily be missed in examinations of commercial alloys – hence why it has not been noticed and reported previously. As commercially available Zr-containing Mg alloys include having other alloying elements in the alloy composition, such as Zn and RE elements, these ternary and quaternary alloying elements also influence the anodic and cathodic reaction kinetics as well. The subtle, yet influential effect of Zr activating the anodic corrosion reaction kinetics of Mg can be minor compared to the extra changes in both the anodic and cathodic reaction kinetics due to these additional elements. Moreover, most commercial Zr-containing Mg alloys also have post-casting heat treatments to improve their mechanical properties. These heat treatments usually increase the amount of Zr that is dissolved in solid solution, leading to fewer Zr particles in the matrix. Thus, the heat treatments reduce the likelihood of the Zr additions forming Zr particles in the matrix that create micro-galvanic couples and accelerate the cathodic reaction kinetics.
- The Mg-Mn-Zr alloy series produced herein has shown that despite the formation of the Mn_2Zr particle when both Mn and Zr are added to Mg, there can still be significant levels of Mn and Zr additions present together in the Mg matrix. Moreover, the electrochemical polarisation and immersion test results indicate that adding both elements concurrently may be beneficial for the corrosion resistance of

Mg-alloys. The development of Mg-alloys with both Mn and Zr as alloying constituents may open up a new avenue for future Mg-alloy development.

8.2 Future work

Future experiments continuing this research may further the development and understanding of Mg technology. Some areas of note that could constitute further research based on the outcomes of this study include the following:

- The metallurgical aspects underlying the Mn-Fe particle interaction, where Mn forms an encapsulating layer around Fe, can be further studied. It is this observed interaction, coupled with the Mn-Fe particles that do not form an encapsulating layer that reduces the detrimental impact of Fe on Mg corrosion behaviour. However, the exact metallurgical reasons, such as cooling rate and alloy composition, for this interaction are not understood fully at present and require a more in-depth investigation to confirm the precise cause and reasons why these elements interact in this manner. One suggested course of analysis is to conduct computer simulations through a CALPHAD-based program which can calculate the interaction between the two elements in a molten magnesium environment. Another suggested technique is TEM analysis to confirm the atom lattice structures differentiating the Fe core from the Mn encapsulation layer and the mixed Mn-Fe particles.
- The results presented herein demonstrate how Zr is an anodic activator of Mg. It is not clear why, compared to other alloying elements, that even a small addition of Zr is able to activate the anodic reaction kinetics of Mg. Further investigation into this interaction is required to understand fully the exact mechanism as to how Zr activates Mg anodically. XPS and cross-sectional TEM analysis of the alloy microstructure and surface film, similar to the methods used by Taheri [36], would help elucidate this anodic activation effect.
- The effect of anodic activation of Zr on Mg has not been reported previously in published studies. However, as presented herein, this activation effect is also observed in current commercial Zr-containing Mg alloys. It would be beneficial to determine to what degree this effect affects the corrosion rate of these alloys and if there is any way to counteract or minimise the impact without interfering with the grain refinement desired for increased mechanical properties. Corrosion testing via immersion, electrochemical and possibly salt-spray testing, involving the adjustment of Zr in solid solution in currently available commercial Mg alloys should be conducted and the

corrosion behaviour analysed in order to determine which alloys are more susceptible to this effect of Zr on the anodic reaction kinetics.

- A more in-depth analysis of the Mg-Mn-Zr alloy system would be enlightening; hopefully opening up the possibility to developing a new series of Mg alloys or modifying existing alloys to be used in additional applications. It is known that Zr is a potent grain refiner of Mg alloys and that Mn additions lead to grain growth in Mg alloys. Apart from further researching the effects on the corrosion behaviour via immersion and electrochemical polarisation testing, the effect of both Mn and Zr concurrently on the grain size, alloy microstructure and subsequent mechanical properties should be explored through electron microscopy and tensile testing.
- The main focus of this research was to provide a foundational level of scientific understanding to aide in the future development of Al-free Mg alloys with superior corrosion resistance. Since the commencement of this thesis, there has been growing activity in Mg-alloys (outside the corrosion field). Initially, this was based on the Al-free Mg alloys that have usage in elevated temperature applications (i.e. >200°C) that require creep resistance for applications such as engine blocks. The vision was that this project would inform the development of creep-resistant Mg-RE-(Zn) where RE = Ce, La, Nd, and these alloys may or may not contain Zn. This vision is realistic based on the research network under which the project was executed (the CAST CRC). However, immense growth in R&D has also commenced in wrought Mg-alloys suitable for automotive sheet, based on Al-free compositions such as: Mg-Ca-Zn, Mg-Zn-Ca, Mg-Zn-Y or Mg-Zn-Gd [78, 104, 114, 149, 150]. The work herein is equally valid for such Al-free alloys. As such, the next step would be to use the insight generated in this dissertation in the further development of the properties of new Mg alloys (be it creep-resistant or sheet alloys) that would include the corrosion resistant design criteria reported herein.

This page is intentionally left blank

References

This page is intentionally left blank

[1] I.J. Polmear, Light Alloys. 3rd (Ed). 1995, London, England: Arnold.
[2] J.A. Boyer, The corrosion of magnesium and of the magnesium aluminum alloys containing manganese. 1927, American Magnesium Corporation. 417-454.
[3] H.E. Friedrich and B.L. Mordike, Magnesium Technology. 2006, Berlin: Springer. 708.
[4] D.H. StJohn, Overview of CAST and Australian magnesium research, Materials Science Forum, 546-549, (2007), 49-54.
[5] D.H. StJohn, Overview of current international magnesium research and recent CAST CRC developments, Advanced Materials Research, 29-30, (2007), 3-8.
[6] G. Dunlop, D. StJohn, and M. Frost, The AMC - CAST alliance for advanced magnesium research and development, Materials Science Forum, 419-422, (2003), 565-574.
[7] K.U. Kainer, Magnesium - Alloys and technology. 2003: Wiley-VCH.
[8] E.F. Emley, Principles of Magnesium Technology. 1st edition (Ed). 1966, Manchester: Pergamon Press.
[9] S. Mathieu, C. Rapin, J. Steinmetz, and P. Steinmetz, A corrosion study of the main constituent phases of AZ91 magnesium alloys, Corrosion Science, 45, (2003), 2741-2755.
[10] M.V. Kral, B.C. Muddle, and J.F. Nie, Crystallography of the bcc/hcp transformation in a Mg-8Li alloy, Materials Science and Engineering A, 460-461, (2007), 227-232.
[11] C.P. Liang and H.R. Gong, Phase stability, mechanical property and electronic structure of Mg-Li system, Journal of Alloys and Compounds, 489, (2010), 130-135.
[12] K. Chen and K.P. Boyle, Elastic properties, thermal expansion coefficients, and electronic structures of Mg and Mg-based alloys, Metallurgical and Materials Transactions A 40A, (2009), 2751-2760.
[13] S.M. Zhu, M.A. Gibson, J.F. Nie, M.A. Easton, and T.B. Abbott, Microstructural analysis of the creep resistance of die-cast Mg-4Al-2RE alloy, Scripta Materialia, 58, (2007), 477-480.
[14] T.L. Chia, M.A. Easton, S.M. Zhu, M.A. Gibson, N. Birbilis, and J.F. Nie, The effect of alloy composition on the microstructure and tensile properties of binary Mg-rare earth alloys, Intermetallics, 17, (2009), 481-490.
[15] S.M. Zhu, M.A. Gibson, M.A. Easton, and J.F. Nie, The relationship between microstructure and creep resistance in die-cast magnesium-rare earth alloys, Scripta Materialia, 63, (2010), 698-703.
[16] J. Zhang, J. Wang, X. Qio, D. Zhang, Z. Tian, X. Niu, D. Tang, and J. Meng, Effect of Nd on the microstructure, mechanical properties and corrosion behaviour of die-cast Mg-4Al-based alloy, Journal of Alloys and Compounds, 464, (2008), 556-564.
[17] T. Laser, M.R. Nurnberg, A. Janz, C. Hartig, D. Letzig, R. Schmid-Fetzer, and R. Bormann, The influence of manganese on the microstructure and mechanical properties of AZ31 gravity die cast alloys, Acta Materialia, 54, (2006), 3033-3041.
[18] Y. Fan, G. Wu, H. Gao, G. Li, and C. Zhai, Influence of lanthanum on the microstructure, mechanical property and corrosion resistance of magnesium alloy, Journal of Material Science, 41, (2005), 5409-5416.
[19] L.L. Rokhlin, Dependence of the Rare Earth metal solubility in solid magnesium on its atomic number, Journal of Phase Equilibria, 19(2), (1997), 142-145.
[20] P. Cao, M. Qian, D.H. StJohn, and M.T. Frost, Uptake of iron and its effect on grain refinement of pure magnesium by zirconium, Materials Science and Technology, 20, (2003), 585-592.
[21] H.C. Jung and K.S. Shin, Processing and characterization of magnesium alloys, Materials Science Forum, 488-489, (2005), 401-404.
[22] D. Eliezer, E. Aghion, and F.H. Froes, Magnesium science, technology and applications, Advanced Performance Materials, 5, (1998), 201-212.
[23] J.F. King, Magnesium: commodity or exotic?, Materials Science and Technology, 23(1), (2007), 1-14.

[24] G. Song and D. StJohn, The effect of zirconium grain refinement on the corrosion behavior of magnesium-rare earth alloy MEZ, Journal of Light Metals, 2, (2002), 1-16.
[25] Q. Peng, Y. Huang, K.U. Kainer, and N. Hort, Development of high performance single-phase solid solution magnesium alloy at low temperature, Advanced Engineering Materials, 14(3), (2012), 178-184.
[26] M. Yamasaki, N. Hayashi, S. Izumi, and Y. Kawamura, Corrosion behaviour of rapidly solidified Mg-Zn-rare earth element alloys in NaCl solution, Corrosion Science, 49, (2007), 255-262.
[27] S. Krishnamurthy, M. Khobaib, E. Robertson, and F.H. Froes, Corrosion behaviour of rapidly solidified Mg-Nd and Mg-Y alloys, Materials Science and Engineering, 99, (1988), 507-511.
[28] P.-y. Lin, H. Zhou, N. Sun, W.-P. Li, C.-t. Wang, M.-x. Wang, Q.-c. Guo, and W. Li, Influence of cerium addition on the resistance to oxidation of AM50 alloy prepared by rapid solidification, Corrosion Science, 52, (2009), 416-421.
[29] R.W.K. Honeycombe and H.K.D.H. Bhadeshia, Steels: Microstructure and Properties. 3rd (Ed), ed. E.S. Publishers. 2006: Butterworth-Heinemann.
[30] F. Rosalbino, D. Maccio, A. Saccone, E. Angelini, and S. Delfino, Effect of Nb alloying additions on the characteristics of anodic oxide films on zirconium and their stability in NaOH solution, Solid State Electrochemistry, 14, (2009), 1451-1455.
[31] H. Okamoto, Mg-Mn (Magnesium-Manganese), Journal of Phase Equilibria and Diffusion, 29(2), (2008), 208-209.
[32] H. Okamoto, Mg-Zr (magnesium-zirconium), Journal of Phase Equilibria and Diffusion, 28(3), (2007), 305-306.
[33] G.L. Makar and J. Kruger, Corrosion of magnesium, International Materials Reviews, 38(3), (1993), 138-153.
[34] R.E. McNulty and J.D. Hanawalt, Some corrosion characteristics of high purity magnesium alloys, in: R.B. Mears(Ed) Eighty-first General Meeting, (1942), Trans. Electrochem. Soc., pp. 423-433.
[35] M. Pourbaix, Atlas of Electrochemical Equilibria in Aqueous Solutions. 2nd (Ed). 1974.
[36] M. Taheri, R.C. Phillips, J.R. Kish, and G.A. Botton, Analysis of the surface film formed on Mg by exposure to water using a FIB cross-section and STEM-EDS, Corrosion Science, 59, (2012), 222-228.
[37] M.E. Straumanis and B.K. Bhatia, Disintergration of magnesium while dissolving anodically in neutral and acidic solutions, Journal of the Electrochemical Society, 110(5), (1963), 357-360.
[38] Z. Rong-chang, Z. Jin, H. Wei-Jiu, W. Dietzel, K.U. Kainer, C. Blawert, and K.E. Wei, Review of studies on corrosion of magnesium alloys, Transactions of Nonferrous Metals Society of China, 16, (2006), 763-771.
[39] H.J. Martin, R.B. Alvarez, J. Danzy, M.F. Horstemeyer, and P.T. Wang, Quantification of corrosion pitting under immersion and salt spray environments on an As-Cast AM60 magnesium alloy, Corrosion, 68(6), (2012), 571-585.
[40] J.D. Hanawalt, C.E. Nelson, and J.A. Peloubet, Corrosion studies of magnesium and its alloys, Transactions of the American Institute of Mining and Metallurgical Engineers, 147, (1942), 273-298.
[41] R.C. Phillips and J.R. Kish, Nature of surface film on matrix phase of Mg alloy AZ80 formed in water, Corrosion, 69(8), (2013), 813-820.
[42] J.H. Nordlien, S. Ono, N. Masuko, and K. Nisancioglu, A TEM investigation of naturally formed oxide films on pure magnesium, Corrosion Science, 39(8), (1997), 1397-1414.
[43] J.E. Hillis, The effects of heavy metal contamination on magnesium corrosion performance, in *Light Metal Age*. 1983, SAE: Detroit. 25-29.
[44] N.T. Kirkland, J. Lespagnol, N. Birbilis, and M.P. Staiger, A survey of bio-corrosion rates of magnesium alloys, Corrosion Science, 52(2), (2010), 287-291.

[45] M. Liu, P.J. Uggowitzer, P. Schmutz, and A. Atrens, Calculated phase diagrams, iron tolerance limits, and corrosion of Mg-Al alloys, JOM, 60(12), (2008), 39-44.
[46] G.L. Song and A. Atrens, Corrosion mechanisms of magnesium alloys, Advanced Engineering Materials, 1(1), (1999), 11-33.
[47] A.D. Sudholz, N.T. Kirkland, R.G. Buchheit, and N. Birbilis, Electrochemical properties of intermetallic phases and common impurity elements in Magnesium alloys, Electrochemical and Solid-State Letters, 14(2), (2011), C5-C7.
[48] N.T. Kirkland, N. Birbilis, J. Walker, T. Woodfield, G.J. Dias, and M.P. Staiger, In-vitro dissolution of magnesium-calcium binary alloys: Clarifying the unique role of calcium additions in bioresorbable magnesium implant alloys, Journal of Biomedical Materials Part B: Applied Biomaterials, 95B(1), (2010), 91-100.
[49] E. Ghali, W. Dietzel, and K.-U. Kainer, General and localised corrosion of magnesium alloys: A critical review, Journal of Materials Engineering and Performance, 13(1), (2003), 7-23.
[50] M.G. Fontana, Corrosion Engineering. Vol. 3rd. 2005: Tata McGraw-Hill.
[51] G. Song and A. Atrens, Recent insights into the mechanism of magnesium corrosion and research suggestions, Advanced engineering materials, 9(3), (2007).
[52] R.V. Gadag and A. Nityananda, Engineering Chemistry. 2006, New Delhi, India: I. K. International Publishing House.
[53] G. Williams, K. Gusieva, and N. Birbilis, Localized corrosion of binary Mg-Nd alloys in chloride-containing electrolyte using a scanning vibrating electrode technique, Corrosion, 68(6), (2012), 489-498.
[54] G. Williams, N. Birbilis, and H.N. McMurray, The source of hydrogen evolved from a magnesium anode, Electrochemistry Communications, (2013).
[55] G.S. Frankel, A. Samaniego, and N. Birbilis, Evolution of hydrogen at dissolving magnesium surfaces, Corrosion Science, 70, (2013), 104-111.
[56] D.A. Jones, Principles and Prevention of Corrosion, ed. D. Johnstone. 1992, New York: Macmillan Publishing Company.
[57] S. Bender, J. Goellner, A. Heyn, and S. Schmigalla, A new theory for the negative difference effect in magnesium corrosion, Materials and Corrosion - Werkstoffe und Korrosion, 63(8), (2012), 707-712.
[58] S. Lebouil, A. Duboin, F. Monti, P. Tabeling, P. Volovitch, and K. Ogle, A novel approach to on-line measurement of gas evolution kinetics: Application to the negative difference effect of Mg in chloride solution, Electrochimica Acta, (2013).
[59] G.H. Wu, H.T. Gao, W.J. Ding, and Y.P. Zhu, Study on mechanism of iron reduction in magnesium alloy melt, Journal of Materials Science, 40, (2005), 6175-6180.
[60] H. Gao, G. Wu, W. Ding, L. Liu, X. Zeng, and Y. Zhu, Study on Fe reduction in AZ91 melt by B_2O_3, Materials Science and Engineering, (2004), 311-317.
[61] T. Haitani, Y. Tamura, T. Motegi, N. Kono, and H. Tamehiro, Solubility of iron in pure magnesium and cast structure of Mg-Fe alloy, Materials Science Forum, 419-422, (2003), 697-702.
[62] S. Akavipat and E.B. Hale, Effects of iron implantation on the aqueous corrosion of magnesium, Materials Science and Engineering, 69, (1985), 311-316.
[63] M. Liu, P.J. Uggowitzer, A.V. Nagasekhar, P. Schmutz, M. Easton, G.-L. Song, and A. Atrens, Calculated phase diagrams and the corrosion of die-cast Mg-Al alloys, Corrosion Science, 51, (2008), 602-619.
[64] A.A. Nayeb-Hashemi, J.B. Clark, and L.J. Swartzendruber, The Fe-Mg (Iron-Magnesium) System, Bulletin of Alloy Phase Diagrams, 6(3), (1985), 235-238.
[65] R. Baboian, Corrosion tests and standards: Application and interpretation. 2nd (Ed). 2005, Baltimore, MD: ASTM International, West Conshohocken, PA.

[66] D.S. Gandel, N. Birbilis, M.A. Easton, and M.A. Gibson, Iron and corrosion control in aluminium-free magnesium alloys, in: W.J. Poole and K.U. Kainer(Eds), Mg2012: 9th International Conference on Magnesium Alloys and their Applications, (2012, pp. 197-202.
[67] N. Birbilis and R.G. Buchheit, Electrochemical characteristics of intermetallic phases in aluminium alloys - An experimental survey and discussion, Journal of the Electrochemical Society, 152(4), (2005), B140-B151.
[68] Y.T. Tagashi Haitani, Tetsuichi Motegi, Norio Kono, Hiroshi Tamehiro, Solubility of iron in pure magnesium and cast structure of Mg-Fe alloy, Materials science forum, 419-422, (2003), 697-702.
[69] A. Luo and M.O. Pekguleryuz, Cast magnesium alloys for elevated temperature applications, Journal of Material Science, 29, (1994), 5259-5271.
[70] A.D. Sudholz, N. Birbilis, C.J. Bettles, and M.A. Gibson, Corrosion behavior of Mg-alloy AZ91E with atypical alloying additions, Journal of Alloys and Compounds, 461, (2009), 109-115.
[71] M.D. Bharadwaj, S.M. Tiwari, Y.-M. Wang, and V. Mani, Micro galvanic corrosion behaviour of Mg alloys as a function of aluminium content, in: A.A.L. Randy S. Beals, Neale R. Neelameggham, Mihriban O. Pekguleryuz(Ed) Magnesium Technology, (2008, pp.
[72] Y. Tamura, Y. Kida, H. Tamehiro, N. Kono, H. Soda, and A. McLean, The effect of manganese on the precipitation of $Mg_{17}Al_{12}$ phase in magnesium alloy AZ91, Journal of Material Science, 43, (2008), 1249-1258.
[73] C.R. Hutchinson, J.F. Nie, and S. Gorsse, Modeling the precipitation processes and strengthening mechanisms in a Mg-Al-(Zn) AZ91 alloy, Metallurgical and Materials Transactions A, 36A, (2005), 2093-2105.
[74] Z. Wen, C. Wu, C. Dai, and F. Yang, Corrosion behaviors of Mg and its alloys with different Al contents in a modified simulated body fluid, Journal of Alloys and Compounds, 488, (2009), 392-399.
[75] L.L. Rokhlin, Magnesium alloys containing rare earth metals. 2003: Taylor & Francis Group.
[76] N.T. Kirkland, M.P. Staiger, D. Nisbet, C.H.J. Davies, and N. Birbilis, Performance-driven design of biocompatible Mg alloys, JOM, 63(6), (2011), 28-34.
[77] B.-H. Choi, B.-S. You, W.-W. Park, Y.-B. Huang, and I.-M. Park, Effect of Ca addition on the oxidation resistance of AZ91 magnesium alloys at elevated temperatures, Metals and Materials International, 9(4), (2003), 395-398.
[78] C. Jihua, C. Zhenhua, Y. Hongge, Z. Fuquan, and C. Yingliang, Effects of Sn and Ca additions on microstructure, mechanical properties and corrosion resistance of the as-cast Mg-Zn-Al based alloy, Materials and Corrosion, 59(12), (2008), 934-941.
[79] Y. Terada, R. Sota, N. Ishimatsu, T. Sato, and K. Ohori, A thousandfold creep strengthening by Ca addition in die-cast AM50 magnesium alloy, Metallurgical and Materials Transactions A, 35a, (2004), 3029-3032.
[80] C.J. Bettles, M.A. Gibson, and K. Venkatesan, Enhanced age-hardening behaviour in Mg-4 wt.% Zn micro-alloyed with Ca, Scripta Materialia, 51, (2004), 193-197.
[81] A.F. Smith, The isothermal growth of manganese precipitates in a binary magnesium alloy, Acta Metallurgica, 15, (1967), 1867-1873.
[82] S.A. Khan, Y. Miyashita, Y. Mutoh, and Z.B. Sajuri, Influence of Mn content on mechanical properties and fatigue behaviour of extruded Mg alloys, Materials Science and Engineering A, 420, (2006), 315-321.
[83] X. Zhang, D. Kevorkov, I.-H. Jung, and M. Pekguleryuz, Phase equilibria on the ternary Mg-Mn-Ce system at the Mg-rich corner, Journal of Alloys and Compounds, 482, (2009), 420-428.
[84] C. Liu, F. Pan, and W. Wang, Phase analysis of Al-Mn Compounds in the AZ magnesium alloys, Materials Science Forum, 546-549, (2007), 395-398.

[85] V.Y. Gertsman, J. Li, S. Xu, J.P. Thomson, and M. Sahoo, Microstructure and second-phase particles in low and high-pressure die-cast magnesium alloy AM50, Metallurgical and Materials Transactions A, 36A, (2005), 1989-1997.
[86] P. Cao, M. Qian, and D. StJohn, Effect of manganese on grain refinement of Mg-Al based alloys, Scripta Materialia, 54, (2006), 1853-1858.
[87] S.L. Sin, D. Dube, and R. Tremblay, Characterisation of Al-Mn Particles in AZ91D invesment castings, Materials Characterization, 58, (2007), 989-996.
[88] Y. Hu, Electrochemical polarization behaviour of Mg-Al alloys in near-neutral solutions. 2012, McMaster University: Hamilton. 101.
[89] L.Y. Wei and R. Warren, Microstructural characterisation of several magnesium alloys in AM series, Materials Science and Technology, 23(6), (2007), 745-752.
[90] G.T. Parthiban, N. Palaniswamy, and V. Sivan, Effect of manganese addition on anode characteristics of electrolytic magnesium, Anti-Corrosion Methods and Materials, 56(2), (2009), 79-83.
[91] D.S. Gandel, N. Birbilis, M.A. Easton, and M.A. Gibson, The influence of Mn on the corrosion of Al-free Mg-alloys, in: 18th International Corrosion Congress, (2011), International Corrosion Congress, pp. 1-9.
[92] J.D. Robson, D.T. Henry, and B. Davis, Particle effects on recrystallization in magnesium-manganese alloys: Particle-stimulated nucleation, Acta Metallurgica, 57, (2009), 2739-2747.
[93] J.G. Kim and A.J. Koo, Effect of alloying elements on electrochemical properties of magnesium-based sacraficial anodes, Corrosion Science, 56(4), (2000), 380-388.
[94] J.D. Robson, D.T. Henry, and B. Davis, Particle effects on recrystallization in magnesium-manganese alloys: Particle pinning, Materials Science and Engineering A, 528, (2011), 4239-4247.
[95] D. Pierre, J.C. Viala, N. Peronnet, F. Bosselet, and J. Bouix, Interface reactions between mild steel and liquid Mg-Mn alloys, Materials Science and Engineering A, A349, (2003), 256-264.
[96] M. Qian and D.H. StJohn, Grain nucleation and formation in Mg-Zr alloys, International Journal of Cast Metals Research, 22(1-4), (2009), 256-259.
[97] M. Qian, D.H. StJohn, and M.T. Frost, Zirconium alloying and grain refinement of magnesium alloys, in: H.I. Kaplan(Ed) Magnesium Technology 2003, (2003), The Minerals, Metals and Materials Society pp. 209-214.
[98] M.A. Easton, C.H.J. Davies, M.R. Barnett, and F. Pravdic, Effect of solidification grain refinement on the development of wrought Mg alloys, Materials Science Forum, 539-543, (2007), 1729-1734.
[99] P.Y. Li, H.J. Yu, S.C. Chen, and Y.M. Yu, Factors affecting the corrosion resistance of cast magnesium alloys, in: H.I. Kaplan(Ed) Magnesium Technology 2003, (2003), The Minerals, Metals & Materials Society, pp. 51-58.
[100] W. Yuan, S.K. Panigrahi, J.Q. Su, and R.S. Mishra, Influence of grain size and texture on Hall-Petch relationship for a magnesium alloy, Scripta Materialia, 65, (2011), 994-997.
[101] C.D. Lee, Effect of grain size on the tensile properties of magnesium alloy, Materials Science and Engineering A, 459, (2007), 355-360.
[102] H. Han, S. Liu, L. Kang, and L. Liu, Refinement role of electromagnetic stirring and calcium in AZ91 Magnesium alloy, Journal of Wuhan University of technology - Materials Science Edition, 23(2), (2007), 194-197.
[103] D.H. StJohn, M. Qian, M.A. Easton, P. Cao, and Z. Hildebrand, Grain refinement of magnesium alloys, Metallurgical and Materials Transactions A, 36A, (2005), 1669-1679.
[104] M. Sun, G. Wu, W. Wang, and W. Ding, Effect of Zr on the microstructure, mechanical properties and corrosion resistance of Mg-10Gd-3Y magnesium alloy, Materials Science and Engineering, 523, (2009), 145-151.
[105] P. Lyon, New magnesium alloy for aerospace and specialty applications, in: A.A. Luo(Ed) Magnesium Technology, (2004), TMS, pp. 311-315.

[106] T. Rzychon, J. Michalska, and A. Kielbus, Corrosion resistance of Mg-RE-Zr alloys, Journal of Achievements in Materials and Manufacturing Engineering, 21(1), (2007), 51-54.
[107] C.J. Bettles, M.A. Gibson, and S.M. Zhu, Microstructure and mechanical behaviour of an elevated temperature Mg-rare earth based alloy, Materials Science and Engineering A, 505, (2009), 6-12.
[108] A.C. Hanzi, F.H.D. Torre, A.S. Sologubenko, P. Gunde, R. Schmid-Fetzer, M. Kuehlein, J.F. Loffler, and P.J. Uggowitzer, Design strategy for microalloyed ultra-ductile magnesium alloys, Philosophical Magazine Letters, 89(6), (2009), 377-390.
[109] S.C. Wang and C.P. Chou, Effect of adding Sc and Zr on grain refinement and ductility of AZ31 magnesium alloy, Journal of Materials Processing Technology, 97, (2007), 116-121.
[110] X. Gu, Y. Zheng, Y. Cheng, S. Zhong, and T. Xi, In vitro corrosion and biocompatability of binary magnesium alloys, Biomaterials, 30, (2008), 484-498.
[111] A. Kaya, G. Ben-Hamu, D. Eliezer, K.S. Shin, and S. Kohen, Corrosion and oxidation of alloys of the Mg-Y-Zr-REM system, Metal Science and Heat Treatment, 48(11-12), (2006), 46-50.
[112] D. Pierre, F. Bosselet, M. Peronnet, J.C. Viala, and J. Bouix, Chemical reactivity of iron base substrates with liquid Mg-Zr alloys, Acta Metallurgica, 49, (2000), 653-662.
[113] A. Prasad, P.J. Uggowitzer, Z. Shi, and A. Atrens, Production of high purity magnesium alloys by melt purification with Zr, Advanced Engineering Materials, 14(7), (2012), 477-490.
[114] G. Ben-Hamu, D. Eliezer, K.S. Shin, and S. Cohen, The relation between microstructure and corrosion behaviour of Mg-Y-RE-Zr alloys, Journal of Alloys and Compounds, 341, (2007), 269-276.
[115] W.C. Neil, M. Forsyth, P.C. Howlett, C.R. Hutchinson, and B.R.W. Hinton, Corrosion of magnesium alloy ZE41 - the role of microstructural features, Corrosion Science, 51, (2009), 387-394.
[116] G.L. Song, Recent progress in corrosion and protection of magnesium alloys, Advanced Engineering Materials, 7(7), (2005), 563-586.
[117] D.S. Gandel, M.A. Easton, M.A. Gibson, T. Abbott, and N. Birbilis, The influence of Mg-Zr master alloy microstructure on the corrosion of Mg, in: N. Hort, S.N. Mathaudhu, N.R. Neelameggham, and M. Alderman(Eds), Magnesium Technology 2013, (2013), The Minerals, Metals & Materials Society, pp. 157-162.
[118] M.E. Schlesinger, The Mn-Zr (manganese-zirconium) system, Journal of Phase Equilibria, 20(1), (1999), 79-83.
[119] J.H. Zhang, H.F. Liu, W. Sun, H.Y. Lu, D.X. Tang, and J. Meng, Influence of structure and ionic radius on solubility limit in the Mg-RE systems, Materials Science Forum, 561-565, (2007), 143-146.
[120] N. Birbilis, M.A. Easton, A.D. Sudholz, S.M. Zhu, and M.A. Gibson, On the corrosion of binary magnesium-rare earth alloys, Corrosion Science, 51, (2009), 683-689.
[121] W.J. Liu, F.H. Cao, L.R. Chang, Z. Zhang, and J.Q. Zhang, Effect of rare earth element Ce and La on corrosion behavior of AM60 magnesium alloy, Corrosion Science, 51(6), (2009), 1334-1343.
[122] T. Takenaka, T. Ono, Y. Narazaki, Y. Naka, and M. Kawakami, Improvement of corrosion resistance of magnesium metal by rare earth elements, Electrochimica Acta, 53, (2007), 117-121.
[123] W.E. Mercer and J.E. Hill, SAE Technical Paper 920073, (1992).
[124] N.D. Nam, W.C. Kim, J.G. Kim, K.S. Shin, and H.C. Jung, Effect of mischmetal on the corrosion properties of Mg-5Al alloy, Corrosion Science, 51, (2009), 2942-2949.
[125] Y.L. Song, Y.H. Liu, S.H. Wang, S.R. Yu, and X.Y. Zhu, Effect of neodymium on microstructure and corrosion resistance of AZ91 Magnesium alloy, Journal of Material Science, 42, (2006), 4435-4440.
[126] H. Okamoto, Mg - Zr (Magnesium - Zirconium), Journal of Phase Equilibria and Diffusion, 28(3), (2007), 305-306.

[127] K.V. Kutniy, I.I. Papirov, M.A. Tikhonovsky, A.I. Pikalov, S.V. Sivtzov, L.A. Pirozhenko, V.S. Shokurov, and V.A. Shkuropatenko, Influence of grain size on mechanical and corrosion properties of magnesium alloy for medical implants, Material Wissenschaft Und Werkstofftechnik, 40(4), (2009), 242-246.
[128] M. Sun, M.A. Easton, D.H. StJohn, G. Wu, T.B. Abbott, and W. Ding, Grain refinement of magnesium alloys by Mg-Zr master alloys: The role of alloy chemistry and Zr particle number density, Advanced Engineering Materials, (2012), 1-6.
[129] R.H.A. Crawley, Determination of soluble and insoluble zirconium in magnesium alloys, Analytica Chimica Acta, (1961), 281-284.
[130] M. Sun, G. Wu, M.A. Easton, D.H. StJohn, T. Abbott, and W. Ding, A comparison of the microstructure of three Mg-Zr master alloys and their grain refinement efficiency, in: W.J. Poole and K.U. Kainer(Eds), 9th International Conference on Magnesium Alloys and their Applications, (2012, pp. 873-880.
[131] M. Qian, L. Zheng, D. Graham, M.T. Frost, and D.H. StJohn, Settling of undissolved zirconium particles in pure magnesium melts, Journal of Light Metals, 1, (2001), 157-165.
[132] M. Qian, D.H. StJohn, and M.T. Frost, A new zirconium-rich master alloy for the grain refinement of magnesium alloys, in: K.U. Kainer(Ed) 6th International Conference Magnesium Alloys and their Applications, (2003), Wiley-VCH Verlag Gmbh & Co., pp. 706-712.
[133] M. Qian, D.H. StJohn, M.T. Frost, and M.R. Barnett, Grain refinement of pure magnesium using rolled Zirmax master alloy (Mg-33.3Zr), in: H.I. Kaplan(Ed) Magnesium Technology 2003, (2003), TMS (The Minerals, Metals & Materials Society), pp. 215-220.
[134] M. Qian, D.H. StJohn, and M.T. Frost, Characteristic zirconium-rich coring substructures in Mg-Zr alloys, Scripta Materialia, 46, (2002), 649-654.
[135] M. Qian, D.H. StJohn, and M.T. Frost, Heterogeneous nuclei size in magnesium-zirconium alloys, Scripta Materialia, 50, (2004), 1115-1119.
[136] G. Song and A. Atrens, Understanding Magnesium Corrosion, Advanced Engineering Materials, 5(12), (2003), 837-858.
[137] B. Graver, A.T.J.v. Helvroot, and K. Nisancioglu, Effect of heat treatment on anodic activation of aluminium by trace element indium, Corrosion Science, 52(11), (2010), 3774-3781.
[138] A.R. Despic, D.M. Drazic, M.M. Purenovic, and N. Cikovic, Electrochemical properties of aluminium alloys containing indium, gallium and thallium, Journal of Applied Electrochemistry, 6, (1976), 527-542.
[139] J.T.B. Gundersen, A. Aytac, J.H. Nordlien, and K. Nisancioglu, Effect of heat treatment on electrochemical behaviour of binary aluminium model alloys, Corrosion Science, 46, (2004), 697-714.
[140] F. Kabirian and R. Mahmudi, Effects of Zr additions on the microstructure and impression creep behaviour of AZ91 magnesium alloy, Metallurgical and Materials Transactions A, 41A(13), (2010), 3488-3498.
[141] S.L. Chen, S. Daniel, F. Zhang, Y.A. Chang, X.Y. Yan, F.Y. Xie, R. Schmid-Fetzer, and W.A. Oates, The PANDAT Software Package and its Applications, Calphad, 26(2), (2002), 175-188.
[142] S.L. Chen, F. Zhang, S. Daniel, F.Y. Xie, X.Y. Yan, Y.A. Chang, R. Shcmid-Fetzer, and W.A. Oates, Calculating Phase Diagrams Using PANDAT and PanEngine, JOM, 55(12), (2003), 48-51.
[143] S. Chen, Y. Yang, W. Cao, B. P.Bewlay, K.-C. Chou, and Y.A. Chang, Calculation of two-dimensional sections of liquidus projections in multicomponent systems, Journal of phase Equilibria and Diffusion, 29(5), (2008), 390-397.
[144] U.R. Kattner, The thermodynamic modeling of multicomponent phase equilibria, Journal of Materials, 49(12), (1997), 14-19.
[145] W. Cao, F. Zhang, S.L. Chen, C. Zhang, and Y.A. Chang, An integrated computational tool for precipitation simulation, Journal of Materials, 63(7), (2011), 29-34.

[146] Y. Guo, J. Li, J. Li, Z. Yang, J. Zhao, F. Xia, and M. Liang, Mg-Gd-Y system phase diagram calculation and experimental clarification, Journal of Alloys and Compounds, 450, (2008), 446-451.
[147] D.S. Gandel, N. Birbilis, M.A. Easton, and M.A. Gibson, Influence of Manganese, Zirconium and Iron on the corrosion of Magnesium, in: Corrosion & Prevention 2010, (2010), Australasian Corrosion Association, pp. 1-11.
[148] V.T. Witusiewicz, F. Sommer, and E.J. Mittemeijer, Reevaluation of the Fe-Mn Phase Diagram, Journal of Equilibria and Diffusion, 25(4), (2004), 346 - 354.
[149] J. Grobner and R. Schmid-Fetzer, Selection of promising quaternary candidates from Mg-Mn-(Sc, Gd, Y, Zr) for development of creep-resistant magnesium alloys, Journal of Alloys and Compounds, 320, (2001), 296-301.
[150] T.J. Luo, Y.S. Yang, Y.J. Li, and X.G. Dong, Influence of rare earth Y on the corrosion behavior of as-cast AZ91 alloy, Electrochimica Acta, 54(26), (2009), 6433-6437.

This page is intentionally left blank

Appendices

This page is intentionally left blank

INFLUENCE OF MANGANESE, ZIRCONIUM AND IRON ON THE CORROSION OF MAGNESIUM

D.S. Gandel[1,2], N. Birbilis[1,2], M.A. Easton[1,2], M.A. Gibson[1,3]

[1]CAST Co-operative Research Centre, [2]Department of Materials Engineering, Monash University, Australia, [3]CSIRO Division of Process Science and Engineering, Australia.

Summary: Manganese (Mn) and zirconium (Zr) are two common alloying additions in Magnesium. Both of these elements have very low solubility in Mg, but serve a specific purpose. Mn is known to help produce the Al-Mn-Fe phase that removes Iron (Fe) impurities (dramatically improving corrosion resistance), whilst Zr is utilized as a grain refiner and purifier for Magnesium alloys (dramatically improving strength). The effect of Mn on the corrosion resistance of Mg and subsequent Fe impurity levels in the absence of aluminium is not well documented. Concurrently, the independent contribution Zr has on the corrosion resistance of Zr containing magnesium alloys has not been thoroughly researched. In this study, samples of pure Mg and samples with varying additions of Mn or Zr were prepared. The corrosion resistance of these samples was examined via both electrochemical and immersion tests. The samples containing Zr had a higher corrosion rate than the pure samples and the samples with Mn additions. The samples with Mn additions displayed a tendency to have a reduced corrosion resistance when both the Mn and/or Fe content of the alloy increased.

Keywords: Magnesium, Manganese, Zirconium, Iron, Corrosion.

1. INTRODUCTION

Magnesium (Mg) is the lightest of all the engineering metals and hence, an attractive alternative to metals such as steel and aluminium in an era of light-weighting and energy efficiency. Mg also has excellent castability, particularly in high-pressure die casting (HPDC), however, it is well recognized that the corrosion of Mg and its alloys continues to be a major technological issue preventing wider usage of such alloys [1]. There is an overwhelming demand to develop magnesium alloys with an improved corrosion resistance[2].

Manganese is a common addition in magnesium alloys. While manganese containing Mg alloys can also show some improvements in ductility, Mn additions have little effect on tensile properties. The addition of manganese is usually strategic and aimed at lowering the effect of the iron (Fe) impurity content in order to control the overall corrosion of Mg-Al alloys [3]. In the presence of Al and Fe, additions of Mn produce an $Al_8(Mn,Fe)_5$ phase that can neutralise the Fe impurities. This is important, since when present in Mg, any Fe is nominally insoluble and forms a pure-Fe (bcc) phase in the Mg matrix [4]. This pure Fe has a large potential difference compared to the Mg and is able to support cathodic reactions rather efficiently and hence forms a strong local cathode. The formation of the $Al_8(Mn,Fe)_5$ intermetallic in preference to bcc-Fe can reduce the potential difference and cathodic potency. The exact effect of manganese levels on the corrosion resistance of Mg and subsequent Fe impurity levels in the absence of aluminium is not well documented. Mn also

is sparingly soluble in Mg, and whether in isolation it causes a major corrosion risk needs to be determined. While the phenomenology of the role of Mn is understood, the exact levels of Mn addition necessary to counter-act the detrimental effect of the Fe impurity are still unknown.

Zirconium is mainly added to refine the grain size of magnesium alloys, yet in many cases the corrosion resistance of the alloy is appreciably enhanced as well [2]. Whether this phenomenon is owing to the grain refinement or the presence of Zr itself is not reported in such studies. Zirconium containing Mg alloys tend to be relatively insensitive to iron and nickel impurities. This is because the iron and nickel impurities combine with the zirconium and form insoluble particles, typically Fe_2Zr, which are removed from the magnesium melt during casting and settle at the bottom of moulds and crucibles. Zirconium also combines with Mn to form a Mn_2Zr particle which is also removed during casting [5].

When compared with other common alloying elements in Mg alloys, corrosion studies on the effect of zirconium upon Mg are relatively scarce. In this work, we investigate the role of Fe, Mn and Zr on the corrosion response of Mg.

2. EXPERIMENTAL METHODS

2.1 Samples

Alloys were produced by induction melting and the starting materials were high purity metals (~99.95%). Following melting, alloys were allowed to cool within the furnace. Several samples with low impurity levels were also examined to form a benchmark from which the effects of Mn, Zr and Fe on the change in corrosion resistance can be measured. The levels of manganese and zirconium additions tested vary from below traditional commercial levels to well above commercial levels. Table 1.1 below shows the levels of alloying additions in each of the samples tested. Compositions determined by ICP-AES by Spectrometer Services (Coburg, Vic, Australia).

Table 1.1 – Composition of Mg alloy samples tested in this work (in wt%)

Sample ID	Mg%	Mn%	Zr%	Fe%	Ni%	Cu%	Al%
Pure-Mg1	~Bal	0.01	<0.01	0.004	<0.001	0.002	0.01
Pure-Mg2	~Bal	0.001	0.002	0.001	<0.0001	0.0002	0.001
Pure-Mg3	~Bal	0.001	0.002	0.001	<0.0001	0.0003	0.001
MgZr1	~Bal	0.002	0.37	0.003	0.0002	0.0002	<0.001
MgZr2	~Bal	0.002	0.58	0.009	0.0002	0.0003	0.001
MgZr3	~Bal	0.002	0.22	0.004	0.0009	0.0003	<0.001
MgZr4	~Bal	0.002	1.73	0.008	0.0001	0.0005	<0.001
MgMn1	~Bal	0.61	<0.001	0.012	0.0001	0.0002	<0.001
MgMn2	~Bal	1.13	0.001	0.035	0.0003	0.0004	0.002
MgMn3	~Bal	2.31	<0.001	0.056	0.0001	0.0002	<0.001
MgMn4	~Bal	4.07	<0.001	0.061	0.0013	0.0003	0.008
MgMn5	~Bal	3.94	<0.001	0.002	0.0002	0.0003	<0.001
MgFe1	~Bal	0.008	0.001	0.022	0.002	<0.001	0.002

2.2 Electrochemical Testing

Samples were prepared and ground to a 2000 grit surface finish. A 3-electrode electrochemical flat-cell with an exposed sample area of 1-cm^2 was used. The test electrolyte was 0.1M NaCl in all cases. A VMP 3Z potentiostat was used, with potentiodynamic polarization carried at 1-mV/s. Prior to polarisation, samples were conditioned for ten minutes at open circuit potential to a certain a stable potential. The polarisation curves were used to determine i_{corr} (via a Tafel-type fit) using EC-Lab software. Such fitting is inherently difficult, however the ability of EC-lab to allow manual control is critical. As a general rule, fits were executed by selecting a portion of the curve that commenced >50mV from E_{corr}, and i_{corr} was subsequently estimated from the value where the fit intercepted the potential value of the true E_{corr}. This fit was dominated by cathodic data. More generally, polarisation testing was also able to visually reveal comparative information related to the kinetics of anodic and cathodic reactions between alloys. Each sample was tested five times and an average result was determined.

2.3 SEM and EDX

The microstructures of the alloys were examined via scanning electron microscopy. SEM specimens were polished to a 1µm diamond paste finish and etched with a picric acid solution then imaged using an FEI Phenom SEM. The specimens were also examined via EDX in a JEOL 840A electron microscope to determine the elemental composition of the particles that appeared.

3. RESULTS

3.1 SEM and EDX analyses

The results of microstructural analysis performed herein are included below.

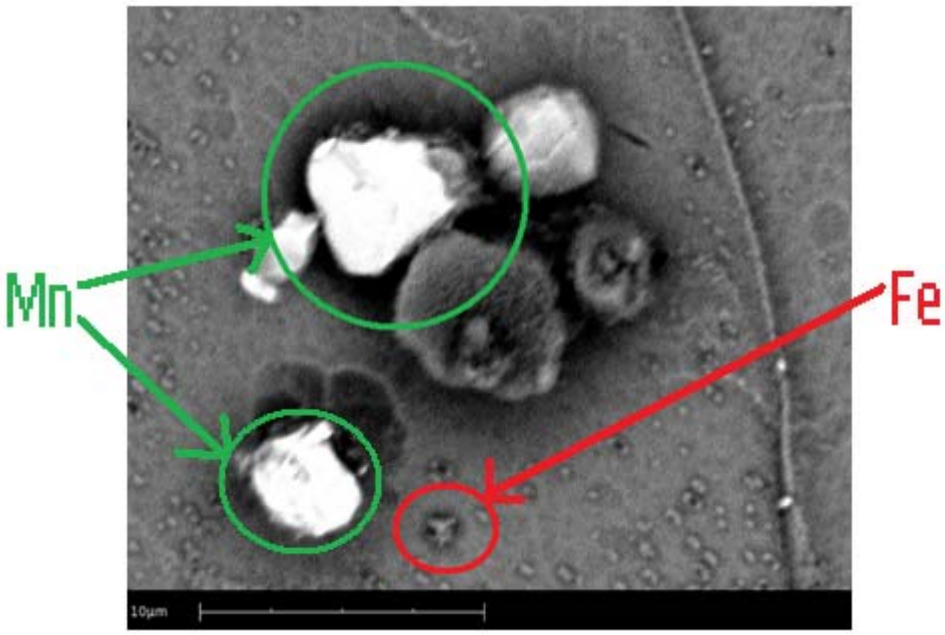

Figure 1 - SEM micrograph of sample with 4.07wt%Mn and 0.061wt%Fe

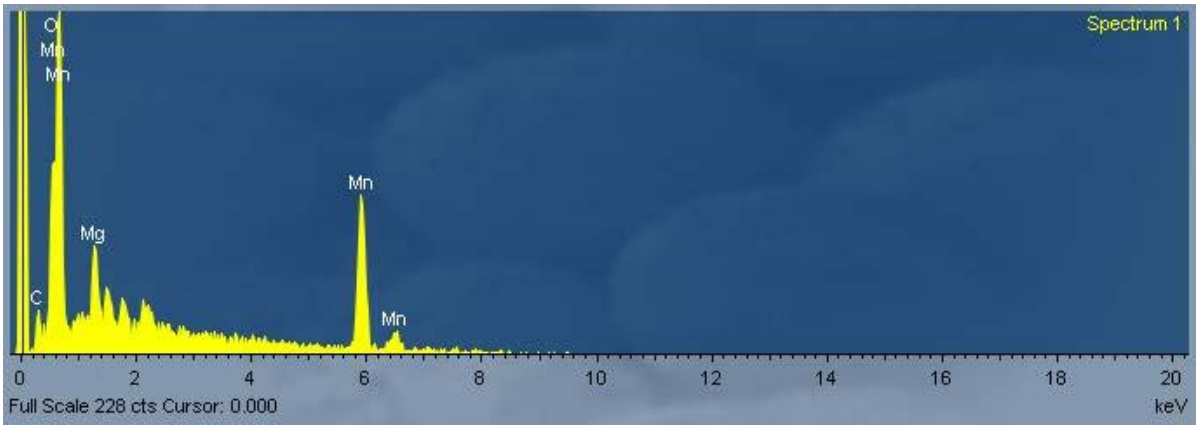

Figure 2 – EDX analysis of Mn particle in Mg alloy depicted in Fig. 1

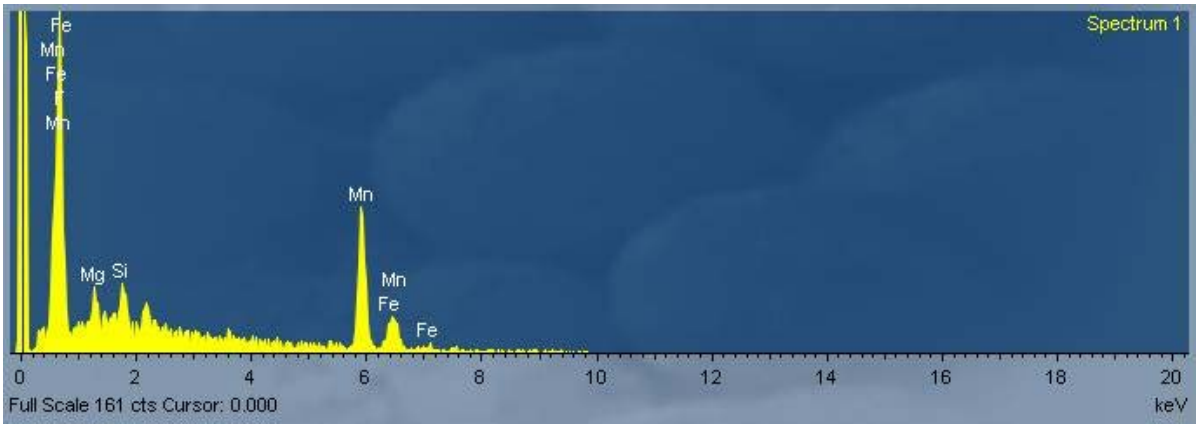

Figure 3 – EDX analysis of Fe particle in Mg alloy with Mn addition depicted in Fig. 1

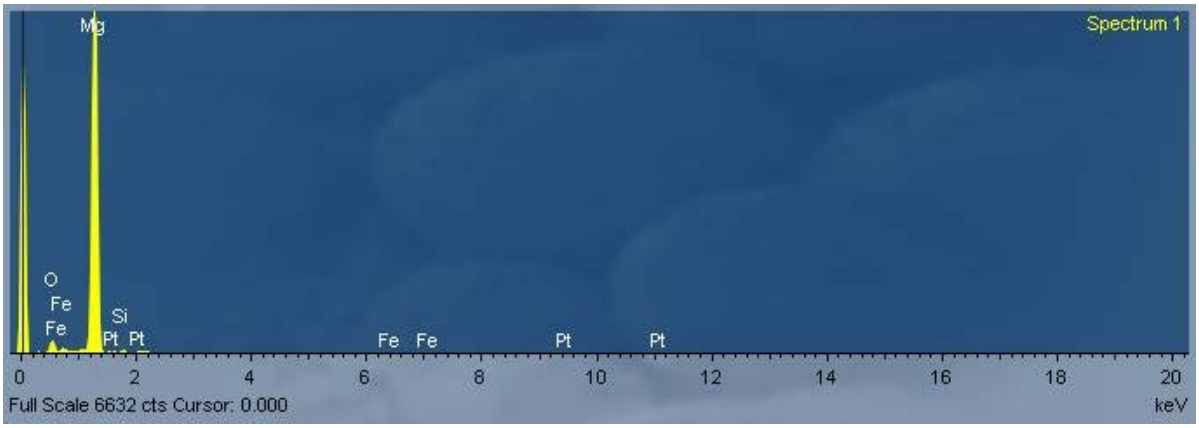

Figure 4 – EDX analysis of Fe particle in Mg alloy without Mn addition (image not shown)

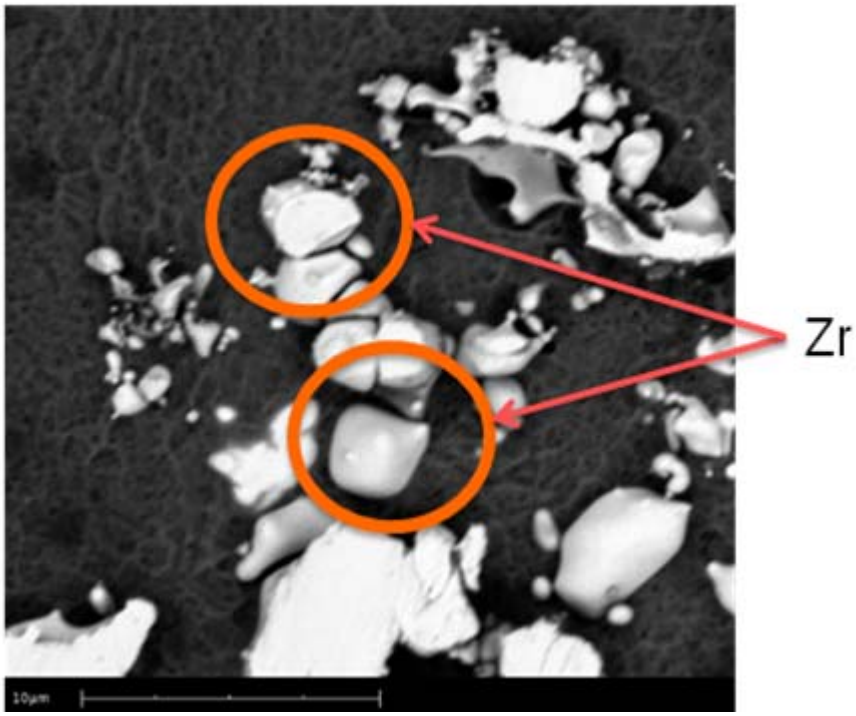

Figure 5 - SEM micrograph of sample with 1.73wt%Zr

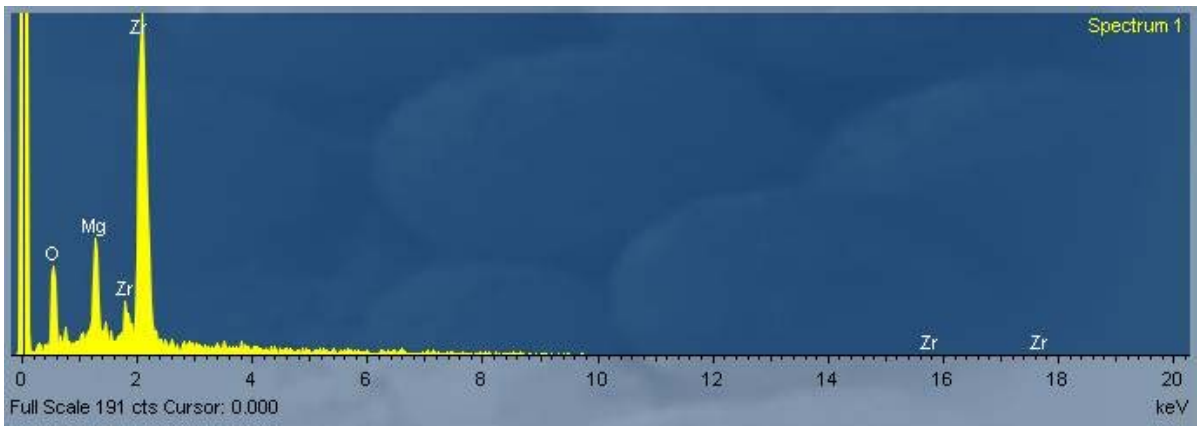

Figure 6 – EDX analysis of Zr particles in Mg alloy depicted in Fig. 4

3.2 Electrochemical tests

The results of potentiodynamic polarisation testing performed are included below.

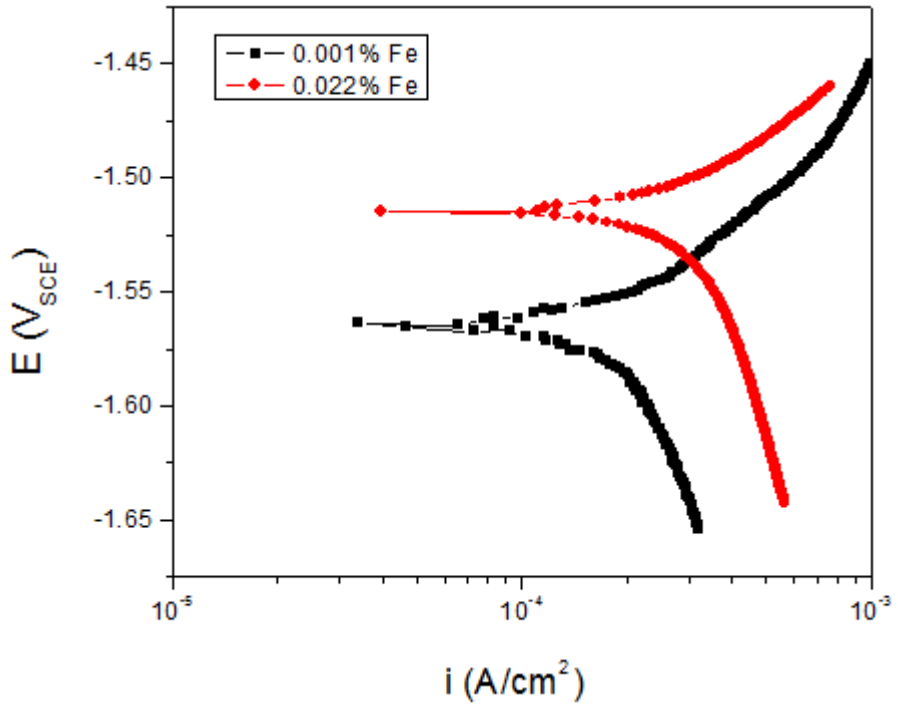

Figure 7 - Potentiodynamic polarization curves for samples with 0.001wt%Fe and 0.022wt%Fe

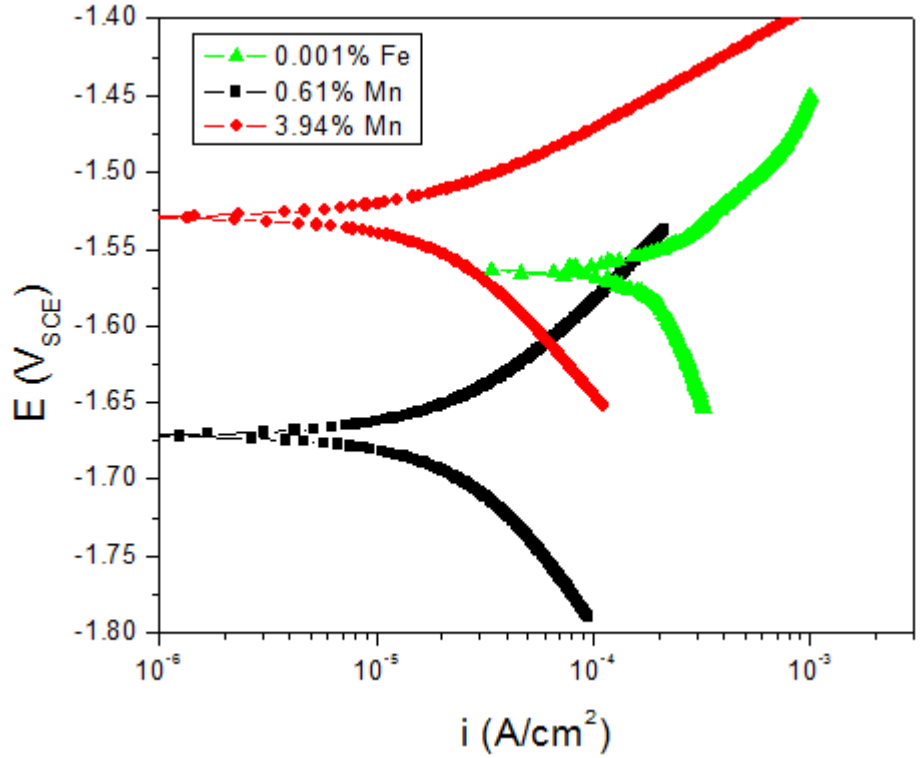

Figure 8 - Potentiodynamic polarization curves for samples with 0.01wt%Mn, 0.61%Mn and 3.94wt%Mn

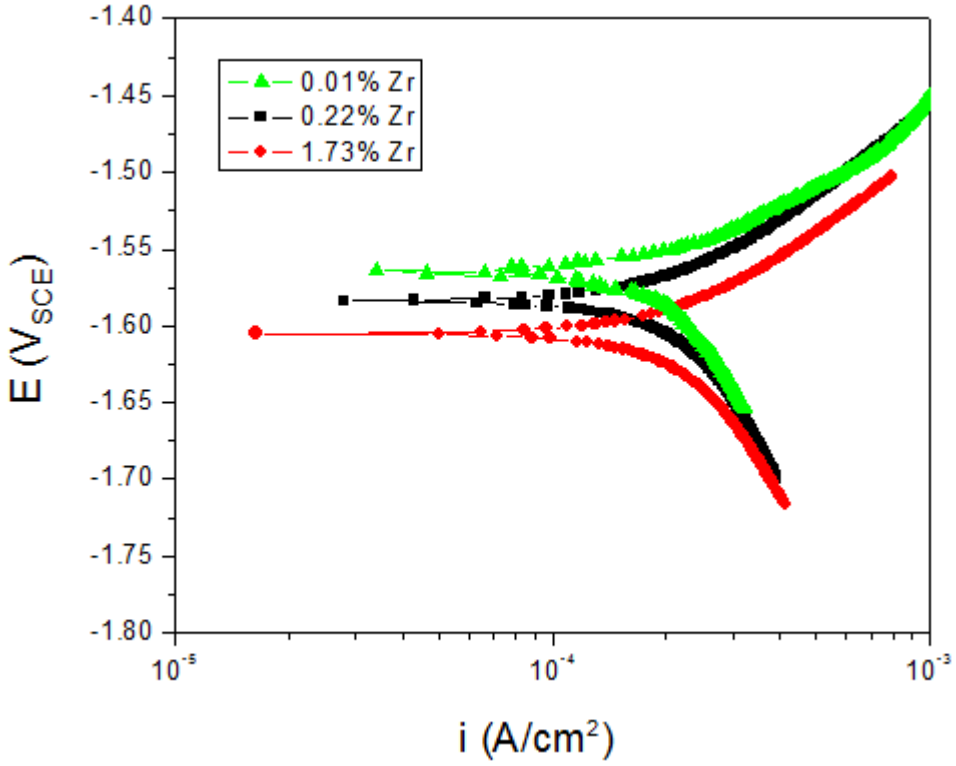

Figure 9 - Potentiodynamic polarization curves for samples with 0.01wt%Zr, 0.61%Zr and 1.73wt%Zr

3.3 Contour maps of composition versus corrosion rates

The results of composition dependant corrosion rate were abridged into the contour plots presented below.

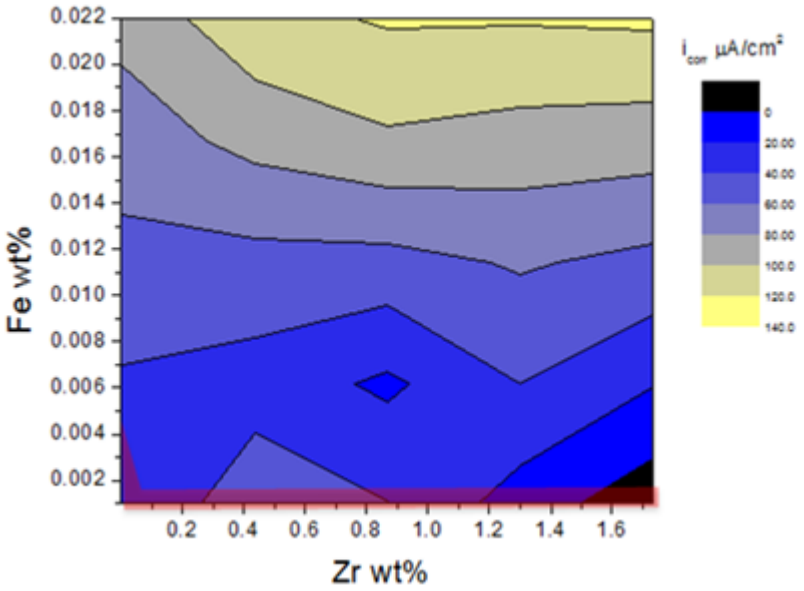

Figure 10 – Contour plot of the corrosion rate as a function of Zr wt% vs. Fe wt%. The red overlay shows a region which corrosion rates are 'acceptable'.

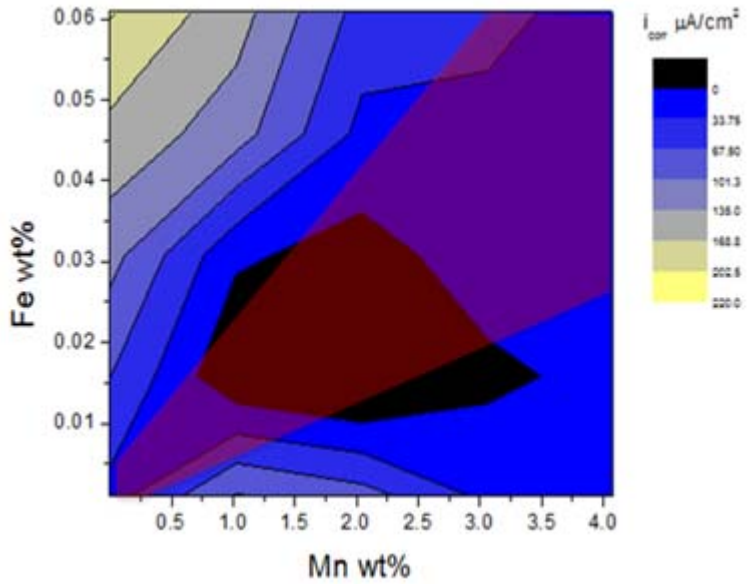

Figure 11 – Contour plot of the corrosion rate as a function of Mn wt% vs. Fe wt%. The red overlay shows a region in which corrosion rates are 'acceptable'

4. DISCUSSION

4.1 SEM and EDX analyses

The SEM image in Figure 1 shows the microstructure of the Mg alloy containing 4.07wt% Mn addition and 0.061wt% Fe. This micrograph shows rather clearly that such elements with low solubility result in the formation of distinct Mn and Fe particles in the Mg matrix. Such particles are essentially pure Mn and pure Fe, and not intermetallic phases that contain Mg. The Mn particles appear to grow up to 15µm in size with an increase of a few weight percent manganese addition while the iron particles are seen to only form up to 1µm in size. As seen in previous work by Robson, these micrographs show that with increasing levels of Mn the particle number density and the volume fraction also increases [6].

The volume fraction of the second phase that forms for a given alloy composition may be estimated from the Lever rule. Using additions of Fe as an example, the Mg-Fe phase diagram allows an estimation for the volume fraction of Fe (BCC) formed [4]. As such:

f_{BCC} = ((Fe content in wt%) – (Fe tolerance limit in wt%)) / (100 – (Fe tolerance limit in wt%)) X 100 = percentage volume fraction

Estimates of the volume fraction of Fe (BCC) phase formed agreed with the observed microstructure where there were very few Fe particles overall in the Mg matrix.

EDX analyses in Figures 2 & 3 confirms that these particles are solely made of manganese and iron with no intermetallic phases with magnesium forming. While the EDX scan in Figure 3 shows that the Fe particle has levels of Mn, there is no intermetallic that forms between Mn and Fe (alone); hence the Mn readings are in this case attributed to the presence of Mn, near or around the Fe particle. Concurrently, the EDX analysis in Figure 4 on the alloys with high Fe and low Mn confirms the iron particles are Mn free.

The SEM image in Figure 5 shows the microstructure of an Mg alloy with 1.73wt% Zr. The EDX analysis in Figure 6 confirms that the particles observed are elemental Zr, and are present in the form up to 20μm in size. The presence of Mg and O in the EDX analysis of Figure 6 can be attributed to the X-rays scanning more than penetrating beyond the Zr particles and also probing the surrounding Mg matrix (and other impurities such as surface O). These Zr regions are undissolved Zr particles due to the level of Zr addition being well above the solid-solubility limit of 0.445wt% [7]. These Zr particles do not form an intermetallic phase with magnesium. A survey of SEM analysis revealed that in the specimens containing Zr, there are practically no separate Fe particles observed. This is likely to be caused by the zirconium reacting with the iron and forming a Fe_2Zr intermetallic which can rapidly settle out in molten magnesium during casting [8].

4.2 Electrochemical tests

Figure 7 shows the effect that Fe-levels have upon the electrochemical response of Mg. An abridged observation from all the data collected, is that the anodic characteristics of the alloys with and without high levels of Fe do not vary as significantly as the cathodic characteristics.

What we see is that specimen with the higher Fe levels exhibits an increase in the rate at which cathodic reaction kinetics are sustained. Fe possesses a greater cathodic efficiency than Mg, and being insoluble, also generates a larger potential difference between the Fe particle and the Mg itself to stimulate microgalvanic corrosion. With higher levels of Fe, more, or larger, Fe particles are expected to form and accelerate this process. As there is almost no Mn in sample MgFe1 to create a buffer between the Fe particles and Mg matrix, the effect of Fe on the cathodic reaction kinetics is more severe, and thus MgFe1 has a higher corrosion rate, despite having less Fe than samples MgMn2, MgMn3 and MgMn4.

Figure 8 shows the changes that occur in the Mn containing Mg alloy samples with increasing Mn content. The cathodic kinetics change when Mn is introduced (again, Mn being a more efficient cathode than Mg), however, other factors which alter the cathodic characteristics must be taken into account as well, such as Fe levels. Yet, when examining the low Mn samples it is seen that the MgMn1 sample with 0.61wt% Mn has higher cathodic reaction rates than the MgMn5 alloy with 3.94wt% Mn, seen by the fact that the alloy with higher Mn content has a lower Fe content. While the cathodic kinetics in sample Pure-Mg2 with 0.001wt% Mn are dominated by the interactions of Fe on the matrix, it is observed that sample MgMn5 has a far lower Fe:Mn ratio than sample MgMn1, and it is seen that increasing cathodic activity follows the increasing Fe;Mn ratio in the trend: MgMn5<MgMn1<Pure-Mg2. This means while Fe does play a detrimental role in the corrosion kinetics of the Mg alloys, the addition of Mn and the apparent ratio of Fe to Mn in the matrix does reduce the detrimental effects of Fe on the cathodic reaction kinetics appreciably. As such, when compared to Pure-Mg2 which has a Fe/Mn ratio of roughly 1 with an overall low level of Fe, samples MgMn1 and MgMn5 have a Fe/Mn well below 1 despite the fact that each alloy has higher levels of Fe. This decrease in the Fe/Mn ratio is seen empirically to be effective. Whilst a detailed understanding of this phenomenon is yet to be presented, one hypothesis was proposed by Kim is that the presence of Mn may allow for the Mn to 'encapsulate' the Fe particles and create a buffer zone between the Fe and Mg matrix which minimises the galvanic coupling effect and reduces the cathodic reaction [9]. Concomitantly, other works such as research by Parthiban have shown that a lower Fe to Mn ratio in magnesium alloys is not always better. Rather, there needs to be a balance where there is not too much Mn added to the alloy to reduce the corrosion resistance [10].

Figure 9 shows the changes that occur in the Zr containing alloys with increasing Zr alloy content. As it can be seen, increasing the zirconium content does not appear to significantly modify cathodic reaction kinetics but it does (albeit slightly) increase anodic activity, contributing to an overall increase in the corrosion rate. The change in Zr content does tend to make the alloy less noble. As a result, this tends to suggest that whilst Fe and Mn dictate the corrosion increase by cathodic control, the role of Zr is one of anodic, or mixed, control. Under some reported circumstances, the Zr in solid-solution is concentrated in Zr-rich cores at the centre of the magnesium grain in the alloy microstructure [11]. It is clear however from the SEM image in Figure 5, that the levels of Zr are well above the solubility limit. Previous studies have shown that such large Zr particles in magnesium alloys can reduce the corrosion resistance as they disrupt the formation and stability of the protective surface film on the alloy surface, opening the alloy to a more aggressive attack from the surrounding environment [12]; however such a situation does not appear to be the principal factor, given that for electrolytes used herein, no protective surface film is expected. The specific role of Zr with respect to corrosion is an avenue that will require further scrutiny in future research.

4.3 Contour maps of composition versus corrosion rates

In order to present the relative effects of the three different additions/impurities being studied herein, the presentation of data as contour plots is presented such that visual assessment of the overall rest results may be obtained. The darker (viz. tending to black) areas display regions with lower corrosion rates where as increasing brightness on the contour plots predicts an increase in the overall corrosion rate.

Figure 10 shows a contour plot of the Mg alloy samples containing Zr and Fe against their i_{corr} values. While it is obvious that the increase in Fe has a negative effect on the corrosion rate of magnesium such high levels are not commonly observed in alloys containing Zr [8]. However, the contour plot does show the effect that changing the Zr levels has on the magnesium. In fact, the direction of the contours upon inspection of Figure 10 does reveal that the shaded scale tends to increase in a manner that aligns with the y-axis and hence Fe content. The shape and scale of these contours tends to show that in combination, the influence of Fe on corrosion will overwhelm that of Zr. Again, a qualitative/tentative zone with respect to threshold limits (based on the empirical data herein) has been overlaid on Figure 10 in red. In the presence of Zr, only low levels of Fe can be tolerated.

Figure 11 shows the contour plot of the Mg specimens containing Mn and Fe against their i_{corr} values. The plot reveals increasing levels of Fe in isolation is detrimental for corrosion. The direction of the contours reveals an interesting relationship, whereby the lowest corrosion rates are seen in a diagonal band that corresponds to an Fe/Mn ratio of 0.02. Most interestingly, a salient feature of Mg alloys is that the common levels of Mn additions in Mg alloys is up to approximately 1wt% and that impurity levels of Fe as high as 300ppm are also not uncommon. This shows that little change to commercial alloy designs are needed when Mn is added.

5. CONCLUSION

1.1 Zr additions beyond a few tenths of a percent increase corrosion rate dramatically. This phenomenon is enhanced in the presence of elevated Mn and/or Fe levels.

1.2 Fe and Mn tend to increase the corrosion rate of Mg by increasing cathodic kinetics.

1.3 The addition of manganese was seen to be beneficial in reducing the impact of Fe impurities, even in the absence of Al. It was seen that a Fe:Mn ratio of 0.02 was a critical ratio for allowing Mn to prove most beneficial.

1.4 The critical threshold limit for any one of Fe, Mn, or Zr is unlikely to be a single value, and the precise threshold will be dependant on the combined relationship between all the three elements (as likely any functional alloying additions to the alloy).

6. ACKNOWLEDGMENTS

The CAST Co-operative Research Centre was established under, and is funded in part by, the Australian Governments Co-operative Research Centres Scheme. Nicholas Kirkland and Daniel East are gratefully acknowledged for their assistance in preparing the alloys used in this research.

7. REFERENCES

1. N. Birbilis, Mark A. Easton., A. D. Sudholz, S. M. Zhu, M. A. Gibson, *On the corrosion of binary magnesiun-rare earth alloys.* Corrosion Science, 2009. **51**: p. 683-689.
2. Guangling Song, David StJohn., *The effect of zirconium grain refinement on the corrosion behavior of magnesium-rare earth alloy MEZ.* Journal of Light Metals, 2002. **2**: p. 1-16.
3. Xin Zhang, Dmytro Kevorkov., In-Ho Jung, Mihriban Pekguleryuz, *Phase equilibria on the ternary Mg-Mn-Ce system at the Mg-rich corner.* Journal of Alloys and Compounds, 2009. **482**: p. 420-428.
4. Ming Liu, Peter J. Uggowitzer., Patrik Schmutz, Andrej Atrens, *Calculated phase diagrams, iron tolerance limits, and corrosion of Mg-Al alloys.* Journal of Materials, 2008. **60**(12).
5. Mark A. Easton, Chris H. J. Davies., Matthew R. Barnett, Franka Pravdic, *Effect of solidification grain refinement on the development of wrought Mg alloys.* Materials science forum, 2007. **539-543**: p. 1729-1734.
6. J.D Robson, D. T. Henry., B. Davis, *Particle effects on recrystallization in magnesium-manganese alloys: particle-stimulated nucleation.* Acta Metallurgica, 2009. **57**: p. 2739-2747.
7. Ma Qian, David H. StJohn., *Grain nucleation and formation in Mg-Zr alloys.* International journal of cast metals research, 2009. **22**(1-4): p. 256-259.
8. P. Cao, Ma Qian., D. H. StJohn, M. T. Frost, *Uptake of iron and its effect on grain refinement of pure magnesium by zirconium.* Materials Science and Technology, 2003. **20**: p. 585-592.
9. J.-G. Kim, A.-J.Koo., *Effect of alloying elements on electrochemical properties of magnesium-based sacraficial anodes.* Corrosion Science, 2000. **56**(4): p. 380-388.
10. G. T. Parthiban, N. Palaniswamy. V. Sivan, *Effect of manganese addition on anode characteristics of electrolytic magnesium.* Anti-Corrosion Methods and Materials, 2009. **56**(2): p. 79-83.
11. Ma Qian, David H. StJohn, M. T. Frost. *Zirconium alloying and grain refinement of magnesium alloys*. in *Magnesium technology 2003*. 2003: The Minerals, Metals and Materials Society
12. W.C Neil, M.Forsyth, P.C. Howlett, C.R. Hutchinson, B.R.W. Hinton, *Corrosion of magnesium alloy ZE41 - the role of microstructural features.* Corrosion Science, 2009. **51**.

8. AUTHOR DETAILS

Darren Gandel is a postgraduate student with the CAST-CRC, working on developing Al-free Mg alloys with improved corrosion resistance.

Nick Birbilis is a senior lecturer in the Department of Materials Engineering at Monash University. His research interests include the broad areas of corrosion and corrosion control.

Mark Easton is the project manager within the CAST CRC. His research focuses on the development of microstructure, particularly during casting processes and its effect on alloy properties.

Dr Mark Gibson is a Senior Principal Research Scientist and Research Group Leader of the Innovation in Process and Production Group at CSIRO Process Science and Engineering. Within the Light Metals Flagship, he leads the high-pressure die casting (HPDC) Magnesium Alloy Development team.

THE INFLUENCE OF MN ON THE CORROSION OF AL-FREE MG-ALLOYS

D.S. Gandel[1,2], N. Birbilis[1,2], M.A. Easton[1,2], M.A. Gibson[1,3]

[1]CAST Co-operative Research Centre, [2]Department of Materials Engineering, Monash University, Australia, [3]CSIRO Process Science and Engineering, Clayton, Australia.

SUMMARY: Manganese is a common addition to magnesium (Mg) alloys. In aluminium (Al) containing Mg alloys, the formation of $Al_8(Mn,Fe)_5$ phase improves the corrosion resistance by removing elemental Fe particles from the Mg. The influence of Mn on the corrosion of Mg alloys in the absence of Al is not well documented. As such, in this study, several commercially pure Mg samples were compared to alloys with varying additions of Mn and Fe. The corrosion rate of these samples was examined via electrochemical and immersion tests. It was seen that samples with Mn additions exhibited an increased Fe impurity tolerance level. This indicates that the Mn addition was able to moderate the effect of the Fe impurity on the corrosion of the Mg alloy even without Al being present.

Keywords: Magnesium, Manganese, Iron, Corrosion.

1. INTRODUCTION

Magnesium (Mg) is the lightest of all the engineering metals and therefore, an attractive alternative to steel and aluminium in an age of light-weighting and energy efficiency. Nonetheless, it is well documented that the corrosion of Mg and its alloys continues to be a major technological challenge preventing wider usage of such alloys in industrial applications [1]. There is an overwhelming demand to develop magnesium alloys with an improved corrosion resistance[2]; with a necessary precursor being a detailed and fundamental understanding of the role of key alloying elements and impurities.

Manganese (Mn) is a common addition in magnesium alloys. While manganese containing Mg alloys can also show some improvements in ductility, Mn additions have little effect on tensile properties. Additions of Mn are aimed at lowering the effect of the iron (Fe) impurity content in order to moderate the corrosion of Mg-Al alloys [3]. In the presence of Al and Fe, additions of Mn produce an $Al_8(Mn,Fe)_5$ phase that can moderate the corrosion rates caused by the impurity Fe. This is important, since when present in Mg, any Fe is nominally insoluble and forms a pure-Fe (bcc) phase in the Mg matrix [4]. This pure Fe has a large potential difference compared to the Mg and is able to support cathodic reactions rather efficiently and hence accelerates the corrosion rate dramatically.

The formation of the $Al_8(Mn,Fe)_5$ intermetallic phase in preference to bcc-Fe can reduce the potential difference by decreasing the iron concentration in the melt. Some of the particles settle at the bottom of the crucible or are

embedded in the casting during solidification [5]. Mn is also sparingly soluble in Mg, and how it affects corrosion is an important consideration for Al-free alloys. While the influence of Mn is known [6], the exact levels of Mn addition necessary to counter-act the detrimental effect of the Fe impurity are still unknown.

When compared with other common alloying elements in Mg alloys, corrosion studies of the effect of Mn upon Al-free Mg are relatively scarce. In this work, we investigate the role of Mn on Fe tolerance limits on the corrosion response of Mg.

2. EXPERIMENTAL METHODS

2.1 Samples

Alloys were produced by induction melting and the starting materials were high purity metals (>99.9%). Following melting, alloys were poured into a cast iron mould and allowed to cool. Several samples with low impurity levels were also examined to form a benchmark from which the effects of the alloying additions on the change in corrosion resistance can be measured. Table 1 below shows the levels of alloying additions in each of the samples tested. Compositions were determined by inductively coupled plasma atomic emission spectroscopy (ICP-AES) by Spectrometer Services (Coburg, Vic, Australia).

Table 1 – Composition of Mg-Mn-Fe alloy samples tested in this work (in wt.%)

Sample ID	Mg%	Mn%	Fe%
1	~Bal	1.92	0.015
2	~Bal	1.91	0.012
3	~Bal	1.08	0.015
4	~Bal	1.12	0.02
5	~Bal	1.11	0.043
6	~Bal	0.72	0.027
7	~Bal	0.7	0.023
8	~Bal	0.65	0.023
9	~Bal	0.59	0.007
10	~Bal	0.52	0.008
11	~Bal	0.44	0.016
12	~Bal	0.35	0.011

Sample ID	Mg%	Mn%	Fe%
13	~Bal	0.6	0.054
14	~Bal	0.77	0.071
15	~Bal	0.81	0.048
16	~Bal	0.61	0.012
17	~Bal	1.13	0.035
18	~Bal	2.31	0.056
19	~Bal	4.07	0.061
20	~Bal	3.94	0.002
21	~Bal	0.01	0.004
22	~Bal	0.001	0.001
23	~Bal	0.001	0.001
24	~Bal	0.008	0.022

2.2 SEM and EDX

The microstructures of the alloys produced were examined via scanning electron microscopy. Specimens were polished to a 1µm diamond paste finish and etched with a picric acid solution then imaged using either an FEI Phenom or JEOL 840A; the latter microscope was also capable of EDXS analysis for determination of elemental composition of the particles that were observed.

2.3 Corrosion Testing

Specimens were ground to a 2000 grit surface finish. A 3-electrode electrochemical flat-cell with an exposed sample area of 1 cm^2 was used for electrochemical testing. The test electrolyte was 0.1M NaCl in all cases. A VMP 3Z potentiostat was used, with potentiodynamic polarisation carried at 1 mV/s. Prior to polarisation, samples were conditioned for ten minutes at open circuit to ascertain a stable potential. The polarisation curves

were used to determine i_{corr} (via a Tafel-type fit) using EC-Lab software. Such fitting is inherently difficult, however the ability of EC-lab to allow manual control is critical. As a general rule, fits were executed by selecting a portion of the curve that commenced >50mV from E_{corr}, and i_{corr} was subsequently estimated from the value where the fit intercepted the potential value of the true E_{corr}. This fit was generally dominated by cathodic data because the cathodic branch of the Tafel plot varied more widely between specimens. More so, polarisation testing was also able to visually reveal comparative information related to the kinetics of both the anodic and cathodic reactions between alloys. Each sample was tested five times and an average result was determined. Weight loss testing was also carried out by immersion of specimens in 0.1M NaCl. Samples were cleaned in 7% HNO3 for approximately 5 seconds to remove any corrosion product, prior to mass loss determination.

3. RESULTS

3.1 Contour maps of composition versus corrosion rates

In order to present the relative effects of both the elements being studied herein, the presentation of data as contour plots is presented such that visual assessment of the overall test results may be obtained. The darker (viz. tending to dark blue) areas display regions with lower corrosion rates where increasing brightness (viz. tending to red) on the contour plots predicts an increase in the overall corrosion rate. The grey dots on the contour plot correspond to the relative spread of the samples tested.

Figure 1 shows the contour plot of the Mg specimens containing Mn and Fe against their immersion weight loss values in grams per centimetre squared per day. As Fe content is increased there is a corresponding increase in the observed corrosion rate. However, as Mn is increased the corrosion rate initially decreases before starting to increase again at higher levels. The effect on the corrosion rate cause by the addition of Mn continues in the presence of higher Fe levels in the alloy. The lowest commercially practical corrosion rates are seen in a diagonal band that corresponds to a Fe:Mn ratio below roughly 0.036.

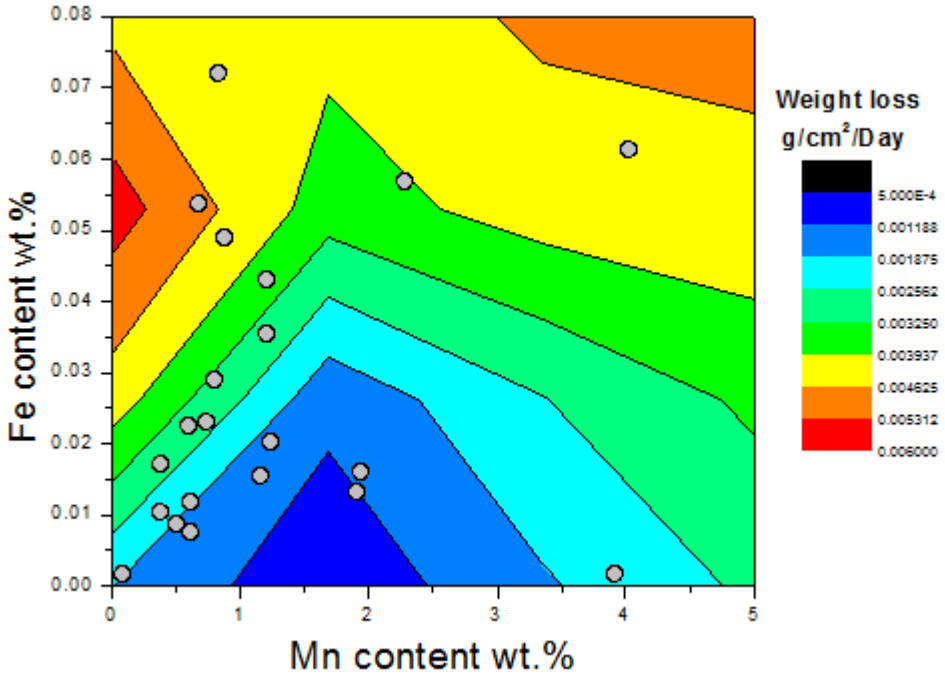

Figure 1 – The corrosion rate as a function of Mn vs. Fe presented from weight loss data.

3.2 SEM and EDX analyses

The SEM image in Figure 2 shows the microstructure of the Mg alloy containing 4.07wt.% Mn addition and 0.061wt.% Fe. The particles seen are essentially pure Mn and pure Fe. The Mg-Mn [7] and Mg-Fe [8] phase diagrams indicate that there are no intermetallic phases that form between Mg and either Mn or Fe. The Mn particles appear to grow up to 15µm in size with an increase of a few weight percent manganese addition while Fe particles are seen only up to 1µm in size. As seen in previous work by Robson, these micrographs show that with increasing levels of Mn the particle number density and the volume fraction also increases [9]. The observed microstructure also shows that there are a few of the very small Fe particles overall in the Mg matrix.

Figure 2 helps clarify how these elements with low solubility result in the formation of distinct Mn and Fe particles in the Mg matrix. When Fe is added to Mg, there is very little solid solubility of roughly 0.00043at.% [8]. Thus, even at low levels, such as the generally quoted Fe tolerance limit of approximately 170ppm [10], Fe particles are numerous enough to cause significant internal galvanic corrosion problems and increase the corrosion rate. Due to the limited temperature range between the liquidus and solidus line seen in the Mg-Fe system [8] there is very little time for the Fe particles to grow into large, well-developed structures [11]. As such, the Fe particles observed are quite small and numerous as increasing Fe content leads to increased distribution rather than increased particle size. Conversely, there is a greater solid solubility for Mn in magnesium than Fe. Mn can be added to just below 1at.% in solid solution under the right processing conditions. As opposed to Fe particle formation, a coarsening reaction takes place with the Mn particles where larger particles grow at the expense of the smaller ones [12]. The driving force for such a reaction is the net decrease of interfacial energy in the system. As such, there are a smaller number of larger Mn particles present [9]. Higher Mn contents are therefore required to increase the total number of Mn particles within the Mg matrix.

Thus, we see a further improvement of the corrosion resistance of the Mg alloy before higher levels of Mn particles begin to act as their own cathodic sites [13]. However, this is not the case for Fe particles. When Mn is added to Mg alloys which contain Fe there is a decrease observed in the negative impact on the corrosion rate that is caused by the Fe impurity. The Mn addition is able to decrease the corrosion rate of the alloy overall despite higher than desired Fe levels.

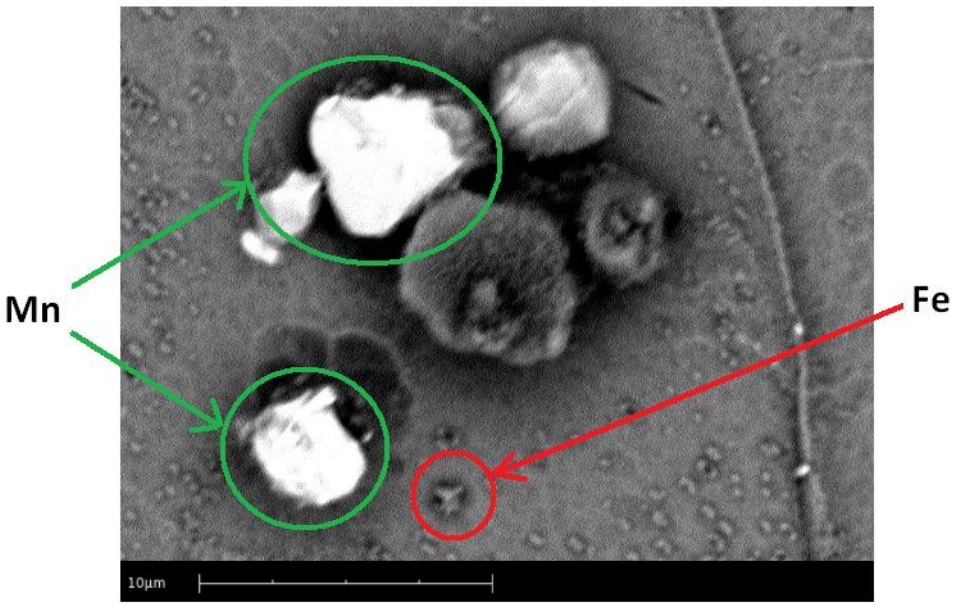

Figure 2 - SEM micrograph of sample with 4.07wt.%Mn and 0.061wt.%Fe

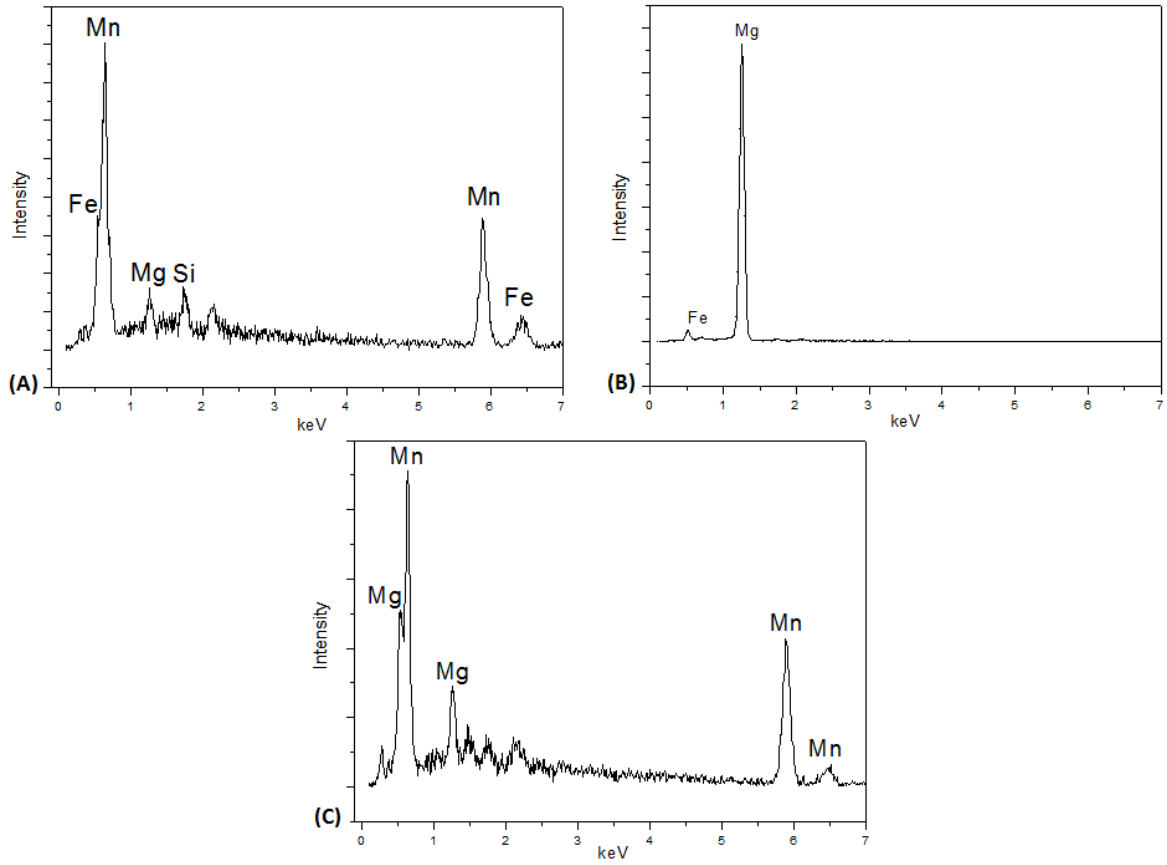

Figure 3 – EDX analysis, (A) Fe particle in alloy containing Mn, (B) Fe particle in alloy that does not contain Mn and (C) Mn particle

3.3 Electrochemical tests

Figure 4(A) shows the effect that Fe-levels have upon the electrochemical response of Mg. The anodic characteristics of the alloys with and without high levels of Fe do not vary as significantly as the cathodic characteristics. This is due to the fact that Fe is not present in solid solution in any significant quantity. The Fe particles that form as a result of this low solid-solubility act as cathodes within the matrix. This causes micro-galvanic coupling within the alloy. As the particles are essentially made of pure Fe, they alter the Tafel plot by moving the cathodic branches due to the interaction of Fe with Mg. Figure 4(B) shows the changes that occur in the anodic and cathodic branches of the Tafel plots in the Mn containing Mg alloy samples with increasing Mn content. The Mn content changes from Sample 22 with low levels of Mn, to Mn in solid solution in Sample 16 and finally to Sample 20 where Mn in solid solution is saturated in the Mg matrix and Mn particles are quite numerous. The corrosion of a multi-phased Mg alloy is typically controlled by three factors: (1) the composition of the α-Mg, (2) the composition of the other phases and (3) the number and size density of the other phases [14].

As Fe does not have a large solid solubility, its effect on factor (1) is not as great as Mn which has a much larger solid solubility. Both Fe and Mn particles are elemental with no Mg intermetallics. This means that they both have an effect of the 2nd factor which contributes to the corrosion characteristics as the Fe and Mn particles are of a different composition to the Mg matrix. The last factor however helps explain how Fe is much more detrimental than other impurities. Fe particles that form in Mg are much smaller and more numerous. As such, their greater distribution leads to a greater negative influence on the corrosion properties. As Mn particles are

observed to be far larger than Fe particles in the alloys tested, a higher Mn content is needed before the Mn particles begin to have the appropriate distribution required to cause a significant impact on the corrosion resistance.

What is observed is that specimens with the higher Fe levels exhibits an increase in the rate at which cathodic reaction kinetics are sustained. Fe possesses a greater cathodic efficiency than Mg [15], and being insoluble, also generates a larger potential difference between the Fe particle and the Mg itself to stimulate microgalvanic corrosion. With higher levels of Fe, more Fe particles are expected to form and accelerate this process.

The cathodic kinetics change when Mn is introduced (again, Mn being a more efficient cathode than Mg), however, as the controlling factors (1) and (3) are different for Mn introduced to Mg as opposed to Fe, the beneficial effects on the cathodic characteristics must be taken into account as well.

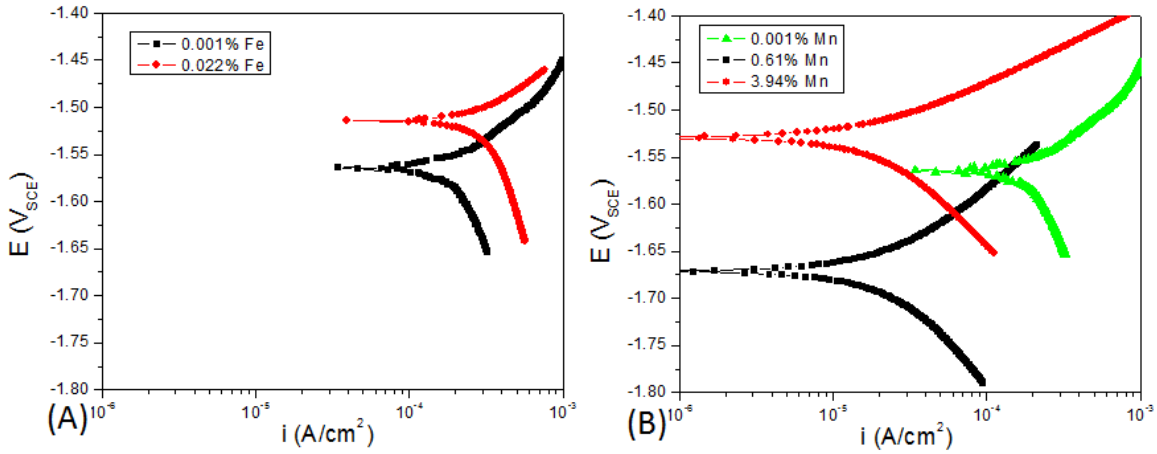

Figure 4 - Potentiodynamic polarization curves, (A) samples 22 & 24 and (B) samples 16, 20 & 22

4. DISCUSSION

4.1 SEM and EDX analyses

EDX analyses in Figures 3(B) & 3(C) confirm that these particles are comprised solely of either Mn or Fe. While the EDX scan in Figure 3(A) shows that the Fe particle has levels of Mn, work on Mn-Fe phase diagrams by Witusiewicz show that no intermetallic phase forms between Mn and Fe (alone), but they are soluble in one another at given conditions [16]; hence the Mn readings are in this case attributed to the presence of Mn, within or around the Fe particle. Whilst a detailed understanding of this phenomenon is yet to be presented, one hypothesis proposed by Kim is that the presence of Mn may allow for the Mn to 'encapsulate' the Fe particles and create a buffer zone between the Fe and Mg matrix which minimises the galvanic coupling effect and reduces the cathodic reaction [6]. This is thermodynamically possible as the Mg-Mn and Mg-Fe phase diagrams show that excess Fe incorporated in the magnesium melt will begin to form solid particles before solidification of Mn begins to take place.

However, this may not necessarily be the case. Witusiewicz's phase diagram [16] shows that there is a large region where a Fe/Mn mixed austenitic phase can exist compared to a ferritic Fe region where Mn is sparingly soluble. Thus, it is possible that the addition of Mn does not merely 'encapsulate' the Fe particles, but rather that it could be dissolved within the Fe to render it less detrimental to the Mg matrix. Concurrently, the EDX analysis in Figure 2(B) on the alloys with high Fe and low Mn confirms the iron particles are Mn free. Future examination of such particles in a TEM will be able to determine if either the ferritic or austenitic Fe particles

exist in the Mg matrix, thereby respectively inferring which of the Fe 'encapsulation' or Mn 'solubility' hypotheses as the cause for the reduction in corrosion rates observed.

4.2 Electrochemical tests

As displayed in Figure 4(A), there is almost no Mn in Sample 24 to moderate the effect of the Fe particles. The shift in the cathodic reaction kinetics results in an increased corrosion rate as Fe is an efficient cathode within Mg. This accelerates the corrosion of the surrounding Mg matrix. As higher levels of Fe are introduced it is expected that the shift in the cathodic branch in the Tafel plot of an Mg alloy will also increase due to the greater number of Fe particles present. Thus, Sample 24 has a higher corrosion rate than other samples tested herein despite having less Fe than samples which also have a high Mn content.

When examining Figure 3(B), it can be seen that the low Mn content Sample 16 with 0.61wt.% Mn has higher cathodic reaction rates than Sample 20, with 3.94wt.% Mn, which is due to the fact that the alloy with higher Mn content has a lower Fe content. Yet, as the Mn content for Sample 16 is below the solid solubility limit we see far less Mn particles, indicating that most of the Mn is in solid solution. This decreases the overall reaction kinetics compared to the commercially pure Sample 22. Sample 20 has a far larger Mn content with the Mg matrix saturated with Mn in solid solution. The cathodic kinetics in Sample 22, with 0.001wt.% Mn, are dominated by the interactions of Fe on the matrix, it is observed that Sample 20 has a far lower Fe:Mn ratio than Sample 16, and it is seen that increasing cathodic activity follows the increasing Fe:Mn ratio in the trend: 20<16<22.

This means while Fe does play a detrimental role in the corrosion kinetics of the Mg alloys, the addition of Mn and the apparent ratio of Fe to Mn in the matrix does reduce the detrimental effects of Fe on the cathodic reaction kinetics appreciably. As such, when compared to Sample 22 which has a Fe/Mn ratio of roughly 1 with an overall low level of Fe, Samples 16 and 20 have a Fe/Mn well below 1 despite the fact that each alloy has higher levels of Fe. This decrease in the Fe/Mn ratio is seen empirically to be effective. Contrary to the work by Kim, other studies such as research by Parthiban have shown that a lower Fe to Mn ratio in magnesium alloys is not always better. Rather, there needs to be a balance where there is not too much Mn added to the alloy before it begins to reduce the corrosion resistance [13].

5. CONCLUSION

- Fe and Mn tend to increase the corrosion rate of Mg by increasing cathodic kinetics; however Fe is a more potent cathode, sustaining reduction reactions at higher rates.
- The addition of manganese was observed to be beneficial in reducing the detrimental impact of Fe impurities, even in the absence of Al. It was seen that a Fe:Mn ratio below roughly 0.036 was a critical ratio for allowing Mn to prove most beneficial.
- The critical threshold limit for Fe in Mg (which is often quoted at a fixed value of ~170ppm) is not observed to be a fixed/single value. We see that with increasing Mn content, the Fe threshold is simultaneously raised, with the precise threshold dependant on the combined relationship between both elements (as likely any functional alloying additions to the alloy). The more Fe present, the more beneficial the impact of Mn. A tolerance level as high as approximately 350ppm is possible based on observations.

6. ACKNOWLEDGMENTS

The CAST Co-operative Research Centre was established under, and is funded in part by, the Australian Governments Co-operative Research Centres Scheme. Andy Yob, Ming Sun, Sherly Simanjuntak, Nicholas

Kirkland and Daniel East are gratefully acknowledged for their assistance in preparing the alloys used in this research.

7. REFERENCES

[1] N. Birbilis, M.A. Easton, A.D. Sudholz, S.M. Zhu, and M.A. Gibson, On the corrosion of binary magnesiun-rare earth alloys, Corrosion Science, 51, (2009), 683-689.

[2] G. Song and D. StJohn, The effect of zirconium grain refinement on the corrosion behavior of magnesium-rare earth alloy MEZ, Journal of Light Metals, 2, (2002), 1-16.

[3] X. Zhang, D. Kevorkov, I.-H. Jung, and M. Pekguleryuz, Phase equilibria on the ternary Mg-Mn-Ce system at the Mg-rich corner, Journal of Alloys and Compounds, 482, (2009), 420-428.

[4] M. Liu, P.J. Uggowitzer, P. Schmutz, and A. Atrens, Calculated phase diagrams, iron tolerance limits, and corrosion of Mg-Al alloys, Journal of Materials, 60(12), (2008).

[5] S.L. Sin, D. Dube, and R. Tremblay, Characterisation of Al-Mn Particles in AZ91D invesment castings, Materials Characterization, 58, (2007), 989-996.

[6] A.-J.K. J.-G. Kim, Effect of alloying elements on electrochemical properties of magnesium-based sacraficial anodes, Corrosion Science, 56(4), (2000), 380-388.

[7] H. Okamoto, Mg-Mn (Magnesium-Manganese), Journal of phase Equilibria and Diffusion, 29(2), (2008), 208-209.

[8] A.A. Nayeb-Hashemi, J.B. Clark, and L.J. Swartzendruber, The Fe-Mg (Iron-Magnesium) System, Bulletin of Alloy Phase Diagrams, 6(3), (1985), 235-238.

[9] J.D. Robson, D.T. Henry, and B. Davis, Particle effects on recrystallization in magnesium-manganese alloys: particle-stimulated nucleation, Acta Metallurgica, 57, (2009), 2739-2747.

[10] S.J. Splinter, N.S. McIntyre, P.A.W.v.d. Heide, and T. Do, Influence of low level iron impurities on the initial interaction of water vapour with polycrystalline magnesium surfaces, Surface Science, 317, (1994), 194-202.

[11] T. Haitani, Y. Tamura, T. Motegi, N. Kono, and H. Tamehiro, Solubility of iron in pure magnesium and cast structure of Mg-Fe alloy, Materials science forum, 419-422, (2003), 697-702.

[12] A.F. Smith, The isothermal growth of manganese precipitates in a binary magnesium alloy, Acta Metallurgica, 15, (1967), 1867-1873.

[13] G.T. Parthiban, N. Palaniswamy, and V. Sivan, Effect of manganese addition on anode characteristics of electrolytic magnesium, Anti-Corrosion Methods and Materials, 56(2), (2009), 79-83.

[14] Z. Shi, M. Liu, and A. Atrens, Measurement of the corrosion rate of magnesium alloys using Tafel extrapolation, Corrosion Science, 52, (2010), 579-588.

[15] A.D. Sudholz, N.T. Kirkland, R.G. Buchheit, and N. Birbilis, Electrochemical properties of intermetallic phases and common impurity elements in Magnesium alloys, Electrochemical and Solid-State Letters, 14(2), (2011), C5-C7.

[16] V.T. Witusiewicz, F. Sommer, and E.J. Mittemeijer, Reevaluation of the Fe-Mn Phase Diagram, Journal of phase Equilibria and Diffusion, 25(4), (2004), 346-354.

8. AUTHOR DETAILS

Darren Gandel is a postgraduate student with the CAST-CRC, working on developing Al-free Mg alloys with improved corrosion resistance.

Nick Birbilis is an Assoc. Professor in the Department of Materials Engineering at Monash University. His research interests include the broad areas of corrosion and corrosion control.

Mark Easton is the Project Manager within the CAST CRC. His research focuses on the development of microstructure, particularly during casting processes and its effect on alloy properties.

Dr Mark Gibson is a Senior Principal Research Scientist and Research Group Leader of the Innovation in Process and Production Group at CSIRO Process Science and Engineering. Within the Light Metals Flagship, he leads the high-pressure die casting (HPDC) Magnesium Alloy Development team.

IRON AND CORROSION CONTROL IN ALUMINIUM-FREE MAGNESIUM ALLOYS

D.S. Gandel[1,2], N. Birbilis[1,2], M.A. Easton[1,2], M.A. Gibson[1,3]

[1]CAST Co-operative Research Centre;
Level 4, Building 43, Coopers Road, University of Queensland; St. Lucia, Brisbane, Queensland, 4072, Australia
[2]Department of Materials Engineering, Monash University; Building 72, Clayton Campus, Monash University; Melbourne, Victoria, 3800, Australia
[3]CSIRO Process Science and Engineering; 71 Normanby Road Clayton; Melbourne, Victoria, 3168, Australia

Keywords: Magnesium, Manganese, Zirconium, Iron, Corrosion

Abstract

There are a number of new and existing magnesium alloys that do not contain aluminium (Al). Often these are used for high performance applications such as aerospace or structural purposes. It is well known that the most important consideration for corrosion performance in Mg alloys is to reduce the presence of impurities such as iron (Fe). Zirconium (Zr) and manganese (Mn) are both common alloying additions in Al-free Mg-alloys. Both Mn and Zr were investigated to understand their effectiveness of mitigating the effect of Fe impurities in Mg alloys. In this study, Mg-alloys are made with additions of Mn, Zr and Fe. The addition of Mn was found to inhibit the negative effects of Fe on the Mg microstructure, yet little Fe was removed from the melt. Zr demonstrated a high propensity for removing Fe; however, the introduced Zr caused micro-galvanic corrosion. When Mn and Zr are added together to the Mg melt at appropriate levels it was found that the beneficial effects of Mn's inhibition and Zr's removal of Fe work in conjunction to create an alloy with superior corrosion resistance to an Mg-alloy with either Zr or Mn additions on their own.

Introduction

Magnesium is the least dense of all the engineering metals. This makes it an attractive substitute for other metals such as steel or aluminium where weight reduction is a key concern in engineering applications. However, it is well documented that the corrosion of Mg and its alloys continues to be a major technical issue preventing increased usage of these alloys [1]. There is a great desire to design Mg alloys with an improved corrosion resistance [2], most notably in relation to the removal or control of deleterious Fe impurities [3-5]. Due to the industrial usage of steel dies for Mg casting it is difficult to avoid introducing some Fe into the alloys [6]. As such, Al containing Mg alloys incorporate Mn additions which form the Al_8Mn_5 phase in which Fe can substitute for Mn and this improves the corrosion characteristics. In Al-free alloys it is not as clear what is the best approach for the removal or mitigation of Fe. However, Mn and Zr are two possible candidates for alloying additions to counter the deleterious effects of Fe.

Mn is reported to act as a excellent scavenger element in Mg alloys that can control the effects of Fe impurities [7]. It is commonly believed to be accomplished by either enveloping or forming intermetallic compounds with the Fe impurities in the Mg melt, making the particles less galvanically active in the Mg matrix [5]. In general, Zr containing Mg alloys show little sensitivity to Fe impurities. It is known that the Fe impurities are scavenged by Zr in the Mg melt prior to casting to form insoluble precipitates. This can be considered to render the Mg-Zr alloys as 'high purity' Mg alloys [2], with commercial Mg alloys containing zirconium generally containing less than 50 ppm of Fe [8].

Very little research has been done on Mg alloys which contain both Mn and Zr. However, previous

work suggests that not only are Fe impurities soluble in the Mn-Zr intermetallic phases, but that Zr, Mn and Fe combine to form additional intermetallic phases in the Mg melt which then settle to the bottom of the processing vessel as sludge [9]. This work focuses on the impact on Fe when Mn and/or Zr are added to Mg during the casting process, expressly on the relative effectiveness of Mn and/or Zr on Fe removal and control.

Experimental Methods

Mg alloys were made by mixing Mg-Mn, Mg-Zr and Mg-Fe master alloys with commercially pure Mg in a resistance furnace with Sulfur Hexafluoride (SF_6) as a cover gas. The pure Mg was initially melted in the furnace and small amounts of the master alloys were weighed and added according to their calculated Mn/Zr/Fe content to achieve specific Mn/Zr/Fe levels in the cast ingots. Following melting, the alloys were poured into a cast iron mould and allowed to cool. Three series were produced, two with only Mn or Zr as singular additions and one with both Mn and Zr as additions. All three series had Fe added into the melt. The compositions of the alloys were determined by inductively coupled plasma atomic emission spectroscopy (ICP-AES).

The samples were machined and cut to an appropriate size and were cold mounted in epoxy resin. The metal surfaces were ground to a 2000 grit surface finish. A 3-electrode electrochemical flat-cell with an exposed sample area of 1 cm^2 was used in conjunction with a 0.1M NaCl electrolyte. A VMP 3Z potentiostat was used, with potentiodynamic polarisation conducted at 1 mV/s. Prior to polarisation, samples were conditioned for ten minutes at open circuit to ascertain a stable potential. The polarisation curves were used to determine i_{corr} (via a Tafel-type fit) using EC-Lab software. Such fitting is inherently difficult; however the ability of EC-lab to allow manual control is critical.

As a general rule, fits were executed by selecting a portion of the curve that commenced >50mV from E_{corr}, and i_{corr} was subsequently estimated from the value where the fit intercepted the potential value of the true E_{corr}. Polarisation testing was also able to visually reveal comparative information related to the kinetics of both the anodic and cathodic reactions of the various Mg specimens. Each sample was tested five times and an average result was determined.

Results

Fe was added to the Mn and Zr containing specimens to roughly 500ppm in order for the Fe content to be above the expected tolerance limit. Figure (1) shows a plot of the Mg-Mn specimens produced in this study according to their Mn and Fe contents. The plot shows that as the Mn content is increased the Fe concentration does not necessarily always decrease in a cast sample, as even samples with up to 1 wt.% Mn still have roughly 500ppm of Fe. The low Fe levels in the high Mn containing samples appears to be fortuitous as previous studies have indicated that at higher Mn contents high Fe levels commonly occur [10]. As such, there does not appear a strong trend where additional Mn reduces the Fe content when compared to Zr in Figure (2), which shows a plot of the Mg-Zr specimens according to their Zr and Fe contents. Unlike Figure (1), the plot indicates that the Fe levels in these alloys are low irrespective of the overall Zr content. This shows that the addition of Zr is more effective at lowering the Fe impurity content in the Mg alloy.

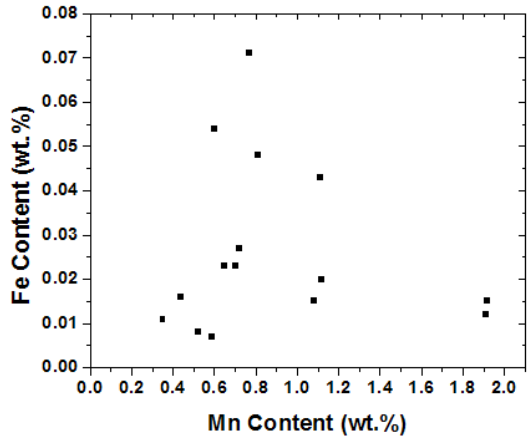

Figure (1) Mn content (wt.%) vs. Fe content (wt.%) for the Mg-Mn alloys investigated.

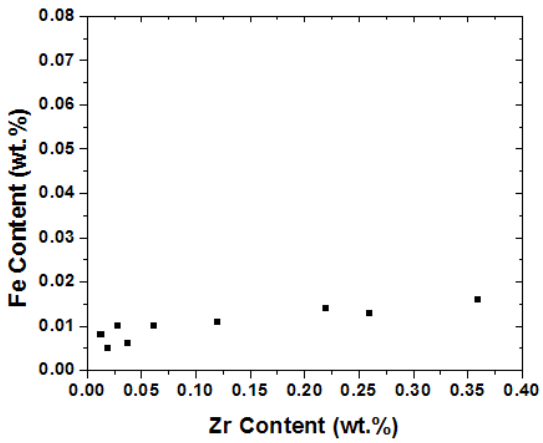

Figure (2) Zr content (wt.%) vs. Fe content (wt.%) for the Mg-Zr alloys investigated.

Figure (3) shows the contour plot of the Mg specimens containing Mn and Fe against their calculated i_{corr} values from Tafel-plot analyses. The plot shows that as the Fe content is increased there is a subsequent increase in the corrosion rate. However, as the Mn content is increased the corrosion rate begins to decrease. The reduction of the corrosion rate caused by the addition of Mn continues in a roughly linear fashion even in the presence of higher Fe levels in the alloy. Figure (4) similarly shows a contour plot of the calculated i_{corr} values for the Mg specimens containing Zr and Fe. As with Figure (3), the plot shows that with increasing Fe content the corrosion rate increases. However, Zr is not as beneficial to Mg corrosion resistance as Mn. As the Zr content increases the corrosion rate continues to increase.

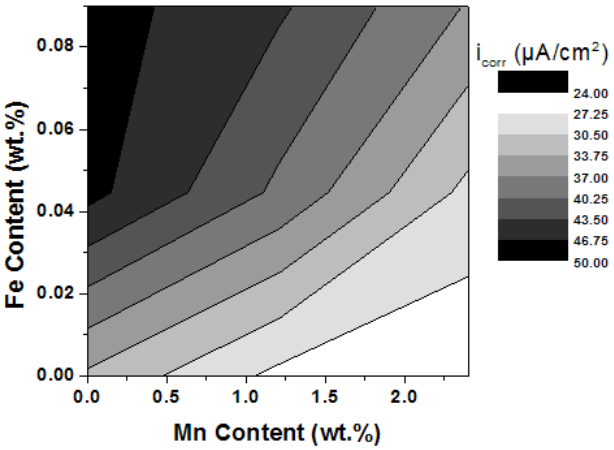

Figure (3) Contour plot of the corrosion rate as a function of Mn wt.% vs. Fe wt.%.

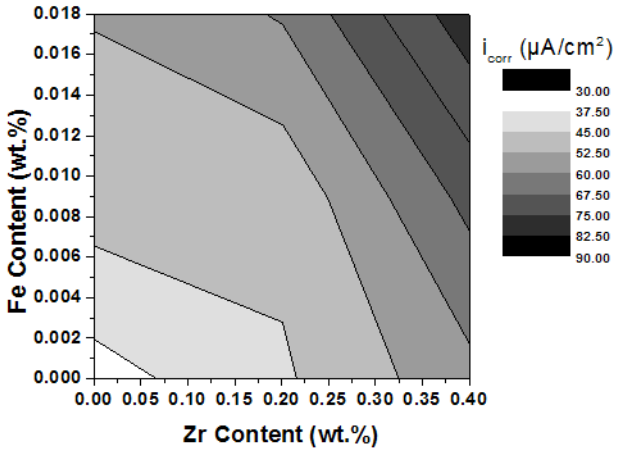

Figure (4) Contour plot of the corrosion rate as a function of Zr wt.% vs. Fe wt.%.

Figure (5) shows a Tafel plot of an Mg-Mn specimen with 1.08wt.% Mn and 150ppm Fe compared to that of Pure Mg with approximately 40ppm Fe. The plot shows that there is a decrease in the cathodic reaction kinetics despite the fact that the Mn containing specimen has an Fe content of 150ppm, which is usually a critical composition of Fe for increased corrosion. This shows that the corrosion rate decreases when the Mn content is increased even without reducing the overall Fe content. Figure (6) shows Tafel plots of an Mg-Zr specimen with 0.037wt.% Zr and 60ppm Fe and Pure Mg with approximately 40ppm Fe. The plot shows that while Zr containing Mg alloy has a similar Fe content that is considered to be below the critical level of 150ppm, there is an increase in the anodic reaction kinetics. It is known that the Zr particles that form which are micro-

galvanically active in a similar manner to Fe [11, 12] and that Zr can increase the anodic reaction kinetics when added to Mg [13]. As such, it is theorised that the Zr particles are responsible for the control and increase in the overall corrosion rate.

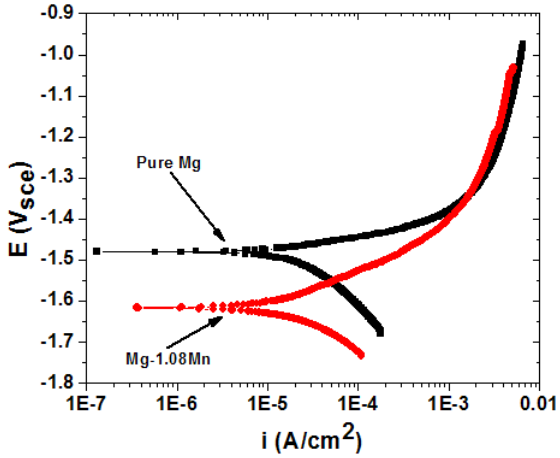

Figure (5) Polarisation curves for Pure Mg and Mg-Mn alloy.

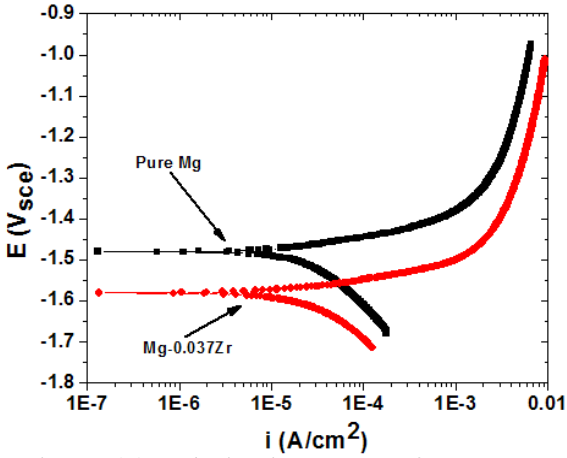

Figure (6) Polarisation curves for Pure Mg and Mg-Zr alloy.

Figure (7) shows the calculated i_{corr} values and standard error for the Mg alloy series containing both Mn and Zr. The Mn content is reasonably constant at approximately 2 wt.% whereas the Zr content is increasing. It shows that initially there is an increase in the corrosion rate as Zr is introduced into the system, then there is a subsequent reduction in the corrosion rate when the specimens contain between 0.05 and 0.15 wt.% Zr. Beyond this region the corrosion rate continues to increase.

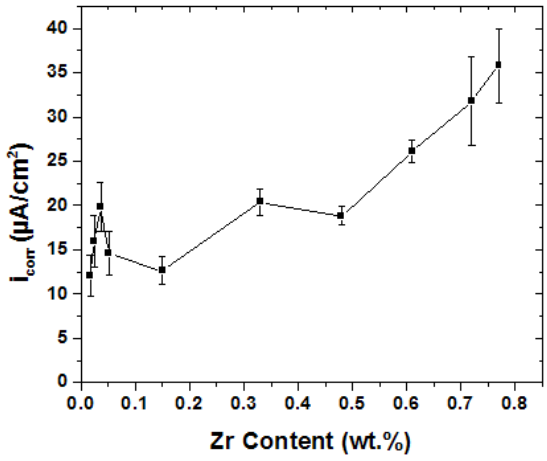

Figure (7) i_{corr} vs. Zr content with constant Mn level of roughly 2wt.%.

Discussion

According to figure (1), there does not appear to be a 'scavenging' effect by Mn as the Fe content in the alloy seems to be unaffected by the Mn content. However, Mn is still able to play a role in the inhibition of the detrimental effect of Fe impurities. As Figure (3) shows, when Fe increases, the corrosion rate increases. Yet, when Mn is added, the corrosion rate decreases. Previous work has shown that at increased Mn levels, Fe particles will be accompanied by Mn [10]. This interaction

is observed in figure (5) where the cathodic corrosion kinetics are reduced when Mn is added, despite the high Fe content. The added Mn prevents the Fe impurities from controlling the cathodic kinetics and increasing the corrosion rate. This interaction is capable of increasing the Fe tolerance limit, allowing higher Fe impurity levels to be present before they begin to cause deleterious micro-galvanic corrosion of the Mg matrix. Hence it appears that Mn does not effectively remove Fe from the melt. Instead Mn reduces the negative impact of Fe on the matrix.

It is well documented that adding even a little Zr to the Mg melt is able to remove Fe impurities [2, 8]. Indeed, figure (2) shows that there are low levels of Fe in the specimens containing Zr. However, too much Zr is itself detrimental for the corrosion of Mg alloys as the Zr particles that form in the Mg matrix can also act as micro-galvanic sites for corrosion to accelerate in a similar manner to Fe impurities [11, 12]. Thus, an increase in the corrosion rate can be observed, as shown Figure (4), when either the Fe or Zr levels are increased. Moreover, figure (6) shows how the anodic corrosion kinetics increase as the Zr content is increased, despite the fact that there is a low Fe content. Thus, while Zr is highly effective at removing the deleterious Fe particles from the initial Mg melt, Zr in the alloy inevitably results in the same problems with enhanced corrosion as caused by the Fe particles that the Zr addition is meant to be removing.

Apart from the known Zr-Fe interactions that remove Fe impurities, it has been suggested that Mn-Zr particles can also remove Fe impurities. However, the Mn-Zr particles that form are also insoluble and settle out of the melt during processing [9]. In the case of the Mg-Mn-Zr specimens produced herein, the Mn content is kept close to its solid solubility limit in Mg at 2 wt.%. Figure (7) shows the changes in i_{corr} values as the Zr content is increased up to roughly 0.8 wt.%. The plot shows how a combined Mg-Mn-Zr alloy with roughly 2 wt.% Mn and 0.15 wt.% Zr can produce an i_{corr} value as low as 12.5 $\mu A/cm^2$ compared to the Mg-Mn and Mg-Zr allows with their lowest i_{corr} values being roughly 25 $\mu A/cm^2$ and 35 $\mu A/cm^2$ respectively in the best of circumstances. This can be attributed to two reasons; firstly that the Zr initially removes the Fe particles and secondly the Zr is subsequently removed by interacting with the Mn in the melt, thereby producing an Mg casting with low Fe and Zr levels.

Conclusion

1. Mn is effective at rendering Fe less detrimental to the corrosion rate of Mg, probably by reducing the micro-galvanic corrosion potential with the Mg matrix, but is inefficient at removing Fe from the melt/alloy.
2. Zr is effective at removing the Fe from the melt, but the Zr itself is deleterious for corrosion resistance of Mg, most likely due to micro-galvanic coupling with the Mg matrix.
3. Higher levels of Mn combined with low levels of Zr demonstrated the highest corrosion resistance. The Zr removed the Fe, and then the Mn removed the excess Zr and rendered the remaining Fe less detrimental.

Acknowledgments

The CAST Co-operative Research Centre was established under, and is funded in part by, the Australian Governments Co-operative Research Centres Scheme. Andy Yob, Ming Sun, Sherly Simanjuntak, Nicholas Kirkland and Daniel East are gratefully acknowledged for their assistance in preparing the alloys used in this research.

References

[1] N. Birbilis, M.A. Easton, A.D. Sudholz, S.M. Zhu, and M.A. Gibson, On the corrosion of binary magnesiun-rare earth alloys, Corrosion Science, 51, (2009), 683-689.
[2] G. Song and D. StJohn, The effect of zirconium grain refinement on the corrosion behavior of magnesium-rare earth alloy MEZ, Journal of Light Metals, 2, (2002), 1-16.

[3] G. Song and A. Atrens, Understanding Magnesium Corrosion, Advanced engineering materials, 5(12), (2003), 837-858.
[4] M. Liu, P.J. Uggowitzer, P. Schmutz, and A. Atrens, Calculated phase diagrams, iron tolerance limits, and corrosion of Mg-Al alloys, Journal of Materials, 60(12), (2008).
[5] G.T. Parthiban, N. Palaniswamy, and V. Sivan, Effect of manganese addition on anode characteristics of electrolytic magnesium, Anti-Corrosion Methods and Materials, 56(2), (2009), 79-83.
[6] T. Haitani, Y. Tamura, T. Motegi, N. Kono, and H. Tamehiro, Solubility of iron in pure magnesium and cast structure of Mg-Fe alloy, Materials science forum, 419-422, (2003), 697-702.
[7] J.G. Kim and A.J. Koo, Effect of alloying elements on electrochemical properties of magnesium-based sacraficial anodes, Corrosion Science, 56(4), (2000), 380-388.
[8] P. Cao, M. Qian, D.H. StJohn, and M.T. Frost, Uptake of iron and its effect on grain refinement of pure magnesium by zirconium, Materials Science and Technology, 20, (2003), 585-592.
[9] M.A. Easton, C.H.J. Davies, M.R. Barnett, and F. Pravdic, Effect of solidification grain refinement on the development of wrought Mg alloys, Materials science forum, 539-543, (2007), 1729-1734.
[10] D.S. Gandel, N. Birbilis, M.A. Easton, and M.A. Gibson, The influence of Mn on the corrosion of Al-free Mg-alloys, in: 18th International Corrosion Congress, (2011), pp. 1-9.
[11] A.E. Coy, F. Viejo, P. Skeldon, and G.E. Thompson, Susceptibilityof rare-earth-magnesium alloys to microgalvanic corrosion, Corrosion Science, 52(12), (2010), 3896-3906.
[12] W.C. Neil, M. Forsyth, P.C. Howlett, C.R. Hutchinson, and B.R.W. Hinton, Corrosion of magnesium alloy ZE41 - the role of microstructural features, Corrosion Science, 51, (2009), 387-394.
[13] D.S. Gandel, N. Birbilis, M.A. Easton, and M.A. Gibson, Influence of Manganese, Zirconium and Iron on the corrosion of Magnesium, in: Corrosion & Prevention 2010, (2010), Australasian Corrosion Association, pp. 1-11

Magnesium Technology 2013
Edited by: Norbert Hort, Suveen N. Mathaudhu, Neale R. Neelameggham, and Martyn Alderman
TMS (The Minerals, Metals & Materials Society), 2013

The influence of Mg-Zr master alloy microstructure on the corrosion of Mg

D.S. Gandel[a,b], M.A. Easton[a,b], M.A. Gibson[a,c], T. Abbott[a,d] and N. Birbilis[a,b]
[a]*CAST Cooperative Research Centre*
[b]*Department of Materials Engineering, Monash University, Clayton VIC. 3800, Australia*
[c]*CSIRO Process Science and Engineering, Clayton, VIC, 3168, Australia*
[d]*Magontec Limited, Sydney, NSW, 2000, Australia*

Keywords: Magnesium, Zirconium, Polarisation, Weight loss, Microstructure

Abstract

In this study, sixteen Mg-Zr alloys were produced to investigate the role of Zr on corrosion of Mg. Alloys were produced using two different commercial Mg-Zr master alloys commonly used for grain refining Mg, but which contain different Zr particle size distributions. It is seen that the master alloy with a smaller Zr particle size leads to an alloy containing more Zr in solid solution. The ratio of Zr in solid solution and in particle form was observed to have a marked effect on the corrosion of Mg.

Introduction

Zirconium (Zr) has a low solid solubility in magnesium (Mg) of 0.73 at.% and it is acknowledged that there are no intermetallic phases that form between Mg and Zr [1]. Zr is commonly and predominantly added to Mg in order to refine the grain size [2-4]. The reduction in grain size in Mg alloys provides greatly improved casting quality and increased mechanical properties [5-7]. As Mg has a Hall-Petch coefficient of 280-320 MPa/μm, the reduction of the grain size in Mg alloys significantly increases the strength of the alloy and allows a greater control over the alloy texture [6, 8, 9]. Thus, Zr is used in the commercial alloys WE43, ZE41 and ZK60. Moreover, newer Mg alloys, such as AM-SC1 and Elektron 21, have recently been developed which also contain Zr for the purpose of grain refinement [10-13]. Given the considerable present interest in Mg alloys a better understanding of the influence of Zr additions on the corrosion of Mg is necessary.

There are reported cases where the addition of Zr to Mg alloys has decreased the corrosion rate through the removal of Fe impurities by the Zr addition [4, 14-16]. Fe impurities in Mg are scavenged by Zr in the melt due to the Zr and Fe combining to form insoluble precipitates, usually Fe_2Zr, which can settle to the bottom of the melt crucible owing to a difference in density. Thus, Mg-Zr alloys are generally considered 'high purity', with commercial Mg alloys that incorporate Zr, usually containing under 50 ppm of Fe [14].

Whilst the removal of Fe by Zr is beneficial in reducing the corrosion rates of Mg alloys, the addition of Zr to the Mg matrix can cause its own corrosion related issues. It has been reported that when Zr is not homogeneously dispersed within the Mg matrix, the corrosion rate can increase compared to a more even distribution of smaller Zr particles [17]. Furthermore, excess Zr in Mg increases the amount of elemental Zr particles that form in the matrix, which is detrimental for corrosion [18]. These elemental Zr particles have been reported to cause micro-galvanic couples with the surrounding Mg matrix and the disruption of the protective oxide film on the alloy surface [19]. As such, further investigation into elucidating the role of Zr in corrosion of Mg is of considerable importance to improve both current and future commercial Mg alloys containing Zr.

In this study, the role of Zr additions on the increasing corrosion rate of Mg and the fundamental effects of different Zr particle sizes and size distributions, added from different Mg-Zr master alloys, is examined. The effect on the corrosion rates for given Mg-Zr alloy mixtures made from two different Mg-Zr master alloys, i.e. Microzir (formally AM-Cast) and Zirmax, are reported.

Experimental Methods

Alloy production and characterization

Sixteen Mg-Zr alloys were produced by adding different amounts of Mg-Zr master alloys to commercially pure Mg. The Mg-Zr master alloys used herein were Microzir, supplied by Magontec, and Zirmax supplied by Magnesium Elektron. Melting was carried out in a resistance furnace using AM-Cover® as a cover gas. The commercially pure Mg was initially melted in a steel crucible at 700°C to which small amounts of the master alloys were added to achieve specific Zr contents in the final castings. The melt was poured into a graphite coated cast iron mould and the ingots were allowed to air cool. Stirred samples were vigorously mixed immediately prior to casting; where as unstirred specimens were held stationary for 20 minutes prior to casting.

The compositions of the alloys were determined independently via inductively coupled plasma atomic emission spectroscopy (ICP-AES) (Spectrometer Services, Coburg, Australia). The precise composition of the experimental alloys is given in Table 1. The values for Zr content in solid solution and overall Zr content were measured by via an acid pre-treatment procedure prior to ICP-AES analysis as per Crawley [20]. The soluble Zr content was determined by dissolving the sample in a 10% HCl solution. The total Zr content was determined by dissolving the specimen in a 50% HCl – 6% HF solution.

Several alloys were examined via scanning electron microscopy. Prepared Mg-Zr alloy specimens and both Mg-Zr master alloys were polished to a 1μm diamond paste finish and then imaged using a JEOL 7001F SEM in back scattered electron (BSE) mode. The microscope was equipped with energy dispersive x-ray spectroscopy (EDX) (Oxford Instruments X-Max 80 detector).

Electrochemical and corrosion testing

Specimen surfaces were ground to a 2000 grit surface finish. A 3-electrode electrochemical flat-cell with an exposed sample area of 1 cm^2 was used in conjunction with a 0.1M NaCl electrolyte. A VMP 3Z potentiostat was used, with potentiodynamic polarisation conducted at 1 mV/s. Prior to polarisation, the samples were conditioned for ten minutes at open circuit to ascertain a stable potential. The polarisation curves were used to determine i_{corr} (via a Tafel-type fit) using EC-Lab software.

Tafel-like fits were executed by selecting a portion of the curve that commenced >50mV from E_{corr}, and i_{corr} was estimated from

the value where the fit intercepted the potential value of the true E_{corr}. Polarisation testing was also able to visually reveal comparative information related to the kinetics of both the anodic and cathodic reactions of the various Mg specimens. Each sample was tested five times and an average result was determined.
Additionally, weight loss was determined by exposing alloy samples via immersion in 0.1M NaCl for a period of 24 hours. Subsequent corrosion products were removed by a light scrubbing following a 3s immersion in 15% HNO_3. The mass loss was determined on three unique samples and an average result was determined and reported.

Results and Discussion

Alloy characterization

All alloys examined in this study have Zr additions below the levels expected for grain refinement to take place. Stirring the Mg melt prior to casting was found to increase the overall Zr content in binary Mg-Zr alloys (Table 1). However, while the unstirred alloys had a lower average total Zr content, they did have similar percentages of Zr in solid solution compared to the stirred alloys. The lower total Zr content in the unstirred alloys compared to the stirred alloys is most likely due to Zr particles contained in the unstirred Mg melt settling down to the bottom of the crucible during the extended holding time prior to casting. This would result in less Zr in suspension in the Mg melt at the point in time where the molten liquid is poured from the crucible to the mould while making the Mg-Zr ingot.
The ICP-AES compositional data (Table 1) confirm that the Mg-Zr alloys made from the Microzir master alloy have on average a much higher percentage of Zr in solid solution than the Mg-Zr alloys made from the Zirmax master alloy. The stirred alloys made with the Microzir master alloy averaged between 36% to 47% of the total Zr content in solid solution compared to the stirred alloys made with the Zirmax master alloy which only averaged between 10% to 25% of the total Zr content in solid solution. This difference between the Microzir and Zirmax samples does not appear to be caused by a stirring effect due to the similarities in percentage of Zr in solid solution in both the stirred and unstirred conditions. The difference in microstructure is caused by the different sizes of Zr particles introduced by the Mg-Zr master alloys (Figures 1 (A & B)) [21].
Both the Zirmax and Microzir Mg-Zr alloys (Figures 2 (A, & C)) contain Zr particles embedded in the Mg matrix. EDX mapping elucidates the difference in microstructure of the two alloy groups due to the difference in Zr particles size introduced by the different Mg-Zr master alloys. Apart from the greater number of Zr particles present, there is a large amount of Zr in solid solution in the Mg matrix of the Microzir sample (Figure 2 (B)). The Zirmax alloy (Figure 2 (D)) does not appear to have much Zr in solid solution, despite having a similar overall Zr content to the Microzir alloy. The finer particle sizes introduced by the Microzir master alloy has allowed a greater amount of Zr to go into solid solution rather than forming insoluble Zr particles in the Mg matrix [22]. Due to the very low Fe content in both of the Mg-Zr alloys, no discernable Fe peaks of note were seen while performing EDX testing on the selected specimens.
There is a noticeable difference in the Zr particle structure between the two Mg-Zr alloy groups. The Microzir alloys generally have smaller Zr particles that cluster together, compared to the Zirmax alloys that have larger and more isolated individual Zr particles. Again, the difference in particle size between the two master alloys is likely to be the cause for the different morphologies in the Zr particles present in the matrix. Vigorous stirring has been shown to minimise the presence of large Zr particle clusters, however, larger individual Zr particles need longer holding times to let the particles settle out of the Mg melt effectively [23]. The extended holding times required to remove the larger individual Zr particles have been shown to reduce the overall Zr content in the Mg alloy. The EDX map of the selected Microzir and Zirmax specimens corroborates the compositional analysis which indicate that the Microzir alloys have a much higher percentage of Zr in solid solution compared to the Zirmax alloys.

Assessment of Zr in solid solution

There is a higher average Zr content in the stirred Mg-Zr alloys compared to the unstirred alloys (Figure 3 (A & B)). This is due to the fact that more Zr particles are able to settle to the bottom of the crucible during processing of the unstirred samples, which were held motionless for an extended period of time prior to casting. It can be seen that there is a trend where the overall percentage of Zr in solid solution increases as the overall Zr content increases in the Microzir containing alloys (Figure 3 (A)). The Zirmax alloys, however, show the opposite effect, in that as the overall Zr content increases the percentage of Zr in solid solution decreases. Despite the reduced uptake of Zr in Mg overall, these trends are also seen in the unstirred Mg-Zr alloys (Figure 3 (B)).
The amount of Zr in solid solution is influenced by the difference in Zr particle size characteristic of the two master alloys. The Zirmax master alloy has a larger and more variable Zr particle size compared to the Microzir master alloy, which has a more even distribution of smaller Zr particles [22, 23]. The finer Zr particle size in the Microzir master alloy, with most Zr particles ranging between 1 and 5 μm in size, allows for more Zr to dissolve into solid solution. This finer distribution is highly desired due to the beneficial effects favouring the alloying effectiveness of the Mg-Zr master alloy and the ensuing grain-refining effect of Zr [4, 24-26]. Moreover, with more Zr in solid solution, less elemental Zr particles will be retained in the Mg matrix to contribute to corrosion related problems and increased corrosion rates.

Effect of Zr alloying additions on Mg corrosion rates

I_{corr} increases in the Zirmax containing alloys as the Zr content in solid solution increases (Figure 4 (A)). The Zirmax alloys, however, typically have only low levels of Zr in solid solution with increasing total Zr content, with only up to 0.012 wt.% Zr observed in solid solution at best. The Microzir alloy, with over 0.1 wt.% Zr in solid solution, displays an initial slight decrease in i_{corr} before increasing, however, the later increase does not exceed the initial measured i_{corr} value.
The i_{corr} values for the Zirmax alloys appear to be quite variable with very little increase in Zr content in solid solution (Figure 4 (B)). The Microzir alloys, with a slightly higher percentage of Zr in solid solution, do have some semblance of a decreasing corrosion rate. There is initially a drop in the measured i_{corr} value as the Zr content in solid solution is increased. However, the overall Zr content is still quite low (Table 1).
In the Microzir alloys, i_{corr} decreases, then increases slightly as the overall Zr content increases (Figure 4 (C)). The higher percentage of Zr in solid solution allows for higher overall Zr contents in Mg

before accelerating the corrosion rate. The Microzir-4 alloy contains five times as much Zr in solid solution as the Zirmax-4 alloy with a similar total Zr content. The greater amount of Zr present as elemental Zr particles in the Zirmax alloys thus contributes to increased i_{corr} values than the Microzir produced Mg-Zr alloys.

The stirred and unstirred samples do not have a similar measured i_{corr} trend. There is an overall decrease in i_{corr} for the unstirred Microzir alloys and a slight overall increase for the unstirred Zirmax alloys (Figure 4 (D)) compared to stirred alloys of a similar content. The greater percentage of Zr in solid solution at a lower overall Zr content in the unstirred Microzir alloys compared to the stirred alloys may account for this difference as a greater amount of Zr has gone into solid solution. The unstirred Zirmax alloys have a lower percentage of Zr in solid solution compared to the stirred alloys with a similar Zr content. The greater amount of Zr particles embedded in the matrix, rather than dissolving into solid solution, is the likely cause of the increase i_{corr} values measured.

Influence of Zr on the corrosion reaction kinetics of Mg

As Zr is introduced into Mg there is an increase in the anodic reaction kinetics whilst the cathodic reaction kinetics are only slightly increased for the Zirmax containing alloy. The changes in the reaction kinetics when Zr is added can be seen in Figure 5. The increase in anodic and cathodic reaction kinetics can be observed through the shifts in the anodic and cathodic branches of the polarisation curves compared to pure Mg. At the alloying content limit of the Mg alloys examined (Table 1), Zr is still below the solid solution limit in Mg according to the phase diagram [1], with a large percentage of the total Zr content in the Mg-Zr alloys in solid solution.

The data reveals that Zr is an anodic activator of Mg and increases the corrosion rate of Mg when added. This anodic activation effect is observed even at very low levels of Zr and does not seen to be influenced by the initial microstructure of the Mg-Zr master alloy used in the manufacturing of the Mg-Zr alloys. This data supports previous work that the initial addition of Zr into Mg increases the anodic kinetics before increasing the cathodic reaction kinetics via micro-galvanic coupling with large Zr particles embedded in the Mg matrix [27]. The increase in anodic kinetics is the key electrochemical reason for the increased corrosion rates seen in the Mg-Zr alloys produced herein. As such, the increase in the cathodic reaction kinetics in the Zirmax containing Mg-Zr alloy can be explained by the increased number of large Zr particles present in the microstructure due to less Zr dissolving into solid solution.

Comparison between Microzir and Zirmax alloys via long corrosion testing

There is a noticeable trend linking the overall Zr content and the mass loss from immersion results (Figure 6). The relationship shows that as the Zr content increases the mass loss also increases per unit time. The data is presented in its native units to avoid problems or errors from assuming uniform corrosion for the immersion weight loss data data.

There is a divergence in the weight loss values for the two Mg-Zr alloy groups. The Microzir alloys not only have a higher average weight loss than the Zirmax alloys but they also have a larger calculated standard error. As the two alloy groups have a similar overall Zr content (Table 1), the most likely cause for the increased weight loss observed in the Microzir alloys is the higher Zr content in solid solution.

General discussion

The increase in Zr content in Mg has a great influence on the anodic corrosion characteristics of Mg. As discussed previously, however, there is no large overall increase in i_{corr} with increasing Zr content in the Microzir alloys, Figure 6 shows that when there is a greater amount of Zr in solid solution there is an increase in the corrosion rate according to the longer term immersion weight loss tests.

The higher levels of Zr in solid solution lead to a greater anodic activating effect in the Mg matrix. This is an indicator that there is a greater anodic activation by the higher amount of Zr in solid solution increasing the long-term corrosion rates. With a higher Zr content in solid solution there should be a greater amount of generalised corrosion attack across the surface area of the alloy as less Zr particles would be present in the matrix to serve as corrosion initiation sites via micro-galvanic coupling.

Despite the desire for a greater content of Zr in solid solution, which is beneficial for grain refinement [27], even low levels of Zr appear to increase the overall corrosion of Mg. The difference in the size of the Zr particles introduced to Mg does appear affect the way in which Zr affects the long-term corrosion rate. Higher percentages of Zr in solid solution for a given total Zr content increase the long-term corrosion rates of Mg, where as lower percentages of Zr in solid solution for a similar Zr content will have a greater impact on the short-term electrochemical corrosion behaviour of Mg.

While other studies have suggested that the addition of Zr is favourable for corrosion resistance of Mg [14, 15], these studies have generally examined Mg-alloys that contain other elements, such as rare earths. As such, they do not reflect the direct interaction between only Zr and Mg. Any decrease in corrosion rates observed in such studies are likely from secondary interactions between Zr and ternary or quaternary elements or the changes in grain sizes - which in turn also impact the corrosion of the particular alloys studied.

Conclusions

1. For the same nominal composition, higher overall Zr contents were obtained through stirring of the Mg melt prior to casting due to settling of Zr in the furnace crucible with the long holding times associate with the unstirred alloys.
2. Stirring of the melt did not greatly affect the average percentage of Zr in solid solution for a given total Zr content.
3. Mg-Zr master alloys with a finer particle size used in the production of Mg-alloys will have an increased amount of Zr in solid solution in Mg-alloys for a given Zr content.
4. The corrosion current density, i_{corr}, increases more significantly with an increasing Zr content when there is a lower percentage of Zr in solid solution.
5. Zr in solid solution in Mg is an anodic activator, increasing the anodic reaction kinetics and thereby accelerating the generalised corrosion attack of the matrix.

6. Mass loss testing indicated that greater (and more highly variable) mass loss occurs with time in alloys which have a higher proportion of Zr in solid solution.

Acknowledgments

The CAST Co-operative Research Centre was established under, and is funded in part by, the Australian Governments Co-operative Research Centres Scheme. Andy Yob, Ming Sun and Sherly Simanjuntak are gratefully acknowledged for their assistance in preparing the alloys used in this research.

[1] H. Okamoto, Mg - Zr (Magnesium - Zirconium), Journal of Phase Equilibria and Diffusion, 28(3), (2007), 305-306.

[2] I.J. Polmear, Light Alloys. 3rd Edition (Ed). 1995, London, England: Arnold.

[3] E.F. Emley, Principles of Magnesium Technology. 1st edition (Ed). 1966, Manchester: Pergamon Press.

[4] M. Qian and D.H. StJohn, Grain nucleation and formation in Mg-Zr alloys, International Journal of Cast Metals Research, 22(1-4), (2009), 256-259.

[5] K.V. Kutniy, I.I. Papirov, M.A. Tikhonovsky, A.I. Pikalov, S.V. Sivtzov, L.A. Pirozhenko, V.S. Shokurov, and V.A. Shkuropatenko, Influence of grain size on mechanical and corrosion properties of magnesium alloy for medical implants, Material Wissenschaft Und Werkstofftechnik, 40(4), (2009), 242-246.

[6] C.D. Lee, Effect of grain size on the tensile properties of magnesium alloy, Materials Science and Engineering A, 459, (2007), 355-360.

[7] H.E. Friedrich and B.L. Mordike, Magnesium Technology. 2006, Berlin: Springer. 708.

[8] W. Yuan, S.K. Panigrahi, J.Q. Su, and R.S. Mishra, Influence of grain size and texture on Hall-Petch relationship for a magnesium alloy, Scripta Materialia, 65, (2011), 994-997.

[9] H. Han, S. Liu, L. Kang, and L. Liu, Refinement role of electromagnetic stirring and calcium in AZ91 Magnesium alloy, Journal of Wuhan University of technology - Materials Science Edition, 23(2), (2007), 194-197.

[10] P. Lyon, New magnesium alloy for aerospace and specialty applications, in: A.A. Luo(Ed) Magnesium Technology, (2004), TMS, pp. 311-315.

[11] T. Rzychon, J. Michalska, and A. Kielbus, Corrosion resistance of Mg-RE-Zr alloys, Journal of Achievments in Materials and Manufacturing Engineering, 21(1), (2007), 51-54.

[12] C.J. Bettles, M.A. Gibson, and S.M. Zhu, Microstructure and mechanical behaviour of an elevated temperature Mg-rare earth based alloy, Materials Science and Engineering A, 505, (2009), 6-12.

[13] A.C. Hanzi, F.H.D. Torre, A.S. Sologubenko, P. Gunde, R. Schmid-Fetzer, M. Kuehlein, J.F. Loffler, and P.J. Uggowitzer, Design strategy for microalloyed ultra-ductile magnesium alloys, Philosophical Magazine Letters, 89(6), (2009), 377-390.

[14] P. Cao, M. Qian, D.H. StJohn, and M.T. Frost, Uptake of iron and its effect on grain refinement of pure magnesium by zirconium, Materials Science and Technology, 20, (2003), 585-592.

[15] G. Song and D. StJohn, The effect of zirconium grain refinement on the corrosion behavior of magnesium-rare earth alloy MEZ, Journal of Light Metals, 2, (2002), 1-16.

[16] M. Qian, D.H. StJohn, and M.T. Frost, Zirconium alloying and grain refinement of magnesium alloys, in: H.I. Kaplan(Ed) Magnesium Technology 2003, (2003), The Minerals, Metals and Materials Society pp. 209-214.

[17] G. Ben-Hamu, D. Eliezer, K.S. Shin, and S. Cohen, The relation between microstructure and corrosion behaviour of Mg-Y-RE-Zr alloys, Journal of Alloys and Compounds, 341, (2007), 269-276.

[18] Z. Rong-chang, Z. Jin, H. Wei-Jiu, W. Dietzel, K.U. Kainer, C. Blawert, and K.E. Wei, Review of studies on corrosion of magnesium alloys, Transactions of Nonferrous Metals Society of China, (2006), 763-771.

[19] W.C. Neil, M. Forsyth, P.C. Howlett, C.R. Hutchinson, and B.R.W. Hinton, Corrosion of magnesium alloy ZE41 - the role of microstructural features, Corrosion Science, 51, (2009), 387-394.

[20] R.H.A. Crawley, Determination of soluble and insoluble zirconium in magnesium alloys, Analytica Chimica Acta, (1961), 281-284.

[21] M. Sun, G. Wu, M.A. Easton, D.H. StJohn, T. Abbott, and W. Ding, A comparison of the microstructure of three Mg-Zr master alloys and their grain refinement efficientcy, in: W.J. Poole and K.U. Kainer(Eds), Mg2012: 9th International Conference on Magnesium Alloys and their Applications, (2012, pp. 873-880.

[22] M. Qian, D.H. StJohn, and M.T. Frost, A new zirconium-rich master alloy for the grain refinement of magnesium alloys, in: K.U. Kainer(Ed) 6th International Conference Magnesium Alloys and their Applications, (2003), Wiley-VCH Verlag Gmbh & Co., pp. 706-712.

[23] M. Qian, L. Zheng, D. Graham, M.T. Frost, and D.H. StJohn, Settling of undissolved zirconium particles in pure magnesium melts, Journal of Light Metals, 1, (2001), 157-165.

[24] M. Qian, D.H. StJohn, M.T. Frost, and M.R. Barnett, Grain refinement of pure magnesium using rolled Zirmax master alloy (Mg-33.3Zr), in: H.I. Kaplan(Ed) Magnesium Technology 2003, (2003), TMS (The Minerals, Metals & Materials Society), pp. 215-220.

[25] M. Qian, D.H. StJohn, and M.T. Frost, Characteristic zirconium-rich coring substructures in Mg-Zr alloys, Scripta Materialia, 46, (2002), 649-654.

[26] M. Qian, D.H. StJohn, and M.T. Frost, Heterogeneous nuclei size in magnesium-zirconium alloys, Scripta Materialia, 50, (2004), 1115-1119.

[27] D.S. Gandel, M.A. Easton, M.A. Gibson, and N. Birbilis, Influence of Mn and Zr on the corrosion of Al-free Mg-alloys, Part 2: Impact of Mn and Zr on Mg-alloy electrochemistry, Corrosion, (Submitted).

List of tables and figures

Table 1: Composition of alloys produced in this study as tested via ICP-AES.

Figure 1: (A): BSE-SEM micrograph of Microzir master alloy, (B): BSE-SEM micrograph of Zirmax master alloy. **Figure 2**: (A): BSE-SEM micrograph of Mg-0.22Zr Microzir alloy, (B): EDX map of Zr content in Mg-0.22Zr Microzir alloy, (C): BSE-SEM micrograph of Mg-0.19Zr Zirmax alloy, (D): EDX map of Zr content in Mg-0.19Zr Zirmax alloy.

Figure 3: (A): Zr in solid solution vs. total Zr content for stirred Mg-Zr alloys (B): Zr in solid solution vs. total Zr content for unstirred Mg-Zr alloys.

Figure 4: (A): Zr content in solid solution (wt.%) vs. i_{corr} for stirred Mg-Zr alloys, (B): Zr content in solid solution (wt.%) vs. i_{corr} for unstirred Mg-Zr alloys, (C): Total Zr content (wt.%) vs. i_{corr} for stirred Mg-Zr alloys, (D): Total Zr content (wt.%) vs. i_{corr} for unstirred Mg-Zr alloys.

Figure 5: Electrochemical polarisation curves for Microzir and Zirmax containing Mg-Zr alloys compared with commercially pure Mg.

Figure 6: Weight loss vs. Zr content for Mg-Zr alloys made with Microzir and Zirmax master alloys.

Sample ID	Mg wt.%	Zr wt.% (Total content)	Overall % of Zr in solid solution	Fe wt.%
Microzir-1 Stirred	~Bal	0.028	42.86	0.01
Microzir-1 Unstirred	~Bal	0.012	33.33	0.008
Microzir-2 Stirred	~Bal	0.061	36.07	0.01
Microzir-2 Unstirred	~Bal	0.014	42.86	0.008
Microzir-3 Stirred	~Bal	0.12	45	0.011
Microzir-3 Unstirred	~Bal	0.019	47.37	0.005
Microzir-4 Stirred	~Bal	0.22	47.27	0.014
Microzir-4 Unstirred	~Bal	0.037	51.35	0.006
Zirmax-1 Stirred	~Bal	0.028	25	0.006
Zirmax-1 Unstirred	~Bal	0.018	22.22	0.006
Zirmax-2 Stirred	~Bal	0.057	15.79	0.006
Zirmax-2 Unstirred	~Bal	0.025	16	0.005
Zirmax-3 Stirred	~Bal	0.12	10	0.001
Zirmax-3 Unstirred	~Bal	0.056	8.93	0.005
Zirmax-4 Stirred	~Bal	0.19	10.53	0.006
Zirmax-4 Unstirred	~Bal	0.075	8	0.013

Table 1: Composition of alloys produced in this study as tested via ICP-AES.

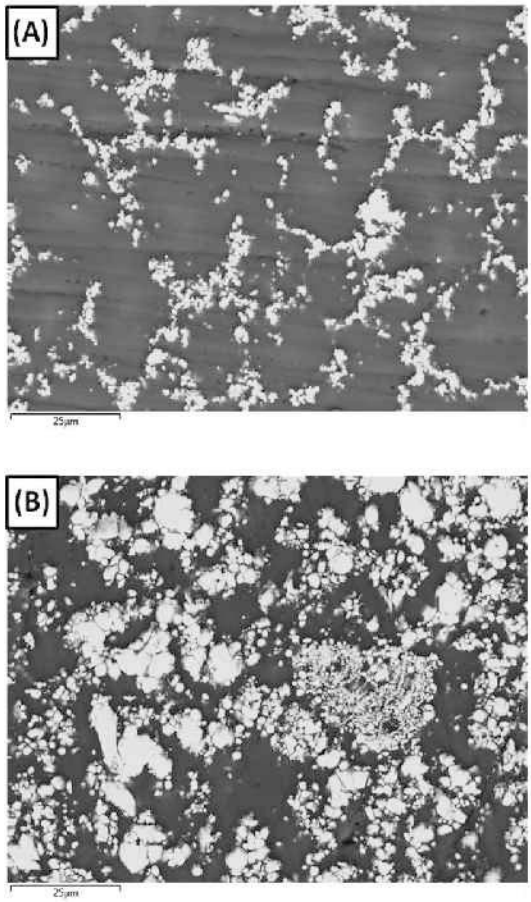

Figure 1: (A): BSE-SEM micrograph of Microzir master alloy, (B): BSE-SEM micrograph of Zirmax master alloy.

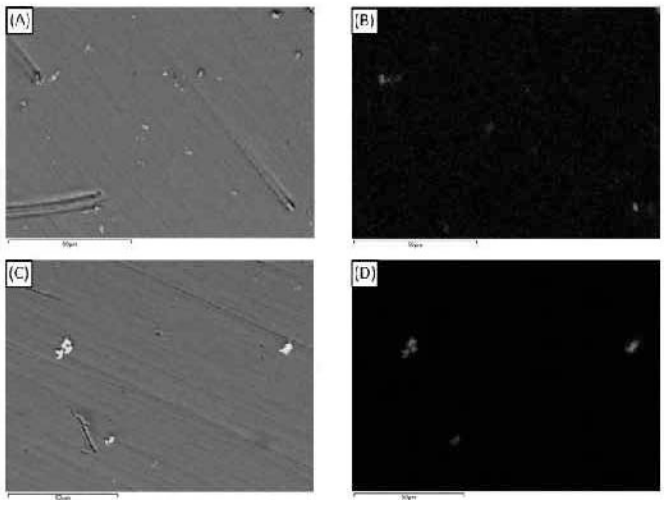

Figure 2: (A): BSE-SEM micrograph of Mg-0.22Zr Microzir alloy, (B): EDX map of Zr content in Mg-0.22Zr Microzir alloy, (C): BSE-SEM micrograph of Mg-0.19Zr Zirmax alloy, (D): EDX map of Zr content in Mg-0.19Zr Zirmax alloy.

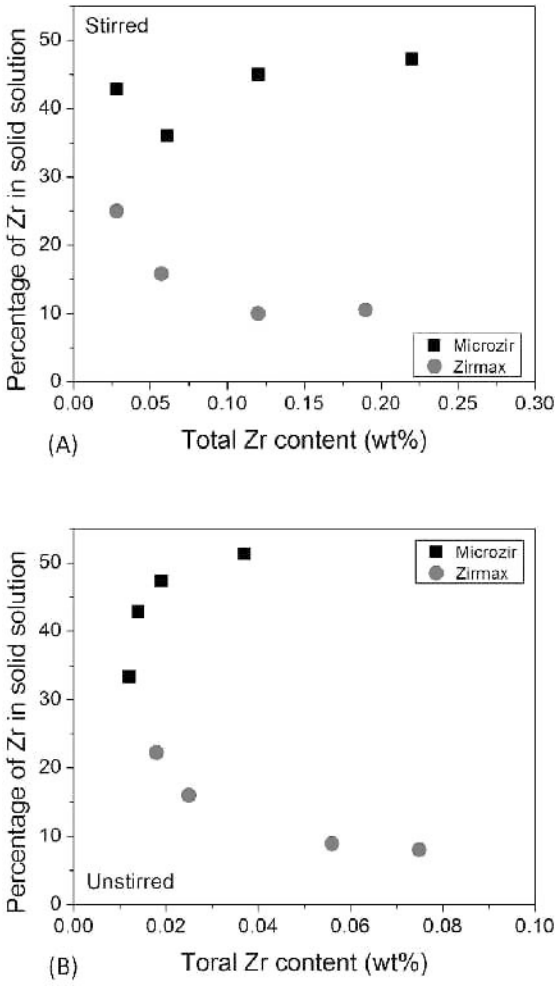

Figure 3: (A): Zr in solid solution vs. total Zr content for stirred Mg-Zr alloys (B): Zr in solid solution vs. total Zr content for unstirred Mg-Zr alloys.

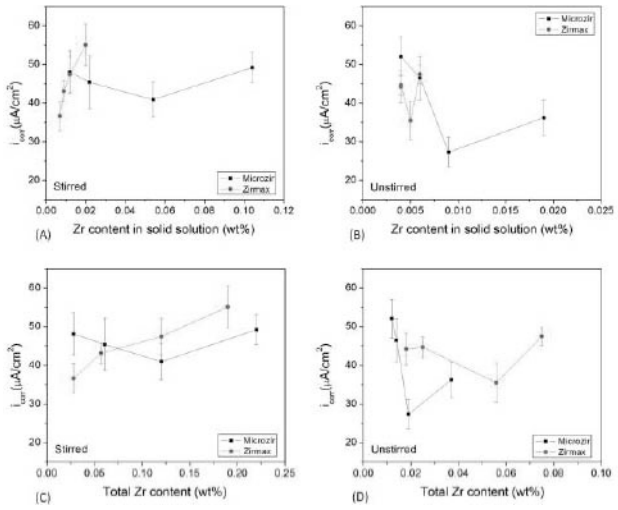

Figure 4: (A): Zr content in solid solution (wt.%) vs. i_{corr} for stirred Mg-Zr alloys, (B): Zr content in solid solution (wt.%) vs. i_{corr} for unstirred Mg-Zr alloys, (C): Total Zr content (wt.%) vs. i_{corr} for stirred Mg-Zr alloys, (D): Total Zr content (wt.%) vs. i_{corr} for unstirred Mg-Zr alloys.

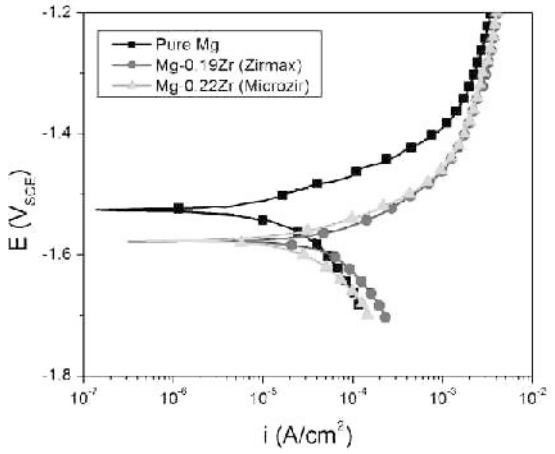

Figure 5: Electrochemical polarisation curves for Microzir and Zirmax containing Mg-Zr alloys compared with commercially pure Mg.

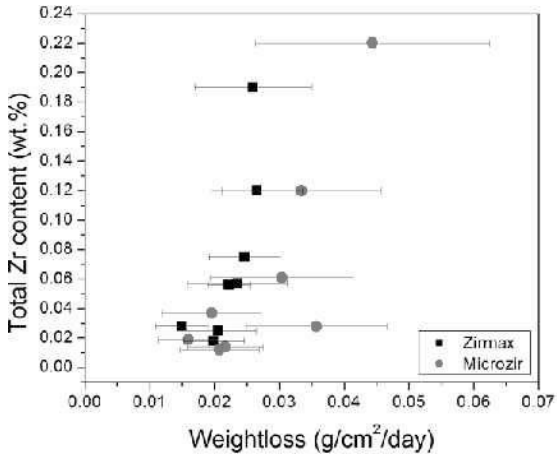

Figure 6: Weight loss vs. Zr content for Mg-Zr alloys made with Microzir and Zirmax master alloys.